THE UNIVERSITY OF MICHIGAN

INDUSTRY PROGRAM OF THE COLLEGE OF ENGINEERING

THE DOORWAY STATE THEORY OF NEUTRON NUCLEAR REACTIONS

Kenji Takeuchi

A dissertation submitted in partial fulfillment
of the requirements for the degree of
Doctor of Philosophy in the
University of Michigan
Department of Nuclear Engineering
1967

March, 1968

IP-812

ACKNOWLEDGMENTS

The author gratefully acknowledges the following:

To Professor F. C. Shure, the committee chairman, for his introductory guidance to the material of this thesis, particularly Part I; for his patient help in completing the thesis; and for his technical and editorial corrections of the thesis.

To Dr. P. A. Moldauer for his invaluable information, guidance, and assistance over the entire thesis work which could not have been accomplished without him.

To the remaining committee members, for their assistance: I am indebted to Professor R. K. Osborn for the shell model theory, to Professor G. C. Summerfield and Professor A. Z. Akcasu for the scattering theory.

To Dr. D. Kurath, the Argonne National Laboratory, for his technical assistance for the work in Part III.

To Professor A. Arima, the Argonne National Laboratory on leave from the Tokyo University, for his suggestions in setting up the model in Part III.

To Professor W. Kerr and Professor P. F. Zweifel through whom the financial support, under the contract with the Brookhaven National Laboratory, and the opportunity for working at the Argonne National Laboratory were provided.

To Dr. P. A. Moldauer, Dr. A. B. Smith, and Dr. S. A. Cox for their hospitality at the Argonne National Laboratory.

To the Argonne National Laboratory and the Associated Midwestern Universities for the opportunity of performing the investigation under the excellent staff members of the institute.

To the fellow students, James Davidson, Ellen Leonard, and Donald Oliver, for their corrections of the English in parts of this thesis.

The author is indebted to the Department of Nuclear Engineering, where he was a research assistant (July, 1964 - June, 1966, and May-July, 1967), and to the Associated Midwestern Universities and the Argonne National Laboratory where he was a student research associate (July, 1966 - March, 1967), for financial support during the thesis work.

Finally the author would like to express his thanks to the Industry Program for printing this thesis.

TABLE OF CONTENTS

TABLE OF CONTENTS (CONT'D)

TABLE OF CONTENTS (CONT'D)

LIST OF TABLES

LIST OF FIGURES

LIST OF FIGURES (CONT'D)

LIST OF APPENDICES

INTRODUCTION

In this thesis, we shall expand the doorway state theory for neutron nucleus reactions in the energy region below 10 Mev. In particular, we will improve the optical model in the very low energy region (1-500 Kev) and study the intermediate structure of cross sections. Further, we will investigate the analytic structure of T-matrix so that the properties of the fine structure of doorway states may be obtained. The results will be applied to the study of fine structure as well as intermediate structure of total cross section. Finally, the doorway state formation probability of Ni^{58} will be calculated by application of the shell model.

For more than ten years, the giant resonances of the total cross section and of the strength functions have been known and explained by the optical model.[29] Both the experimental data and the theory have been refined.[24,38-48] Recently, the deviations of the results of optical model (O.M.) calculations from the experimental data have been explained in terms of the simplest internal degree of freedom of the compound nucleus (the doorway state). This doorway state approximation has been applied to the strength functions of individual nuclei,[22] the intermediate structure of cross sections,[61,62] and the total cross section in the very low energy region. The last problem is our main concern in Part I and the detailed discussion may be seen in 5.1 of Part I.

The intermediate structure of the cross section is composed of the resonance structure smaller than the giant resonances but larger than the fine resonances. In the high energy region where the experimental energy

resolution is limited, the fluctuating part of the measured cross section from the smoothed cross section may be considered to be the intermediate structure. In the low energy region where fine resonances may be observed, the E-averaged cross sections show bumps whose sizes are smaller than the giant resonances. These are the intermediate structures (named for the appearance).

The intermediate structure of the measured cross sections in the high energy region are discussed by Kerman et.al.[62] Those in the low energy region are discussed by Feshbach et.al.[61] Further detailed search for intermediate structure has been actively conducted by by various experimentalists. Some of the observations are as follows: Cross sections of Cr, Ti, Ni, Fe, and Ce from 0.5 to 1.5 Mev are measured and the intermediate structures are observed by Smith[92] and by Cox.[93] Taking the E-average over a certain energy range, and varying the range, they observed bumps in the E-averaged cross sections. If a bump exists over a reasonable variation of the energy range, the bump is considered to be as the intermediate structure.[83] The cross sections of heavy nuclei[89,92] such as Mo and Ag do not reveal a clear intermediate structure.

Feshbach established the unified theory of nuclear reactions in 1958.[1] This theory is more convenient for dynamical description of the nuclear reactions than the R-matrix theory.[4] Weisskopf[21] proposed a reaction mechanism of cascade-like development of the nuclear reactions in contrast to the Bohr's mechanism. Based on the unified theory and the Weisskopf's model, Block and Feshbach[2] established the original form of the doorway state theory in 1963: Considering

that the cascade is proceeded by the residual two particle interaction potential and that the ground state of a target nucleus plus the incident neutron is one particle state, they called the simplest excited state of the compound nucleus, 2 particle-1 hole, the doorway state. We will interpret this definition of the doorway state as a subspace of (A+1) nucleon wave functions in the closed channel which is directly coupled to the open channel through an interaction Hamiltonian. The theoretical formalism itself is not changed by the extension. But the doorway state can be a vibrational or a rotational state and is determined by choice of the Hamiltonian.

The doorway state theory for the intermediate structure has been developed by MIT-group.(61) We will also apply the doorway state theory to a complex potential model (the modified O.M.), in Part I. Our formalism has a closer relation of the doorway-state effects to the complex potential than the MIT's; for example, we may take an energy average of the complex potential. Some results of these theories are as follows; the E-averaged cross section has a Breit-Wigner form around a doorway state. The effects of the doorway state may be represented by three dynamical constants: the doorway state formation and decay probabilities, and the doorway state energy.

The above theory improve the O.M. In particular, we may expect that the deviation of the complex potential for the smoothed cross sections of individual nuclei from the O.M. potential (to yield over-all averaged cross sections and the strength functions) may be explained in terms of the doorway states. Here, the complex potential is determined by the dynamical constants of the doorway states.

The shape of the measured intermediate structure has a sort of similarity to that predicted by the doorway state theory, and their widths are of the order of 100 kev which are extrapolated from the values of the doorway state formation probability of the simple nuclei. Because of the above reasons, the doorway state Ansatz has been justified. However, for example, the intermediate structure in the high energy region may be explained by the lumping effects of the fluctuation cross section (References 90 and 91) or by the statistical theory.(84) In the low energy region, the total cross section with fine resonances and with the intermediate structure may be explained by multi-level Breit-Wigner formula.(4,85) Under this situation, we consider that we must justify the existence of the doorway state upon stronger bases than the usual shape identification.

The dynamical constants of a doorway state have not been obtained except for the case of simple-structure nuclei for which measured resonances themselves may be considered to be the intermediate structure. (References 71, 77 and 80). Since these constants are important, we will develop a method to analyze the experimental data.

We may naturally expect more information on the doorway state from the fine structure of doorway states. We may also expect that the shapes of fine resonances are different from those of Breit-Wigner form due to difference in the reaction mechanisms of Bohr's and Weisskopf's. If so, the resonance shape provides any information and we must find out the condition under which the shape is reduced to the Breit-Wigner form.

For the above purposes, we will develop Mahaux-Weidenmuller's study[82] on the analytic structure of the T-matrix[96] when the doorway state exists. First, we will found the general theory of a single doorway state including multi-open channels.[94] By assuming the infinite Picket Fence model, we may almost completely trace the poles and residues of the T-matrix as functions of the doorway state formation and decay probabilities. From the pole and residue distributions, we may also investigate the fine structure of total cross section.

Based on the above results, we have discovered systematic resonance width distributions[63] from Ca- to Ni- isotopes which are obtained from experiments at Duke University[85] and will analyze the distributions to evaluate the dynamical constants. The obtained values well be applied to estimate the total cross section. The results are in good agreement with the measured cross section. These as well as brief discussion on the intermediate structure in the continuum region will be contained in Part II. The dynamical constants are also applied to the modified O.M. potential of Part I. The result indicates double $\gamma\sigma$ in the total cross section of Ni^{58} in good numerical agreement with the measured cross section.

In Part III, we will estimate the doorway state formation probability of Ni^{58} by nuclear structure calculation. The nuclear structure models for the highly excited states have not been much developed. It is mainly because the many configurations involved make calculation unfeasible. For simple-structure nuclei, however, the structure analyses of neutron elastic scattering cross sections and the resonance widths have recently been developed by Lemmer and Shakin,[71] by Shakin,[77] and by Lovas.[80] Lemmer and Shakin, and Lovas have calculated the

elastic scattering cross sections of N^{15} and C^{12} respectively. Shakin has calculated the resonance widths of Pb isotopes. These nuclei are considered to have simple nuclear structures because they took into account only doorway states for the compound states and because the calculation agrees with the fine structures of cross sections.

Our particular interest lies in the intermediate heavy nuclei of which observed cross sections exhibit excitation of more complicated states than the doorway states (Part II). For the highly excited states of such nuclei, Lande and Brown proposed a model. Their calculation, however, did not show the intermediate structure. Taking full advantage of the doorway state theory for these nuclei, we decouple the more complicated states and calculate the doorway state formation probability. Namely, we calculate only the intermediate structure and do not estimate fine resonance widths which involve mixture of highly complicated configurations.

We will take the quasi-particle model (pairing force plus 2^l pole-2^l pole force) which has been developed for the low lying excited states of vibrational type nuclei by Kisslinger and Sorensen, (Reference 99) Baranger,(100) and Yoshida.(97) For Ni isotopes, the levels are estimated by Kisslinger and Sorensen,(99) recently by Hsu and French,(108) and by Auerbach.(110) Lawson et.al.(107) calculated these levels by the shell model. We will also calculate the low excited levels and adjust the force constants to yield the above calculated as well as measured levels. With thus determined Hamiltonian, we calculate the doorway state formation probabilities. The results agree fairly well with the measured values. The relation with the Lande-Brown model will be briefly discussed in Part III.

PART I

INTERMEDIATE STRUCTURE OF CROSS SECTIONS

INTRODUCTION

In this part of the thesis, we improve the Optical Model in the very low energy region and provide some information for the intermediate structure of cross sections. Chapter 1 contains some historical background. In Chapter 2, adopting the formalism of the unified theory, we present the theoretical preliminaries for the thesis. In Chapter 3 we outline a new method for the derivation of the optical model potential. This method has the advantage that it permits straightforward calculation of the doorway-state effects upon the optical model potentials, and such calculations are carried out in Chapters 4 and 5. Chapter 6 contains a brief comparison between our results and the results of Feshbach and his co-workers.

CHAPTER 1

REVIEW OF EXISTING THEORIES

1.1 Bohr's Compound Nucleus

A comprehensive history of the early research on nuclear reactions may be found in the works of Breit,[5] Evans,[6] and Darow.[7]

The nuclear transmutation reaction of $N(\alpha, p)O$ was discovered by Rutherford[8] in 1919. Until 1930, (α, p) - reactions with light nuclei, particularly, B , N , and Al , were investigated by the Cavendish school.[7] In 1930, the resonance reaction was first discovered by Pose[9] from the $Al(\alpha, p)Si$ experiments. In the same year, Bothe and Becker[10] discovered (α, n) - and (α, γ) - reactions, although they did not distinguish between the two. In 1932, the neutron was discovered by Chadwick[11] from $Be(\alpha, n)C$. Since then, many neutron experiments have been performed. In 1935 and 1936, neutron moderation, $1/v$ - absorption, and resonance capture were discovered by Fermi,[6] and by Moon and Tillman.[13]

In the 1930's, prototypes of the modern nuclear reaction theories were developed: the resonance theory,[14,15,16] the direct reaction model,[16] the statistical model,[17] the continuum theory,[17,18] and the general theory.[19]

In the resonance theory, the compound nucleus was proposed by Bohr.[14] The Breit-Wigner formula[15] was derived taking γ -decay channels into account. Bohr's classical compound nucleus has recently been reconsidered by Breit[20] from a quantum mechanical standpoint, referring to Blatt and Weisskopf's text.[3] "Bohr's assumption" is stated as follows:[20]

"The nuclear reaction is separated into two 'stages':
(a) the formation of the compound system C, and
(b) the disintegration of the compound system into the products of the reaction.

"The following approximation has been proved valid, or at least approximately valid in many cases: the two stages can be treated as independent processes, in the sense that the mode of disintegration of C depends only on its energy, angular momentum, and parity, but not on the specific way in which it has been produced.

"The reaction mechanism is that the incident particle comes within the short range of nuclear forces and shares its energy quickly among all constituents well before any re-emission can occur."

Calling Bohr's assumption the case of very strong interactions between nuclear constituents, Weisskopf[21] proposed another reaction mechanism for weak interactions which will be reviewed in section 1.7. His ideas have been first formulated as the doorway state theory by Block and Feshbach.[22] Weisskopf's compound nucleus is the basis of the entire work of this thesis.

1.2 The R-Matrix Theories

The general theory of nuclear reactions by Kapur and Peierls[18] formed the basis of the R-matrix theory which is reviewed in the classic paper of Lane and Thomas.[4] The Breit-Wigner formulae[4,15] were originally derived using time-dependent perturbation theory in which a single particle plays a significant role and the interactions are weak (electron-photon interaction). The form of the theoretical cross section fits well to the measured resonances. However, difficulties appear when attempts are made to interpret the values of the parameters. The unsatisfactory reliance on the perturbation theory was removed by Kapur and Peierls.

There are various formalisms of the R-matrix theory,[4] among them, those of Kapur-Peierls, of Wigner-Eisenbud, and of Moldauer. These formalisms are interrelated by choice of the boundary conditions (References 17 and 18) which will be set on the eigenfunctions. Each is characterized by a different choice of B_c, the logarithmic derivative of the internal eigenfunction evaluated at the nuclear boundary.

The R-matrix theory is constructed as follows: In each channel, a relative space coordinate is separated into two parts by a channel radius, a_c, such that outside the channel radius no strong nuclear reactions occur. The regions inside and outside the radius a_c are called the internal and external regions respectively. By this separation of the space region, the collision matrix* $\underset{\sim}{U}$ (= S -matrix) is separated into kinematical and dynamical factors.

The kinematical factors are given by diagonal matrices $\underset{\sim}{L}$, $\underset{\sim}{\Omega}$, and $\underset{\sim}{\rho}$ which depend on a_c but not on B_c. By denoting the incoming and outgoing channel waves by $\mathcal{I}_c$ and $\mathcal{O}_c$, the radial wave functions $I_{\alpha l}$ and $O_{\alpha l}$ are related by

$$\left.\begin{aligned} \mathcal{I}_c &= \frac{I_{\alpha l}}{\sqrt{v_\alpha}}\varphi_c\ ; \quad I_{\alpha c} \sim \exp\left\{-i\left(\rho_\alpha - \frac{l\pi}{2}\right)\right\} \\ \mathcal{O}_c &= \frac{O_{\alpha l}}{\sqrt{v_\alpha}}\varphi_c\ ; \quad O_{\alpha c} \sim \exp\left\{i\left(\rho_\alpha - \frac{l\pi}{2}\right)\right\}, \end{aligned}\right\} \quad (1.2.1)$$

where φ_c is called the surface function, v_α is the relative speed, $\rho_\alpha \equiv k r_\alpha$ and the channel index $c \equiv (\alpha l s J M)$. Another kinematical

---

* The rows and columns of matrices correspond to the channel indices.

factor, $\underset{\sim}{W}$, is the wronskian which is independent of ρ_c in the external region and in normalized to $2i\,(=W_c)$ for the open channel. The matrix elements of $\underset{\sim}{L}$ are the logarithmic derivatives of the outgoing radial wave function at the channel surface $(L_c \equiv [\rho_c O_c' / O_c]_{a_c})$. Those of $\underset{\sim}{\Omega}$ are the ratios of the incoming to the outgoing wave amplitudes $(\Omega_c \equiv [I_c / O_c]_{a_c})$. $\underset{\sim}{P}$ is defined by its diagonal elements $P_c \equiv [\rho_c / I_c O_c]_{a_c}$. The real and imaginary parts of $\underset{\sim}{L}$ are called the shift factor, $\underset{\sim}{S}$, and the penetration factor, $\underset{\sim}{P}$, $(\underset{\sim}{L} = \underset{\sim}{S} + i\underset{\sim}{P})$.

The dynamical factor is given by the R-matrix, $\underset{\sim}{R}$. The R-matrix depends on the channel radius, a_c , and on the boundary condition, B_c . In the internal region, the function space of the system Hamiltoniam is represented by an orthonormalized and complete set of eigenfunctions χ_λ within the internal region which are specified by a_c and B_c. The R-matrix is given by the eigenvalue e_λ and the reduced width $\gamma_{\lambda c}$. The reduced width is proportional to a channel* component, c , of the radial wave of the eigenfunction,** χ_λ , on the channel surface. Denoting $\gamma_{\lambda c}$ by a column matrix $\underset{\sim}{\gamma}_\lambda$, the R-matrix is given by

$$\underset{\sim}{R} = \sum_\lambda \frac{\underset{\sim}{\gamma}_\lambda \times \underset{\sim}{\gamma}_\lambda}{E - e_\lambda} , \qquad (1.2.2)$$

where $\underset{\sim}{\gamma}_\lambda \times \underset{\sim}{\gamma}_\lambda$ is the direct product.

---

*The channel indices are good quantum numbers in the external region.

**

$$\gamma_{\lambda c} \equiv \sqrt{\frac{\hbar^2}{2M_c a_c}} \int \varphi_c^* \chi_\lambda \, dS ,$$

where M_c is the reduced mass of the channel c .

The collision matrix $\underset{\sim}{U}$ and the R-matrix are related by

$$\underset{\sim}{U} = \underset{\sim}{\Omega}^2 + 2i\,\underset{\sim}{\Omega}\,\rho^{1/2}\frac{1}{1-\underset{\sim}{R}\,\underset{\sim}{L}^0}\,\underset{\sim}{R}\,\rho^{1/2}\,\underset{\sim}{\Omega}, \qquad (1.2.3)$$

where $\underset{\sim}{L}^0 \equiv \underset{\sim}{L} - \underset{\sim}{B}$ and $\underset{\sim}{B}$ is a diagonal matrix of components B_c .

The Kapur-Peierls formalism[4] is obtained by choice of the Boundary condition, $\underset{\sim}{L}^0 = \underset{\sim}{0}$; i.e. $\underset{\sim}{B} = \underset{\sim}{L}$. Therefore, the boundary condition depends on E and is complex.

Now consider a certain range of E. The R-matrix of Equation (1.2.2) may be divided into two parts

$$\underset{\sim}{R} = \underset{\sim}{R}^0 + \underset{\sim}{R}',$$

where in $\underset{\sim}{R}^0$ all the distant levels are included. $\underset{\sim}{R}^0$ varies only slowly with E in the above energy range. Then, Equation (1.2.3) becomes

$$\underset{\sim}{U} = \underset{\sim}{\Omega}^2 + 2i\,\underset{\sim}{\Omega}\,\rho^{1/2}\frac{1}{1-\underset{\sim}{R}^0\underset{\sim}{L}^0}\,\underset{\sim}{R}^0\,\rho^{1/2}\,\underset{\sim}{\Omega} + \qquad (1.2.4)$$

$$+ 2i\,\underset{\sim}{\Omega}\,\rho^{1/2}\sum_{\lambda\mu}(\underset{\sim}{\alpha}_\lambda \times \underset{\sim}{\alpha}_\mu)\,A_{\lambda\mu}\,\rho^{1/2}\,\underset{\sim}{\Omega},$$

where

$$\left.\begin{aligned}
&\underset{\sim}{A} \equiv \left(\underset{\sim}{e} - E\underset{\sim}{1} - \underset{\sim}{\xi}\right)^{-1} \qquad \text{; the level matrix,}\\
&(\underset{\sim}{e})_{\lambda\mu} \equiv e_\lambda\,\delta_{\lambda\mu},\\
&(\underset{\sim}{\xi})_{\lambda\mu} \equiv \underset{\sim}{\gamma}_\lambda^{T}\left[\underset{\sim}{L}^0\left(\underset{\sim}{1} - \underset{\sim}{R}^0\underset{\sim}{L}^0\right)^{-1}\right]^{T},\\
&\underset{\sim}{\alpha}_\lambda \equiv \left(\underset{\sim}{1} - \underset{\sim}{R}^0\underset{\sim}{L}^0\right)^{-1}\underset{\sim}{\gamma}_\lambda,
\end{aligned}\right\} \qquad (1.2.5)$$

and $\underset{\sim}{\gamma}_\lambda^T$ is the transpose of $\underset{\sim}{\gamma}_\lambda$. If we may attribute the slowly varying part of the S-matrix to the direct reactions, then the direct reaction is given by the distant levels in the language of the R-matrix theory. In the unified theory, such a contribution is given by the distorted waves, or by a single particle potential, or by the real parts of the potential of the generalized optical model.

In Moldauer's formalism,[23] the S-matrix is sought which is correct in a certain energy range Δ centered at E_0, instead of that which is correct over the entire energy region such as Equation (1.2.3) or that of Kapur-Peierls. The statistical region, I, centered at E_0 $(I >> \Delta)$ is also considered. The choice of the boundary condition is $\underset{\sim}{B} = \underset{\sim}{L}(E_0)$. Then, the R-matrix is divided into two parts;

$$\underset{\sim}{R} \equiv \sum_\mu \frac{\underset{\sim}{\theta}_\mu \times \underset{\sim}{\theta}_\mu}{\varepsilon_\mu - E - \frac{i}{2}\Gamma_\mu} = (\underset{\sim}{R}^{(0)} - \underset{\sim}{R}^{(2)}) + (\underset{\sim}{R}^{(1)} + \underset{\sim}{R}^{(2)}), \tag{1.2.6}$$

where the notation follows Reference 23, and, here, we will see values in comparison with Equation(1.2.2). The matrix $\underset{\sim}{R}^{(2)}$ depends upon parameters for which the statistics is the same as those of $\underset{\sim}{R}^{(1)}$. Its levels are extended from $-\infty$ to $+\infty$ outside the region I. Equation (1.2.3) becomes, in the energy region Δ,

$$\underset{\sim}{U}^S(E;E_0) = \underset{\sim}{U}^{(0)}(E_0) - i\sum_\mu \frac{\underset{\sim}{g}_\mu \times \underset{\sim}{g}_\mu}{E - \varepsilon_\mu + \frac{i}{2}\Gamma_\mu}, \tag{1.2.7}$$

where

$$\underset{\sim}{U}^{(0)}(E_0) \equiv \underset{\sim}{\Omega}^2 + 2i\,\underset{\sim}{\Omega}\,\underset{\sim}{P}^{1/2}(\underset{\sim}{R}^{(0)} - \underset{\sim}{R}^{(2)})\,\underset{\sim}{P}^{1/2}\,\underset{\sim}{\Omega}\,,$$

and (1.2.8)

$$\underset{\sim}{\mathcal{G}}_\mu \equiv \underset{\sim}{\Omega}\,(2\underset{\sim}{P})^{1/2}\,\underset{\sim}{\vartheta}_\mu\,.$$

$\underset{\sim}{U}^S$ is called the statistical collision matrix and will be often referred to in this thesis.

Humblet and Rosenfeld[84] expressed the S-matrix by a Mittag-Leffler series which is valid on the entire Riemann surface. The parameters are independent of energy. This form of S-matrix is ideal in its simplicity. However, it has been pointed out[23] that it is not clear what conditions must be placed on the Hamiltonian to insure covergence of the series.

In the above formalism, the dynamical constants depend crucially on the choice of the channel radius, within the frame of one formalism. In the unified theory,[68,69] the radius dependence is removed and this formalism is most easily combined with a nuclear structure theory.

Although the unified theory has the above advantage, it is least tractable as far as the analytic structure of the S-matrix is concerned. The dynamical constants are energy-dependent, and there is the same difficulty in the inversion of the matrix as is in the R-matrix theory. In addition, the finite number[34] of compound states causes a serious difficulty in carrying out an average of the S-matrix over energy.

We will adopt the shell model for the dynamics of the reactions; i.e., the Hamiltonian is taken to be a single particle potential plus two body residual interactions. The rotational model[66] and the vibrational model[67] may be formally derived from the shell model. In the highly excited states of interest to us, a high degree of configuration mixture makes calculation unfeasible. However, combined with Weisskopf's reaction picture, configurations may be limited to only simple modes of excitation; doorway states. These do not in general give the compound states. However, they show up their existence in various ways in the observed resonance data which will be studied in Part II. Hence, a quantity $\Gamma^{\uparrow}$ * associated with the simple mode is obtained from both experiment and calculation.

In Part I, the more complicated states will be averaged out and their effects are represented by the doorway state strength function*, $\Gamma^{\downarrow}$. Instead of smearing out the more complicated states, in Part II we assume one doorway state and the Picket Fence model for the more complicated states. Analytic properties of the T-matrix and the fine structure of total cross section will be investigated as a function of the coupling strengths $\Gamma^{\uparrow}$ and $\Gamma^{\downarrow}$. From the observed resonance width distribution and the total cross section, $\Gamma^{\uparrow}$ and $\Gamma^{\downarrow}$ are obtained. Also, the relation between Weisshopf's and Bohr's reaction pictures will be derived. In Part III, the Hamiltonian which explains low excited states of Ni^{58} will be applied to the calculation of $\Gamma^{\uparrow}$.

---

* $\Gamma^{\uparrow}$ and $\Gamma^{\downarrow}$ are measures of coupling strengths of the doorway state to the open channel and to the closed channel respectively.

An E-average of the T-matrix is involved in Part I. We adopt Feshbach's calculation which becomes a good approximation for $\langle\Gamma\rangle/\langle D\rangle \ll 1$. As far as this calculation applies, the averaged quantity is given by a simple form and the inversion of the matrix is unnecessary.

As mentioned above, analytic properties of the T-matrix will be studied in Part II. By limiting the energy region as is done in Moldauer's treatment of the statistical collision matrix, the single particle effects may be taken to be independent of energy. Then, resonance parameters become independent of energy. By the assumption of the single doorway state, the multi-channel T-matrix becomes reduced to the form of a branching ratio times a structure factor, and the inverse of the matrix may be calculated easily.

1.3 The Phenomenological Optical Model

The essentials of the optical model (O.M.) approach are as follows:[24] (1) The many-body problem is approximated by a two-body problem. (2) The imaginary part of the potential appears through the elimination of open channels and by an energy average of the T-matrix. Based on the empirical fact that the complex potential gives good fit to the E-averaged total cross section, the O.M. potential has been defined as the potential which will produce the average S- or T-matrix.[1]

The early development of the O.M. is reviewed by Feshbach in Reference 24. The replacement of the target nucleus by a potential well was first suggested by Bethe[25] in 1935. He hoped to understand nuclear reactions and, in particular, the slow neutron resonances which have been successfully explained by Bohr[14] and by Breit and Wigner.[15]

The resonances obtained by Bethe are now referred to as "single-particle resonances" or "giant resonances." Bethe[26] pointed out that the single particle potential was actually a single-particle approximation to the Bohr theory, and discussed that it gives the E-averaged cross sections.[16]

The giant resonances* as a function of mass number, A , and energy, E , have been discovered by Ford and Bohm[27] and by Barshall.[28] Feshbach, Porter, and Weisskopf[29] have calculated the total cross section by the square complex well. The fit is obtained at

$$U(r) = \begin{cases} -U_0(1+i\zeta) & r < R \\ 0 & r > R \end{cases},$$

$$U_0 = 42.\ \text{Mev}, \quad \zeta = 0.03 \ (\text{Im}U \cong 1.26\ \text{Mev}),$$

and

$$R = 1.45 \times 10^{-13}\ A^{1/3}\ \text{cm}.$$

Thomas[32] and Lane, Thomas, and Wigner[33] have shown that the giant resonances are derived directly from the R-matrix theory by a suitable Ansatz on the distribution of the reduced widths. A similar Ansatz is used by Moldauer[34] for the intermediate structure of cross sections. The results of Part II can be thought of as a justification of the Ansatz, for a particular doorway state model.

As mentioned above, the imaginary part of the potential is produced by elimination of open channels and by the E-average process. The many-body problem may be formally reduced to the two-body problem without

---

*The terminology "giant resonance" refers to wide resonances over E and A .[30]

the process of E-averaging.[24] Such a potential is called the "generalized optical potential."[24] If open channels are eliminated, it becomes a complex potential.[24]

Another cause of the imaginary part of the O.M. potential has been justified by taking the E-average of the T-matrix[1,24] (see § 1.5 and § 3.1). This E-average process corresponds to the experimental situation of "bad resolution". Namely, the experimentally measured cross sections with the bad resolution may be calculated by the O.M. A physical interpretation of the bad resolution was once given by Friedman and Weisskopf[35] to the effect that the E-average appears as a consequence of the formation of the wave packet.[1,24] However, the well-known fact that the wave packet changes its original form as it moves indicates that the wave function becomes indefinite at large distances from the target nucleus (see Equations (3.2.2) and (1.5.1)).

We will show in § 3.2 that the O.M. is derived from the E-average of the Schrödinger equation* rather than from the quantum mechanical resolution. Namely, each incident neutron has an ideal resolution. A group of incident neutrons and target nuclei forms an ensemble. Each element of the ensemble follows an equation of motion independently. The energies of the elements distribute around an energy E_o of the O.M. Therefore, observed cross sections are the ensemble average of the independent events. This is parallel to the E-average of the statistical theory.

---

*This method for derivation of the O.M. equation is developed in order to derive the doorway state strength function (Chapter 4). On this particular point, the author acknowledges the assistance of extensive discussions with Dr. P. A. Moldauer and Dr. R. Coester. Also, Dr. S. A. Cox's explanation of the experimental resolution was very suggestive of the correct approach to this problem.

1.4 Refinement of the O.M. Potential

The optical model (O.M.) was proposed in order to explain the giant resonances.[29] In combination with the Hauser-Feshbach (H-F) statistical theory[36] (further improved by Moldauer[37]), the O.M. has been used to obtain theoretical values of elastic, elastic differential, and inelastic scattering cross sections in addition to the total cross section.[46-48] At higher energies where there are many competing compound-nucleus decay channels, the compound elastic cross sections may be neglected compared to the shape elastic cross sections so that the shape elastic and the absorption cross sections of O.M. may be put equal to the average elastic and average total reaction cross sections respectively.[24] At such high energies, the O.M. potential (without H-F correction) is expected to yield the E-averaged total, total elastic, differential elastic, and total reaction cross sections.

Originally, an energy independent complex square well was used for the O.M. potential,[29] with fair success, but many refinements were applied subsequently; Wood-Saxon potential, $\underset{\sim}{\ell}\cdot\underset{\sim}{s}$ potential, etc.[24] Furthermore, deformation of nuclei has been taken into account to explain the double peaks of the strength function at $A \sim 160$.[44~47] Surface absorption (peaking of the imaginary potential near the nuclear surface) has been introduced to improve the differential elastic, total, and total elastic cross sections at higher energies,[38,39] and the strength function at $A \sim 100$.[40-43] One would hope to be able to choose an energy independent form for the O.M. potential, but it was found necessary to admit a slow variation of the potentials with energy.[38] Even so, various energy dependent potentials have been shown to be equivalent to non-local potentials.[24,47,48]

In the usual O.M. the target nucleus is not assumed to have internal degrees of freedom. Scattering into inelastic channels appears only via absorption followed by decay of the compound nucleus (see next section). Yoshida's "Generalized Optical Model"(52) incoorporates target nucleus internal degrees of freedom, thereby yielding direct inelastic reactions. This approach was applied to the deformed nuclei, treating the nucleus as a rigid rotator, and may be regarded as a forerunner of the doorway state theory.

Moldauer(23,37) has developed a statistical theory which takes into account the correlations of the R-matrix parameters. He obtains an optical model potential which fits both the strength function and the low-energy ($\sim$1 Mev) average experimental values of the total, differential elastic, and inelastic scattering cross sections.(43,37) We have done χ^2-fit calculation to the total, total elastic, and differential elastic scattering cross sections on Na^{23}. The energy range from 1 to 4 Mev is used for the fit. Calculations were performed on the IBM-7090 using the ABACUS II code which has O.M. with H-F correction. The result is applied to the inelastic scattering cross sections with fair success. The total cross section is calculated extending the energy range up to 10 Mev with good fit to the measured value.(51) However, extension to the lower energy region was not satisfactory. The discrepancy becomes larger below 0.5 Mev and the calculated total cross section turns into the well-known $1/v$-region of the O.M., while the measured σ_t is fairly constant in E. In order to improve the O.M. fit, the imaginary part of the O.M. potential must be allowed to vary rapidly with energy in the very low energy region. Part I of this thesis is devoted to the theoretical justification of this variation. The detailed discussion on the method for development may be seen in Chapter 4.

On the other hand, the MIT-group[61] has developed the theory for the intermediate structure of cross sections in the higher energy region.[62] Our motivation and method for the approach to the problem (see Chapter 3-5) are different from those of MIT, and are worked out independently. However, both are dealing with the same theoretical objects. So, we will follow our formalism and notations up through Chapter 5. In the last chapter, the notations will be compared and, in the following parts of this thesis, we will adopt MIT's notation, since it is more commonly used.

1.5 The O.M. and the Statistical Theory

Feshbach, Porter, and Weisskopf[29] introduced the average cross sections: the shape elastic cross section, the compound elastic cross section, and the compound-nucleus formation cross section. The phenomenological optical model and the statistical theory[36,56] have been related through the transmission coefficient. Moldauer[37] and Porter[57] extended the average cross sections to correspond to those of the generalized O.M. theory. Moldauer[37] further improved the statistical theory taking into account the statistics of the R-matrix parameters.[58]

By partial wave analysis, the asymptotic wave function becomes

$$\psi_l \longrightarrow \text{const.} \left[e^{-i(kr - \frac{l\pi}{2})} - \eta_l e^{i(kr - \frac{l\pi}{2})} \right]. \tag{1.5.1}$$

where no spin is considered and $|\eta_\ell| < 1$. The cross sections are

$$\left.\begin{aligned} \sigma_{el}^{(l)} &= \pi \lambda^2 (2l+1) \left| 1 - \eta_l \right|^2, \\ \sigma_r^{(l)} &= \pi \lambda^2 (2l+1) \left(1 - |\eta_l|^2 \right), \\ \sigma_t^{(l)} &= 2\pi \lambda^2 (2l+1) \left(1 - \mathrm{Re}\, \eta_l \right). \end{aligned}\right\} \qquad (1.5.2)$$

the subscripts referring to elastic, reaction, and total cross sections respectively. Taking the E-average, the total cross section becomes

$$\bar{\sigma}_t^{(l)} = 2\pi \lambda^2 (2l+1) \left(1 - \mathrm{Re}\, \bar{\eta}_l \right). \qquad (1.5.3)$$

The shape elastic, compound elastic, and compound-nucleus formation cross sections are defined respectively by

$$\sigma_{se}^{(l)} \equiv \pi \lambda^2 (2l+1) \left| 1 - \bar{\eta}_l \right|^2, \qquad (1.5.4a)$$

$$\sigma_{ce}^{(l)} \equiv \pi \lambda^2 (2l+1) \left(\overline{|\eta_l|^2} - |\bar{\eta}_l|^2 \right), \qquad (1.5.4b)$$

and

$$\sigma_c^{(l)} \equiv \sigma_{ce}^{(l)} + \bar{\sigma}_r^{(l)} = \pi \lambda^2 (2l+1) \left(1 - |\bar{\eta}_l|^2 \right). \qquad (1.5.4c)$$

$$\therefore \quad \sigma_{el}^{(l)} = \sigma_{se}^{(l)} + \sigma_{ce}^{(l)}. \qquad (1.5.5)$$

Having the empirical fact that the O.M. gives the E-averaged total cross section, Feshbach, Porter, and Weisskopf identified the E-averaged S-matrix with the S-matrix which is yielded by the O.M. potential. This then becomes the definition of the O.M. potential[1] (§ 3.1).

The question immediately arises as to whether the shape elastic and compound nucleus cross sections σ_{se} and σ_c (i.e., those obtained by replacing η_ℓ by $\bar{\eta}_\ell$ in the expressions for σ_e and σ_r)have physical significance. This is discussed in detail by Feshbach, Porter, and

Weisskopf[29] who show that quite generally the shape elastic cross section is approximately equal to σ_p , the potential scattering part of the scattering cross section. Therefore, the compound elastic cross section σ_{ce} of (1.5.4b) is equal to the energy average of $\sigma_e - \sigma_p$.

The compound nucleus formation cross section is also related to the imaginary part of the potential by Porter[59] (see § 2.3 and 2.4). This is further related to the transmission coefficient by

$$\sigma_c^{(\ell)} = \pi \lambda\!\!\!^{-2} (2\ell+1)\, T_\ell \,. \qquad (1.5.6)$$

The computer code ABACUS II[55] is available for the optical model combined with Hauser-Feshbach statistical model.

To take the direct reactions into account, the O.M. is replaced by the generalized O.M. The T-matrix elements obtained from the generalized O.M. is equated to the E-averaged T-matrix elements.[37] In this case, the average cross sections are redefined by Moldauer.[37] As mentioned above, the statistical theory is further developed.[37] Modern statistical theory is developed based on the R-matrix theory[4,23] and the statistics of the R-matrix parameters.[58] The consequences on the intermediate structure of cross sections are given by Moldauer.[89]

1.6 Direct Reaction and the Unified Theory

The nuclear reaction models have been composed of two models:[4,60] the compound nucleus model and the direct reaction model. The basic physical idea[4,60] for the direct reaction mechanism is that, as a consequence of the fairly onlg mean free path against collision, it is possible for an incident nucleon to enter a nucleus and to exchange energy

with a target nucleon, and for the one or the other particle to escape directly (or in one step) without formation of the compound nucleus. The compound reaction mechanism has been represented by Bohr's model.

These reaction mechanisms are distinguished by the angular distribution and the energy dependence of cross sections. In the direct reaction, there is the strong forward peaking in the angular distribution. Also, the cross sections predicted by the direct reaction theory do not show the sharp resonances characteristic of the compound-nucleus theory.[4,60]

In the R-matrix theory, the direct reaction is usually ascribed to the distant levels[4] which appear in the S-matrix as the first two terms of Equation (1.2.4) and the first term of Equation (1.2.7). On the other hand, the Hamiltonian of the direct reaction model[60] is constructed by adding to the O.M. potential an interaction which causes the transition to the inelastic channels. In other words, the Hamiltonian of the generalized O.M. is the model Hamiltonian of the direct reaction theory.

The formal theory of the direct reactions has been developed by many authors[65] and is reviewed by Austern.[64] These works were forerunners of Feshbach's unified theory of nuclear reactions.[68,69] This formalism can easily be applied to the theory of the nuclear structure. The nuclear structure studies have been recently started in the highly excited states, based on the unified theory. We will contribute to the study in Part III where the target nucleus is one of the intermediate nuclei.

The part of the Hamiltonian corresponding to the direct reaction is PHP in this thesis (see Chapter 2). The parts of the T-matrix and cross sections due to PHP will often be considered to be constant in energy within a certain energy range, Δ .

1.7 Weisskopf's Compound Nucleus

In 1961, Weisskopf[15] suggested a unified view of the nuclear models. The nucleon-nucleus interaction is separated into a single particle potential plus residual interactions. Based on the success of the O.M., a weak coupling reaction model is proposed to understand both the occurrence of direct reactions and the formation of a compound nucleus.

In Weisskopf's scheme, nuclear reactions proceed as a succession of collisions of two nucleous. At the first collision, the incident nucleon may experience a direct reaction or enter the first stage of the compound nucleus such as "2 particle - 1 hole" state. At the second collision, it may go to the end of the reaction as well as to the more complicated states of the compound nucleus such as "3 particle - 2 hole" states. The first step of this reaction picture is drawn in Figure I.1 of Chapter 2.

Block and Feshbach[22] reintroduced Weisskopf's reaction mechanism as the doorway state theory. The doorway state is defined to be the first stage for the formation of the compound nucleus; e.g. 2p - 1h states in the above picture.

As a natural extention, we may consider the doorway states which are rotation excitation plus one particle states or vibration excitation plus one particle states, etc., depending on the target nucleus. There

is no difference in the formalism. The relation between the two-body residual interaction and collective interactions may be seen in References 66 and 67.

CHAPTER 2

THEORETICAL PRELIMINARY

In this chapter and in Appendices A and B, the theoretical background of the unified theory will be given. Notations and physical constants which will appear in the later chapters will be specified. Section 2.1 outlines the many-body Hamiltonian. In section 2.2, Feshbach's projection operator formalism will be reviewed. Relations between the T-matrix elements and the cross sections will be given in Appendix A based on the projection operator formalism. Appendix B discusses the partial wave analysis thoroughly and relates cross sections to Blatt and Biedenharn's expressions. Some of the results in the Appendices will be listed at the end of section 2.2. The resonance parameters introduced by Feshbach will be reviewed in section 2.3. The absorption cross sections of the S-wave single channel have been related to the imaginary part of the complex potential by Porter. This is applied to the unified theory and generalized in section 2.4 to the multi-channel cases. There the strength function and transmission coefficients are defined. In section 2.5, Feshbach's energy average of the T-matrix will be reviewed. Finally, the T-matrix and the compound states will be defined in section 2.6.

2.1 Hamiltonian for $A(n,n')A^*$ Reactions

We deal with the nuclear reaction problem of the type $A(n,n')A^*$, that is, elastic and inelastic scattering of neutrons by nuclei. The many-body Hamiltonian is discussed in this section. The total energy of the system of $A+1$ particles interacting pairwise is

$$H_L = \sum_{i=0}^{A} \frac{p_i^2}{2m} + \sum_{i>j} V_{ij}, \qquad (2.1.1)$$

where the coordinates are referred to the laboratory system,

A ; the mass number of the target,

$\underset{\sim}{p}_i$; the momentum of the i-th nucleon,

m ; nucleon mass,

V_{ij} ; the two-body interaction potential between the i-th and j-th nucleons,

and subscript i = 0 indicates the incident neutron. The coordinates are transformed to the center of mass system as follows.

$$H_c = H_L - \frac{M}{2}(\dot{\underset{\sim}{R}})^2$$

$$= \frac{\mu}{2}(\dot{\underset{\sim}{r}})^2 + \frac{m}{2}\sum_{i=1}^{A}(\dot{\underset{\sim}{x}}_i)^2 + \sum_{i>j(\geq 1)}^{-} V_{ij} + \sum_{j=1}^{A} V_{0j} \,, \qquad (2.1.2)$$

where

$$M = (A+1)\,m \,,$$

$\underset{\sim}{R}$; center of mass (c. of m.) of the whole system,

$\underset{\sim}{R}_1$; c. of m. of the target,

$\underset{\sim}{r}$; relative coordinate of the incident neutron

$$\underset{\sim}{r} \equiv \underset{\sim}{x}_0 - \underset{\sim}{R}_1 \qquad (2.1.3)$$

and $\underset{\sim}{x}_0$ is referred to the laboratory system,

μ ; reduced mass

$$\mu \equiv \frac{Am}{1+A} \,, \qquad (2.1.4)$$

$\underset{\sim}{x}_i$; coordinate of the i-th target nucleon referred to $\underset{\sim}{R}_1$

and so

$$\sum_{i=1}^{A} \underset{\sim}{x}_i = 0 \,. \qquad (2.1.5)$$

For $A>1$, the coordinates in Equation (2.1.2) are not linearly independent. If $\underset{\sim}{x}_i$'s are further transformed to $3(A-1)$-independent coordinates, however, the equation and the symmetrization operation are expected to become complicated.(70,31)

In the Shell Model, all the coordinates $\underset{\sim}{X}_i \ (i=0,1,\cdots,A)$ are referred to $\underset{\sim}{R}$. The total energy corresponding to the shell-model Hamiltonian becomes

$$H = \frac{m}{2}\sum_{i=0}^{A}(\dot{\underset{\sim}{x}}_i)^2 + \sum_{i>j} V_{ij} \tag{2.1.6}$$

and

$$\sum_{i=0}^{A} \underset{\sim}{x}_i = 0 \ . \tag{2.1.7}$$

All the coordinates are taken as independent variables, in spite of the constraint Equation (2.1.7). The error due to the redunduncy is proportional to $1/(1+A)$.(31) It causes the spurious states amoung the shell-model states which have been investigated for light nuclei and for low excitation states.* We assume that this effect on our problem is very small.

In the case of the R-matrix theory, the same problem must exist. However, in this theory, all the dynamics are represented by the reduced widths $\gamma_{\mu c}$ and the energy eigenvalue e_μ .

Under the above assumptions, the Hamiltonian is obtained from Equation (2.1.2),

$$H^{A+1} = K(\underset{\sim}{r}_0) + H^A(\underset{\sim}{r}_1, \cdots, \underset{\sim}{r}_A) + \\ + V(\underset{\sim}{r}_0; \underset{\sim}{r}_1, \cdots, \underset{\sim}{r}_A) \ , \tag{2.1.8}$$

---

*The author is indebted to Professor R. K. Osborn for clarification of this material.

where

$K(\underset{\sim}{r}_0) \equiv \frac{\hbar^2}{2\mu} \Delta_0$; relative kinetic energy,

$H^A(r_1, \cdots, r_A)$; Hamiltonian of the target with A nucleons,

$V(r_0; r_1, \cdots, r_A) = \sum_{i=1}^{A} V_{0i}$,

$\underset{\sim}{r}_0$; incident neutron coordinate referred to c. of m. of the target,

$\underset{\sim}{r}_i$; target nucleon coordinate referred to c. of m. of the target $(1 \leq i \leq A)$, for neutrons $(1 \leq i \leq N)$ and for protons $(N < i \leq A)$,

and r_i ; spin and space coordinate $(0 \leq i \leq A)$.

The shell model will be assumed to reproduce dynamics of neutron-nucleus reactions. The main idea of the shell model[72] is that the interaction is represented by a single particle potential as a first approximation and by the effective residual interaction. For the single particle potential of the open channel,[21] it is reasonable to choose the Wood-Saxon potential. The problem is then to determine the residual interaction potential. Since the shell model has been originally developed to explain the ground states and the low excited states of nuclei,[71,77,80] there may be question of its application to the highly excited states where one neutron can be free. However, the success of Lemmer and Shakin's calculation[71] of neutron - N^{15} elastic scattering cross section encourages the more extensive application of the shell-model Hamiltonian. Then the potential in Equation (2.1.8) may be written as

$$V(r_0; r_1 \cdots r_A) = U'(r_0) + \sum_{i=1}^{A} V(r_0, r_i) , \qquad (2.1.9)$$

where $U'(r_0)$; single particle potential,

and $V(r_0, r_i)$; residual two-body interaction potential.

Now, the equation of motion of the system is given by the following Schrödinger equation

$$H^{A+1}\Psi = E\Psi, \tag{2.1.10}$$

where

$$H^{A+1} = H^A + K + U'(r_0) + \sum_{i=1}^{A} V(r_0, r_i), \tag{2.1.11}$$

with the incident wave

$$\upsilon_{\underset{\sim}{k}} \equiv \frac{1}{(2\pi)^{3/2}} e^{i\underline{k}\cdot\underline{r}_0}\, u_{s\nu}\, \Psi_0^A(r_1, \cdots, r_A), \tag{2.1.12}$$

where

$\hbar\underline{k}$; momentum of the incident neutron,

$u_{s\nu}$; spin state of the incident neutron,

Ψ_0^A ; ground state vector of the target

$$H^A\Psi_0^A = E_0^A\Psi_0^A,$$

E ; total energy of the system which will be normalized to zero at zero incident energy

$$E = E_0^A + \frac{\hbar^2k^2}{2\mu} = \frac{\hbar^2k^2}{2\mu}. \tag{2.1.13}$$

2.2 Feshbach's Projection Operators

Since 1958, the unified theory of nuclear reactions[1] has been developed by Feshbach. This theory does not have the channel radii. Instead, the function space of $(A+1)$ - nucleons is projected into subspaces of closed and open channels, and the problem is reduced to an A-nucleon problem. This formalism has been most easily combined with

the dynamics of the nucleus, such as the shell model.[71,77,80] The incident neutron is treated as a distinguishable particle from the target nucleons.

The theory has been further developed in 1962[1] so that the space is totally antisymmetrized and the Kapur-Peierls formalism is also derived. Assuming projection operators on the totally antisymmetrized space, problems are handled by operator calculus. However, the projection operator themselves are difficult to obtain in practice. For a single open channel, these are exhibited by Feshbach.[1] The radial wave function projected on the open channel is given by the solution of a second order integrodifferential equation.

Lemmer and Shakin[71] tried to calculate the open channel radial wave function by a simpler method on the totally antisymmetrized space. However, their treatment of exchange effects seems to be incorrect since the "projection operators" they introduced are not idenpotent. For multi-channel cases including the inelastic channels, furthermore, the relation of the T-matrix to the cross sections becomes complicated.

Here, the problem of the type $A(n,n')A^*$ will be treated by the unified theory[1] developed in 1958. The incident neutron will be distinguished from the target nucleus, and the exchange reactions will be neglected.

Denoting the vector space of functions of 3A spatial and A spin coordinates by $\mathcal{E}^A$, the antisymmetrized subspace of the target states will be denoted by $\tilde{\mathcal{E}}^A$. So, we consider a vector on $\mathcal{E}' \otimes \tilde{\mathcal{E}}^A$ where the direct product is denoted by $\otimes$.[70]

In this section, the projection operators defined by Feshbach[68] will be given. In terms of these operators, the Schrödinger equation will be decomposed into a system of equations. Some meanings of these operators will be schematically described in relation to a simple shell model picture corresponding to Weisskopf's picture.[21] Then, the effective open channel Schrödinger equation will be obtained. Notations for the basis vectors will be summarized.

According to Feshbach,[1] the projection operators on $\mathcal{E}' \otimes \tilde{\mathcal{E}}^A$ may be defined by

$$P \equiv \sum_{j=0}^{N} |\Psi_j^A\rangle\langle\Psi_j^A| , \tag{2.2.1}$$

and

$$Q \equiv \sum_{j>0} |\Psi_j^A\rangle\langle\Psi_j^A| , \tag{2.2.2}$$

where

$$H^A \Psi_j^A = E_j^A \Psi_j^A , \tag{2.2.3}$$

j indicates the j-th excited states, and N is determined by

$$E_{N+1}^A > E > E_N^A \tag{2.2.4}$$

(see Equation (2.1.13)). The operators P and Q are projection operators on both $\tilde{\mathcal{E}}^A$ and $\mathcal{E}' \otimes \tilde{\mathcal{E}}^A$.

$$\left.\begin{aligned} P + Q &= 1 \\ PQ &= QP = 0 . \end{aligned}\right\} \tag{2.2.5}$$

By these operators, the Schrödinger equation of Equation (2.1.10) is written as a pair of simultaneous equations.

$$\left.\begin{aligned}(PHP-E)P\Psi &= -PHQ\,Q\Psi \\ \text{and}\qquad (QHQ-E)Q\Psi &= -QHP\,P\Psi,\end{aligned}\right\} \tag{2.2.6}$$

where the superscript of H^{A+1} is suppressed. The incident wave of Equation (2.1.12) belongs to the open channel subspace on which $\mathcal{E}\otimes\tilde{\mathcal{E}}^{A}$ is projected by P ,

$$Q\,\upsilon_{\underline{k}} = 0. \tag{2.2.7}$$

Since P commutes with K, H^{A} , and $U'(r_0)$, PHP (when operating in the open channel subspace, $P(\mathcal{E}'\otimes\tilde{\mathcal{E}}^{A})$) may be thought of as a Hamiltonian of the form

$$\begin{aligned}PHP &= K(\underline{r}_0) + H^{A} + U'(r_0) + \\ &\qquad + \sum_{i=1}^{A} P\,V(r_0, r_i)\,P \\ &= H_0 + U(r_0),\end{aligned} \tag{2.2.8}$$

where

$$H_0 \equiv K(\underline{r}_0) + H^{A}, \tag{2.2.9}$$

and

$$U(r_0) \equiv U'(r_0) + \sum_{i=1}^{A} P\,V(r_0, r_i)\,P. \tag{2.2.10}$$

Similarly, it follows that

$$QHQ = H_0 + U_Q(r_0), \tag{2.2.11}$$

where

$$U_Q(r_0) \equiv U'(r_0) + \sum_{i=1}^{A} Q\,V(r_0, r_i)\,Q\,. \tag{2.2.12}$$

In this case, QHQ operates in the closed channel subspace, $Q(\mathcal{E}' \otimes \tilde{\mathcal{E}}^A)$.

A rough discussion on the meanings of the projection operators will be given based on the perturbational viewpoint, and independent particle model. Expanding Ψ into a series of eigenfunctions of H^A

$$\Psi = \sum_{j=0}^{N} v_j \Psi_j^A + \sum_{l>N} u_l \Psi_l^A , \tag{2.2.13}$$

the equations for v_j and u_l of the incident neutron become:

$$\left[K + U' + V_{jj} - (E - E_j^A)\right] v_j = - \sum_{k(\neq j)}^{N} V_{jk} v_k - \sum_{l>N} V_{jl} u_l , \tag{2.2.14}$$

$$\left[K + U' + V_{ll} - (E - E_l^A)\right] u_l = - \sum_{m(\neq l)>N} V_{lm} u_m - \sum_{j=0}^{N} V_{lj} v_j , \tag{2.2.15}$$

where $0 \leq j, k \leq N < l, m$, and where

$$V_{jk} \equiv \left\langle \Psi_j^A \sum_{i=1}^{A} V_{0i} \Psi_k^A \right\rangle , \text{ etc.} \tag{2.2.16}$$

The r.h.s. of Equations (2.2.14) and (2.2.15) are the transition terms among different neutron states of a single particle Hamiltonian of the form $K + U' + V_{jj} + E_j^A$. Neglecting these transition terms entirely, Equation (2.2.14) gives the scattering of the neutron by a rigid target, and Equation (2.2.15) determines the bound states of the neutron in this single particle potential. If we consider only the first terms on the r.h.s. of Equations (2.2.14) and (2.2.15), the first equation gives the

direct reactions and Equation (2.2.15) gives the bound states whose energy levels may be split into more levels. The last terms gives the transitions among the free states and the bound states.

Consider the initial state such that the incident neutron is only in U_0 . Then, the reaction picture given by Equations (2.2.14) and (2.2.15) may be drawn in Figures I.1.a and I.1.b corresponding to those of Weisskopf.[21] The figures correspond to the first order perturbation. Figure I.1.a illustrates the direct reaction in which the incident neutron goes from U_0 to U_i while the target is transferred from Ψ_0^A to Ψ_j^A .

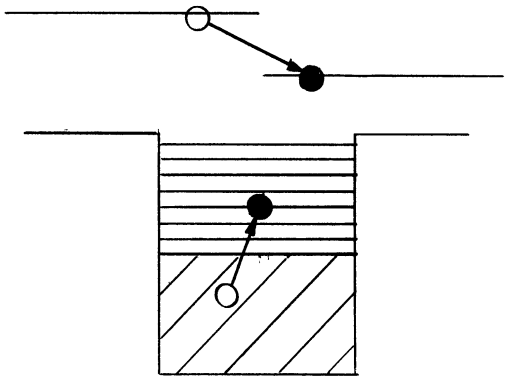

Figure I.1.a. Direct Reaction.

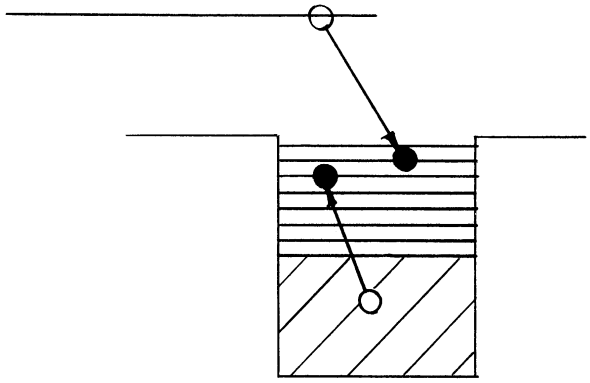

Figure I.1.b. Compound Reaction.

This transition is made by the first term of the r.h.s. of Equation (2.2.14). By the last term, the incident neutron is transferred to one of the bound states given by the l.h.s. of Equation (2.2.13).

This is of course only a rough semiclassical picture of the reactions. For example, setting the l.h.s. of Equation (2.2.15) = 0 does not always give the bound states due to failure to satisfy the boundary conditions.

Some terms of $u_\ell \Psi_\ell^A$ in which a target nucleon is unbound can be excited as intermediate states. Among such states, a target neutron can be free energetically and the incident neutron is bound

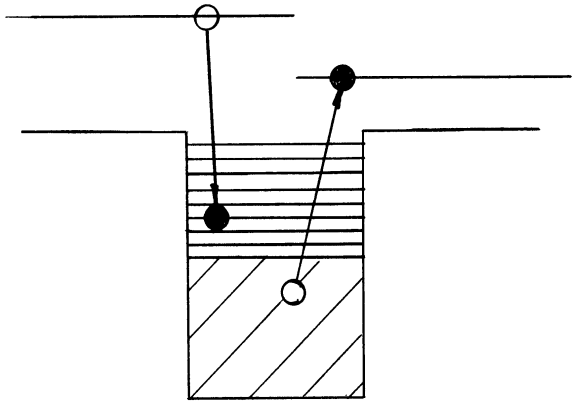

Figure I.1.c. Exchange Reaction.

(Figure I.1.c). This is actually the exchange reaction. We are assuming that the exchange reactions do not occur. Namely, the interaction potential which causes the exchange reactions is considered to be null.

The effective open channel Schrödinger equation is obtained formally from Equations (2.2.6)

$$(PHP-E)P\Psi = -PHQ\,\frac{1}{E-QHQ}\,QHP\,P\Psi. \qquad (2.2.17)$$

We will abbreviate the potential operator on the r.h.s. by W,

$$W \equiv PHQ\,\frac{1}{E-QHQ}\,QHP. \qquad (2.2.18)$$

The following notations will be used for the target nucleus states: the subscript j of the wave function Ψ_j^A signifies the j-th excited state. $\alpha(j)$ indicates the quantum numbers of this state. When there occurs no confusion, j will be often suppressed and only α will be used and vice versa. When we use some of the quantum numbers of the

target state, we write quantum numbers with subscript α . For example, nuclear spin and its z -component of Ψ_j^A or $\Psi^A_{\alpha(j)}$ are denoted by S_α and ν_α .

The eigenstates of H_0 and PHP describe the free state and the distorted wave including the direct reactions. These will be denoted as follows:

(I) Eigenfunctions of H_0 ; $\mathcal{U}_{[\alpha(j)\, \underline{k}_j s \nu_j]}(\underline{r}_0)$

or $\mathcal{U}_{[j\, \underline{k}_j s \nu]}(\underline{r}_0)$

$$(H_0 - E)\, \mathcal{U}_{[j\, \underline{k}_j s \nu]}(\underline{r}_0) = 0 , \tag{2.2.19}$$

and

$$E = E_j^A + \frac{\hbar^2}{2\mu} k_j^2 . \tag{2.2.20}$$

For example,

$$\mathcal{U}_{[j\, \underline{k}_j s \nu]}(\underline{r}_0) = \frac{1}{(2\pi)^{3/2}} e^{i \underline{k}_j \cdot \underline{r}_0} u_{s\nu}\, \Psi^A_{\alpha(j)}(r_1 \cdots r_A) . \tag{2.2.21}$$

(II) Eigenfunctions of PHP (Distorted wave);

$$\chi^{(+)}_{[\alpha(j)\, \underline{k}_j s \nu_j]}(\underline{r}_0) \quad \text{or} \quad \chi^{(+)}_{[j\, \underline{k}_j s \nu]}(\underline{r}_0)$$

$$(PHP - E)\, \chi^{(+)}_{[\alpha(j)\, \underline{k}_j s \nu_j]} = 0 , \tag{2.2.22}$$

where the incident wave is given by Equation (2.1.11)

$$\mathcal{U}_{[\alpha(j)\, \underline{k}_j s \nu_j]} = \frac{1}{(2\pi)^{3/2}} e^{i \underline{k}_j \cdot \underline{r}_0} u_{s\nu_j}\, \Psi^A_{\alpha(j)} . \tag{2.2.23}$$

The plus sign of χ indicates the outgoing wave boundary condition. Taking this boundary condition into account, Equation (2.2.22) may then be written as an integral equation:[70,73]

$$\chi^{(+)}_{[\alpha(j)\,\underline{k}_j\,s\,\nu_j]} = v_{[\alpha(j)\,\underline{k}_j\,s\,\nu_j]} + \frac{1}{E^{(+)} - H_0}\, U\, \chi^{(+)}_{[\alpha(j)\,\underline{k}_j\,s\,\nu_j]}. \qquad (2.2.24)$$

In the above notations, the space coordinate $\underline{r}_0$ is sometimes suppressed. The subscripts $[\alpha(0)\,\underline{k}\,s\,\nu]$ and $[\alpha(j)\,\underline{k}_j\,s\,\nu_j]$ will be abbreviated by [i] (initial) and [f] (final) respectively.

The T-matrix and the scattering amplitudes are defined by Equations (A.1) and (A.2) of Appendix A respectively. The T-matrix elements based on the free wave v will be related to the scattering amplitudes by Equation (A.6) and then to the cross sections by Equation (A.12).

The effects of the potential W may be emphasized by incorporating the potential U into the unperturbed Hamiltonian H_0. The T-matrix elements based on the distorted wave[70] χ will be called the distorted wave T-matrix, while χ of Equation (2.2.24) includes effects of the direct inelastic scattering. The two matrix elements are related by Equation (A.8).

In the subscript $[\alpha\,\underline{k}\,s\,\nu]$ the numbers s, ν refer to the neutron spin state. When we wish to refer to overall channel spin states, the brackets are dropped and we write $\alpha\,\underline{k}\,s\,\nu$. The transformations of wave functions are given by Equations (B.2), (B.4), and (B.5).

The scattering amplitudes and the cross sections are given by Equations (B.11) and (B.12) respectively.

Transformations between wave functions defined by sets of indices $\alpha \underline{k} s \nu$ and $\alpha \mathcal{E} l s J M$ are given in Appendix B. Some of them which will be used in the later chapters will be listed below. l, s, and J are orbital, channel spin, and total angular moments respectively. M is the z-component of the total angular momentum. $\mathcal{E}$ is the total energy which is related to the neutron wave vector by Equation (2.2.20).

$[\alpha \underline{k} s \nu]$, $\alpha \underline{k} s \nu$ and $\alpha \mathcal{E} l s J M$ are sets of good quantum numbers for the free waves. They are <u>not</u> good quantum numbers for the distorted waves. However, the distorted wave and the total wave are well defined by any set of indices through Equations (2.2.24) and (2.2.17) respectively.

The free waves in $\alpha \underline{k} s \nu$ and in $\alpha \mathcal{E} l s J M$ are given by Equations (2.2.23) and (B.2) and by Equations (B.23) and (B.24) respectively. The relations are given by

$$U_{\alpha \underline{k} s \nu} = \frac{1}{\sqrt{\rho_{\mathcal{E}}}} \sum_{l m J M} \langle l s m \nu | J M \rangle \, Y_{lm}^{*}(\hat{\underline{k}}) \, U_{\alpha \mathcal{E} l s J M} \qquad (2.2.25)$$

with the inverse relations

$$U_{\alpha \mathcal{E} l s J M} = \sqrt{\rho_{\mathcal{E}}} \sum_{m \nu} \langle l s m \nu | J M \rangle \int d\hat{\underline{k}} \, Y_{lm}(\underline{k}) \, U_{\alpha \underline{k} s \nu}, \qquad (2.2.26)$$

where $\hat{\underline{k}}$ is the unit vector along $\underline{k}$.

The T-matrix elements are denoted as

$$T^{J}_{\alpha' l' s'; \alpha l s}(\mathcal{E}', \mathcal{E}) \equiv \left\langle U_{\alpha' \mathcal{E}' l' s' J M} \, T \, U_{\alpha \mathcal{E} l s J M} \right\rangle. \qquad (2.2.27)$$

On the energy shell $(\varepsilon'=\varepsilon)$, it will be written as

$$T^{J}_{\alpha'\ell's';\,\alpha\ell s} \equiv T^{J}_{\alpha'\ell's';\,\alpha\ell s}(\varepsilon,\varepsilon) \tag{2.2.28}$$

Transformations of the T-matrix elements based on $\alpha \underset{\sim}{k} s\nu$ and $\alpha\varepsilon\ell sJM$ are given by Equation (B.26). Cross sections are expressed in terms of the T-matrix elements of Equation (2.2.28) in § B.3 of the Appendix B. Among them, the total cross section is given by

$$\sigma_\alpha^{T} = 2\pi\lambda^2 \sum_J g_\alpha^J \sum_{\ell s} \mathcal{R}e\left(i\, T^{J}_{\alpha\ell s;\,\alpha\ell s}\right), \tag{2.2.29}$$

where α refers to the initial state of the target.

The distorted waves with indices $\alpha\varepsilon\ell sJM$ are related to those with $\alpha \underset{\sim}{k} s\nu$ by similar relations to Equations (2.2.25) and (2.2.26). Equation (B.39) corresponds to Equation (2.2.26);

$$\chi^{(+)}_{\alpha\varepsilon\ell sJM} = \sqrt{\rho_\varepsilon} \sum_{m\nu} \langle \ell s m\nu / JM\rangle \times$$

$$\times \int d\hat{\underset{\sim}{k}}\, Y_{\ell m}(\hat{\underset{\sim}{k}})\, \chi^{(+)}_{\alpha \underset{\sim}{k} s\nu}. \tag{2.2.30}$$

The orthonormality of the distorted waves is given by Equation (B.41) and the completeness, Equation (B.42), is given by

$$\sum_{\ell sJM} \int d\varepsilon\; \chi^{(+)}_{\alpha\varepsilon\ell sJM}(\underset{\sim}{r}) \langle \chi^{(+)}_{\alpha\varepsilon\ell sJM}(\underset{\sim}{r}')$$

$$= \Psi^A_\alpha \rangle\langle \Psi^A_\alpha\; \delta(\underset{\sim}{r}-\underset{\sim}{r}'). \tag{2.2.31}$$

The distorted wave, Equation (2.2.30), and the free wave, Equation (2.2.26), are related by

$$\chi^{(+)}_{\alpha\varepsilon\ell sJM} = \sum_{\alpha'\ell's'm'\nu'} \chi^{(+)}_{\alpha'\ell's';\alpha\ell sJ\varepsilon} \times$$

$$\times Y_{\ell'm'}(\hat{r})\, u_{s'\nu'} \langle \ell's'm'\nu' | JM \rangle, \tag{2.2.32}$$

where

$$\chi^{(+)}_{\alpha'\ell's';\alpha\ell sJ\varepsilon} \equiv v_{\alpha\varepsilon\ell}\, \delta(\alpha\ell s;\alpha'\ell's') +$$

$$+ 2\pi\mu^2 \sqrt{\frac{2\ell+1}{4\pi}} \int d\varepsilon' \frac{1}{E^{(+)}_{\alpha} - \varepsilon'} v_{\alpha'\varepsilon'\ell'} \times$$

$$\times T^{J}_{\alpha'\ell's';\alpha\ell s}(\varepsilon', \varepsilon), \tag{2.2.33}$$

and $v_{\alpha\varepsilon\ell}$ is related to the free wave by Equation (B.23).

Often, the channel indices $\alpha\ell sJM$ will be abbreviated by C. For example, completeness will be denoted by

$$\sum_{c} \int d\varepsilon\, \chi^{(+)}_{c\varepsilon}(r) \rangle\langle \chi^{(+)}_{c\varepsilon}(r') = P\,\delta(r - r'), \tag{2.2.34}$$

where the sum over α is taken up to that of the N-th excited states (see Equation (2.2.4)).

The channel indices of the initial and final states are denoted by i and f respectively. Applying the same transformation as Equations (2.2.26) and (2.2.30) to the total wave function, the Schrodinger equations are given by

$$\chi^{(+)}_{i} = v_i + \frac{1}{E^{(+)} - H_0} U \chi^{(+)}_{i}, \tag{2.2.35}$$

$$\chi_f^{(-)} = v_f + \frac{1}{E^{(-)} - H_0} U \chi_f^{(-)} , \qquad (2.2.36)$$

and

$$P\Psi_i^{(+)} = \chi_i^{(+)} + \frac{1}{E^{(+)} - PHP} WP\Psi_i^{(+)} , \qquad (2.2.37)$$

where Equations (B.2), (B.4), (B.5), (2.2.26), and (2.2.30) are applied to Equations (2.2.24), (A.7), and(2.2.17). The T-matrix elements are related to the potentials U and W

$$T_{fi} = 2\pi \left\{ \langle v_f U \chi_i^{(+)} \rangle + \langle \chi_f^{(-)} W P \Psi_i^{(+)} \rangle \right\} \qquad (2.2.38)$$

as is shown in Appendix B.

2.3 Resonance Parameters

In the unified theory, the resonance parameters have been defined so that, in the isolated resonance region, the T-matrix of the unified theory becomes equal to that of the R-matrix theory.(1) The resonance widths in the many resonance region are chosen by extending the formula obtained above.(1) Applying the energy averaged T-matrix the optical model Schrödinger equation is derived.(1) These are briefly reviewed in this section. Considering the case of no spin and S-wave, the absorption cross section and the strength function will be derived. The transmission coefficient will be derived from the absorption cross section.

Under the isolated resonance approximation where only one of the eigenvalues of QHQ

$$(QHQ - E_\mu)\psi_\mu = 0 \qquad (2.3.1)$$

becomes significant in the T-matrix of Equation (2.2.38) and Equation (2.2.18), the T-matrix becomes

$$T_{fi} \cong 2\pi \left\{ \langle U_f U \chi_i^{(+)} \rangle + \right.$$

$$\left. + \frac{\langle \chi_f^{(-)} PHQ\psi_\mu \rangle \langle \psi_\mu QHP \chi_i^{(+)} \rangle}{E - E_\mu + \left\langle \psi_\mu QHP \frac{1}{E^{(+)} - PHP} PHQ\psi_\mu \right\rangle} \right\}. \qquad (2.3.2)$$

The denominator may then be written in the form $E - E_\mu + (\Delta_\mu - i\Gamma_\mu/2)$, where the level shift and the resonance width[4] are defined by[1]

$$\Delta_\mu \equiv \sum_c P \int_0^\infty \frac{|\langle \psi_\mu QHP \chi_{c\varepsilon}^{(+)} \rangle|^2}{E - \varepsilon} d\varepsilon , \qquad (2.3.3)$$

$$\Gamma_\mu \equiv \sum_c \Gamma_{\mu c} , \qquad (2.3.4)$$

and

$$\Gamma_{\mu c} \equiv 2\pi \left| \langle \psi_\mu QHP \chi_{c\varepsilon}^{(+)} \rangle \right|^2 . \qquad (2.3.5)$$

We have made use of the completeness relations, Equation (2.2.34).

In the many resonance region, the energy averaged T-matrix element is given by

$$\overline{T_{fi}} = 2\pi \left\{ \langle U_f U \chi_i^{(+)} \rangle - \pi i \langle \chi_f^{(-)} PHQ \Lambda QHP \chi_i^{(+)} \rangle \right\}. \qquad (2.3.6)$$

The derivation of this formula will be given in § 2.5, and the operator Λ is defined according to

$$\Lambda \equiv \frac{1}{\langle D \rangle} \frac{1}{N} \sum_\mu \psi_\mu \rangle \langle \psi_\mu , \qquad (2.3.7)$$

$\langle D \rangle$ is the average resonance spacing, and N is the number of the resonances within the energy range for averaging.

The optical model (O.M.) Schrödinger equation is derived by Feshbach[1] in such a way that the resulting T-matrix becomes equal to the energy averaged T-matrix of Equation (2.3.6). The O.M. Schrödinger equation becomes

$$\left(E - PHP - H_{CN}\right)\varphi = 0 \tag{2.3.8}$$

where

$$H_{CN} \equiv -i\pi PHQ \frac{1}{1 - i\pi \Lambda QHP \frac{1}{E^{(+)} - PHP} PHQ} \Lambda QHP. \tag{2.3.9}$$

The derivation may be seen in § 3.1.

For the no spin case, the S-wave absorption cross section has been related to the imaginary part of the O.M. potential by Porter.[59] The S-wave absorption cross section is obtained from Equation (2.3.8)

$$\sigma_{ab}^{OM} \cong 2\pi^2 \lambda^2 \frac{\langle \Gamma \rangle}{\langle D \rangle} \left(1 - \frac{\pi}{2} \frac{\langle \Gamma \rangle}{\langle D \rangle}\right), \tag{2.3.10}$$

where second order perturbation theory with respect to H_{CN} is applied and where, by the use of the definition of Equation (2.3.5), the average resonance widths are given by[1]

$$\frac{\langle \Gamma \rangle}{\langle D \rangle} = 2\pi \left\langle \chi_{l=0}^{(+)} PHQ \Lambda QHP \chi_{l=0}^{(+)} \right\rangle \tag{2.3.11}$$

The strength function is defined by[116]

$$S_l \equiv \sqrt{\frac{E^0}{E}} \frac{\langle \Gamma_l \rangle}{\langle D \rangle}, \tag{2.3.12}$$

where E^0 is the fixed energy to which widths at E are normalized. The S-wave strength function becomes

$$S_0 = 2\pi \sqrt{\frac{E^0}{E}} \left\langle \chi_{l=0}^{(+)} PHQ \Lambda QHP \chi_{l=0}^{(+)} \right\rangle. \tag{2.3.13}$$

The S-wave transmission coefficient is defined by[3,4,37]

$$\sigma_{ab}^{OM} = \pi \lambda^2 \mathcal{T}_{\ell=0} \tag{2.3.14}$$

$$\therefore \mathcal{T}_{\ell=0} = 2\pi \frac{\langle \Gamma \rangle}{\langle D \rangle} \left(1 - \frac{\pi}{2} \frac{\langle \Gamma \rangle}{\langle D \rangle}\right). \tag{2.3.15}$$

2.4 Absorption Cross Section

Porter's relation between the S-wave absorption cross section and the imaginary part of the O.M. potential will be generalized to include more than one open channel. The generalization will then be applied to the O.M. Schrödinger Equation (2.3.8) to determine the absorption cross section. Strength functions and transmission coefficients will be obtained in the context of the unified theory.

The O.M. Schrödinger equation is written as

$$(PHP - iV - E)\, \psi_{\alpha \underline{k} s \nu} = 0 \tag{2.4.1}$$

where V is Hermitian. In the case of Equation (2.3.8), $H_{CN} = \delta U - iV$ and δU may be neglected relative to PHP. The incident wave is

$$\upsilon_{\alpha \underline{k} s \nu} = \frac{1}{(2\pi)^{3/2}} e^{i \underline{k} \cdot \underline{r}} u_{\alpha s \nu}. \tag{2.4.2}$$

The absorption cross section by partial wave analysis is defined by[3]

$$\sigma_{\alpha}^{ab} \equiv \pi \lambda^2 \sum_{J} g_{\alpha}^{J} \sum_{\ell s} \frac{I_{net}^{c}}{I_{in}^{c}} \tag{2.4.3}$$

where $c = \alpha \ell s J M$, α is referred to the initial state of the target nucleus, I_{in}^{c} is the incoming current in a channel c, and I_{net}^{c} is the net current of a channel c.

The asymptotic solution of Equation (2.4.1) is given by

$$\psi_{\alpha \underline{k} s \nu} \sim \upsilon_{\alpha \underline{k} s \nu} - \sum_{\alpha' s' \nu'} \langle \upsilon_{\alpha' \underline{k}' s' \nu'} T \upsilon_{\alpha \underline{k} s \nu} \rangle \times \frac{\mu}{2\pi\hbar^2} \frac{e^{ik'r}}{r} u_{\alpha' s' \nu'}. \tag{2.4.4}$$

The T-matrix elements in Equation (2.4.4) is related to those of the partial wave analysis by

$$\langle \mathcal{U}_{\alpha' \underline{k}' s' \nu'} T \mathcal{U}_{\alpha \underline{k} s \nu} \rangle = \sum_{l m l' m' J M} T^{J}_{\alpha' l' s'; \alpha l s} \sqrt{\frac{2\pi}{\rho_\varepsilon \rho_{\varepsilon'}}} \times$$

$$\times \langle l s m \nu | J M \rangle \langle l' s' m' \nu' | J M \rangle Y_{l'm'}(\hat{\underline{k}}') Y^{*}_{lm}(\hat{\underline{k}}) \tag{2.4.5}$$

This relation becomes

$$\sqrt{\rho_\varepsilon} \sum_{m'' \nu} \int d\hat{\underline{k}} \langle l'' s m'' \nu | J'' M'' \rangle Y_{l'' m''}(\hat{\underline{k}}) \langle \mathcal{U}_{\alpha' \underline{k}' s' \nu'} T \mathcal{U}_{\alpha \underline{k} s \nu} \rangle$$

$$= \sum_{l' m'} T^{J'}_{\alpha' l' s'; \alpha l s} \sqrt{\frac{2\pi}{\rho_{\varepsilon'}}} \langle l' s' m' \nu' | J'' M'' \rangle Y_{l'm'}(\hat{\underline{r}}) \tag{2.4.6}$$

where $\hat{\underline{k}}'$ is replaced by $\hat{\underline{r}}$ because $\underline{r} /\!/ \underline{k}'$. By operating with

$$\int d\hat{\underline{k}} \sqrt{\rho_\varepsilon} \langle l s m \nu | J M \rangle Y_{lm}(\hat{\underline{k}})$$

upon Equation (2.4.4), therefore, the asymptotic form of the partial waves is obtained,

$$\varphi_{\varepsilon c}(\underline{r}) \sim \mathcal{U}_{\alpha c}(\underline{r}) - \frac{\mu}{2\pi\hbar^2} \sum_{\alpha' l' s' m' \nu'} \sqrt{\frac{2\pi}{\rho_{\varepsilon'}}} \frac{e^{ik'r}}{r} \times$$

$$\times \langle l' s' m' \nu' | J M \rangle T^{J}_{\alpha' l' s'; \alpha l s} Y_{l'm'}(\hat{\underline{r}}) u_{\alpha' s' \nu'} \tag{2.4.7}$$

$$= \frac{\mu}{2i\hbar^2} \sqrt{\frac{2}{\pi}} \left\{ \sum_{m \nu} \frac{(-)^{l+1}}{\sqrt{\rho_\varepsilon}\, r} e^{-ikr} \langle l s m \nu | J M \rangle Y_{lm}(\hat{\underline{r}}) u_{\alpha s \nu} + \right.$$

$$\left. + \sum_{\alpha' l' s' m' \nu'} \frac{1}{\sqrt{\rho_{\varepsilon'}}\, r} e^{ik'r} \langle l' s' m' \nu' | J M \rangle S^{J}_{\alpha' l' s'; \alpha l s} Y_{l'm'}(\hat{\underline{r}}) u_{\alpha' s' \nu'} \right\} \tag{2.4.8}$$

where we have used Equation (B.35). Therefore, we have

$$I^{c}_{im} = \frac{1}{2\pi\hbar} \tag{2.4.9}$$

and

$$I^{c}_{net} = \frac{1}{2\pi\hbar}\left\{1 - \sum_{\alpha'\ell's'} \left| S^{J}_{\alpha'\ell's';\alpha\ell s} \right|^2 \right\}. \qquad (2.4.10)$$

The absorption cross section is obtained

$$\sigma^{ab}_{\alpha} = \pi\lambda^2 \sum_{J} g^{J}_{\alpha} \sum_{\ell s} \left\{1 - \sum_{\alpha'\ell's'} \left| S^{J}_{\alpha'\ell's';\alpha\ell s} \right|^2 \right\}. \qquad (2.4.11)$$

On the other hand, the net current is related to the non-Hermitian part of Equation (2.4.1). By operating with

$$\sum_{m\nu} \int d\hat{\underset{\sim}{k}} \sqrt{\rho_\varepsilon}\; \varphi^{*}_{\varepsilon c}(\underset{\sim}{r}) \langle \ell s m\nu | J M \rangle Y_{\ell m}(\hat{\underset{\sim}{k}})$$

upon Equation (2.4.1) and with its complex conjugate upon the Hermitian conjugate of Equation (2.4.1), subtracting one from the other, and then integrating over $\underset{\sim}{r}$ in a large sphere, we have

$$\begin{aligned} & 2i \langle \varphi_{\varepsilon c} V \varphi_{\varepsilon c} \rangle \\ &= \frac{\hbar^2}{2\mu} \int \left\{ \varphi^{*}_{\varepsilon c} \Delta \varphi_{\varepsilon c} - \varphi_{\varepsilon c} \Delta \varphi^{*}_{\varepsilon c} \right\} d\underset{\sim}{r} \\ &= \frac{\hbar^2}{2\mu} \int \left\{ \varphi^{*}_{\varepsilon c} \frac{\partial}{\partial r} \varphi_{\varepsilon c} - \varphi_{\varepsilon c} \frac{\partial}{\partial r} \varphi^{*}_{\varepsilon c} \right\} r^2 d\hat{\underset{\sim}{r}} \\ &= i\hbar\, I^{c}_{net}. \end{aligned} \qquad (2.4.12)$$

Therefore, we have relations between the imaginary part of the O.M. potential and the absorption cross section

$$\sigma^{ab}_{\alpha} = 4\pi^2\lambda^2 \sum_{J} g^{J}_{\alpha} \sum_{\ell s} \langle \varphi_{\varepsilon c} V \varphi_{\varepsilon c} \rangle \qquad (2.4.13)$$

This is the generalization of Porter's result.

Under the distorted wave Born approximation (DWBA), the solution of Equation (2.4.1) in the partial wave analysis is given by

$$\varphi_{\varepsilon c}^{(+)} = \chi_{\varepsilon c}^{(+)} + \frac{1}{E^{(+)} - PHP}(-iV)\,\chi_{\varepsilon c}^{(+)} . \qquad (2.4.14)$$

The matrix elements in Equation (2.4.13) will be obtained in this approximation.

$$\begin{aligned}
&\langle \varphi_{\varepsilon c}^{(+)} V \varphi_{\varepsilon c}^{(+)} \rangle \\
&= \Big\langle \Big(1 + \frac{1}{E^{(+)} - PHP}(-iV)\Big)\chi_{\varepsilon c}^{(+)} \Big| V \Big| \Big(1 + \frac{1}{E^{(+)} - PHP}(-iV)\Big)\chi_{\varepsilon c}^{(+)} \Big\rangle \\
&= \Big\langle \chi_{\varepsilon c}^{(+)} \Big(1 + iV\frac{1}{E^{(-)} - PHP}\Big) V \Big(1 - \frac{1}{E^{(+)} - PHP} iV\Big)\chi_{\varepsilon c}^{(+)} \Big\rangle \\
&\cong \Big\langle \chi_{\varepsilon c}^{(+)} \Big(V - iV\Big\{\frac{1}{E^{(+)} - PHP} - \frac{1}{E^{(-)} - PHP}\Big\} V \Big)\chi_{\varepsilon c}^{(+)} \Big\rangle \\
&= \langle \chi_{\varepsilon c}^{(+)} V \chi_{\varepsilon c}^{(+)} \rangle - 2\pi \langle \chi_{\varepsilon c}^{(+)} V \delta(E - PHP) V \chi_{\varepsilon c}^{(+)} \rangle \\
&= \langle \chi_{\varepsilon c}^{(+)} V \chi_{\varepsilon c}^{(+)} \rangle - 2\pi \sum_{\alpha' l' s'} \left| \langle \chi_{\varepsilon c}^{(+)} V \chi_{\varepsilon c'}^{(+)} \rangle \right|^2 ,
\end{aligned} \qquad (2.4.15)$$

where $c' \equiv \alpha' l' S' J M$.

Now we will apply the results to the case of the O.M. Equation (2.3.8). Expanding H_{CN} to second order in $PHQ\Lambda QHP$, the potential V becomes

$$\begin{aligned}
V &= \pi\, PHQ\Lambda QHP + \pi^3\, PHQ\Lambda QHP\, \delta(E - PHP)\, PHQ\Lambda QHP \\
&= \pi\, PHQ\Lambda QHP + \\
&\quad + \pi^3 \sum_{c''} PHQ\Lambda QHP\, \chi_{\varepsilon c''}^{(+)} \rangle\langle \chi_{\varepsilon c''}^{(+)}\, PHQ\Lambda QHP ,
\end{aligned} \qquad (2.4.16)$$

where $c'' \equiv \alpha'' l'' s'' J'' M''$.

Thus, the first term of Equation (2.4.15) becomes

$$\langle \chi_{\varepsilon c}^{(+)} V \chi_{\varepsilon c}^{(+)} \rangle = \frac{\pi}{\langle D \rangle} \frac{1}{N} \sum_{\mu} |\langle \psi_\mu | QHP | \chi_{\varepsilon c}^{(+)} \rangle|^2 +$$

$$+ \frac{\pi^3}{\langle D \rangle^2} \frac{1}{N^2} \sum_{\alpha' \ell' s'} \left| \sum_{\mu} \langle \chi_{\varepsilon c}^{(+)} | PHQ | \psi_\mu \rangle \langle \psi_\mu | QHP | \chi_{\varepsilon c'}^{(+)} \rangle \right|^2 \qquad (2.4.17)$$

and the second term becomes

$$\sum_{\alpha' \ell' s'} |\langle \chi_{\varepsilon c}^{(+)} V \chi_{\varepsilon c'}^{(+)} \rangle|^2$$

$$\cong \frac{\pi^2}{\langle D \rangle^2} \frac{1}{N^2} \sum_{\alpha' \ell' s'} \left| \sum_{\mu} \langle \chi_{\varepsilon c}^{(+)} | PHQ | \psi_\mu \rangle \langle \psi_\mu | QHP | \chi_{\varepsilon c'}^{(+)} \rangle \right|^2 . \qquad (2.4.18)$$

The random phase approximation will be applied to Equation (2.4.18) and the second term of Equation (2.4.17). Namely, $\sum_{\mu} \langle \chi_{\varepsilon c} | PHQ | \psi_\mu \rangle \langle \psi_\mu | QHP | \chi_{\varepsilon c'} \rangle = 0$ for $c \neq c'$. Equation (2.4.15) then becomes

$$\langle \varphi_{\varepsilon c}^{(+)} V \varphi_{\varepsilon c}^{(+)} \rangle = \frac{\pi}{\langle D \rangle} \frac{1}{N} \sum_{\mu} |\langle \psi_\mu | QHP | \chi_{\varepsilon c}^{(+)} \rangle|^2 -$$

$$- \frac{\pi^3}{\langle D \rangle^2} \left\{ \frac{1}{N} \sum_{\mu} |\langle \psi_\mu | QHP | \chi_{\varepsilon c}^{(+)} \rangle|^2 \right\}^2$$

$$= \pi \frac{\langle \Gamma_c \rangle}{\langle D \rangle} - \pi^3 \left(\frac{\langle \Gamma_c \rangle}{\langle D \rangle} \right)^2 . \qquad (2.4.19)$$

The absorption cross section becomes

$$\sigma_\alpha^{ab} = \pi \lambda^2 \sum_J g_\alpha^J \sum_{\ell s} T_{\alpha \ell s}^J , \qquad (2.4.20)$$

where

$$T_{\alpha \ell s}^J \equiv S_{\alpha \ell s}^J \left(1 - \frac{1}{4} S_{\alpha \ell s}^J \right) \qquad (2.4.21)$$

which is the transmission coefficient,[37] and

$$S_{\alpha \ell s}^J \equiv 2\pi \frac{\langle \Gamma_c \rangle}{\langle D \rangle}$$

$$= \langle \chi_{\varepsilon c}^{(+)} | PHQ \Lambda QHP | \chi_{\varepsilon c}^{(+)} \rangle . \qquad (2.4.22)$$

The transmission coefficient is related to V by Equation (2.4.13)

$$T_c = \langle \varphi_{2c} V \varphi_{2c} \rangle \qquad (2.4.23)$$

2.5 Energy Average of the T-Matrix

The energy average of the T-matrix is concerned with the following problems: derivation of formulas for E-averaged cross sections; derivation of the Optical Model Schrödinger equation; calculation of the upper bound of the strength function.

The distorted wave T-matrix is separated into two terms, Equation (2.2.38). The first term depends only on the single particle potential. Typically, for a given set of quantum numbers its poles lie along a line in the lower half complex E-plane approximately parallel to the real E-axis. The spacings between poles is of the order of 10 Mev. Hence, this term may be approximated by a constant in the energy interval over which the averaging is performed. On the other hand, the second term is expected to vary much within the range of spacings of fine resonances ($\lesssim 10$ kev).

Precisely speaking, the calculation of the E-average of the resonant part of the T-matrix is known only if the poles and residues of the T-matrix distribute evenly from $-\infty$ to $+\infty$ along the real E-axis. In more realistic cases, the number of poles is finite. The calculation of the E-average of such a T-matrix becomes difficult due to edge effects.[34] However, Feshbach's calculation[1] will be briefly reviewed. The result will be applied in Chapters 3 and 4 of Part I.

The energy average is taken over a range Δ centered at E_0 within which the single particle effects such as $\langle v_f U \chi_i^{(+)} \rangle$ are

approximated by a constant; e.g. their values at E_0 . Terms of the resonant part of the T-matrix whose poles lie outside the range Δ are effectively absorbed into the potential part of the T-matrix, T^P, as follows.

The effective open channel Schrödinger equation of (2.2.17) is written as

$$\left\{ PHP + \int_j \frac{PHQ\psi_j\rangle\langle\psi_j QHP}{E - E_j} - E \right\} P\Psi$$

$$= -\sum_{k=1}^{N} \frac{PHQ\psi_k\rangle\langle\psi_k QHP}{E - E_k} P\Psi, \qquad (2.5.1)$$

where the ψ_ℓ's are eigenfunctions of QHQ ,

$$QHQ\psi_\ell = E_\ell \psi_\ell, \qquad (2.5.2)$$

E_k ; E_ℓ such that $E_0 - \frac{\Delta}{2} \leq E_\ell \leq E_0 + \frac{\Delta}{2}$,

E_j ; the remaining spectrum of QHQ,

$\int$; notation for the sum over the discrete spectrum and the integral over the continuum spectrum.

Supposing that the second term of the l.h.s. of Equation (2.5.1) does not vary much with E, this term is effectively represented by a single particle potential operator U'' .

$$U'' = U + \int_j \frac{PHQ\psi_j\rangle\langle\psi_j QHP}{E - E_j} . \qquad (2.5.3)$$

The notation PHP for $H_0 + U$ in Equation (2.5.1) will be used for $H_0 + U''$ in the following. The distorted wave which is an eigenfunction of $H_0 + U''$ will be again denoted by the same notation χ as before. Then, the

T-matrix elements of Equation (2.2.38) becomes

$$T_{fi} = 2\pi \langle \chi_f U'' \chi_i^{(+)} \rangle + $$

$$+2\pi \sum_{k=1}^{N} \frac{\langle \chi_f^{(-)} PHQ\psi_k \rangle \langle \psi_k QHP \chi_i^{(+)} \rangle}{E - E_k} . \qquad (2.5.4)$$

The integral form of Equation (2.5.1) is

$$P\Psi_i^{(+)} = \chi_i^{(+)} + \frac{1}{E^{(+)} - PHP} \sum_{k=1}^{N} \frac{PHQ\psi_k \rangle \langle \psi_k QHP P\Psi_i^{(+)} \rangle}{E - E_k}, \qquad (2.5.5)$$

with the new definition of $\chi_i^{(+)}$.

The wave functions χ and χ are considered to be known. The T-matrix elements of Equation (2.5.4) involve $P\Psi_i^{(+)}$ which is unknown. The next problem is to express

$$\langle \psi_k QHP P\Psi_i^{(+)} \rangle / (E - E_k),$$

in terms of the $\langle \psi_k QHP \chi_i^{(+)} \rangle$'s . By applying Equation (2.5.5) to $\langle \psi_k QHP P\Psi_i^{(+)} \rangle$, we have

$$\langle \psi_k QHP P\Psi_i^{(+)} \rangle = \langle \psi_k QHP \chi_i^{(+)} \rangle +$$

$$+ \sum_{k=1}^{N} \left\langle \psi_k QHP \frac{1}{E^{(+)} - PHP} PHQ\psi_{k'} \right\rangle \frac{\langle \psi_{k'} QHP P\Psi_i^{(+)} \rangle}{E - E_{k'}} . \qquad (2.5.6)$$

Equations (2.5.4) and (2.5.6) are compactly written using the following notations:

$$
\left.
\begin{aligned}
g_k^{i(\pm)} &\equiv \langle \psi_k \, QHP \, \chi_i^{(\pm)} \rangle , \\
f_k^i &\equiv \langle \psi_k \, QHP \, P \Psi_i^{(+)} \rangle / (E - E_k) , \\
W_{kk'} &\equiv \langle \psi_k \, QHP \, \frac{1}{E^{(+)} - PHP} \, PHQ \, \psi_{k'} \rangle , \\
(\underset{\sim}{\Xi})_{kk'} &\equiv E_k \delta_{kk'} - W_{kk'} , \\
\underset{\sim}{F}_i &\equiv \{ f_1^i , f_2^i , \cdots , f_N^i \} , \\
\underset{\sim}{G}_i &\equiv \{ g_1^{i(\pm)} , \cdots , g_N^{i(\pm)} \} ,
\end{aligned}
\right\} \qquad (2.5.7)
$$

where $\{ \cdots \}$ is a column matrix. Then, Equations (2.5.4) and (2.5.6) become

$$
T_{fi} = 2\pi \langle V_f U'' \chi_i^{(+)} \rangle + 2\pi \left(\underset{\sim}{G}_f^{(-)} \right)^{\dagger} \underset{\sim}{F}_i , \qquad (2.5.8)
$$

and

$$
\left(\underset{\sim}{\Xi} - E \, \underset{\sim}{1} \right) \underset{\sim}{F}_i = - \underset{\sim}{G}_i^{(+)} , \qquad (2.5.9)
$$

respectively. If the inverse of $E\underset{\sim}{1} - \underset{\sim}{\Xi}$ exists, Equation (2.5.8) becomes

$$
T_{fi} = 2\pi \langle V_f U'' \chi_i^{(+)} \rangle + 2\pi \left(\underset{\sim}{G}_f^{(-)} \right)^{\dagger} \frac{1}{E\underset{\sim}{1} - \underset{\sim}{\Xi}} \, \underset{\sim}{G}_i^{(+)} . \qquad (2.5.10)
$$

The problem is reduced to the diagonalization of the matrix $\underset{\sim}{\Xi}$ which is symmetric but non-Hermitian. This diagonalization is generally not covered in this thesis except for the model of Part II. Instead, we assume the following properties:

(a) All the singularities of the T-matrix are simple poles.

(b) From the conservation of flux, the poles of the T-matrix are required to exist on the unphysical E-plane.

From these properties, the eigenvalues of $\underset{\sim}{\Xi}$ may be shown to be all discrete and simple. In addition, these lie below the real axis in the complex E-plane. Therefore, the inverse of $E\underset{\sim}{1} - \underset{\sim}{\Xi}$ exists and $\underset{\sim}{\Xi}$ is diagonalizable.(79)

Denoting eigenfunctions of $\underset{\sim}{\Xi}$ and its Hermitian conjugate $\underset{\sim}{\Xi}^{+}$ by $\underset{\sim}{X}_i$ and $\underset{\sim}{\widetilde{X}}_i$ respectively,

$$\underset{\sim}{\Xi}\,\underset{\sim}{X}_i = \mathcal{E}_i\,\underset{\sim}{X}_i \tag{2.5.11}$$

$$\underset{\sim}{\Xi}^{+}\,\underset{\sim}{\widetilde{X}}_i = \mathcal{E}_i^{*}\,\underset{\sim}{\widetilde{X}}_i . \tag{2.5.12}$$

The orthonormal and completeness relations are given by

$$\underset{\sim}{\widetilde{X}}_i\,\underset{\sim}{X}_j = \delta_{ij} \tag{2.5.13}$$

$$\sum_{j=1}^{N} \underset{\sim}{X}_j\,\underset{\sim}{\widetilde{X}}_j = \underset{\sim}{1} . \tag{2.5.14}$$

Then, we have

$$T_{fi} = 2\pi\langle V_f U'' \chi_i^{(+)}\rangle + 2\pi\sum_{j=1}^{N} \frac{\langle \underset{\sim}{G}_f^{(-)}\underset{\sim}{X}_j\rangle\langle\underset{\sim}{\widetilde{X}}_j\,\underset{\sim}{G}_i^{(+)}\rangle}{E-\mathcal{E}_j} . \tag{2.5.15}$$

The energy average of Equation (2.5.15) is taken as follows:

$$\begin{aligned}\overline{T_{fi}} &= 2\pi\langle V_f U''\chi_i^{(+)}\rangle + \\ &\quad + 2\pi\frac{1}{\Delta}\int_{E_0-\Delta/2}^{E_0+\Delta/2}\sum_j \frac{\langle \underset{\sim}{G}_f^{(-)}\underset{\sim}{X}_j\rangle\langle\underset{\sim}{\widetilde{X}}_j\,\underset{\sim}{G}_i^{(+)}\rangle}{E-\mathcal{E}_j}\,dE \\ &\cong 2\pi\langle V_f U''\chi_i^{(+)}\rangle - i\frac{2\pi^2}{\Delta}\sum_{j=1}^{N}\langle \underset{\sim}{G}_f^{(-)}\underset{\sim}{X}_j\rangle\langle\underset{\sim}{\widetilde{X}}_j\,\underset{\sim}{G}_i^{(+)}\rangle \\ &= 2\pi\langle V_f U''\chi_i^{(+)}\rangle - i\frac{2\pi^2}{\Delta}\left(\underset{\sim}{G}_f^{(-)}\right)^{\dagger}\underset{\sim}{G}_i^{(+)} .\end{aligned} \tag{2.5.16}$$

The approximation in the second step of Equation (2.5.16) is not clear. But if the residues and the poles evenly distribute over Δ and if $\operatorname{Im}\mathcal{E}_i \simeq 0$, then it is a good approximation. Equation (2.5.16) is rewritten as

$$\overline{T_{fi}} = 2\pi\left\{\langle v_f U'' \chi_i^{(+)}\rangle - \pi i \langle \chi_f^{(-)} PHQ\,\Delta\, QHP\,\chi_i^{(+)}\rangle\right\}, \qquad (2.5.17)$$

with Δ given by Equation (2.3.7).

This is Feshbach's derivation of the E-averaged T-matrix.[1] The approximation in Equation (2.5.16) will be extensively used in the remainder of Part I, although the same shifting of T-matrix terms, Equation (2.5.9), will not always be applied.

2.6 The τ-Matrix and the Compound States

The T-matrix is defined on the basis of free waves by

$$P\Psi_i^{(+)} = v_i + \frac{1}{E^{(+)} - H_0} P T v_i . \qquad (2.6.1)$$

We decompose T into two parts:

$$\begin{aligned} T &= T^P + T^R \\ T^P &= \lim_{W\to 0} T . \end{aligned} \qquad (2.6.2)$$

The potential part T^P includes only the single particle interaction and satisfies

$$\chi_i^{(+)} = v_i + \frac{1}{E^{(+)} - H_0} P T^P v_i . \qquad (2.6.3)$$

The matrix elements are further related to the distorted wave T-matrix by

$$T_{fi} = \langle \upsilon_f T \upsilon_i \rangle = 2\pi \left\{ \langle \upsilon_f U'' \chi_i^{(+)} \rangle + \langle \chi_f^{(-)} W P \Psi_i^{(+)} \rangle \right\} . \qquad (2.6.4)$$

Let us define the τ-matrix according to

$$P\Psi_i^{(+)} = \chi_i^{(+)} + \frac{1}{E^{(+)} - PHP} \tau \chi_i^{(+)} \qquad (2.6.5)$$

so that

$$\langle \upsilon_f T^R \upsilon_i \rangle = \langle \chi_f^{(-)} \tau \chi_i^{(+)} \rangle . \qquad (2.6.6)$$

Equation (2.6.6) is derived from Equations (2.6.1), (2.6.2), (2.6.3), and (2.6.5).

In the following, τ will be related to the potential W and the Hamiltonian PHP. First, we rearrange the Schrödinger equation of Equation (2.2.37):

$$P\Psi_i^{(+)} = \chi_i^{(+)} + \frac{1}{E^{(+)} - PHP} \cdot \frac{1}{1 - W \frac{1}{E^{(+)} - PHP}} W \chi_i^{(+)} . \qquad (2.6.7)$$

Then, comparing Equations (2.6.4) and (2.6.7) and noting that τ is defined only in terms of its effects on the χ_i, we may identify

$$\tau = \frac{1}{1 - W \frac{1}{E^{(+)} - PHP}} W .$$

Using the definition of W (Equation (2.2.18)), this may be written

$$\tau = PHQ \frac{1}{E - QHQ - QHP \frac{1}{E^{(+)} - PHP} PHQ} QHP . \qquad (2.6.8)$$

Later, we will define the compound states as being the eigenfunctions of the operator Ξ , defined according to:

$$\Xi \equiv QHQ + QHP \frac{1}{E^{(+)} - PHP} PHQ ,$$

where E is real. On the basis of ψ_s which are eigenfunctions of QHQ, this operator may be expressed by a complex symmetric matrix which will be denoted by $\underset{\sim}{\Xi}$, where

$$\Xi_{ss'} \equiv E_s \delta_{ss'} + \Delta_{ss'} - \pi i \Gamma_{ss'} ,$$

and $\Delta_{ss'}$ and $-\pi\Gamma_{ss'}$ are the real and imaginary parts of

$$\langle \psi_s QHP \frac{1}{E^{(+)} - PHP} PHQ \psi_{s'} \rangle .$$

Assuming that all the eigenvalues of $\underset{\sim}{\Xi}$ are different, then $\underset{\sim}{\Xi}$ may be diagonalized by a similarity transformation $\underset{\sim}{V}$.(77)

Denote the compound state by Φ_α ,

$$\left(QHQ - QHP \frac{1}{E^{(+)} - PHP} PHQ - \mathcal{E}_\alpha \right) \Phi_\alpha = 0 . \qquad (2.6.9)$$

The Φ_α is related to ψ_s by

$$\underset{\sim}{\Phi} = \underset{\sim}{V} \underset{\sim}{\psi} . \qquad (2.6.10)$$

This formulation will be applied in Chapter 3 (Part I) and in Chapters 1 and 2 of Part II.

CHAPTER 3

THE OPTICAL MODEL POTENTIAL

One of the advantages of the unified theory is that the optical model potential is easily expressed by operators. Our aim is to improve the optical model in the low energy region. As will be discussed later, this will be accomplished by extracting the doorway state contribution in which all the compound states are smeared out by the energy average process. For this purpose, a new method for derivation of the O.M. potential will be developed in this chapter.

In § 3.1, Feshbach's method will be briefly reviewed. In § 3.2, the new method will be shown.

3.1 Optical Model Potential

The optical model potential is defined by Feshbach[68,24] such that it yields the energy averaged T-matrix elements, Equation (2.5.17). We will review the derivation of Reference 68, in this section.

Consider an O.M. Schrödinger equation

$$\varphi_i^{(+)} = \chi_i^{(+)} + \frac{1}{E^{(+)} - PHP} H_{CN} \varphi_i^{(+)}, \qquad (3.1.1)$$

where $\varphi_i^{(+)}$ is the O.M. wave function and H_{CN} is to be obtained. The distorted wave T-matrix elements of Equation (3.1.1) are given by (see Equation (2.4.16))

$$T_{fi}^{OM} = 2\pi \left\{ \langle v_f U'' \chi_i^{(+)} \rangle + \langle \chi_f^{(-)} H_{CN} \varphi_i^{(+)} \rangle \right\}. \qquad (3.1.2)$$

H_{CN} will be determined from $\overline{T_{fi}} = T_{fi}^{OM}$. By comparing Equation (3.1.2) with Equation (2.5.17), we obtain

$$H_{CN}\,\psi_i^{(+)} = -i\pi\, PHQ\,\Lambda\, QHP\,\chi_i^{(+)} \qquad (3.1.3)$$

Applying this to Equation (3.1.1),

$$\psi_i^{(+)} = \chi_i^{(+)} + \frac{1}{E^{(+)} - PHP}(-i\pi)\, PHQ\,\Lambda\, QHP\,\chi_i^{(+)}. \qquad (3.1.4)$$

Or,

$$\chi_i^{(+)} = \frac{1}{1 - i\pi \dfrac{1}{E^{(+)} - PHP} PHQ\,\Lambda\, QHP}\,\psi_i^{(+)}. \qquad (3.1.5)$$

In order to derive the Schrödinger equation for $\psi_i^{(+)}$, we operate with $E - PHP$ on both sides of Equation (3.1.5) with the result

$$(E - PHP)\,\frac{1}{1 - i\pi \dfrac{1}{E^{(+)} - PHP} PHQ\,\Lambda\, QHP}\,\psi_i^{(+)} = 0,$$

which may be rearranged as

$$\left(E - PHP - H_{CN}\right)\psi_i^{(+)} = 0, \qquad (3.1.6)$$

with

$$H_{CN} = -i\pi\, PHQ\,\frac{1}{1 - i\pi\,\Lambda\, QHP \dfrac{1}{E^{(+)} - PHP} PHQ}\,\Lambda\, QHP. \qquad (3.1.7)$$

Thus, H_{CN} is related to PHQ and its Hermitian conjugate, and to the density of the compound states. If Λ and $QHP[E^{(+)} - PHP]^{-1} PHQ$ are independent of energy, then H_{CN} is constant with energy except for a slow variation through the non-locality of $PHQ\,\Lambda\, QHP$. This is the usual justification for the Optical Model.

3.2 O.M. Schrödinger Equation

The average cross section is that which is measured when the incident neutron has what is called "bad resolution". This resolution is often referred to as the spread of the wave packet.(1) Instead, we consider it as follows: N neutrons are incident on the target nuclei. Each neutron has an ideal resolution. But the number of neutrons with energy E is distributed as n(E) with spread Δ centered at E_0 . For example, see Figure I.2.

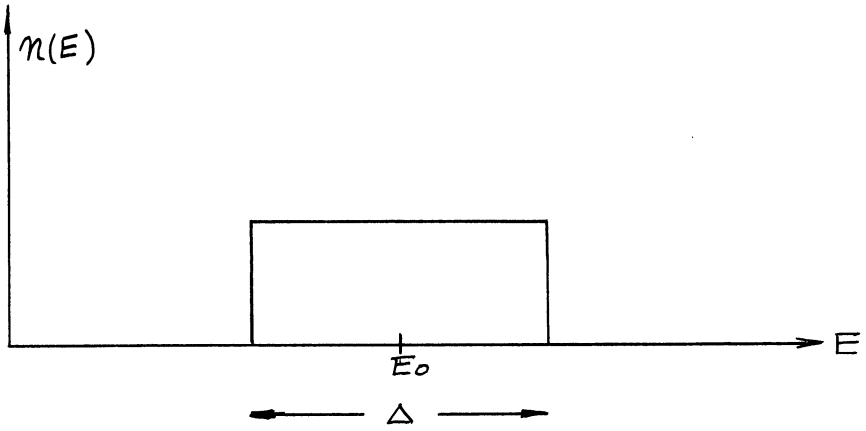

Figure I.2. Neutron Distribution.

The n-th neutron with energy E_n obeys the n-th Schrödinger equation

$$(E_n - PHP)P\Psi_n = W(E_n)P\Psi_n \qquad \text{for } n = 1, 2, \cdots, N. \tag{3.2.1}$$

The Optical Model is considered to represent these N independent events by a single Schrödinger equation.

The first problem is to reduce the system of Schrödinger equations to a single Schrödinger equation. Next, we will consider whether the obtained equation is the same as Equation (3.16); the O.M. Schrödinger equation.

Consider the free waves and the distorted waves whose energies are within the spread Δ. At large distances,

$$\left.\begin{array}{ll} \text{(a)} & U_E(r) \neq U_{E_0}(r) \\ & \chi_E(r) \neq \chi_{E_0}(r) \end{array}\right\} \quad \text{for } E \neq E_0 \text{ at } |r| \to \infty \tag{3.2.2}$$

However, we may assume that

$$\left.\begin{array}{ll} \text{(b)} & U_E(r) \cong U_{E_0}(r) \\ & \chi_E(r) \cong \chi_{E_0}(r) \end{array}\right\} \quad \text{for } |r| < R$$

$$\text{e.g. } \langle U_E \cup \chi_E^{(+)} \rangle \cong \langle U_{E_0} \cup \chi_{E_0}^{(+)} \rangle . \tag{3.2.3}$$

Furthermore, we assume that

(c) the shift functions, Equation (2.3.3), and the resonance widths, Equation (2.3.5), are independent of energy within Δ. Or,

$$QHP \frac{1}{E_n^{(+)} - PHP} PHQ \cong QHP \frac{1}{E_0^{(+)} - PHP} PHQ. \tag{3.2.4}$$

The conditions (b) and (c) are assumed not only in this section but in this entire thesis.

If we replace the operator $E_n - PHP$ of equation (3.2.1) by $E_0 - PHP$, we obtain

$$(E_0 - PHP)\,\varphi_n = W(E_n)\,\varphi_n . \tag{3.2.5}$$

We intend to average this equation over n, and use the function $\bar{\Phi}$ defined according to

$$\bar{\Phi} \equiv \frac{1}{N} \sum_n \varphi_n$$

as our optical model wave function.

It is important to note that the φ_n's, the solutions to Equation (3.2.5), are not equal to the $P\Psi_n^{(+)}$'s, the solutions to the actual Schrödinger equation (3.2.1), nor are they approximately equal. In fact, by Equation (2.6.5) we have $P\Psi_n^{(+)}$ and its asymptotic form:

$$P\Psi_n^{(+)} = \chi_{in}^{(+)} + \frac{1}{E_n^{(+)} - PHP}\, T(E_n)\, \chi_{in}^{(+)} \qquad (3.2.6)$$

$$\xrightarrow[r_0 \to \infty]{} \chi_{in}^{(+)} - \frac{\mu}{\sqrt{2\pi}\,\hbar^2} \sum_{f_n} \frac{e^{ik_n r_0}}{r_0}\, U_{sv} \left\langle \chi_{fn}^{(-)} T(E_n)\, \chi_{in}^{(+)} \right\rangle, \qquad (3.2.7)$$

where we have used Equation (2.2.36). Similarly,

$$\varphi_n^{(+)} = \chi_{i0}^{(+)} + \frac{1}{E_0^{(+)} - PHP}\, T'(E_n)\, \chi_{i0}^{(+)} \qquad (3.2.8)$$

$$\xrightarrow[r_0 \to \infty]{} \chi_{i0}^{(+)} - \frac{\mu}{\sqrt{2\pi}\,\hbar^2} \sum_{f_0} \frac{e^{ik_0 r_0}}{r_0}\, U_{sv} \left\langle \chi_{f0}^{(-)} T'(E_n)\, \chi_{i0}^{(+)} \right\rangle, \qquad (3.2.9)$$

where the subscripts i_0 and f_0 refer to initial and final states with energy E_0, and the subscripts i_n and f_n refer to similar states with energy E_n (e.g. $(E_n - PHP)\chi_{in} = 0$), and where we have defined $T'(E_n)$ according to

$$T'(E_n) \equiv W(E_n) + W(E_n) \frac{1}{E_0^{(+)} - PHP - W(E_n)}\, W(E_n). \qquad (3.2.10)$$

However, it is not difficult to show that the T-matrices obtained from both Equations (3.2.1) and (3.2.5) are equal within the approximations implied by assumptions (b) and (c). That is, the observables given by Equation (3.2.5) are approximately equal to those given by Equation (3.2.1).

In fact, by rearranging Equation (3.2.10), we find

$$\tau'(E_n) = PHQ \frac{1}{E_n - QHQ - QHP \frac{1}{E^{(+)} - PHP} PHQ} QHP$$
$$\cong \tau(E_n), \tag{3.2.11}$$

by assumption (c). In addition, by Equations (2.2.38) and (2.6.2), and by Equation (2.6.6), we have

$$\langle v_{fn} U'' \chi_{in}^{(+)} \rangle \cong \langle v_{fo} U'' \chi_{io}^{(+)} \rangle, \tag{3.2.12}$$

and

$$\langle \chi_{fn}^{(+)} \tau(E_n) \chi_{in}^{(+)} \rangle \cong \langle \chi_{fo}^{(+)} \tau'(E_n) \chi_{io}^{(+)} \rangle, \tag{3.2.13}$$

where assumptions (b) and (c) and the fact that τ' and τ are sandwiched by PHQ and QHP are applied. Therefore, for the purpose of obtaining the T-matrix, Equation (3.2.5) may be considered to be the Schrödinger equation for the n-th neutron.

Taking average of Equation (3.2.5) over n, we have

$$(E_o - PHP)\,\bar{\Phi} = \overline{W \varphi_n}. \tag{3.2.14}$$

Or, Equations (3.2.8) and (3.2.5) lead to

$$(E_o - PHP)\,\bar{\Phi} = \overline{\tau'}\, \chi_{in}^{(+)}. \tag{3.2.15}$$

Both are, of course, equivalent.

Equation (3.2.15) may be shown to be equivalent to the O.M. Schrodinger equation of Equation (3.1.6) within the approximations (b) and (c). In fact, from Equations (3.2.11), (2.6.9) and (2.6.10), we

have

$$\overline{\tau}' = 2\pi i\, PHQ \wedge QHP. \tag{3.2.16}$$

Applying this result to Equation (3.2.15) and using the same argument as that below Equation (3.1.3), we obtain:

$$(E_0 - PHP - H_{CN})\,\overline{\Phi} = 0, \tag{3.2.17}$$

where H_{CN} is given by Equation (3.1.7). Thus, $\overline{\Phi}$ is equivalent to the O.M. wave function.

For later convenience, we will examine an approximation

$$\overline{W \varphi_n^{(+)}} \cong \overline{W}\ \overline{\varphi_n^{(+)}} = \overline{W}\,\overline{\Phi}. \tag{3.2.18}$$

It will be tested by comparing O.M. equations derived before and after this approximation.

The eigenvalues of QHQ are real, and W is given by Equation (2.2.18). To integrate W along the real E-axis, we need to know how to integrate W around the eigenvalues.

To assist in the contour integration, it is convenient to include an additional infinitesimal dissipative perturbation (such as might occur from spontaneous γ -decay). Thus we write the Schrödinger equation as

$$\lim_{\delta \to +0} (H - i\delta - E)\,\Psi = 0 \tag{3.2.18}$$

where the limit $\delta \to +0$ is implied to satisfy the experimental boundary condition. Therefore,

$$\left.\begin{aligned}(E - PHP + i\delta)\, P\Psi &= PHQ\, Q\Psi \\ (E - QHQ + i\delta)\, Q\Psi &= QHP\, P\Psi .\end{aligned}\right\} \tag{3.2.19}$$

Defining ψ_s and E_s as in Equation (2.5.2), we have an effective open channel Schrödinger equation with a first order perturbation.

$$(E_0 - PHP + i\delta)\,\varphi = \sum_s \frac{PHQ\psi_s\rangle\langle\psi_s QHP}{E - E_s + i\delta}\,\varphi . \tag{3.2.20}$$

This equation corresponds to Equation (3.2.5) and the operator in the r.h.s corresponds to W . Taking the limit $\delta \to +0$ after integrating W over E, we obtain:

$$\overline{W} = \frac{1}{\Delta}\int_{E_0-\frac{\Delta}{2}}^{E_0+\frac{\Delta}{2}} dE \sum_s \frac{PHQ\psi_s\rangle\langle\psi_s QHP}{E^{(+)} - E_s} . \tag{3.2.21}$$

This integral is calculated in § 3.1 with the result

$$\overline{W} \cong -i\pi\, PHQ \wedge QHP . \tag{3.2.22}$$

Therefore, we have

$$\begin{aligned}(E - PHP)\,\overline{\Phi} &= \overline{W}\,\overline{\Phi} \\ &= -i\pi\, PHQ \wedge QHP\,\overline{\Phi} .\end{aligned} \tag{3.2.23}$$

As may be seen from Equations (3.1.6) and (3.1.7), this approximation is as good as the first order approximation of Equation (3.1.7). As is seen below Equation (2.4.16), this first order gives the first two terms of the absorption cross section correctly. The accuracy involved in the approximation, Equation (3.2.18) is surprisingly good.

CHAPTER 4

INTRODUCTION OF THE DOORWAY STATE STRENGTH FUNCTION

The exact Schrödinger equation involves the many-body problem. The cross sections calculated from it must be those measured with ideal resolution. Formally, the equation may be reduced to one with a single particle potential (generalized O.M. potential (§ 1.3)) although the potential is not known.

The O.M. Schrödinger equation, on the other hand, contains a two-body complex potential. As we have seen above, the averaging operation on the exact T-matrix or Schrödinger equation produces the O.M. equation which yields the gross structures of cross sections and strength functions.

Weisskopf's compound nucleus formation process[15] is a cascade sequence into the more and more complicated states (§ 1.7). The first stage of this process is called the doorway state.[22] In the derivation of the O.M. equation, all the processes involving the internal degrees of freedom are smeared out by the averaging process into a single particle complex potential. Block and Feshbach[22] explained the deviation of the strength function of individual nuclei from the gross structure taking into account the effects of the doorway states. We will improve the O.M. by extracting the effects of the doorway states from the O.M.

The two extreme cases, the O.M. Schrödinger equation and the exact Schrödinger equation are related by an average over the range Δ. This suggests to us that if the range is reduced, a degree of internal

freedom (i.e. doorway states) will come out explicitly and the potential derived will be somewhere between the O.M. and the generalized O.M. potentials.

For the energy average to be meaningful, we must assume that the spectrum of the more complicated states is much denser than that of the doorway states. This contrasts with the assumption of Block and Feshbach.[22]

After averaging out the effects of the more complicated states, we will obtain a pair of equations: one for the open channel and another for the doorway states. The potentials are composed of the single particle potential, the coupling between the open channel and the doorway states, and the imaginary potential. The imaginary potential will be called the "doorway state strength function". It appears in the equation for the doorway states and represents the effects of the more complicated states.

4.1 Introduction of the Doorway State Strength Function

Following Block and Feshbach,[22] the closed channel states $Q\Psi$ are divided into two components: the doorway state component $q_1\Psi$ and the more complicated state component $q_2\Psi$.

$$Q\Psi = q_1\Psi + q_2\Psi. \tag{4.1.1}$$

Thus we assume, from the beginning, the existence of the projection operators q_1 and q_2 such that

$$\left.\begin{aligned} &Q = q_1 + q_2 \;, \quad q_1 q_2 = 0 \\ &PHq_1 \neq 0 \;, \text{ and } PHq_2 = 0. \end{aligned}\right\} \tag{4.1.2}$$

Given these projection operators, we may then define the doorway states, φ_s , and the more complicated states, ϕ_n , according to

$$q_1 H q_1 \varphi_s = E_s \varphi_s , \tag{4.1.3}$$

$$q_2 H q_2 \phi_n = E_n \phi_n . \tag{4.1.4}$$

The relations between Equation (4.1.1) and Equations (4.1.3) and (4.1.4) will be discussed in Part II.

The Schrödinger equation

$$H\Psi = E\Psi \tag{4.1.5}$$

is decomposed into a system of three equations by means of the projection operators P , q_1 , and q_2 .

$$(PHP-E)P\Psi = -PHq_1 q_1\Psi , \tag{4.1.6}$$

$$(q_1 H q_1 - E) q_1\Psi = -q_1 HPP\Psi - q_1 H q_2 q_2\Psi , \tag{4.1.7}$$

$$(q_2 H q_2 - E) q_2\Psi = -q_2 H q_1 q_1\Psi . \tag{4.1.8}$$

Within the range Δ centered at E_0 of §3.2, we may replace (PHP-E) by (PHP-E_0). Now, we will consider replacement of (q_1Hq_1-E) by (q_1Hq_1-E_0). Substituting the formal solution of Equation (4.1.6) to Equation (4.1.7), we have

$$\left[q_1 H q_1 - E + i\pi q_1 HP \delta(E_0 - PHP) PHq_1 + \right.$$

$$\left. + q_1 HP \frac{\mathcal{P}}{E_0 - PHP} PHq_1 \right] q_1\Psi$$

$$= -q_1 HP \chi_i^{(+)}(E_0) - q_1 H q_2 q_2\Psi . \tag{4.1.9}$$

By assumption on the spectra of q_1Hq_1 and q_2Hq_2, only one doorway state φ_s is significant in a certain energy interval Δ which contains a subinterval Δ' in which there exist many eigenvalues of q_2Hq_2 (see Figure I.3). The bound state $q_1\Psi$ is given in terms of $\chi_i^{(+)}$ and $q_2\Psi$ and by a Green's operator which is inverse of the operator on the l.h.s. of Equation (4.1.9). If the energy range of interest Δ' can be small so that

$$\Delta' \ll \pi \left| \langle \varphi_s \, q_1 H P \chi^{(+)}(E_0) \rangle \right|^2, \tag{4.1.10}$$

then E in the Green's operator may be replaced by E_0. This implies the replacement of $(q_1Hq_1 - E)$ by $(q_1Hq_1 - E_0)$ in Equation (4.1.7).

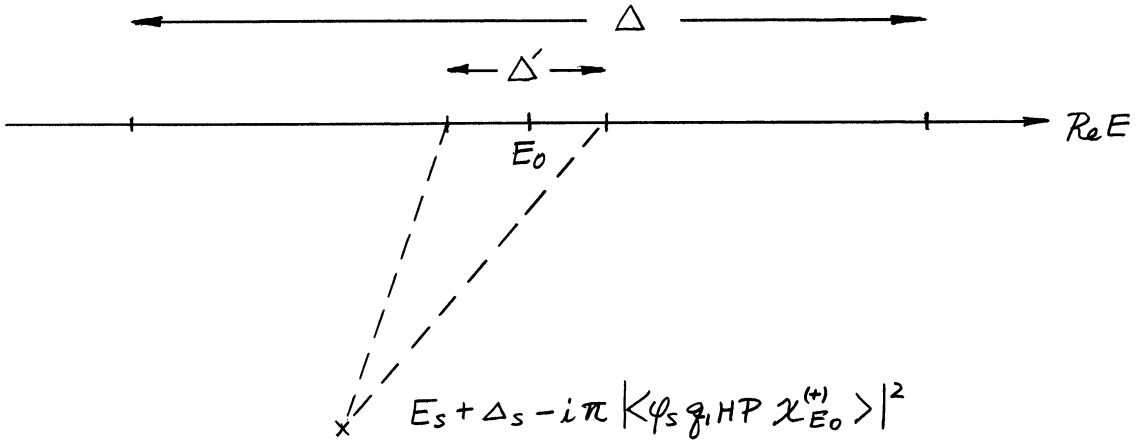

Figure I.3. Ranges Δ and Δ', and the Singular Point of Equation (4.1.9).

Now, we have

$$(PHP - E_0)\,\widetilde{P\Psi} = -PHq_1 q_1 \Psi, \tag{4.1.11}$$

$$(q_1Hq_1 - E_0)\,q_1\Psi = -q_1HP\widetilde{P\Psi} - q_1Hq_2\,q_2\Psi, \tag{4.1.12}$$

$$(q_2Hq_2 - E)\,q_2\Psi = -q_2Hq_1\,q_1\Psi. \tag{4.1.13}$$

Since $q_1\Psi$ and $q_2\Psi$ are bound states and close to those of Equations (4.1.6), (4.1.7), and (4.1.8), we use the same notation.

From Equations (4.1.12) and (4.1.13), the effective doorway state equation is obtained,

$$(q_1Hq_1 - E_0)\,q_1\Psi = -q_1HP\,\widetilde{P\Psi} - q_1Hq_2\frac{1}{E-q_2Hq_2}\,q_2Hq_1\,q_1\Psi. \tag{4.1.14}$$

We assume that the spectrum of q_2Hq_2 is dense so that

$$D \ll \Delta', \tag{4.1.15}$$

where D is the spacing of the eigenvalues.

The E-average of Equation (4.1.14) will be taken over Δ' and the averaged values denoted by e.g. $\widetilde{\Psi}$ instead of $\overline{\Psi}$ of § 3.2. The approximation of § 3.2 will be used (c.f. the discussion after Equation (3.2.18)).

$$\overline{q_1Hq_2\frac{1}{E-q_2Hq_2}\,q_2Hq_1\,q_1\Psi} \simeq \overline{q_1Hq_2\frac{1}{E^{(+)}-q_2Hq_2}\,q_2Hq_1}\;\widetilde{q_1\Psi}. \tag{4.1.16}$$

We then write

$$\overline{q_1Hq_2\frac{1}{E^{(+)}-q_2Hq_2}\,q_2Hq_1} = -i\pi\,q_1Hq_2\lambda\,q_2Hq_1 \equiv -i\frac{\alpha_{op}}{2}, \tag{4.1.17}$$

where we have used the abbreviation:

$$\lambda \equiv \frac{1}{\Delta'}\sum_n |\phi_n\rangle\langle\phi_n|. \tag{4.1.18}$$

Therefore, Equations (4.1.6), (4.1.7), and (4.1.8) are reduced to a pair of simultaneous equations

$$\left.\begin{aligned} (PHP-E)\widetilde{P\Psi} &= -PHq_1\widetilde{q_1\Psi}, \\ (q_1Hq_1 - i\frac{\alpha_{op}}{2} - E)\widetilde{q_1\Psi} &= -q_1HP\widetilde{P\Psi}. \end{aligned}\right\} \qquad (4.1.19)$$

By comparison with Equation (2.2.6), we see that the effects of the more complicated states have been replaced by the Hermitian operator α_{op}. We will call α_{op} the doorway state strength function operator.

4.2 Concluding Remarks

We have performed the E-average of the Schrödinger equation over Δ'. As is expected, the doorway states are extracted from the O.M. complex potential. In Equation (4.1.19), the doorway states explicitly appear and the more complicated states are represented by a complex potential in the doorway state equation.

This energy average operation may be set at any stage of the cascade scheme.

Comparing Equation (4.1.19) with Equation (3.2.19), the complex potential appears in the doorway state equation, while the complex potential of the O.M. appears in the open channel equation. Both potentials are expected equally to be independent of energy. The theoretical structures are similar to each other. The diagonal part of $PHQ\Lambda QHP$ is proportional to the strength function

$$\frac{\bar{\Gamma}}{\bar{D}} = 2\pi \langle \chi_E^{(+)} PHQ\Lambda QHP\chi_E^{(+)} \rangle .$$

and $\alpha_{op} = 2\pi q_1 H q_2 \lambda q_2 H q_1$. In this sense, α_{op} is called the doorway state strength function operator.

The conditions for the energy average are Equations (4.1.10) and (4.1.15). These are satisfied if

$$-v_0 \left(\equiv \frac{\pi |\langle \psi_s q_1 H P \chi^{(+)} \rangle|^2}{\bar{D}} \right) \gg 1$$

at any situation of coupling strengths (see Part II). Furthermore, the condition that the density of spectrum of the more complicated states are much denser than that of the doorway states has been applied. This implies that the results apply to nuclei with rather complicated structure.

CHAPTER 5

MODIFIED OPTICAL MODEL IN THE ISOLATED DOORWAY STATE REGION

5.1 Optical Model Calculation for Na^{23}

We have calculated the optical model cross sections for Na^{23} Figure I.5 shows the measured and calculated total cross sections of Na^{23}.(54) The Wood-Saxon real well with Gaussian surface absorption was chosen for the optical model potential shape (see Figure I.4).

$$V_{re}(r) = \frac{-VRE}{1 + \exp\frac{r-R_1}{a_1}} \qquad \text{for } r \le R_1 + 4a_1,$$

$$V_{im}(r) = -VIM \exp\left\{-\left(\frac{r-R_1}{a_2}\right)^2\right\},$$

$$V_{so}(r) = -VSR \frac{1}{r}\left|\frac{d}{dr} V_{re}(r)\right| \vec{\ell}\cdot\vec{s}.$$

The six parameters of the potential are determined for the best fit to the total cross section, the total elastic cross section, and the differential elastic cross section from 1 to 4 Mev with Hauser-Feshbach correction. The best set of the parameters is

$$VRE = 40.5 \text{ Mev},$$
$$VIM = 8.0 \text{ Mev},$$
$$VSR = 10.0 \text{ Mev},$$
$$R_1 = 3.92 \text{ fm},$$
$$a_1 = 0.60 \text{ fm},$$
$$a_2 = 1.04 \text{ fm}.$$

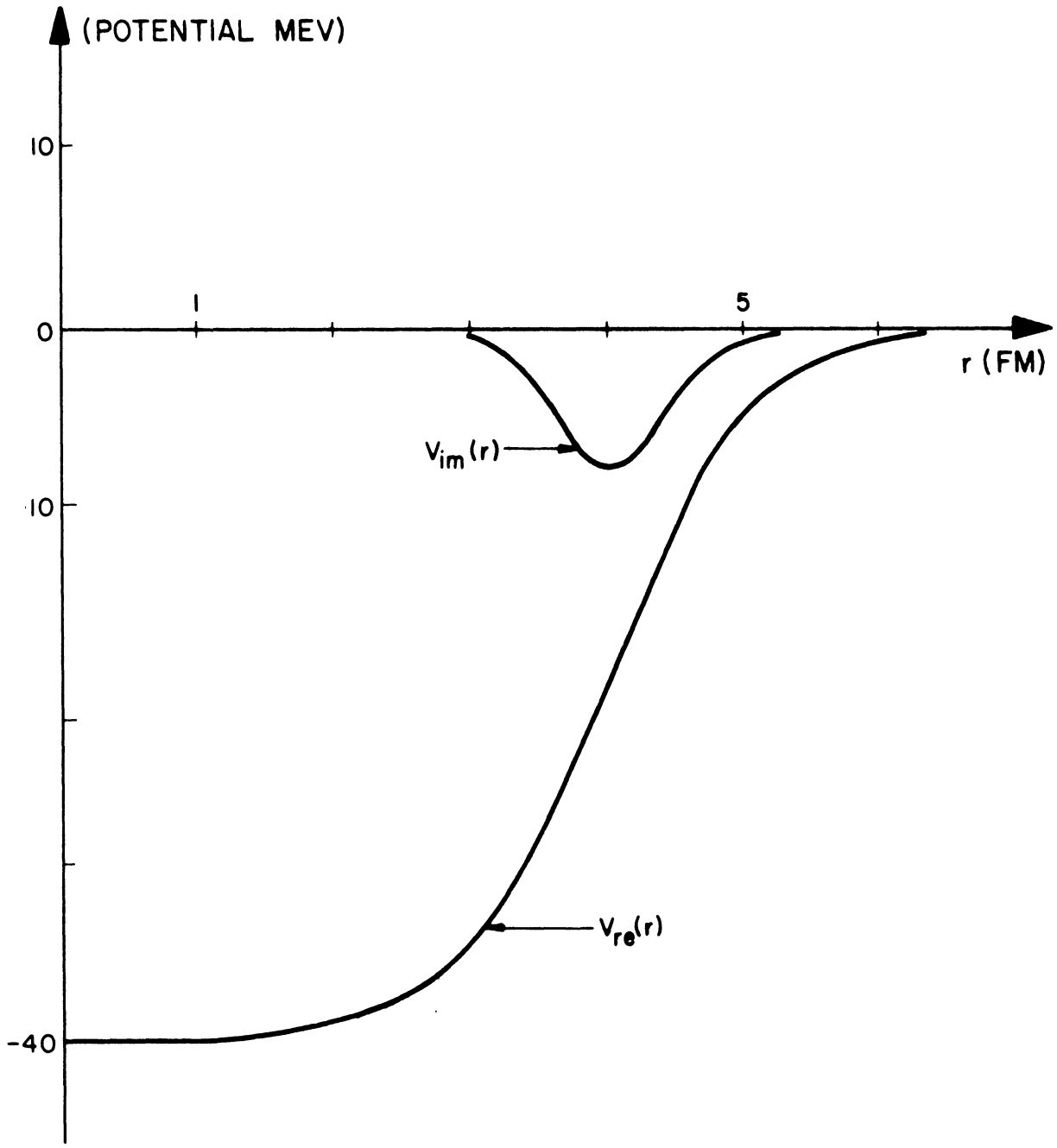

Figure I.4. Optical Model Real and Imaginary Potentials.

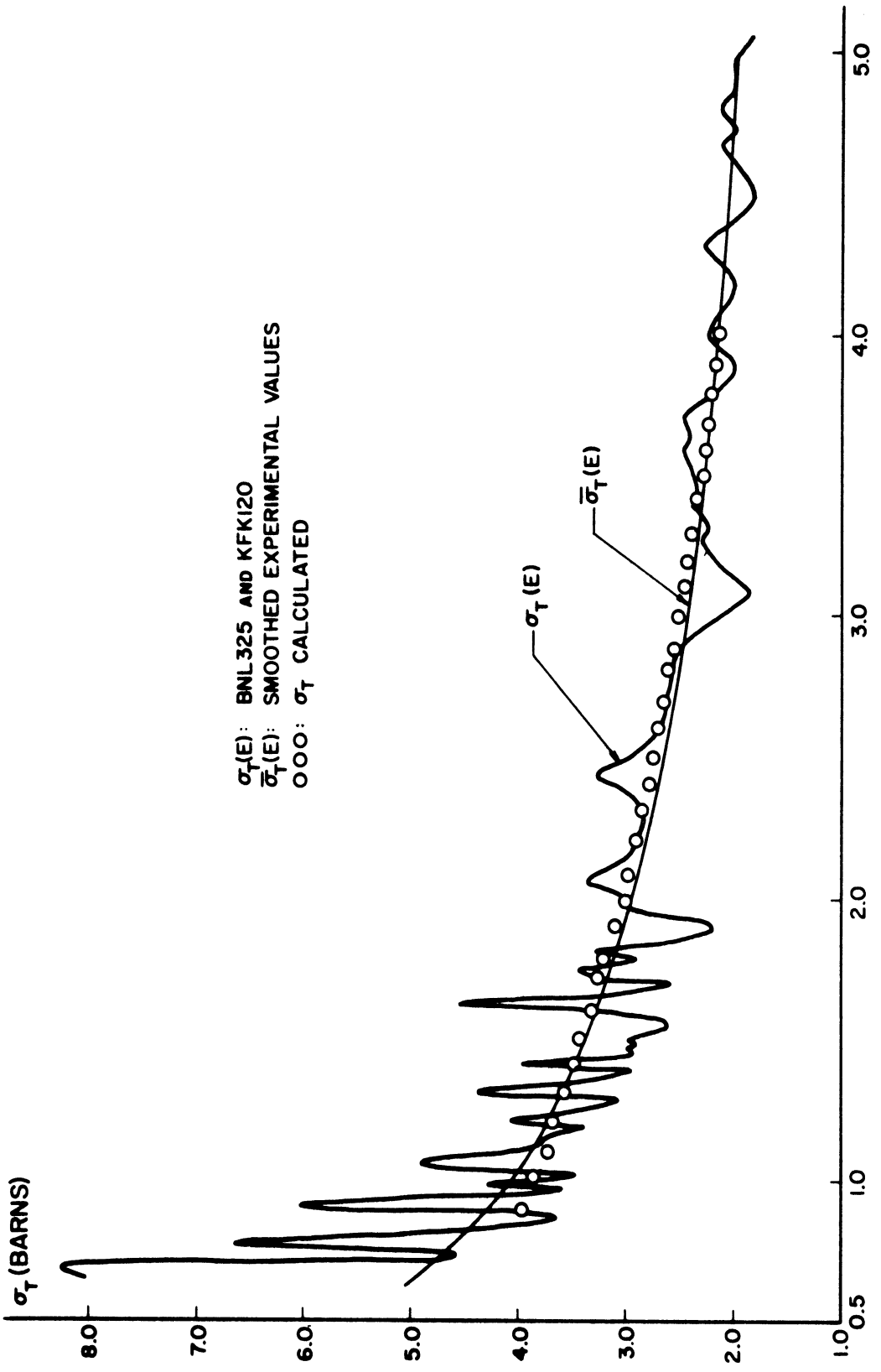

Figure I.5. Optical Model Fit to the Total Cross Section of N_a-23.

The resulting potential is applied to the calculation of the inelastic cross section to see the fit.[54] The fit there is very good except around thresholds where Moldauer's correction[23,27] must be applied. The total cross section is calculated up to 10 Mev. The fit is also very good. However, when the calculation is extended below 1 Mev, agreement of the calculation to the measured values disappears with decreasing neutron energy. Namely, the calculated total cross section turns into the $1/v$ region of the O.M. below 0.5 Mev, while the measured cross section stays almost constant as a whole. The discrepancy is caused by the increasing calculated absorption cross section.

We will try to indicate in this chapter how the O.M. should be modified to eliminate this discrepancy.

The O.M. usually explains well the gross structure: the E-averaged cross section including the giant resonances, and the strength function, (§ 1.3). Another characteristic is the $1/v$ -dependence of the O.M. absorption cross section which occurs when $ka \ll 1$. In fact, the O.M. strength function is defined by the behavior of the O.M. absorption cross section at low energies[59,29,43](§ 2.3),

$$\sigma_a^{OM} = \frac{1}{k}\frac{2M}{\hbar^2}\int_0^\infty |M(r)|^2 W(r)\,dr = \frac{1}{\sqrt{E}}\frac{2\pi^2 E}{k^2}\left[\frac{\overline{\Gamma_n^0}}{D}\right]_{OM}.$$

On the other hand, the statistical theory yields for the E-averaged reaction cross section,[29,36]

$$\overline{\sigma_r} \cong \frac{1}{\sqrt{E}}\frac{2\pi E}{k^2}\left[\frac{\overline{\Gamma_n^0}}{D}\right].$$

Measured values for $\bar{\Gamma}_n^0/\bar{D}$ agree well with direct measurements of σ_a in the $1/v$ region for most nuclei.

However, the O.M. strength function gives only the average distribution of the strength functions for different nuclei. Its deviation from the measured strength function of an individual nucleus is inevitable. This deviation was explained in terms of the doorway states by Block and Feshbach.[22] To obtain such individual strength function or $1/v$ -cross section, it is necessary to adjust the O.M. potential, particularly its imaginary part. It is not clear if the adjusted O.M. potential will yield the average cross section in the high energies.

At high energies, giant resonances and resonances with large widths have been measured. As the energy decreases, individual resonances may be more closely observed. Below the resonance region, the cross section becomes flat and small. We denote the lower and upper limits of the resonance region by E_1 and E_2 respectively. In the usual situation (S-wave scattering predominant), the E-averaged total cross section has a $1/v$ dependence for $E \gtrsim E_1$. Also, it is easily observed that E_2 varies cyclically in accordance with the cycle of the strength function although it becomes larger for lighter nuclei as a whole. These are overall tendencies for nuclei with mass numbers larger than 30.

For very light nuclei, the lower end of the resonance region, E_1 , becomes as high as 1 Mev. We will briefly describe the cross sections of F, Na, Mg, and Al . The energy corresponding to $ka = 1$ for these nuclei is about 1 Mev. Therefore, the $1/v$ cross section

above 1 Mev does not correspond to the O.M. $1/v$ we are discussing. Our calculation of Na^{23} yields a σ_{se} of the form of one side of a giant resonance shape, with the resonance lying somewhat below 1 Mev. The cross sections of F and Mg are similar: $1/v$ behavior from ~ 0.5 to above 3 Mev, and a few isolated resonances, which do not belong to this $1/v$, below ~ 0.5 Mev. In this case, it is not clear how a part of this $1/v$ (0.5 - 1 Mev) is to be treated. Na and Al have almost the same total cross section. The resonance region extends down to 1 kev and the average measured cross section becomes flat below 1 Mev. For most heavier nuclei, the O.M. $1/v$ fits well at least above E_1. But, for nuclei from F to Al, particularly Na and Al, the O.M. $1/v$ is clearly incorrect.

Consideration of the extremely low energy range suggests an *ad hoc* way to improve the O.M. in the intermediate and the low energy regions. The total cross section calculated and measured disagree greatly. But the shape elastic cross section agrees well with the measured total cross section even at extremely low energies ~ 1 ev. This calculation suggests that the real part of the O.M. potential might be correct even at very low energies and that only the imaginary part should be changed. In fact, when the imaginary part of the potential is decreased gradually to zero below 0.5 Mev, we obtain a complete fit of the calculation to the E-averaged measured total cross sections.

The theoretical justification of this tentative approach follows from a treatment based on Weisskopf's reaction picture discussed in Chapters 3 and 4. The generalized O.M. is supposed to yield the exactly measured cross sections, e.g. the lowest resonance of Na^{23}. The

transient region between the lowest resonance and the lower end of the O.M. may be analyzed by constructing a theory intermediate between the generalized O.M. and the O.M. In other words, we will describe a modification to the O.M. in which the energy averaging is carried out over a shorter range than ordinarily. The results of the improvement of the O.M. will be seen in this chapter.

Equation (4.1.14) may be written as an effective open channel Schrödinger equation,

$$(PHP-E)P\tilde{\Psi} = -PHq_1 \frac{1}{E-q_1Hq_1+i\frac{\alpha_{op}}{2}} q_1HP\tilde{\Psi}. \qquad (5.1.1)$$

Let us call it the "modified Optical Model" Schrödinger equation, the modification being that the energy range is not so coarse as in the original O.M. In the case that the interference between the doorway states may be neglected, the complex potential will be obtained in § 5.2. The total cross section and the absorption cross section will also be obtained to illustrate the result. In § 5.3, the imaginary potential in the low and the intermediate energy regions will be given. This discussion is based on a coarse assumption; nevertheless, it is very suggestive.

5.2 Modified Optical Model

In this section, the modified O.M. potential will be obtained in the isolated doorway state region. The total cross section and the absorption cross section will also be obtained.

We expand the Green's operator of Equation (5.1.1) in terms of the doorway state eigenfunctions of Equation (4.1.3),

$$q_1 = \sum_s \varphi_s \rangle\langle \varphi_s \quad , \tag{5.2.1}$$

$$\alpha_{op} = \alpha_{op}^{D} + \alpha_{op}^{ND} \quad , \tag{5.2.2}$$

where

$$\alpha_{op}^{D} \equiv \sum_s \varphi_s \rangle\langle \varphi_s \, \alpha_{op} \, \varphi_s \rangle\langle \varphi_s \quad , \tag{5.2.3}$$

$$\alpha_{op}^{ND} \equiv \sum_{s \neq s'} \varphi_s \rangle\langle \varphi_s \, \alpha_{op} \, \varphi_{s'} \rangle\langle \varphi_{s'} \quad . \tag{5.2.4}$$

Equation (5.1.1) becomes

$$(PHP - E)\widetilde{P\Psi} = -\sum_{l=0}^{\infty} PHq_1 \left(G\, i\frac{\alpha_{op}}{2} \right)^{l} G\, q_1 HP\, \widetilde{P\Psi} \quad , \tag{5.2.5}$$

where

$$G \equiv \frac{1}{E - q_1 H q_1 + i\frac{\alpha_{op}^{D}}{2}} \tag{5.2.6}$$

In the intermediate energy region where doorway states are separated sufficiently so that

$$|E_s - E_{s'}| \gg |\langle \varphi_s \, \alpha_{op}^{ND} \, \varphi_{s'} \rangle| \quad , \tag{5.2.7}$$

the interference terms $(l > 0)$, containing the effects of α_{op}^{ND}, may be neglected. Equation (5.2.5) becomes

$$(PHP - E)\widetilde{P\Psi} = -\sum_s \frac{PHq_1 \varphi_s \rangle\langle \varphi_s q_1 HP}{E - E_s + i\alpha_s/2}\, \widetilde{P\Psi} \quad , \tag{5.2.8}$$

where

$$\alpha_s \equiv \langle \varphi_s \, \alpha_{op} \, \varphi_s \rangle . \tag{5.2.9}$$

We may then write Equation (5.2.8) in the form:

$$\left(PHP - F_1(E) - i F_2(E) - E \right) \widetilde{P\Psi} = 0 , \tag{5.2.10}$$

where the modified O.M. potential operators F_1 and F_2 are given by

$$F_1(E) \equiv \sum_s \mathcal{R}e[f_s(E)] \, PHq_1 \varphi_s \rangle \langle \varphi_s q_1 HP , \tag{5.2.11}$$

$$F_2(E) \equiv \sum_s \mathcal{I}m[f_s(E)] \, PHq_1 \varphi_s \rangle \langle \varphi_s q_1 HP , \tag{5.2.12}$$

and

$$f_s(E) \equiv \frac{1}{E - E_s + i \alpha_s/2} . \tag{5.2.13}$$

This result shows that around the doorway state energies the real and imaginary parts of the complex potential vary like the interference and resonance terms of the Breit-Wigner expressions. Far below the lowest doorway state energy, the imaginary part goes to a constant value, very small compared to that of the O.M. Transients around the lowest doorway state energy will be discussed in § 5.3.

We now obtain the total cross section. Applying Equation (2.2.38), the T-matrix element of Equation (5.2.10) is calculated as

$$T_{fi} = 2\pi \Big\{ \langle v_f \, U'' \chi_i^{(+)} \rangle + $$

$$+ \sum_s f_s(E) \langle \chi_f^{(-)} PHq_1 \varphi_s \rangle \langle \varphi_s q_1 HP \tilde{\Psi}_i^{(+)} \rangle \Big\}. \qquad (5.2.14)$$

Applying the formal solution of Equation (5.2.10) to Equation (5.2.14) as § 2.5, we have

$$\langle \varphi_s q_1 HP \tilde{\Psi}_i^{(+)} \rangle$$

$$\cong \frac{\langle \varphi_s q_1 HP \chi_i^{(+)} \rangle}{1 - f_s(E) \langle \varphi_s q_1 HP \frac{1}{E^{(+)} - PHP} PHq_1 \varphi_s \rangle}. \qquad (5.2.15)$$

Now $\chi^{(-)}$ defined by Equation (2.2.36) will be related to $\chi^{(+)}$ so that $\langle \chi^{(-)} PHq_1 \varphi_s \rangle$ may be written in terms of $\langle \chi^{(+)} PHq_1 \varphi_s \rangle$.

$$\chi_f^{(-)} = v_f + \frac{1}{E - i\eta - PHP} U'' v_f$$

$$= \chi_f^{(+)} + \left(\frac{1}{E - i\eta - PHP} - \frac{1}{E + i\eta - PHP} \right) U'' v_f$$

$$= \chi_f^{(+)} + 2\pi i \, \delta(E - PHP) \, U'' v_f . \qquad (5.2.16)$$

By Equations (5.2.16) and (2.2.34), we have

$$\langle \chi_f^{(-)} PHq_1 \varphi_s \rangle = \langle \chi_f^{(+)} PHq_1 \varphi_s \rangle - 2\pi i \sum_c \langle v_f \, U'' \chi_c^{(+)} \rangle \langle \chi_c^{(+)} PHq_1 \varphi_s \rangle$$

$$= \sum_c (\underset{\sim}{S}^P)_{fc} \langle \chi_c^{(+)} PHq_1 \varphi_s \rangle, \qquad (5.2.17)$$

where

$$(PHP - E)\,\chi_c^{(+)} = 0$$

and where

$$(\underset{\sim}{S}^P)_{cc'} \equiv \delta_{cc'} - 2\pi i \langle U_c \, U'' \chi_{c'}^{(+)} \rangle , \qquad (5.2.18)$$

which is the S-matrix element of the potential scattering. Applying Equations (5.2.15) and (5.2.17), Equation (5.2.14) becomes

$$T_{fi} = 2\pi \langle U_f \, U'' \chi_i^{(+)} \rangle +$$

$$+ 2\pi \sum_s \sum_c S_{fc}^P \frac{\langle \chi_c^{(+)} PHq_1 \varphi_s \rangle \langle \varphi_s q_1 HP \chi_i^{(+)} \rangle}{E - E_s - \Delta_s + \frac{i}{2}(\alpha_s + \Gamma_s^{(D)})} , \qquad (5.2.19)$$

where

$$\Delta_s \equiv \sum_c \mathcal{P} \int_0^\infty d\varepsilon \, \frac{|\langle \varphi_s q_1 HP \chi_c^{(+)}(\varepsilon) \rangle|^2}{E - \varepsilon} , \qquad (5.2.20)$$

and

$$\Gamma_s^{(D)} \equiv 2\pi \sum_c |\langle \varphi_s q_1 HP \chi_c^{(+)}(E) \rangle|^2 . \qquad (5.2.21)$$

In the case of a single open channel $(\alpha l S J M)$, the potential scattering S-matrix is given by

$$S_{cc}^P = e^{2i\delta_{ls}^J} , \qquad (5.2.22)$$

where δ^J_{ls} is the phase shift. Denoting the n-th doorway state constants with subscript n, the total cross section is obtained from Equation (2.2.29)

$$\sigma^T = 2\pi\lambda^2 g^J Re\left[i\, T^J_{\alpha ls;\alpha ls}\right]$$

$$= \pi\lambda^2 g^J \left\{ 4\sin^2\delta^J_{ls} - \right.$$

$$- \frac{2(E-E_n-\Delta_n)\Gamma_n^{(D)}\sin 2\delta^J_{ls} + (\alpha_n+\Gamma_n^{(D)})\Gamma_n^{(D)}(1-\cos 2\delta^J_{ls})}{(E-E_n-\Delta_n)^2 + \frac{1}{4}(\alpha_n+\Gamma_n^{(D)})^2}$$

$$\left. + \frac{(\alpha_n+\Gamma_n^{(D)})\Gamma_n^{(D)}}{(E-E_n-\Delta_n)^2 + \frac{1}{4}(\alpha_n+\Gamma_n^{(D)})^2} \right\}. \qquad (5.2.23)$$

This is the Breit-Wigner form[4] with modified resonance parameters. The first term is the potential scattering. The third term is the doorway state resonance and the second is the interference between the potential scattering and the doorway state resonance. From the form, $\Gamma_n^{(D)}$ is the formation probability of the n-th doorway state. After the doorway state is formed, it decays into the more complicated states with probability α_n, as well as into the free state.

Next, the S-wave absorption cross section may be calculated using Equations (2.4.11) and (5.2.19).

$$\alpha' = \alpha \quad , \quad \ell' = \ell = 0 \quad , \text{ and } J = S \text{ (channel spin).}$$

We obtain

$$\sigma_{\ell=0}^{ab} = \pi \lambda^2 \left(1 - |S_{os}^{s}|^2 \right)$$

$$= \pi \lambda^2 \left\{ 2i \, \mathrm{Im} \, T_{os;os}^{s} - |T_{os;os}^{s}|^2 \right\}$$

$$= \pi \lambda^2 \sum_n \frac{\alpha_n \Gamma_n^{(D)}}{(E - E_n - \Delta_n)^2 + \frac{1}{4}(\alpha_n + \Gamma_n^{(D)})^2} \, . \qquad (5.2.24)$$

In the absorption cross section as well as the total cross section, the doorway state strength function, α_n, appears in the place of Γ_γ, the γ-decay width in the single level Breit-Wigner formula. α_n is, in general, energy dependent, but is expected to be almost constant. The transmission coefficient is obtained as

$$T_{\ell=0} = \sum_n \frac{\alpha_n \Gamma_n^{(D)}}{(E - E_n - \Delta_n)^2 + \frac{1}{4}(\alpha_n + \Gamma_n^{(D)})^2} \qquad (5.2.25)$$

$$\cong \frac{2\pi \langle \alpha_n \Gamma_n^{(D)} \rangle}{D_d \langle \alpha_n + \Gamma_n^{(D)} \rangle} \, , \qquad (5.2.26)$$

where D_d is the spacing between the doorway states. The S-wave absorption cross section at very low energy has a $1/v$-dependence as in the usual O.M. result:

$$\sigma^{ab}_{\ell=0} = \pi\lambda^2 \sum_n \sqrt{\frac{E_n}{E}}\ \frac{\alpha_n}{E_n^2}\ \Gamma_n^{(D)}(E_n). \qquad (5.2.27)$$

However, the magnitude of the coefficients is very different. This will be discussed in § 5.3.

5.3 Concluding Remarks

From Equations (5.2.12) and (5.2.13), the imaginary potential tends towards a constant value below the lowest doorway state (further illustration for the transient variation of the potential may be seen later). Furthermore, the results indicate the local fluctuation of the O.M. potential. The total cross section has the Breit-Wigner form in the vicinity of the doorway state. Such variations may be seen around 0.2, 0.4, and 0.7 Mev in the Na^{23} cross section.

A crude picture of the modified O.M. potential may be given by making the assumption that

$$PHq_1\varphi_n\rangle\langle\varphi_n q_1 HP \cong PHq_1\varphi_{n'}\rangle\langle\varphi_{n'} q_1 HP. \qquad (5.3.1)$$

This implies that the formation probabilities of all the doorway states are the same. The imaginary part of the modified O.M. potential near a doorway state is given by

$$F_2(E) \cong \left[\frac{\alpha_n/2}{(E-E_n)^2+(\alpha_n/2)^2} + \sum_{\substack{n' \\ (E_{n'}>E_n)}} \frac{\alpha_{n'}/2}{(E_{n'})^2} + \right.$$

$$\left. + \sum_{\substack{n'' \\ (E_{n''}<E)}} \frac{\alpha_{n''}/2}{(E_n)^2} \right] PHq_1\varphi_n\rangle\langle\varphi_n q_1 HP. \qquad (5.3.2)$$

Some properties of this potential may be described in relation to the imaginary part of the O.M. potential. Taking another average of the modified O.M. equation over a wide energy range so that the doorway states are smeared out, the O.M. potentials are derived with the results:

$$\left.\begin{aligned} \overline{F_1} &\cong 0 , \\ \overline{F_2} &\cong \frac{\pi}{D_\alpha} P H q_1 \varphi_n \rangle\langle \varphi_n q_1 H P . \end{aligned}\right\} \qquad (5.3.3)$$

The potential F_2 varies as a Lorentzian and the ratio of the peak value to the O.M. imaginary potential is given by

$$\frac{F_2(E_n)}{\overline{F_2}} \cong \frac{2D_\alpha}{\pi \alpha_n}\left[1 + \frac{1}{4}\sum_{n'}\frac{\alpha_n \alpha_{n'}}{(E_{n'})^2} + \frac{1}{4}\sum_{n'}\frac{\alpha_n \alpha_{n''}}{(E_n)^2}\right] . \qquad (5.3.4)$$

The ratio of F_2 at $E = 0$ to the O.M. imaginary potential is obtained by

$$\frac{F_2(0)}{\overline{F_2}} \cong \frac{1}{2\pi}\sum_n \frac{\alpha_n D_\alpha}{(E_n)^2} . \qquad (5.3.5)$$

The variation of F_2 with energy may be illustrated using Ni^{58} as an example. The constants $\alpha_n (= \Gamma^{\downarrow})$, $\Gamma^{(D)} (= \Gamma^{\uparrow})$, and D_α are given in Table II.2 of Part II. The values for the ratio $F_2(E_n)/\overline{F_2}$ are approximately 1 for the doorway state at 205 kev, and 2 for the doorway states at 410 and 580 kev. Another doorway state exists at 65 kev with $\alpha_s \simeq$ 40 kev and $F_2(E_n)/\overline{F_2} \simeq 1$.

The constants of the last doorway state are obtained from the resonance width distribution in BNL - 325 . The value of the ratio $F_2(0)/\overline{F_2}$ is approximately 0.17. The imaginary part of the modified O.M. potential is thus drawn in Figure I.6.

The curve in this figure indicates four properties. First, it shows a decrease of the imaginary potential to a small value below the lowest doorway state. Second, it shows the overall decrease of the

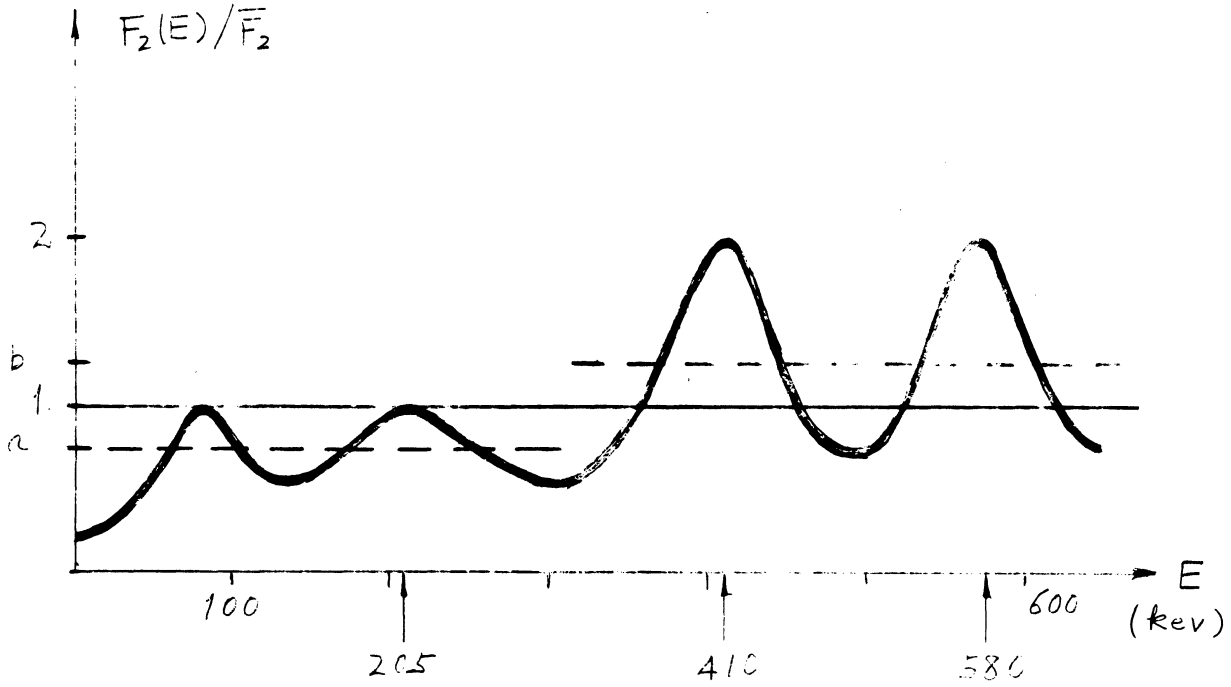

Figure I.6. Imaginary Potentials of the Modified O.M. and the O.M. for N_i-58.

imaginary potential with decreasing energy. These two properties are in accordance with O.M. calculations fitting energy dependent problems to N_a^{23} data. The following two additional properties were not expected at the stage of the ad hoc calculation. Third, there are local variations of the imaginary potential around the doorway states.

Corresponding to it, the total cross section has a Breit-Wigner form, Equation (5.2.23). This form of the E-dependence of the E-averaged measured total cross section may be observed in Figure II.29. The last property which is obtained from the curve is the existence of the two groups of $1/v$ dependent resonances separated at $\sim$ 300 kev. By close observation of the total cross section in Figure II.29 connected to that (below 100 kev) of the natural N_i (the abundance of N_i^{58} is 67.88%) in BNL - 325, the two $1/v$ separated at $\sim$ 300 kev may be found and the ratio of the proportional constants is observed to be 1.6. Taking a local average of $F_2(E)/\overline{F_2}$ above and below 300 kev (b and a respectively), the ratio b/a is approximately 1.6. Besides the first three properties, this result indicates that the curve in Figure I.6 is fairly meaningful without regard to the assumption, Equation (3.3.1).

CHAPTER 6

SUMMARY

In Chapter 4 we have smeared out the more complicated states by the energy-average process and left explicitly only the doorway states. The result is given in Equation (4.1.19). We may expect that this modified O.M. works well in the lower energy region where cross section data are required by reactor physicists. Furthermore, the interpolation and extrapolation of the modified O.M. over nearby nuclei is possible if we know the systematics of the doorway state constants.

In the case of the single doorway state, the total cross section is calculated in Equation (5.1.25) which shows the Breit-Wigner form.

As mentioned in the introduction to Part I, this part of the work has been independently worked out and published by the MIT-group.[61] For convenience of detailed comparison, equations obtained in Reference 61 will be listed below. Our work has been done for the specific purpose of improving the O.M. However, their theoretical objects and our theoretical objects are the same, and moreover the MIT-group's work has been better known among physicists. From now on, therefore, we call the theory as a whole "the intermediate structure of cross sections", and notations will be changed to theirs:

$$\alpha_s \longrightarrow \Gamma^{\downarrow}$$

$$\Gamma_s^{(D)} \longrightarrow \Gamma^{\uparrow}$$

$$\Delta_s \longrightarrow \Delta^{\uparrow} \ (\text{or} \ \Delta_d)$$

$$\alpha_s + \Gamma_s^{(D)} \longrightarrow \Gamma_d \ (= \Gamma^{\uparrow} + \Gamma^{\downarrow})$$

The physical discussions and conclusions which are not given in the previous chapters may be seen in Reference 61. One may also find many observed cross sections in that reference.

Reference 61	Ours
(2.31)	(4.1.2)
(2.91)	(4.1.19)
(2.49)	(5.2.9)
(2.88)	(5.2.10)
(2.50), (2.75)	(5.2.17)
(2.51), (2.52), (2.76)	(5.2.18)
(2.56)	S-wave part of (5.2.22)

The O.M. potential is well known. It yields only a coarse result. At the opposite extreme is the generalized O.M. which yields exact results, while its potential is not known in general. The modified O.M. yields better cross sections than the O.M. Its potential form is known and depends only on the doorway state constants. These constants will be obtained by analysis of the resonance width distribution and the cross section in Part II.

There is a lower limit even for the modified O.M. to apply. The spacings of the resonances are almost constant in energy, but the experimental resolution as well as the interval of interest takes smaller energy intervals into account at low energies. Below a certain

energy, the range Δ' cannot contain enough resonances for the averaging process discussed in Section 4.1 to be used.

On the other hand, the modified O.M. applies in the higher energy region. There, we meet with the MIT's problem of the intermediate structure of cross sections; for example, the bump-type deviation from the O.M. cross section which may be seen above 2 Mev in Figure I.6. The bumps resulting from E-averaging of cross sections with fine resonances are also called the intermediate structure. In our case of Ni^{58}, such structures exist at 580, 410, 205, and 65 Mev. This aspect of the problem is the subject matter of Part II of this thesis.

PART II

THE FINE STRUCTURE OF DOORWAY STATES

Introduction

In this part of the thesis, we determine the details of the total cross section around a doorway state. We find poles of the T-matrix, evaluate their residues, and analyze their detailed effects on the energy dependence of cross section. These properties mainly depend on the magnitudes of the doorway state constants $\Gamma^{\uparrow}$ and $\Gamma^{\downarrow}$, and on the average resonance spacing $\overline{D}$. The results of the study will be applied to the analysis of the measured cross section and resonance parameters in the low energy region to find the doorway states and to determine their constants.

In Chapter 1, we present the general theory of a single doorway state. In Chapter 2, the analytic properties of the T-matrix are investigated in detail, applying the infinite Picket-Fence model. In Chapter 3, the fine structure and intermediate structure of the total cross section, and the resonance width distribution around the doorway state, will be given and compared with experiments. Finally, the intermediate structure at high energies will be discussed.

CHAPTER 1

FINE STRUCTURE OF THE DOORWAY STATES

In this chapter the fine structure of the doorway states will be investigated in a general way. The detailed properties will be pursued in the subsequent chapters.

In § 1.1, under the single doorway state assumption, we decompose the resonant part of T-matrix into two factors: the branching ratio, $\underset{\sim}{G}$, and the structure factor (see Equation (1.1.14)). There may be more than one open channel, and inelastic channels may be included.

In § 1.2, we will demonstrate the unitarity of the S-matrix on the real E-axis. In § 1.3, we show that the poles of the S-matrix are confined to the lower half E-plane (more precisely, the unphysical E-plane). In other words, the single doorway state model does not violate the general requirements placed on the S-matrix.

In § 1.4, we expand the T-matrix into a series of the multichannel Breit-Wigner form. The fine structure of the total cross section may then be obtained. Corresponding to the above series expansion of the T-matrix, the total cross section is expressed by a series. The first, second, thrid terms, etc., of the total cross section represent the doorway state resonance, the isolated resonance under the influence of the doorway state, the interference of two resonances, etc. Carrying out the expansion through the isolated resonance terms, the cross section is written in a form as close as possible to the Breit-Wigner formula. To do so, we will define the "doorway state phase shift".

Comparing the form of the cross section to the Breit-Wigner formula, we will show that the existence of the doorway state is reflected in the fine structure of the total cross section.

In § 1.5, we will define terminologies "weak coupling limit" (WCL), "strong coupling limit" (SCL). We then exhibit the behavior of the fine structure in these limits.

In § 1.6, sum rules for the poles of the T-matrix will be given. Their possible applications will be discussed.

1.1 T-Matrix of a Single Doorway State

A system of equations in the projection operator formalism will be rederived similar to those in Part I. Then, the T-matrix element of a single doorway state will be obtained.

The Schrödinger equation of our system has been decomposed into a system of equations, Equation (2.2.6) of Part I. We will limit the problem to an energy interval $(E - I/2,\ E + I/2)$ such that

$$E_j^A < E \pm I/2 < E_{j+1}^A , \tag{1.1.1}$$

where E_j^A is the j-th excitation energy of the target nucleus. Equation (2.5.2) of Part I is

$$(QHQ - E_\ell)\chi_\ell = 0. \tag{1.1.2}$$

Now, we will define two projection operators Q_1 and Q_2 in terms of the orthonormal eigenfunctions of Equation (1.1.2) according to

$$\begin{aligned} Q_1 &\equiv \sum_k{}' \chi_k \rangle\langle \chi_k , \\ \text{and} \qquad Q_2 &\equiv Q - Q_1 , \end{aligned} \tag{1.1.3}$$

where the sum over k ranges over all eigenfunctions whose energies E_k satisfy

$$E - I/2 \leq E_k \leq E + I/2 . \tag{1.1.4}$$

Obviously, the projection operators P and Q_1 satisfy the following relations,

$$\left.\begin{aligned} PQ_1 = Q_1 P = 0 , \quad P^2 = P, \quad Q_1^2 = Q_1 \\ P + Q_1 \neq 1 \quad (\text{in } \mathcal{E}^1 \otimes \tilde{\mathcal{E}}^A) . \end{aligned}\right\} \tag{1.1.5}$$

Applying $Q = Q_1 + Q_2$ to Equation (2.2.6) of Part I, we may rederive the same form of equations,

$$\left.\begin{aligned} (P\mathcal{H}P - E)P\Psi &= -P\mathcal{H}Q_1 Q_1 \Psi \\ (Q_1 \mathcal{H} Q_1 - E) Q_1 \Psi &= - Q_1 \mathcal{H} P P \Psi , \end{aligned}\right\} \tag{1.1.6}$$

where

$$\begin{aligned} \mathcal{H} &\equiv H + H Q_2 \frac{1}{E - Q_2 H Q_2} Q_2 H \\ &= H^A + K + U'' + Q_1 V_2 Q_1 + P(H + V_2) Q_1 + \\ &\quad + Q_1 (H + V_2) P , \end{aligned} \tag{1.1.7}$$

$$V_2 \equiv H Q_2 \frac{1}{E - Q_2 H Q_2} Q_2 H , \tag{1.1.8}$$

and U'' is given by Equations (2.1.9), (2.2.10), and (2.5.3) of Part I;

$$U'' = U + PV_2P.$$

Next we presume the existence of projection operators q_1 and q_2 (e.g. § 4.1 of Part I) such that

$$\left.\begin{aligned} &Q_1 = q_1 + q_2, \\ &PHq_1 \neq 0, \text{ and } PHq_2 = 0. \end{aligned}\right\} \tag{1.1.9}$$

Equation (1.1.6) becomes

$$\begin{aligned} &(PHP - E)P\Psi = -PHq_1q_1\Psi, \\ &(q_1Hq_1 - E)q_1\Psi = -q_1Hq_2q_2\Psi - q_1HPP\Psi, \\ &(q_2Hq_2 - E)q_2\Psi = -q_2Hq_1q_1\Psi. \end{aligned} \tag{1.1.10}$$

The distorted wave T-matrix of Equation (1.1.10) is obtained from Equations (2.2.38), (2.6.6), and (2.6.8) of Part I. After some algebra, it becomes

$$T_{fi} = T^P_{fi} + T^R_{fi}, \tag{1.1.11}$$

where

$$T^P_{fi} \equiv 2\pi \langle U_f U'' \chi_i^{(+)} \rangle, \tag{1.1.12}$$

and

$$\begin{aligned} T^R_{fi} \equiv 2\pi \Big\langle \chi_f^{(-)} PHq_1 \Big[&E - q_1Hq_1 - \\ &- q_1Hq_2 \frac{1}{E - q_2Hq_2} q_2Hq_1 - q_1HP \frac{1}{E^{(+)} - PHP} PHq_1 \Big]^{-1} \times \\ &\times q_1HP\chi_i^{(+)} \Big\rangle. \end{aligned} \tag{1.1.13}$$

By the single doorway state assumption, Equation (1.1.13) is reduced to a simple form (the tilde underneath denotes a matrix)

$$\underset{\sim}{T}^{R} = \underset{\sim}{G}\,\frac{\Gamma^{\uparrow}}{E - E_0 - \sum_n \frac{a_n^2}{E - E_n}}\,, \tag{1.1.14}$$

where

$$\underset{\sim}{G} \equiv \underset{\sim}{S}^{P}\cdot\underset{\sim}{\Gamma}^{\uparrow}/\Gamma^{\uparrow}\,, \tag{1.1.15}$$

$$\underset{\sim}{S}^{P} \equiv \underset{\sim}{1} - i\,\underset{\sim}{T}^{P}\,, \tag{1.1.16}$$

$$(\underset{\sim}{\Gamma}^{\uparrow})_{ji} \equiv 2\pi \langle \chi_j^{(+)} P\mathcal{H} q_1 \psi_s \rangle \langle \psi_s q_1 \mathcal{H} P \chi_i^{(+)} \rangle\,, \tag{1.1.17}$$

$$E_0 \equiv E_s + \Delta_d - i\,\frac{\Gamma^{\uparrow}}{2}\,, \tag{1.1.18}$$

$$\Gamma^{\uparrow} \equiv \mathrm{Trace}\,(\underset{\sim}{\Gamma}^{\uparrow})\,, \tag{1.1.19}$$

$$\Delta_d \equiv \mathrm{Trace}\,(\underset{\sim}{\Delta})\,, \tag{1.1.20}$$

$$(\underset{\sim}{\Delta})_{ji} \equiv \mathcal{P}\int_0^{\infty} \frac{\langle \chi_{\varepsilon j}^{(+)} P\mathcal{H} q_1 \psi_s \rangle \langle \psi_s q_1 \mathcal{H} P \chi_{\varepsilon i}^{(+)} \rangle}{E - \varepsilon}\, d\varepsilon\,, \tag{1.1.21}$$

and

$$a_n^2 \equiv |\langle \psi_s q_1 \mathcal{H} q_2 \phi_n \rangle|^2\,. \tag{1.1.22}$$

The constants Δ_d and $\Gamma^{\uparrow}$ are the generalizations of the doorway state shift and doorway state formation probability.(61) a_n^2 is related to $\Gamma^{\downarrow}$, the decay probability of the doorway state to the more complicated states, by

$$\Gamma^{\downarrow} = \frac{2\pi}{D}\langle a_n^2 \rangle\,. \tag{1.1.23}$$

In Equation (1.1.14), the factor $\underset{\sim}{G}$ will be called the "branching ratio". It becomes a significant factor to determine the existence of giant poles due to the doorway states. The remaining factor will be called the "structure factor" which determines the fine structure of doorway states.

1.2 Unitarity of the S-matrix

We will first prove that the unitarity of $\underset{\sim}{S}^P$, the potential part of the S-matrix. Then, we will first prove that the entire S-matrix is unitary. In this way, we show that the single doorway state assumption does not violate the requirement of flux conservation.

The S-matrix is related to the T-matrix by

$$\underset{\sim}{S} = \underset{\sim}{1} - i\,\underset{\sim}{T}. \tag{1.2.1}$$

The matrix element of $\underset{\sim}{T}^P$ is given by Equation (1.1.12). By Equation (1.1.16),

$$(\underset{\sim}{S}^P)^+ \underset{\sim}{S}^P = \underset{\sim}{1} + i\left(\underset{\sim}{T}^{P\,+} - \underset{\sim}{T}^P\right) + \underset{\sim}{T}^{P\,+}\,\underset{\sim}{T}^P. \tag{1.2.2}$$

After some algebra, we have the following relation;

$$\begin{aligned}\langle \chi_f^{(+)} U'' v_i \rangle &= \langle v_f\, U''\, \chi_i^{(+)} \rangle + \\ &\quad + 2\pi i \langle v_f\, U''\, \delta(E - PHP)\, U''\, v_i \rangle \\ &= \langle v_f\, U''\, \chi_i^{(+)} \rangle + 2\pi i \sum_c \langle v_f\, U'' \chi_{Ec}^{(+)} \rangle \langle \chi_{Ec}^{(+)}\, U''\, v_i \rangle,\end{aligned} \tag{1.2.3}$$

where Equation (2.2.34) of Part I has been applied. This implies that

$$i(\underset{\sim}{\Gamma}^{P\dagger} - \underset{\sim}{\Gamma}^{P}) + \underset{\sim}{\Gamma}^{P\dagger}\underset{\sim}{\Gamma}^{P} = 0. \tag{1.2.4}$$

Thus, $\underset{\sim}{S}^{P}$ is unitary,

$$(\underset{\sim}{S}^{P})^{+}\underset{\sim}{S}^{P} = \underset{\sim}{1}. \tag{1.2.5}$$

Now, Equations (1.1.11), (1.1.12), (1.1.14), (1.1.15), (1.1.16), and (1.2.1) yield

$$\begin{aligned}\underset{\sim}{S} &= \underset{\sim}{S}^{P} - i\frac{\underset{\sim}{S}^{P}\underset{\sim}{\Gamma}^{\uparrow}}{E - E_0 - \sum_n \frac{a_n^2}{E-E_n}} \\ &= \underset{\sim}{S}^{P}\underset{\sim}{S}^{R},\end{aligned} \tag{1.2.6}$$

where we have defined

$$\underset{\sim}{S}^{R} \equiv \underset{\sim}{1} - i\frac{\underset{\sim}{\Gamma}^{\uparrow}}{E - E_0 - \sum_n \frac{a_n^2}{E-E_n}} \tag{1.2.7}$$

which will be called the resonant part of S-matrix. Since $\underset{\sim}{S}^{P}$ is unitary, we have

$$\begin{aligned}\underset{\sim}{S}^{+}\underset{\sim}{S} = \underset{\sim}{S}^{R+}\underset{\sim}{S}^{R} &= 1 + \frac{1}{\left|E - E_0 - \sum_n \frac{a_n^2}{E-E_n}\right|^2} \times \\ &\times \Big\{(\underset{\sim}{\Gamma}^{\uparrow})^{+}\underset{\sim}{\Gamma}^{\uparrow} + i(\underset{\sim}{\Gamma}^{\uparrow})^{+}\Big(E - E_0 - \sum_n \frac{a_n^2}{E-E_n}\Big) - \\ &- i\,\underset{\sim}{\Gamma}^{\uparrow}\Big(E - E_0^{*} - \sum_n \frac{a_n^2}{E-E_n}\Big)\Big\}.\end{aligned} \tag{1.2.8}$$

By the definition of $\Gamma^{\uparrow}$, Equation (1.1.17), we may show that

$$(\underset{\sim}{\Gamma}^{\uparrow})^{+} = \underset{\sim}{\Gamma}^{\uparrow}, \qquad (1.2.9)$$

and $$(\underset{\sim}{\Gamma}^{\uparrow})^{2} = \Gamma^{\uparrow}\,\underset{\sim}{\Gamma}^{\uparrow}.$$

From these properties together with Equations (1.1.18) and (1.1.19), we see immediately that the expression in braces vanishes. Thus,

$(\underset{\sim}{S}^{R})^{+}\underset{\sim}{S}^{R} = \underset{\sim}{1}$ and $\underset{\sim}{S}$ is unitary.

1.3 Poles of the T-Matrix

We will study the fine structure of the doorway states through consideration of analytic structure of the T-matrix. We, therefore, analytically continue the T-matrix defined for real E by Equation (1.1.14) onto the complex E-plane.

Let us call the analytically continued T-matrix the "extended T-matrix". The E-dependence of this extended T-matrix is quite complicated. To avoid the complexity, the T-matrix will be approximated on a limited domain by the "statistical T-matrix". Then, properties of the poles of the statistical T-matrix will be studied.

We assume that we may deal with intervals I and Δ which satisfy the following conditions: In addition to the condition given by Equation (1.1.2), the interval I is large enough so that

(a) $\langle a_n^2 \rangle$ and $\bar{D}$ distribute uniformly over I .

(b) V_2 can be independent of E .

(c) Edge effects may be neglected around the center of I .[34]

Such an interval will be fixed centered at E_c (Figure II.1).

The subinterval Δ will be set centered at E_c satisfying the following:

(d) Δ is small enough for $\underset{\sim}{S}^P$, $\underset{\sim}{\Gamma}^\uparrow$, and $\Delta - \frac{i}{2}\Gamma^\uparrow$ to be independent of E, c.f. Equations (3.2.3) and (3.2.4) of Part I.

(e) $\Delta \gg \bar{D}$

Similar to the statistical collision matrix (§ 1.2 of Part I), we thus define the statistical T-matrix according to:

$$J_{fi}(E, E_c) \equiv T^P_{fi}(E_c) + \frac{\underset{\sim}{G}_{fi}(E_c)\,\Gamma^\uparrow(E_c)}{E - E_0(E_c) - \sum_n \frac{a_n^2}{E - E_n}} , \qquad (1.3.1)$$

where $T^P_{fi}(E_c)$ is T^P_{fi} at $E = E_c$, etc. By the assumptions (b) and (d), we have

$$T_{fi} \cong J_{fi}(E, E_c) , \qquad (1.3.2)$$

for E in the subinterval Δ. The statistical T-matrix is easily continued analytically over the entire E-plane. We expect that the extended T-matrix is well approximated by the statistical T-matrix on the domain $\mathcal{d}$ sketched in Figure II.1.

The analytic structure of the statistical T-matrix will be studied. First we note that the statistical T-matrix is a meromorphic function with poles located at the n + 1 zeroes ζ_i of the expression

$$f(E) \equiv E - E_0 - \sum_{n=1}^{N} \frac{a_n^2}{E - E_n} . \qquad (1.3.3)$$

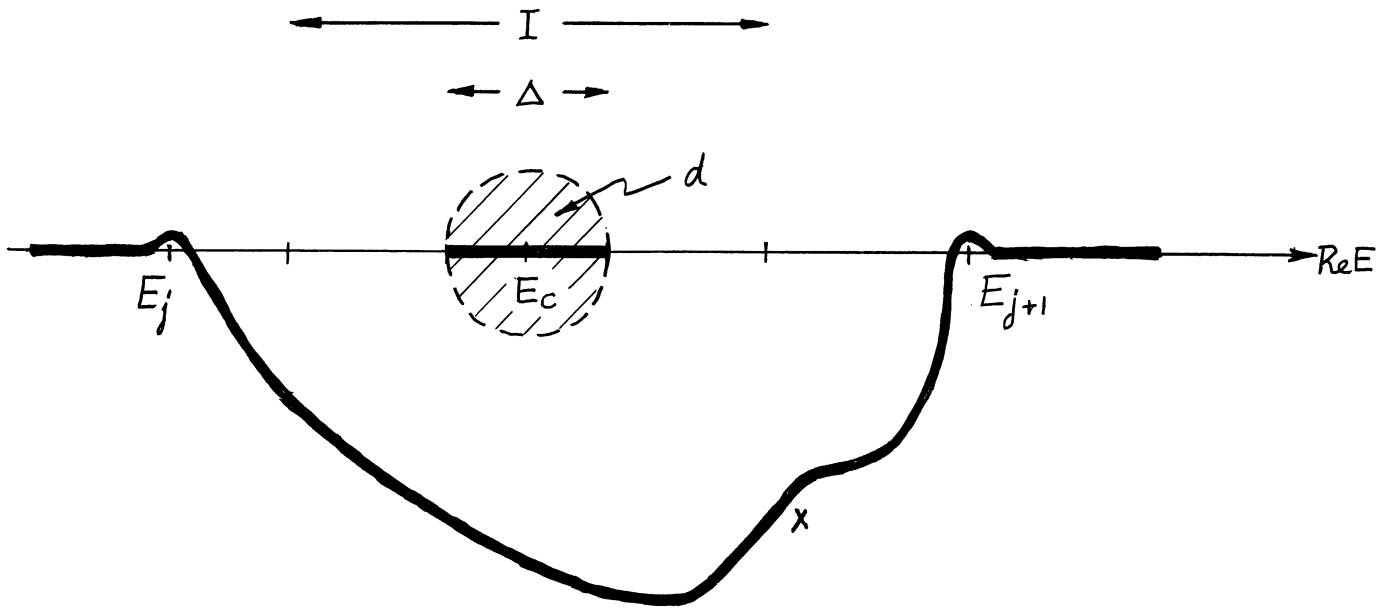

Figure II.1. Intervals I and Δ, and Domain d on a Complex E-plane.

It is easy to see that these zeroes lie in the lower half E-plane, since writing $\zeta_i = \alpha_i + i\beta_i$ we obtain

$$\beta_i + \beta_i \sum_n \frac{a_n^2}{(\alpha_i - E_n)^2 + \beta_i^2} = \mathrm{Im}\, E_0 < 0 .$$

The zeroes are sometimes expressed by ξ_i, where $\zeta_i \equiv E_i + \xi_i$ for i = 0, 1, ... , N. In terms of these zeroes, f(E) becomes

$$f(E) = E - E_0 - \sum_{i=1}^{N} \frac{a_i^2}{E - E_i} = \frac{\prod_{k=0}^{N} (E - \zeta_k)}{\prod_{i=1}^{N} (E - E_i)} , \qquad (1.3.4)$$

and Equation (1.1.14) becomes

$$\underset{\sim}{T}^R = \underset{\sim}{G}\, \Gamma^{\uparrow} \prod_{i=1}^{N} (E - E_i) \Big/ \prod_{k=0}^{N} (E - \zeta_k) . \qquad (1.3.5)$$

We call the pole at $E=\zeta_0$, the "doorway state" pole.

The resonant part of T-matrix, $\underset{\sim}{I}^R$, will be expanded into a series of the form of the multi-level formula. We may easily show the following formula:

$$\prod_{m=1}^{N}(E-\zeta_m) = \prod_{m=1}^{N}(E-E_m) - \sum_{k=1}^{N}\sum_{m_1<\cdots<m_k}^{N}\xi_{m_1}\xi_{m_2}\cdots\xi_{m_k}\prod_{m(\neq m_1\cdots m_k)}^{N\prime}(E-\zeta_m). \tag{1.3.6}$$

Then, $\underset{\sim}{I}^R$ becomes

$$\underset{\sim}{I}^R = \frac{\underset{\sim}{G}\Gamma^{\uparrow}}{E-E_0}\left\{1+\sum_{m_1=1}^{N}\frac{\xi_{m_1}}{E-\zeta_{m_1}}+\cdots\right.$$

$$\left.\cdots+\sum_{m_1<\cdots<m_k}\frac{\xi_{m_1}\cdots\xi_{m_k}}{(E-\xi_{m_1})\cdots(E-\xi_{m_k})}+\cdots\right\}. \tag{1.3.7}$$

When the ξ's are small, this expression is useful.

All information is given in terms of the poles of $\underset{\sim}{I}^R$. We may immediately write sum rules for these poles. From Equation (1.3.4) we have

$$(E-E_0)\prod_{i=1}^{N}(E-E_i) - \sum_{n=1}^{N}a_n^2\prod_{i(\neq n)}^{N\prime}(E-E_i)$$

$$= \prod_{k=0}^{N}(E-E_k-\xi_k). \tag{1.3.8}$$

By comparison of the coefficients of E^N , we have[82]

$$\sum_{k=0}^{N} \xi_k^{\,r} = 0, \tag{1.3.9}$$

$$\sum_{k=0}^{N} \xi_k^{\,i} = 0, \tag{1.3.10}$$

and from the coefficients of E^{N-1} and Equations (1.3.9) and (1.3.10),

$$\sum_{n=1}^{N} a_n^2 \sum_{\substack{i=1 \\ (\neq n)}}^{N} E_i = \sum_{i=0}^{N} \left\{ (\zeta_i^{\,r})^2 - (\zeta_i^{\,i})^2 - E_i^2 + 2i\, \zeta_i^{\,r} \zeta_i^{\,i} \right\}. \tag{1.3.11}$$

$$\therefore \quad \sum_{i=0}^{N} \zeta_i^{\,r} \xi_i^{\,i} = 0, \tag{1.3.12}$$

where the superscripts r and i refer to the real and imaginary parts of the constants. The imaginary part of the doorway state pole is related to those of the remaining poles by

$$\zeta_0^{\,i} = -\frac{\Gamma^{\uparrow}}{2} + \xi_0^{\,i} = -\frac{\Gamma^{\uparrow}}{2} - \sum_{k=1}^{N} \xi_k^{\,i}. \tag{1.3.13}$$

Applying the condition that all the poles are in the lower half plane to Equation (1.3.13), we have

$$(0 \leq) \; -\sum_{k=1}^{N} \xi_k^{\,i} < \frac{\Gamma^{\uparrow}}{2}. \tag{1.3.14}$$

From Equations (1.3.8) and (1.3.10), we have

$$\zeta_0^r = \frac{\sum_{k=1}^{N} \xi_k^i \zeta_k^r}{\sum_{k=1}^{N} \xi_k^i} . \qquad (1.3.15)$$

The doorway state energy, ζ_0^r , is given by an average of fine resonance energies weighted by their widths. Formally, this is the same as the center of mass theorem in the direct reaction theory where the single particle energy is equal to an average of excitation energy weighted by a spectroscopic factor.(106)

1.4 Fine Structure of Total Cross Sections

If the potential scattering S-matrix is diagonal, $S_{cc'} = \delta_{cc'} \times$ $\times \exp(2i\delta_{ls}^J)$, the diagonal part of the T-matrix,

$$\underset{\sim}{T} = \frac{1}{i}\left(\underset{\sim}{1} - \underset{\sim}{S}\right) + \underset{\sim}{G}\Gamma^{\uparrow} \frac{\prod_n (E - E_n)}{(E-\zeta_0)\prod_n (E-\zeta_n)}, \qquad (1.4.1)$$

gives the total cross section (see Equation (2.2.29) of Part I);

$$\sigma_T = 2\pi\lambda^2 \sum_J g^J \sum_{ls} \mathrm{Re}\left(i\, T^J_{\alpha ls;\alpha ls}\right)$$

$$= 2\pi\lambda^2 \sum_J g^J \sum_{ls} \left[1 - \cos 2\delta_{ls}^J - \right.$$

$$\left. - \mathrm{Im}\, G^J_{\alpha ls;\alpha ls} \Gamma^{\uparrow} \frac{\prod_n (E - E_n)}{(E-\zeta_0)\prod_n (E-\zeta_n)} \right]. \qquad (1.4.2)$$

Corresponding to the expansion given in Equation (1.3.5), we have

$$\sigma_T = \sigma^P + \sigma^R_d + \sigma^R_{f_1} + \sigma^R_{f_2} + \cdots , \qquad (1.4.3)$$

where the potential scattering cross section σ^P is given by

$$\sigma^P \equiv 2\pi \lambda\!\!\!^{-2} \sum_J g^J \sum_{ls} (1 - \cos 2\delta) , \qquad (1.4.4)$$

(the super- and sub-scripts of the phase shifts are suppressed), and where we have written

$$\sigma^R_d \equiv 2\pi \lambda\!\!\!^{-2} \sum_J g^J \times$$

$$\times \sum_{ls} \frac{-\Gamma^{\uparrow}_{lsJ} (E - \zeta_0^r) \sin 2\delta - \Gamma^{\uparrow}_{lsJ} \zeta_0^i \cos 2\delta}{(E - \zeta_0^r)^2 + (\zeta_0^i)^2} ; \qquad (1.4.5)$$

the doorway state cross section,

$$\sigma^R_{f_1} \equiv 2\pi \lambda\!\!\!^{-2} \sum_J g^J \sum_{ls} \sum_{m=1}^{N} \frac{|\xi_m|}{|E - \zeta_0|} \times$$

$$\times \frac{-\Gamma^{\uparrow}_{lsJ} (E - \zeta_m^r) \sin 2(\delta + \delta_d) - \Gamma^{\uparrow}_{lsJ} \zeta_m^i \cos 2(\delta + \delta_d)}{(E - \zeta_m^r)^2 + (\zeta_m^i)^2} ; \qquad (1.4.6)$$

corresponding to isolated fine resonances, and where $\sigma^R_{f_2}$,..., etc. are interference cross sections. In Equation (1.4.6), we have defined the doorway state phase shift δ_d by

$$\tan 2\delta_d \equiv \frac{\zeta_0^i (\zeta_m^r - E_m) + \zeta_m^i (E - \zeta_0^r)}{(E - \zeta_0^r)(\zeta_m^r - E_m) - \zeta_0^i \zeta_m^i} . \qquad (1.4.7)$$

Since the expansion of the total cross section in Equation (1.4.3) has the same form as the Breit-Wigner multi-level expansion,[4] any discrepancy of σ_{α}^{R} and $\sigma_{f_1}^{R}$ from the single level Breit-Wigner formula[4] is a reflection of the effects of the doorway state. Compared results are as follows:

(a) σ_{α}^{R} and $\sigma_{f_1}^{R}$ have the Breit-Wigner forms[4] with resonance parameters given by the poles of the doorway state T-matrix.

(b) In $\sigma_{f_1}^{R}$, there is an additional phase shift $\delta\alpha$.

(c) In $\sigma_{f_1}^{R}$, a modulation factor,

$$|\xi_m| / |E - \zeta_0|,$$

indicates another effect of the presence of the doorway state on the shape of the fine resonance.

A Limiting Case

The simplest model from which immediate results may be obtained is the "weak coupling limit", WCL, which is treated in detail in Chapter 2. In this model $\Gamma^{\downarrow} \ll \Gamma^{\uparrow}$ which implies that the a_n^2 in the dispersion relation (1.3.1) may be treated as a perturbation. Thus,

$$\zeta_0 \cong E_0' - \frac{i}{2}\Gamma^{\uparrow}, \qquad (1.4.8)$$

and

$$\zeta_n \cong E_n + \frac{a_n^2}{E_n - E_0}.$$

The poles distribute in the complex E-plane as a Lorentizian with width $\Gamma^{\uparrow}$.[82] In this model, for the single open channel case, the cross

sections become

$$\sigma_d^R = 2\pi \lambda^2 g^J \frac{-\Gamma^\uparrow (E-E_0') \sin 2\delta + \frac{1}{2}(\Gamma^\uparrow)^2 \cos 2\delta}{(E-E_0')^2 + \frac{1}{4}(\Gamma^\uparrow)^2} , \quad (1.4.9)$$

$$\sigma_{fl}^R = -2\pi \lambda^2 g^J \sum_n \frac{\Gamma^\uparrow |\xi_n|}{|E-\zeta_0|} \times$$

$$\times \frac{(E-\zeta_n^r)\sin 2(\delta+\delta_d) + \zeta_n^i \cos 2(\delta+\delta_d)}{(E-\zeta_n^r)^2 + (\zeta_n^i)^2} . \quad (1.4.10)$$

The modulation factor becomes

$$\frac{|\xi_n|}{|E-\zeta_0|} = \frac{a_n^2}{(E_n-E_0')^2 + \frac{1}{4}(\Gamma^\uparrow)^2} \quad (1.4.11)$$

at $E \simeq E_n$, and the doorway state phase shift is simply

$$\tan 2\delta_d = \frac{-\Gamma^\uparrow (E_n-E_0')}{(E_n-E_0')^2 - \frac{1}{4}(\Gamma^\uparrow)^2} . \quad (1.4.12)$$

Finally, the total cross section is sketched in Figure II.2 for the case where the potential phase shift $\delta = 0$.

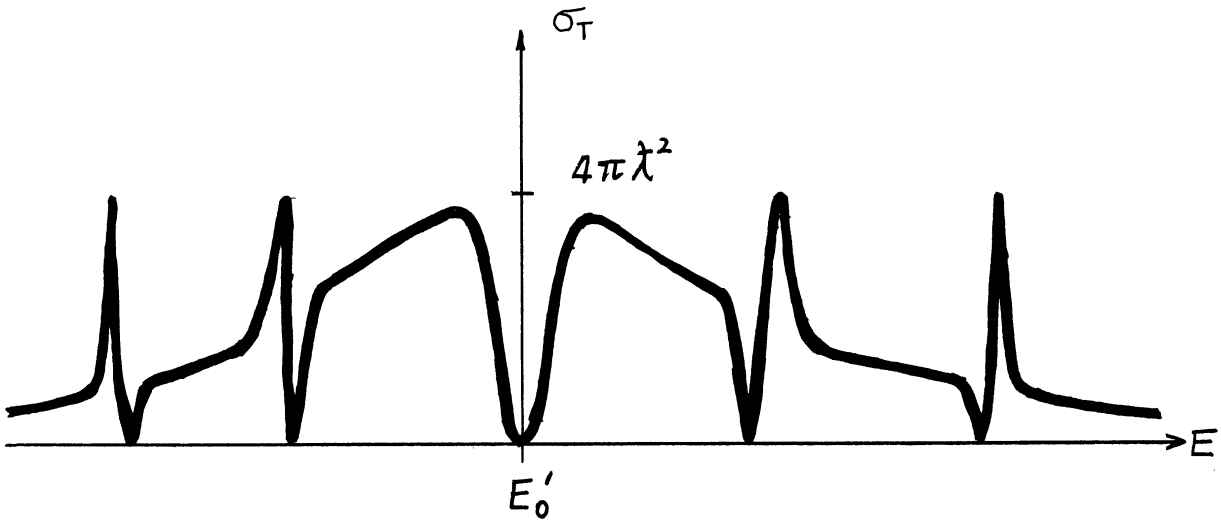

Figure II.2. Fine Structure of Total Cross Section at WCL.

CHAPTER 2

INFINITE PICKET FENCE MODEL

In this chapter, we investigate the analytic properties of the T-matrix using the infinite Picket-Fence model. We expand the T-matrix into a Mittag-Leffler series, and evaluate the poles and residues.

In § 2.1, the existing region of poles and the paths are obtained. In § 2.2, the pole distributions will be calculated as a function of $\Gamma^{\uparrow}/\bar{D}$ and $\Gamma^{\downarrow}/\bar{D}$. In § 2.3, the residues will be estimated.

In the Picket-Fence model, it is assumed that the R-matrix constants, i.e., the reduced widths and the spacings, do not vary from one level to another.[34] We apply this model to the more complicated states. In this case, a_n^2 and $E_{n+1} - E_n$ are independent of n, and are equated to $\langle a_n^2 \rangle$ and $\bar{D}$ respectively. If the number of states, N, is finite, we call the model the finite Picket Fence model (see Appendix C). When N is infinite and when the sum over n is taken as a double limit,

$$\sum_n = \lim_{N\to\infty} \sum_{n=-N}^{N}, \tag{2.0.1}$$

we call the model the infinite Picket Fence model. Deviation from the above models will be discussed in Appendix C.

The resonant part of the T-matrix, Equation (1.1.14), is written as

$$\underset{\sim}{T}^R = \underset{\sim}{G}\,\frac{\Gamma^{\uparrow}}{E - E_0 - \lim\limits_{N\to\infty}\sum\limits_{n=-N}^{N}\frac{\langle a_n^2\rangle}{E - n\bar{D}}}\,. \qquad (2.0.2)$$

The sum may be evaluated using the identity,

$$\sum_{n=-\infty}^{\infty}\frac{1}{x - n\pi} = \cot x, \qquad (2.0.3)$$

with the result

$$\underset{\sim}{T}^R = \underset{\sim}{G}\,\frac{-2V_0\tan z}{(z - z_0)\tan z - t}\,, \qquad (2.0.4)$$

where we have defined the non-dimensional parameters z , z_0 , V_0 , and t according to

$$\left.\begin{aligned} z &= \frac{E}{\bar{D}/\pi}\,, \\ z_0 &= \frac{E_0}{\bar{D}/\pi} = v_0 + i V_0 \\ V_0 &= -\frac{\Gamma^{\uparrow}/2}{\bar{D}/\pi}\,, \\ t &= \frac{\Gamma^{\downarrow}/2}{\bar{D}/\pi}\,. \end{aligned}\right\} \qquad (2.0.6)$$

For the single open channel case, the T-matrix element is just

$$T = \frac{1}{i}\left(1 - e^{2i\delta}\right) + e^{2i\delta}\,\frac{-2V_0\tan z}{(z - z_0)\tan z - t}\,. \qquad (2.0.7)$$

2.1 Poles of the T-matrix

The equation for the poles of the T-matrix is given by

$$t = (z - z_0) \tan z , \tag{2.1.1}$$

where t is real and positive,

$$z \equiv u + iv ,$$

$$z_0 \equiv u_0 + iv_0 ,$$

$$v_0 < 0 , \text{ and } -\pi/2 \leq u_0 \leq \pi/2 .$$

We may take $u_0 \geq 0$ without loss of generality and we shall do so.

Taking the real and imaginary parts of Equation (2.1.1), we have

$$\frac{1}{2} \cdot \frac{(u-u_0)\sin 2u - (v-v_0)\sinh 2v}{\cos^2 u + \sinh^2 v} = t \geq 0 , \tag{2.1.2}$$

and

$$-\frac{v-v_0}{\sinh 2v} = \frac{u-u_0}{\sin 2u} . \tag{2.1.3}$$

From Equations (2.1.2) and (2.1.3),

$$\frac{1}{2} \frac{u-u_0}{\sin 2u} \left\{ \frac{\sin^2 2u + \sinh^2 2v}{\cos^2 u + \sinh^2 v} \right\} = t \geq 0 . \tag{2.1.4}$$

Since the expression in the braces is positive, we have

$$-\frac{v-v_0}{\sinh 2v} = \frac{u-u_0}{\sin 2u} \geq 0. \tag{2.1.5}$$

Therefore, the regions in which poles are located may be obtained:

$$v_c \leq v \leq 0,$$

$$n\pi \leq u \leq (n+\tfrac{1}{2})\pi \qquad \text{for } n \geq 1,$$

$$u_0 \leq u \leq \pi/2,$$

$$(n-\tfrac{1}{2})\pi \leq u \leq n\pi \qquad \text{for } n \leq 0,$$

and

$$-\frac{v-v_0}{\sinh 2v} = \frac{|u-u_0|}{|\sin 2u|} \geq |u-u_0|. \tag{2.1.6}$$

The regions are shown in Figure II.3.

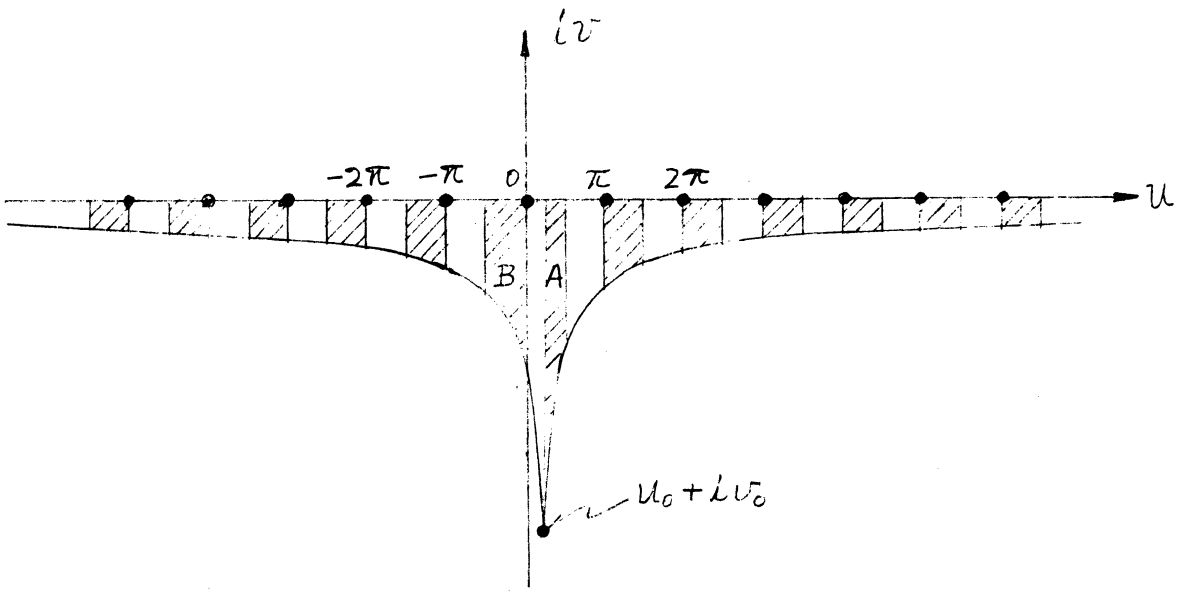

Figure II.3. Existing Regions of Poles. The anomalous pole is in the region A, and the central poles are in the regions A and B. The remaining poles are in the other shadowed areas. The dots show the locations when t = 0.

There is one and only one pole in each of the shaded regions in Figure II.3. This may be shown directly by application of the argument principle. However, it is sufficient to point out that, for $t = 0$, the roots of $(z-z_0)\tan z = 0$ are simple roots, and that the roots are continuous functions of the parameter t.

For $t=0$, the poles lie at

$z = z_0$ (anomalous pole),

$z = 0$ (regular central pole),

and $z = n\pi$, $n \neq 0$ (other regular poles).

These poles are marked on the corner of each shaded region (Figure II.3) by a black dot.

Paths of the Poles

As t increases, each pole traverses a path in its region from the point $z = n\pi$ to the point $z = (n+\frac{1}{2})\pi$ which is its limiting value at $t \to \infty$. The general shape of such a path is shown in Figure II.4, while the path is determined by Equation (2.1.3).

We call this path the n-th path. If, for comparison, we move all paths into the strip $0 \leq u \leq \pi/2$, we see that the n-th path contains the (n + 1)-st path. In fact, we have

$$-\frac{v_n - v_0}{\sinh 2v_n} = \frac{u_n - u_0}{\sin 2u_n},$$

and

$$-\frac{v_{n+1} - v_0}{\sin 2v_{n+1}} = \frac{u_{n+1} - u_0}{\sin 2u_{n+1}}.$$

But $v_{n+1} = v_n + \pi$. Thus

$$-\frac{v_n - v_0}{\sin 2v_n} = -\frac{v_{n+1} - v_0}{\sinh 2v_{n+1}} \left[1 + \frac{\pi}{v_n - v_0}\right],$$

which implies $v_n < v_{n+1}$. This situation is pictured in Figure II.5.

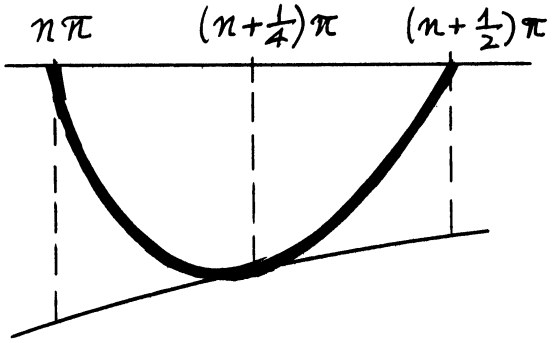

Figure II.4. The n-th Path.

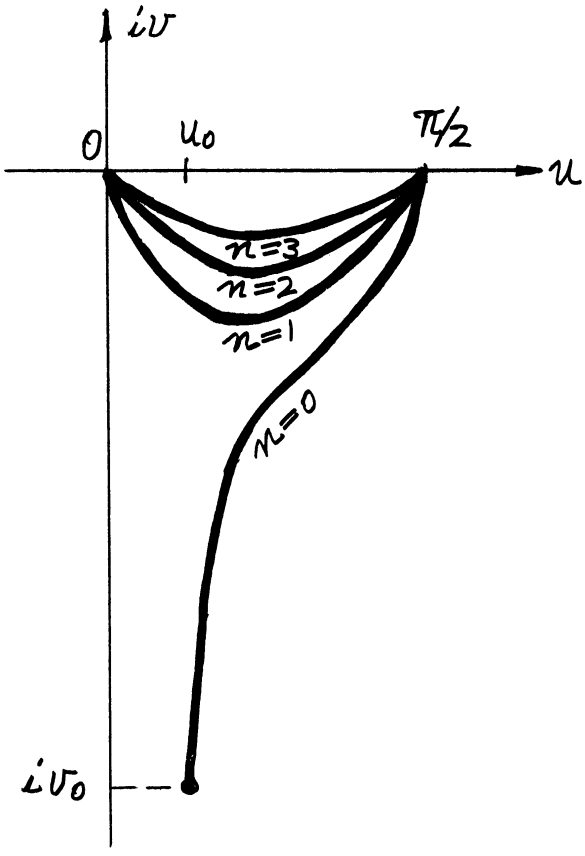

Figure II.5 Paths of the Poles.

2.2 Pole Distributions

In this section, the distribution of poles will be studied as a function of the coupling strengths. Let us call the two poles in a strip $-\pi/2 < u \leq \pi/2$ the "central poles". In § 2.2.1, properties of the central poles will be studied. These are classified according to the value of the parameter t . More specifically, the classification will be given by $t \gg t_\alpha$, $t > t_\alpha$, $t \sim t_\alpha$, $t < t_\alpha$, and $t \ll t_\alpha$ which will be called the "weak coupling limit" (WCL), "weak coupling" (WC), "intermediate coupling" (IC), "strong coupling" (SC), and "strong coupling limit" (SCL) respectively, where t_α will be defined later. Let us call these altogether the "situation of coupling strengths" (SCS). Enough data for IC will be supplied by the study of only the central pole. In §§ 2.2.2, the pole distributions for WCL and WC will be calculated. In §§ 2.2.3, those for SCL and SC will be obtained.

2.2.1 Central Poles

Consider first the case $u_0 = 0$. When t = 0 , the two central poles lie on the imaginary axis at the points 0 and $i v_0$. We are thus led to look for these poles on the imaginary axis for non-zero values of t as well. With this ansatz (u = 0) , Equation (2.1.2) becomes

$$-\frac{1}{2}\,\frac{(v - v_0)\sinh 2v}{1 + \sinh^2 v} = t \geq 0 . \qquad (2.2.1)$$

The left hand side of this equation is sketched in Figure II.6.

As can be seen from Figure II.6, there are two solutions of Equation (2.2.1) when t is sufficiently small. As t increases, these

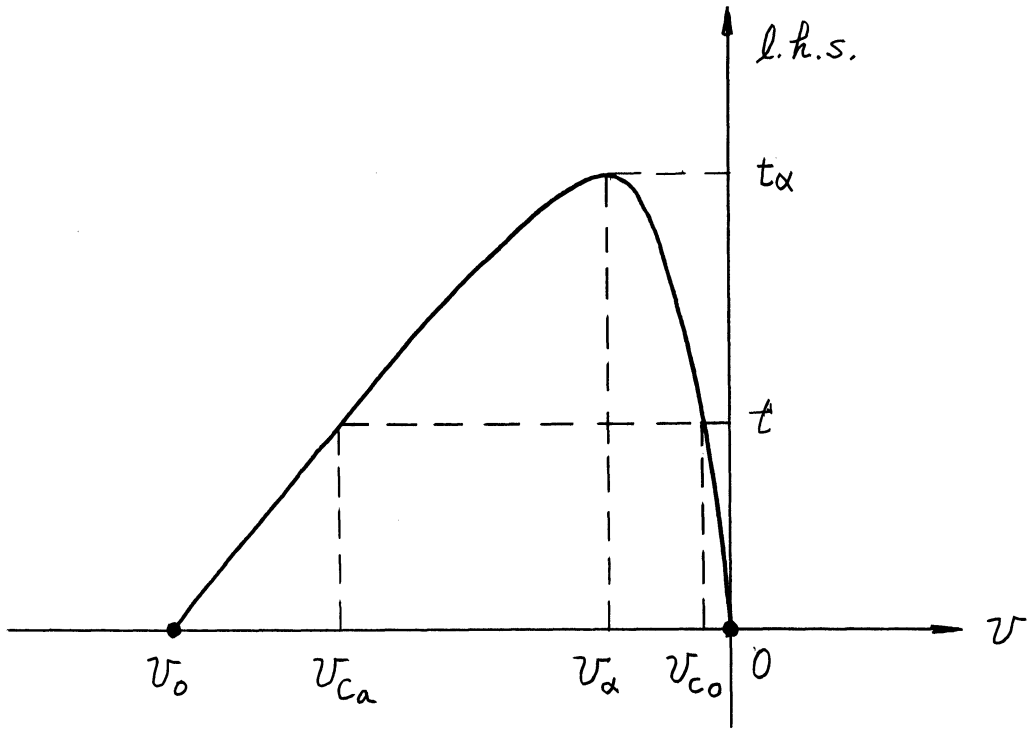

Figure II.6. Graphical Determination of Central Poles at $u_0 = 0$.

solutions, starting at 0 and $i v_\alpha$, move towards each other along the imaginary axis. They coalesce at $v = v_\alpha$ when $t = t_\alpha$. This defines t_α , the determining parameter for the SCS . t_α depends upon v_0 . In fact, the following relations are easy to show:

$$\sqrt{t_\alpha^2 + t_\alpha} + \sinh^{-1}\sqrt{t_\alpha} = -v_0 , \tag{2.2.2}$$

and

$$v_\alpha = -\sinh^{-1}\sqrt{t_\alpha} . \tag{2.2.3}$$

Hence, the SCS depends upon both v_0 and t, i.e., upon $\Gamma^{\uparrow}/\bar{D}$ and $\Gamma^{\downarrow}/\bar{D}$.

For $t > t_\alpha$, the ansatz $u = 0$ is no longer valid, and in fact the two central poles depart from the imaginary axis, as shown by the paths labelled $u_0 = 0$ in Figure II.7.

Note that in the limit of large $-v_0$, t_α approaches $-v_0$, or

$$\lim_{-v_0 \to \infty} \frac{t_\alpha}{t} = \frac{\Gamma^{\uparrow}}{\Gamma^{\downarrow}}.$$

Thus, for large values of $\Gamma^{\uparrow}/\bar{D}$, the SCS is determined entirely by the ratio $\Gamma^{\uparrow}/\Gamma^{\downarrow}$.

When $u_0 = 0$, the two central poles coalesce as $t \to t_\alpha$. For $t \gtrsim t_\alpha$, the anomalous pole is no longer distinct from the regular poles. This has a marked effect upon the T-matrix, and is the basic difference between the SC and the WC, since in the WC the anomalous poles makes a distinctly different contribution to the T-matrix.

For $u_0 \neq 0$, the general situation is shown in Figure II.7. Here again the parameter t_α may be used to determine the SCS. If we define $t^*(u_0)$ to be that value of t which, for a given value of u_0, leads to a pole at $\zeta_\alpha^i = v_\alpha$, (e.g. $t^*(0) = t_\alpha$), we find

$$t^*(\pi/2) = t_\alpha + 1,$$

and

$$\frac{dt^*}{du_0} \geq 0.$$

In other words, $t_\alpha \leq t^*(u_0) \leq t_\alpha + 1$. In fact, t^* can be shown to satisfy

$$2f = \sin 2(u_0 + f).$$

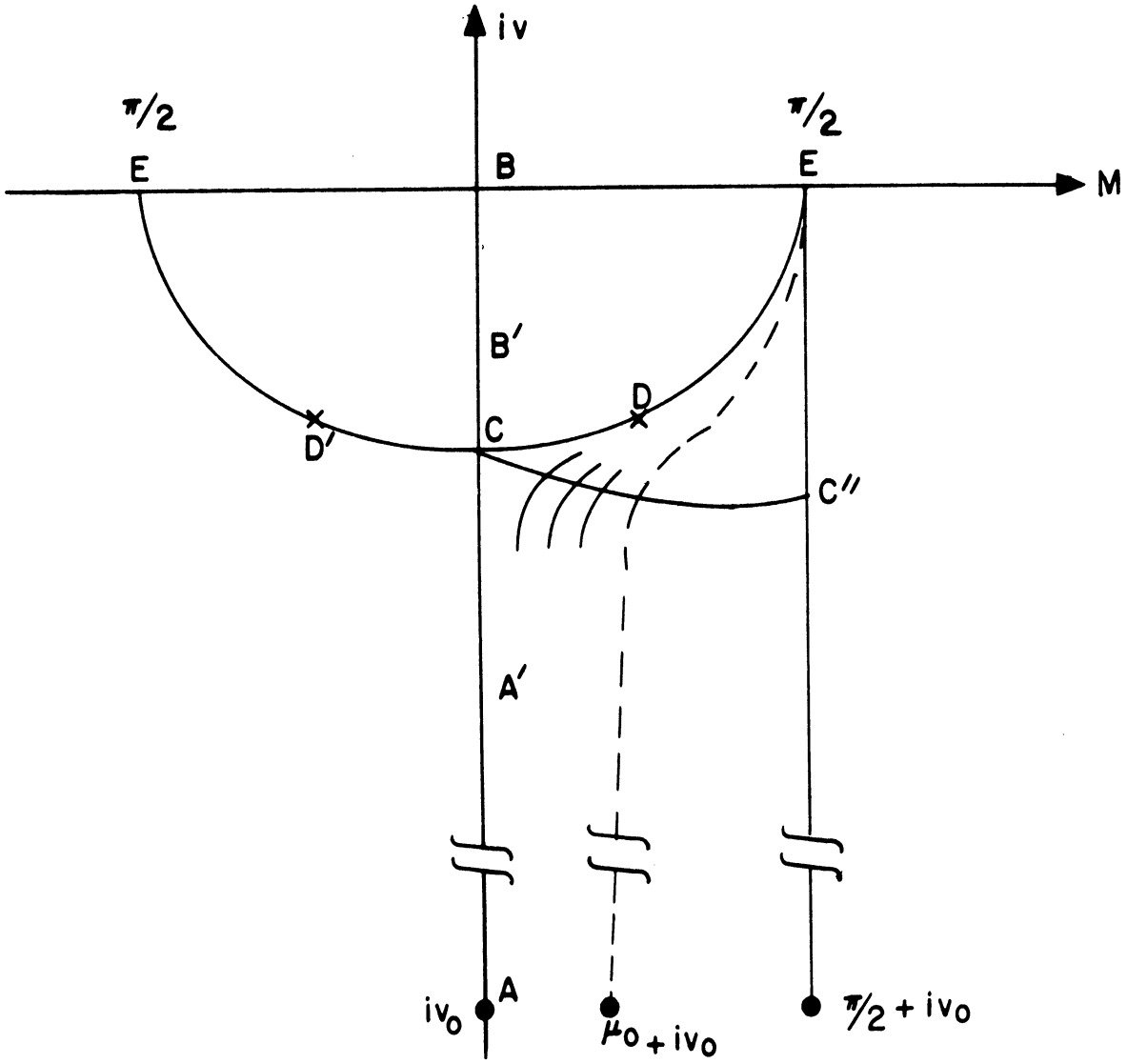

Figure II.7. Paths of the Central Poles. For $u_0 = 0$, the central poles move along the lines AA'CDE and BB'CD'E' for $t = 0$, $t < t_\alpha$, $t \sim t_\alpha$ and $t > t_\alpha$. For $u_0 \neq 0$, the path is given by the broken line. Particularly when $u_0 = \pi/2$, the path is the straight line perpendicular to the u-axis. The location of the anomalous pole when $t = t_\alpha$ is on the line CC'' when the u_0 is varied.

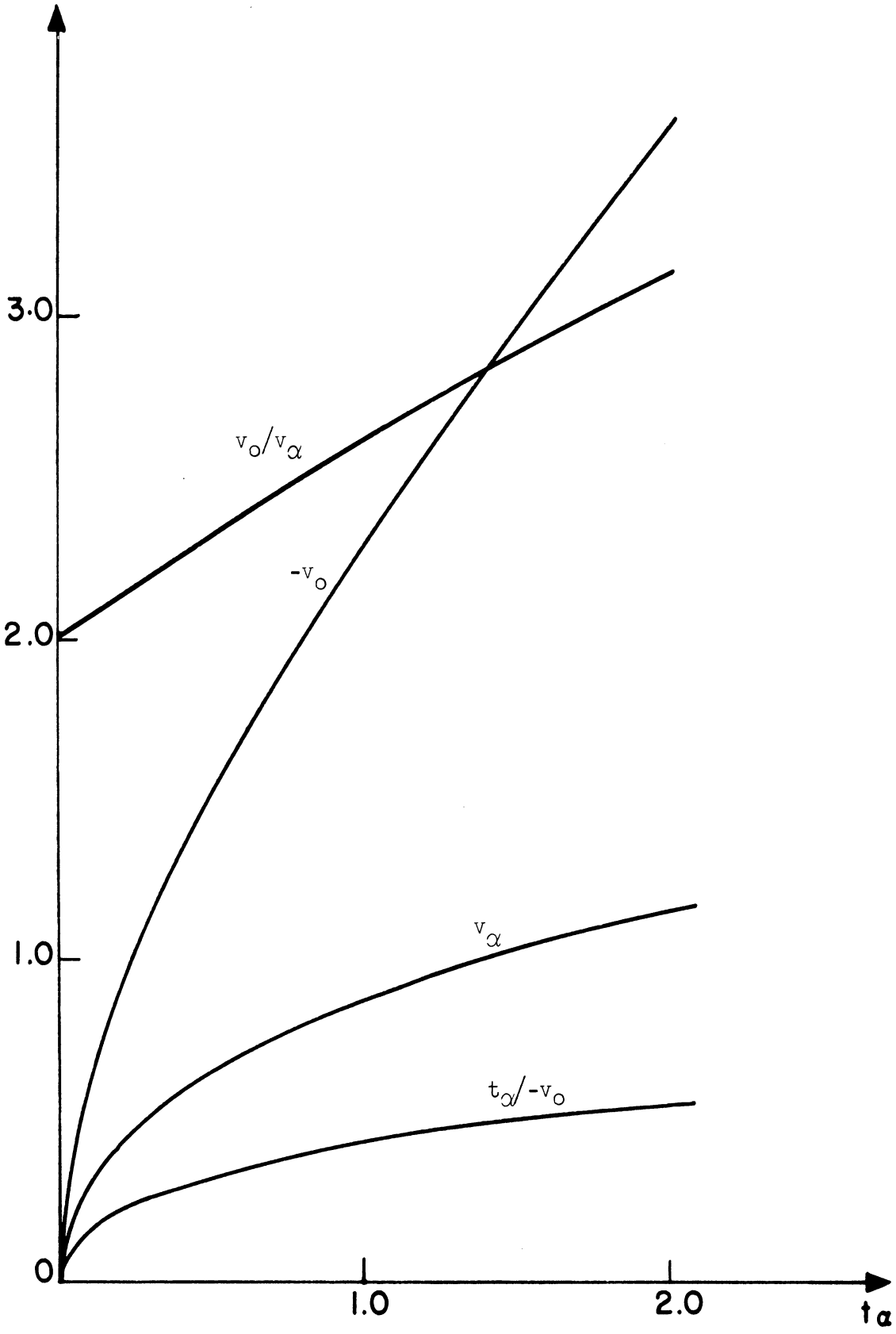

Figure II.8. Constants at the Point C of Figure II.16.

TABLE II.1

CONSTANTS AT THE POINT C OF FIGURE 7

v_α' ; v of the anomalous pole at $t = t_\alpha$ and $u_0 = \pi/2$

t_α	$-v_0$	$-v_\alpha$	v_0/v_α	$t_\alpha/-v_0$	$-v_\alpha'$
0	0	0	2	0	0
0.1	0.642	0.310	2.071	0.156	0.571
0.2	0.924	0.434	2.129	0.216	0.817
0.3	1.148	0.524	2.191	0.261	0.928
0.4	1.345	0.597	2.253	0.297	1.04
0.5	1.524	0.658	2.316	0.328	1.12
0.6	1.692	0.712	2.376	0.355	1.19
0.7	1.852	0.761	2.434	0.378	1.26
0.8	2.005	0.805	2.491	0.400	1.31
0.9	2.152	0.844	2.550	0.418	1.37
1.0	2.296	0.882	2.603	0.435	1.43
1.2	2.572	0.947	2.716	0.475	1.49
1.4	2.839	1.006	2.822	0.494	1.50
1.6	3.097	1.057	2.930	0.517	1.62
1.8	3.349	1.103	3.036	0.538	1.67
2.0	3.596	1.146	3.138	0.556	1.72
5.0	7.021	1.543	4.550	0.713	2.16
10.0	12.36	1.87	6.610	0.812	2.52
20.0	22.70	2.20	10.32	0.880	2.83
30.0	32.90	2.40	13.71	0.913	3.03
40.0	43.04	2.54	16.94	0.929	3.18
50.0	53.13	2.63	20.20	0.940	3.29
60.0	63.24	2.74	23.08	0.950	3.39

where $f^2 \equiv (t^* - t_\alpha)(1 + t_\nu - t^*)$. Thus, except for $-v_0 \ll 1$, t_α is a valid measure for the SCS .

2.2.2 Weak and Strong Couplings

For $t = 0$, the poles are located at z_0 (anomalous pole) and at $n\pi$. Solving Equation (2.1.1) iteratively we obtain

$$\zeta_n \cong n\pi + \frac{t}{n\pi - z_0} \qquad \text{for the regular poles,} \qquad (2.2.4)$$

and

$$\zeta_a \cong z_0 + \frac{t}{\tan z_0} \qquad \text{for the anomalous pole.} \qquad (2.2.5)$$

For WC , it is necessary to use the expressions obtained by iterating one more time.

$$\zeta_n \cong n\pi + \frac{t}{n\pi - z_0 + \dfrac{t(1 + t/3)}{n\pi - z_0}}$$

for the regular poles, (2.2.6)

$$\zeta_\alpha \cong z_0 + \frac{t}{\tan\left(z_0 + \dfrac{t}{\tan z_0}\right)}$$

for the anomalous pole . (2.2.7)

For SC , we must be more careful. It is true that as $t \to \infty$, $\zeta_n \to (n + \frac{1}{2})\pi$. However, this limit is not uniform in n . Hence, the limiting value of $(n + 1/2)\pi$ is not a useful starting point for an iterative calculation designed to obtain approximate locations of all the poles. Instead we write

$$g \equiv t - v_0 \gg -v_0, \qquad (2.2.8)$$

and consider solutions of

$$\left[z-(u_0+iv_0)\right]\tan z = q+v_0,$$

for a fixed value of g in the neighborhood of $v_0 \approx 0$. The results are

(a) 0th approximation, $\zeta_n = u_n^\infty$, where u_n^∞ is real and satisfies:

$$(u_n^\infty - u_0)\tan u_n^\infty = q, \qquad n\pi < u_n^\infty < (n+\tfrac{1}{2})\pi. \tag{2.2.9}$$

(b) 1st approximation:

$$\zeta_n = u_n^\infty + \frac{(u_n^\infty - u_0)v_0 + iqv_0}{q^2+q+(u_n^\infty-u_0)^2}. \tag{2.2.10}$$

(c) 2nd approximation:

$$\zeta_n = u_n^\infty + \frac{v_0 + \dfrac{iv_0q}{u_n^\infty-u_0}}{u_n^\infty + \dfrac{tq}{u_n^\infty-u_0} - z_0 + \dfrac{\left(v_0+\dfrac{iv_0q}{u_n^\infty-u_0}\right)\left(1+\dfrac{v_0}{3}+\dfrac{i}{3}\dfrac{v_0q}{u_n^\infty-u_0}\right)}{u_n^\infty+\dfrac{tq}{u_n^\infty-u_0}-z_0}}. \tag{2.2.11}$$

The substitution $q = t - v_0$ is implied in the above results.

One could also write approximate expressions for the central poles in IC , but these results are not included here, since numerical analysis is required in any event.

2.2.3 Summary

The paths and locations of the poles are illustrated by a numerical calculation in Figures II.9 and II.10. The sample is $-U_0 = 58.5$ and t is varied from 0 to ∞ . The curves of A_0 , A_1 , A_2 , A_5 , A_{10} , and A_{15} are the paths of the cells of n = 0, 1, 2, 5, 10, and 15 respectively. In addition, 6 curves B_i have been drawn through the points $\zeta_n(t_i)$ for a fixed value of t_i . The values of t_i and $t_i/-U_0$ are listed below for B_i .

$-U_0 = 58.5$ and $u_0 = 0$

B_i	t_i	$t_i/-U_0$
B_1	13.6	0.232
B_2	50.2	0.857
B_3	55.3 ($= t_\alpha$)	0.944
B_4	56.0	0.956
B_5	75.2	1.285
B_6	87.8	1.500

The point C is the position of the two poles in coincidence. The value of t_α is $55.3 (\simeq -U_\alpha)$.

Figure II.10a illustrates the pattern of the pole distribution.

(1) The black circles indicate the poles when t = 0 . There is no coupling between the doorway state and the more complicated states.

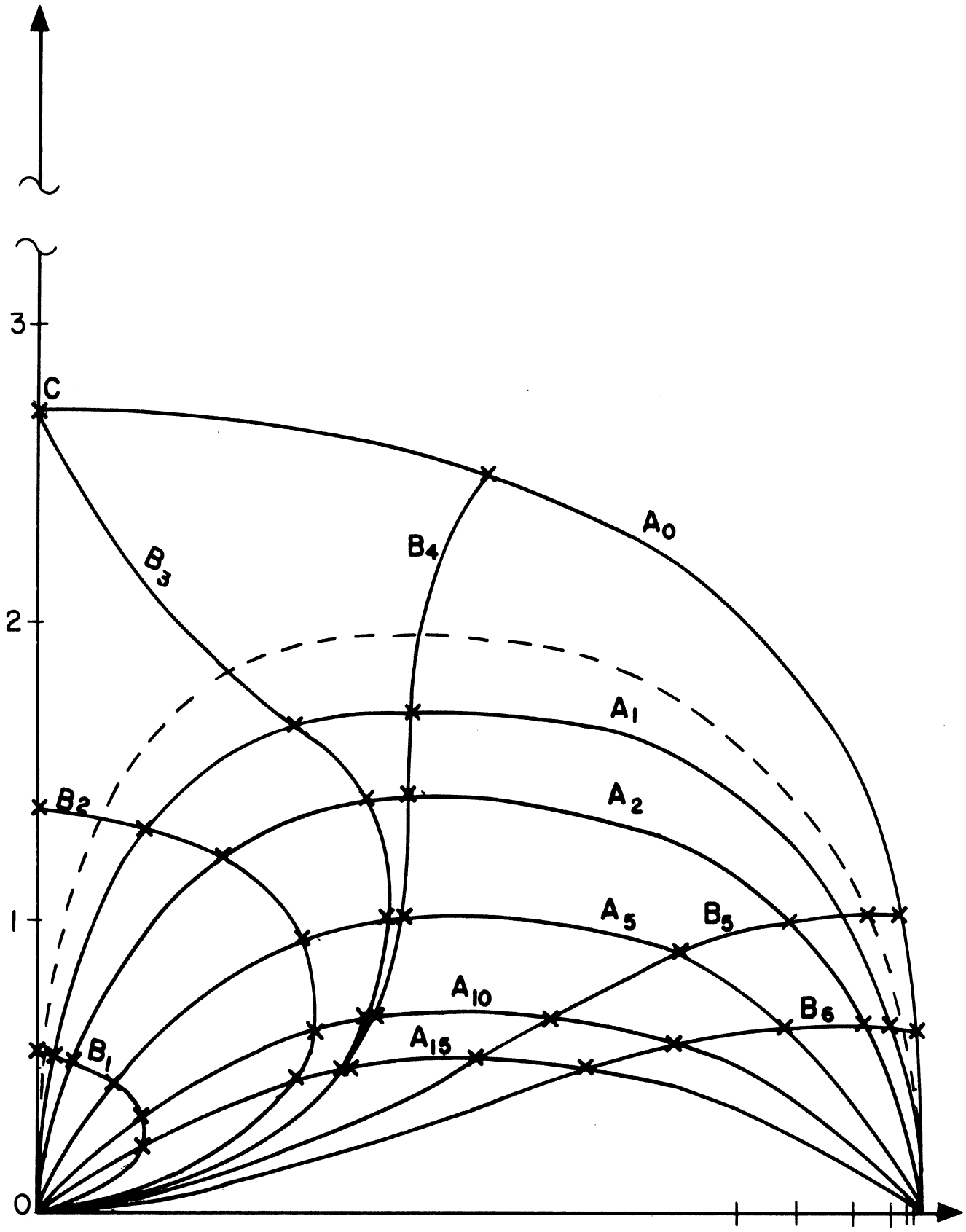

Figure II.9. Numerical Illustration of Paths and Poles.

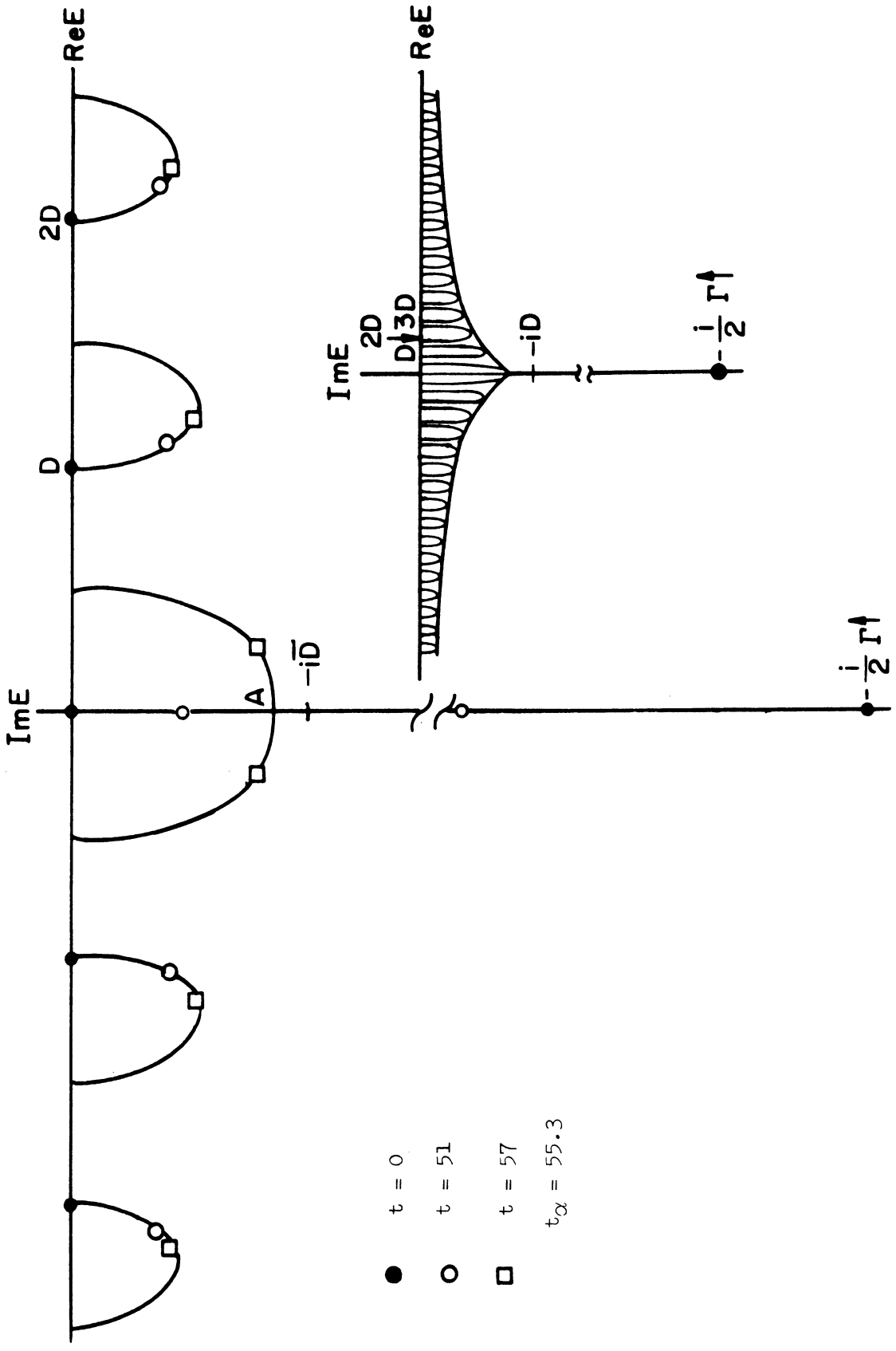

Figure II.10. Illustrations of Paths.

(2) As t increases, the poles move towards the points shown by the open circles. This illustrates the situation of the WC , $t < t_\alpha$. Namely, the coupling strength of the doorway state to the more complicated states is weaker than to the open channel. Here, we have one wide doorway state pole and many narrow regular poles with a Lorentzian distribution.

(3) When $t = t_\alpha$, the doorway state pole coalesces with the other central pole at the point A .

(4) As t increases further, we enter the SC region $t > t_\alpha$, and poles are indicated by the squares in Figure II.10a. In this situation, there is no clearly distinguishable doorway state pole. Nevertheless, the existence of the doorway state is indicated by the energy dependence of the imaginary part of the poles.

2.3 Pole Residues

Having obtained the poles, we may expand the structure factor of the T-matrix into a Mittag-Leffler series[78] and evaluate the resides.

2.3.1 General Properties and Doorway State Phase Shift

After the Mittag-Leffler series expansion, the T-matrix element of Equation (2.0.7) becomes

$$i T = \left(1 - e^{2i\delta}\right) + i e^{2i\delta} \sum_{n=-\infty}^{\infty} \left(\frac{b_n}{z - \zeta_n} - \frac{b_n}{\zeta_n} \right) , \qquad (2.3.1)$$

where

$$b_n = \frac{i(z_0 - z_0^*)\,t}{t^2 + t + (\zeta_n - z_0)^2} \quad . \tag{2.3.2}$$

The T-matrix of the multi-channel case is also expanded into the same series:

$$i\,\underset{\sim}{T} = \underset{\sim}{1} - \underset{\sim}{S}^P + i\,\underset{\sim}{G} \sum_{n=-\infty}^{\infty} \left(\frac{b_n}{z - \zeta_n} - \frac{b_n}{\zeta_n} \right) . \tag{2.3.3}$$

There is no effect of the number of the open channels on the distribution of the poles except through $\Gamma^{\uparrow}$.

The residue, Equation (2.3.2), may be expressed by

$$b_n = |b_n|\, e^{2i\delta_\alpha^{(n)}} , \tag{2.3.4}$$

where the phase $\delta_\alpha^{(n)}$ is given by

$$\tan 2\delta_\alpha^{(n)} = \frac{-2(\zeta_n^r - u_0)(\zeta_n^i - v_0)}{t^2 + t - (\zeta_n^i - v_0)^2 + (\zeta_n^r - u_0)^2} , \tag{2.3.5}$$

and will be called the "doorway state phase shift".

For $u_0 = 0$, the range of $\delta_\alpha^{(n)}$ of the regular poles is distinguished according to the sign of

$$\Delta \equiv t^2 + t - (\zeta_0^i - v_0)^2 \tag{2.3.6}$$

which is zero at $t = t_\alpha$. In the case of the SC , and IC , Δ is non-negative and $2\delta_\alpha^{(n)}$ ranges from 0 to $\pi/2$ and $3\pi/2$ to 2π . Otherwise, $2\delta_\alpha^{(n)}$ ranges from 0 to 2π . For $u_0 \neq 0$, the distinction becomes slightly ambiguous particularly at $-v_0 = O(1)$, see Figure II.3.

The doorway state phase shift of the anomalous pole behaves quite differently and will be treated later, §§ 2.3.4.

The absolute values of the residues are expanded into a series,

$$|b_n| = \frac{-2v_0 t}{t^2+t+(\zeta_n^r-u_0)^2+(\zeta_n^i-v_0)^2} \times$$

$$\times \left\{ 1 + \frac{2t(t+1)(\zeta_n^i-v_0)^2}{\left[t^2+t+(\zeta_n^r-u_0)^2+(\zeta_n^i-v_0)^2\right]^2} + \cdots \right\} . \quad (2.3.7)$$

This series is covergent except for the central pole at $u_0 = 0$ and $t = t_\alpha$. The first term is a good approximation except for the IC .

For $u_0 = 0$, the residues will be calculated further in the following cases: WCL (regular poles) in §§ 2.3.2 and SCL in §§ 2.3.3.

2.3.2 Weak Coupling Limit (Regular Poles)

For the WCL , the regular poles are given by Equation (2.2.3). Applying it to Equations (2.3.5) and (2.3.7), we obtain

$$|b_n| \cong \frac{-2v_0 t}{t(t+1)+v_0^2+(n\pi)^2} , \quad (2.3.8)$$

and

$$\tan 2\delta_d^{(n)} \cong \frac{2v_0(n\pi)}{t(t+1)-v_0^2+(n\pi)^2} . \quad (2.3.9)$$

The results are shown in Figures II.11 and II.12.

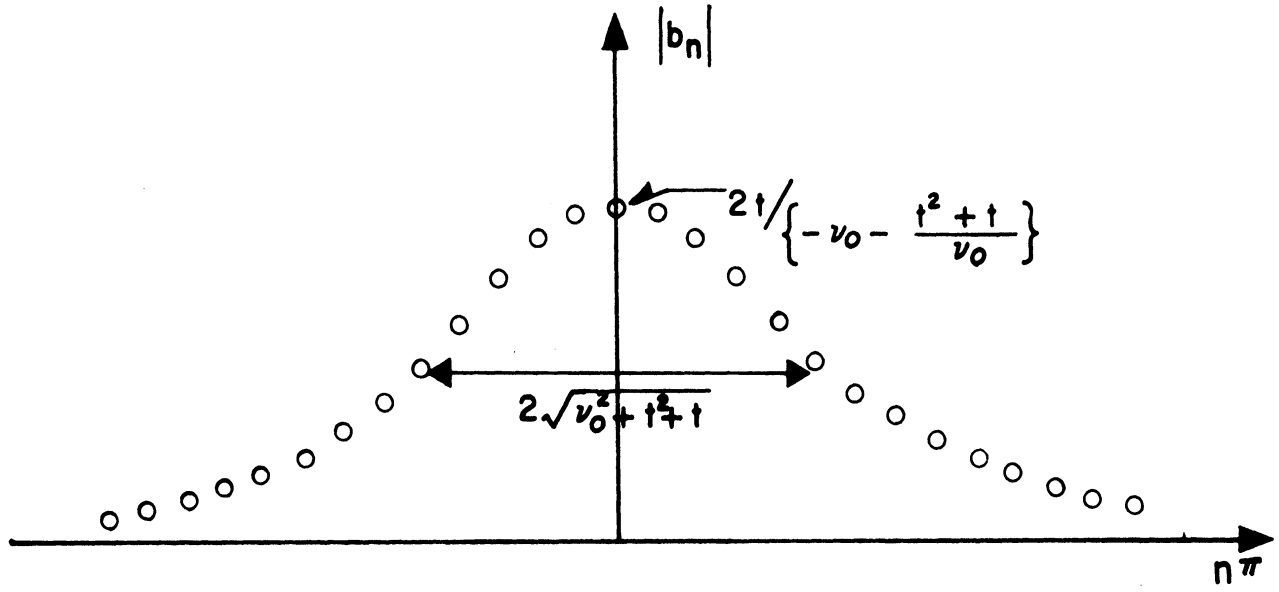

Figure II.11. Absolute Value of the Residues (Regular Poles at WCL).

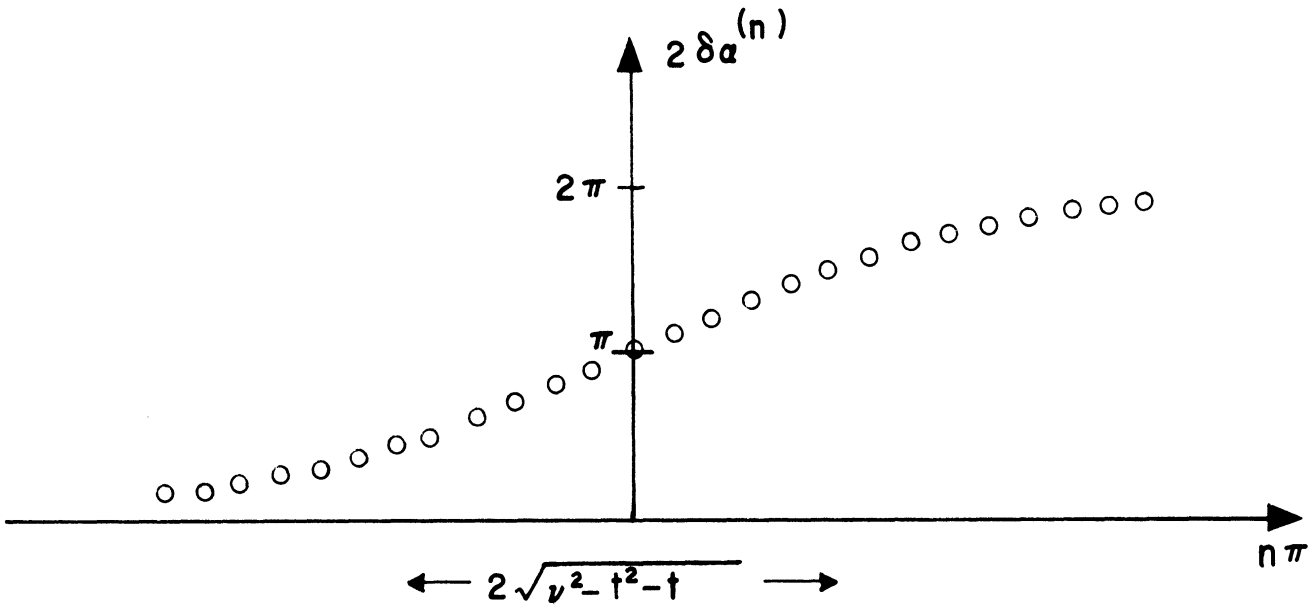

Figure II.12. Doorway State Phase Shift.

2.3.3 Strong Coupling Limit

For the SCL $(t \gg t_\alpha)$, the poles are given by Equation (2.2.10). The residues are calculated with the results:

$$|b_n| \cong \frac{-2U_0 t}{t(t+1) + U_0^2 + (u_n^\infty - u_0)^2}, \tag{2.3.10}$$

and

$$\tan 2\delta_\alpha \cong \frac{2U_0 (u_n^\infty - u_0)}{t(t+1) - U_0^2 + (u_n^\infty - u_0)^2}. \tag{2.3.11}$$

These results show no significant difference in the forms of Equations (2.3.8) and (2.3.10) and of Equations (2.3.9) and (2.3.11). However, a difference in the magnitudes of t and $-U_0$ makes a great difference in the doorway state phase shift. The results are shown in Figure II.13 and II.14. These are a maximum and a minimum which are attained at

$$\zeta_n^r = u_0 \mp \sqrt{t(t+1) - U_0^2} \qquad \text{for } t > t_\alpha. \tag{2.3.12}$$

The values are given by

$$\tan 2\delta_\alpha |_{m\,M} = \mp \frac{U_0}{\sqrt{t(t+1) - U_0^2}}. \tag{2.3.13}$$

Corresponding to each term in the series expansion of the structure factor (Equation (2.3.3)), there is a resonance. For both single and multi-channel cases, the resonance has the Breit-Wigner shape if the corresponding term of the structure factor becomes equivalent to the single channel Breit-Wigner T-matrix.[4] The condition for this equivalence is:

$$\delta_\alpha = 0 \quad \text{and} \quad |b_n| / |\zeta_n^i| = 2. \tag{2.3.14}$$

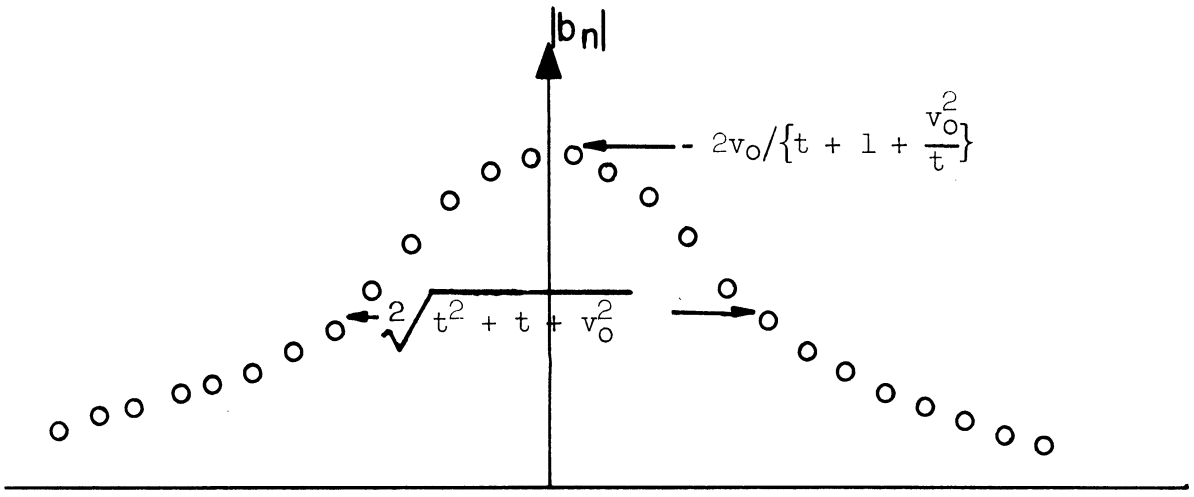

Figure II.13. Absolute Values of the Residues (SCL).

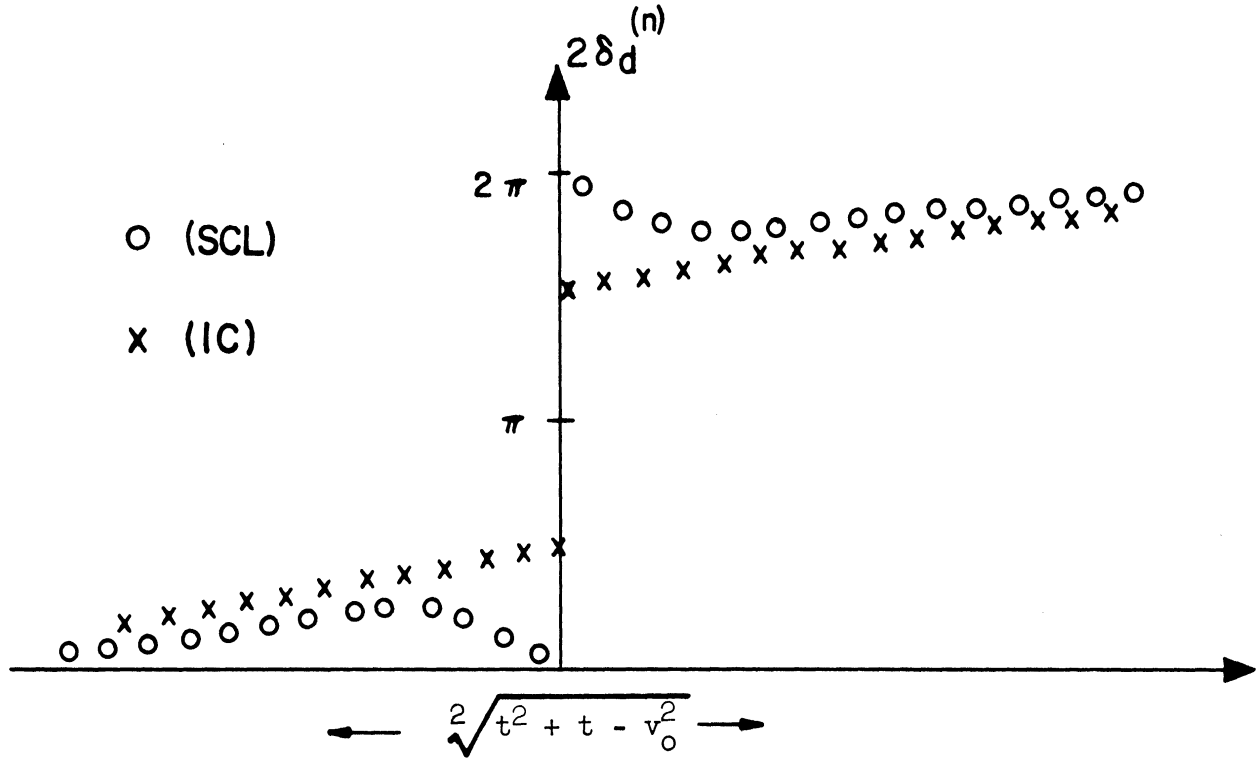

Figure II.14. Doorway State Phase Shift.

Although the residues do not exactly satisfy Equation (2.3.14) in any situation, they approach it in the following cases.

(a) The residues of the poles distant from the doorway state approximately satisfy Equation (2.3.14) without regard to the situation of coupling strengths. Actually, however, the other doorway states are expected in such distant regions.

(b) All the residues at SCL approximately satisfy Equation (2.3.14).

(c) In the case of WCL , the residue of the anomalous pole approximately satisfies the condition, Equation (2.3.14). (The residues of the regular poles near the doorway state do not.)

For a given nucleus, we expect $\Gamma^{\downarrow}$ or $\langle a_n^2 \rangle$ to be a slowly varying function of energy because the levels are saturated in the highly excited states.(58) On the other hand, $\Gamma^{\uparrow}$ varies with energy as the potential barrier and the number of the open channels. That is, as the energy becomes zero, $\Gamma^{\uparrow}$ approaches zero proportional to the penetration factor. Hence, in the low energy region, $\Gamma^{\uparrow}$ becomes small. But $\Gamma^{\uparrow}/\Gamma^{\downarrow} = -U_0/t$ which implies SC . Therefore, in the low energy region, the resonances take on the Breit-Wigner form.

2.3.4 Residues of the Central Poles

The residues of the central poles will be calculated for the cases: (a) WCL (regular central pole) and SCL (both central poles), (b) the anomalous pole at WC , and (c) the central poles at $u_0 = 0$ and $t \sim t_\alpha$. Finally, a part of the T-matrix corresponding to

the central poles will be obtained at $u_0 = 0$ and $t = t_\alpha$ to see the effect of the coalescence of the two central poles.

(a) The residue of the regular central pole is given by Equations (2.3.8) and (2.3.9),

$$b_0 \cong \frac{-2t}{v_0\left(1 - \frac{t^2+t}{v_0^2}\right)}, \tag{2.3.15}$$

at the WCL . For the SCL , the residues of the central poles are given by Equations (2.3.10) and (2.3.11),

$$b_{a,0} \cong \frac{-2v_0}{t\left(1 + \frac{1}{t} - \frac{v_0^2}{t^2}\right)} \mp i\,\frac{2\pi v_0}{t^3}, \tag{2.3.16}$$

where $\mp$ signs refer to the anomalous and regular poles respectively.

(b) The anomalous pole at the WCL is given by Equation (2.2.4). The residue is calculated by applying it to Equation (2.3.2),

$$b_a \cong \frac{-2v_0}{1 - \frac{t}{\sinh(2v_0 + t)}\, e^{2iu_0}}. \tag{2.3.17}$$

It follows that, for $-v_0 \gg 1$, b_a is almost independent of u_0 .

(c) The central poles at $u_0 = 0$ and $t \sim t_\alpha$ are estimated from Equations (2.1.3), (2.1.4), and (2.2.1)-(2.2.3). Then, the residues are calculated with the result:

$$b_{a,0} \cong \frac{-v_0 t}{\pm i\sqrt{(t-t_\alpha)(t_\alpha^2 + t_\alpha)} + (t-t_\alpha)(t_\alpha + 1)}, \tag{2.3.18}$$

where $\pm$ signs refer to the regular and anomalous poles respectively.

All the above results (a)-(c) are summarized in Figure II.15.

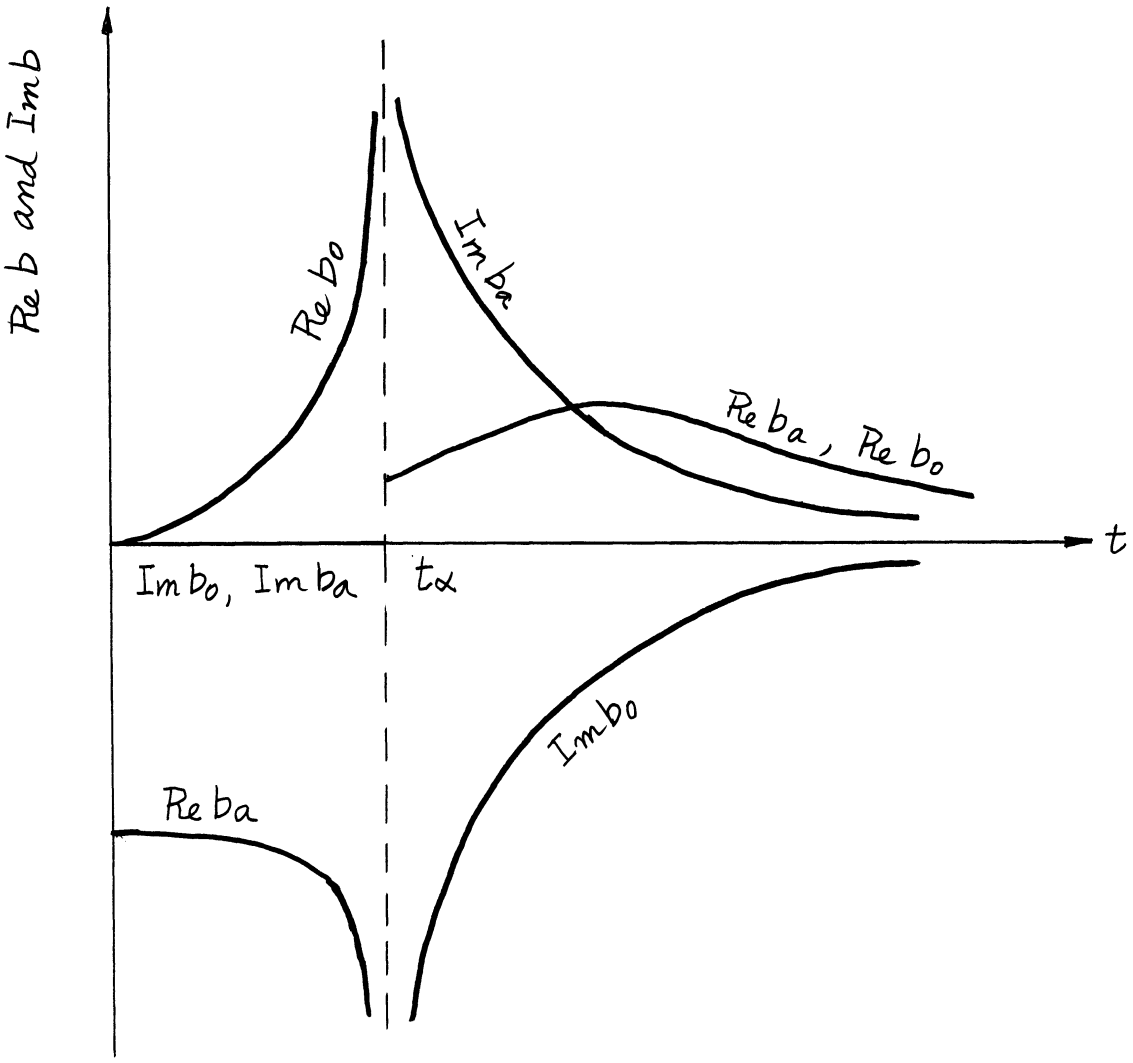

Figure II.15. Residues of the Central Poles.

The singularities of the residues at $t = t_\alpha$ are spurious since the coalescence os the central poles produces a second order pole at $z = i v_\alpha$. If $u_o \neq 0$, then these poles do not coalesce and the residues do not show this singularity. In fact, at $u_o = \pi/2$, the path of the anomalous pole is a straight line parallel to the imaginary axis (see Figure II.7) and the residue is real.

A special situation arises when $v_0 = 0$ and $t = t_\alpha$. Due to the coalescence of the central poles, the T-matrix has a second order pole at $z = i v_\alpha$. The expansion of the T-matrix about $z = i v_\alpha$ yields

$$T^R = \frac{-2 i v_0 \sqrt{1+t_\alpha}}{(z - i v_\alpha)^2} + \frac{2 v_0}{z - i v_\alpha} + \cdots .$$

with the resulting contribution to the cross section,

$$\sigma_t^{\text{cent. pole}} = \frac{2 v_0 \left(v_0 + \sqrt{\frac{t_\alpha}{1+t_\alpha}} - 2 v_\alpha \right)}{z^2 + v_\alpha^2} -$$

$$- \frac{2 v_0 v_\alpha^2 \left(v_0 + \sqrt{\frac{t_\alpha}{1+t_\alpha}} - v_\alpha \right)}{(z^2 + v_\alpha^2)^2} , \qquad (2.3.19)$$

as sketched in Figure II.16.

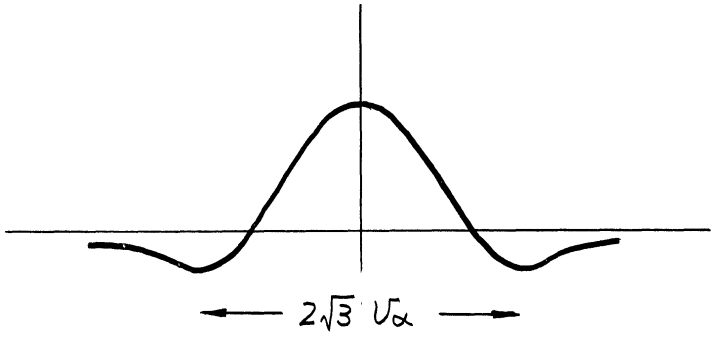

Figure II.16. $\sigma_t^{\text{cent pole}}$.

This result is of academic interest only, since the coalescence of the central poles is an unlikely accident.

CHAPTER 3

APPLICATION, RESULTS, AND CONCLUSION

Through the infinite Picket Fence model, we have investigated the properties of the fine structure of the doorway states in Chapter 2. The effects due to the deviation from the model are studied in Appendix C. The results will be applied in this chapter. The resonance parameters are provided in § 3.1 as preparation for the following sections. In § 3.2, the fine structure of the total cross section will be illustrated. In § 3.3, the average total cross section will be given and in § 3.4 the dynamical constants $\Gamma^{\uparrow}$ and $\Gamma^{\downarrow}$ will be expressed in terms of measurable parameters of the resonance width distribution. In § 3.5, the results obtained above will be applied to the analysis of experiments in the low energy region. In § 3.6, the doorway states in the continuum region will be discussed in relation to the possibility of having bumps in the cross sections which are caused by the doorway states.

3.1 Resonance Parameters

The T-matrix is given by Equation (2.3.3). The total cross section, Equation (1.2.29) of Part I, may therefore be viewed a sum over isolated resonances with average spacing π . For a single open channel, each resonance of the cross section may be specified by the following parameters:

(a) Resonance width $= -2\,\zeta_n^{i}$. (3.1.1)

(b) Values of the extrema

$= \pm 1 + \cos 2(\delta + \delta_d)$ $(2\pi\lambda^2)$, (3.1.2)

where the maximum and the minimum exist at $\mathcal{E} \gtrless \zeta_n^{r}$ and $\mathcal{E} \lesssim \zeta_n^{r}$ according to $\sin 2(\delta+\delta_d) \lesssim 0$ respectively.

(c) Peak of the resonance

$$= \frac{|b_m|}{|\zeta_m^i|} \cos 2(\delta + \delta_d) \qquad (2\pi\lambda^2) \qquad (3.1.3)$$

$$\text{at} \quad z = \zeta_m^r .$$

(d) Area of a resonance divided by π

$$= |b_m| \cos 2(\delta + \delta_d) \qquad (2\pi\lambda^2). \qquad (3.1.4)$$

The dependence of these parameters on the coupling strengths will be briefly discussed in this section and applied in the following sections.

The resonance width distribution will be related to the doorway state constants, $\Gamma^{\uparrow}$ and $\Gamma^{\downarrow}$, in § 3.4 and will be applied to the analysis of the measured width distribution.

The values of the extrema together with the sign of $\sin 2(\delta+\delta_d)$ specify the shape of each resonance. Namely, for $\sin 2(\delta+\delta_d) > 0$, the minimum (dip) of the cross section exists on the left hand side of the maximum (peak). For the other case, the dip exists in the right hand side of the peak. The difference of the values is equal to 2 and the maximum value of the single channel total cross section is 2 in units of $2\pi\lambda^2$. Therefore, the minimum value of the cross section is zero. These results will be applied in § 3.2.

The sign of the peak of the resonance indicates whether the dip of the cross section is due to interference or due to the negative resonance.

The area of a resonance divided by π is approximately equal to the average cross section contributed by the fine resonances. For WC and SC, the areas of the fine resonances are given by

$$\text{Area of Res.} = \frac{-2 U_0 t}{t^2+t+U_0^2+(\bar{z}-u_0)^2} \cos 2(\delta+\delta_d). \qquad (3.1.5)$$

In more detail, they are given by

$$\langle \sigma^T_{R.P.} \rangle_{Area} =$$

$$\frac{2U_0 t\left[\left\{t^2+t-(\zeta_n^i-U_0)^2+(\bar{z}-u_0)^2\right\}\cos 2\delta - 2(\bar{z}-u_0)(\zeta_n^i-U_0)\sin 2\delta\right]}{\left[t^2+t+(\zeta_n^i-U_0)^2+(\bar{z}-u_0)^2\right]^2 + 4(t^2+t)(\zeta_n^i-U_0)^2}, \qquad (3.1.6)$$

where Equations (3.1.4) and (2.3.2) have been used. The total cross section corresponding to the anomalous pole is given by

$$\sigma^T_{D.S} = \frac{2U_0\left\{(\bar{z}-u_0)\sin 2\delta + (t+U_0)\cos 2\delta\right\}}{(\bar{z}-u_0)^2+(t+U_0)^2}. \qquad (3.1.7)$$

These results will be applied in § 4.3.

3.2 Fine Structure of the Total Cross Section

The fine structures of the total cross sections with WC and with SC are shown in Figures II.17a and II.17c respectively. In Figure II.17b, the standard Breit-Wigner form of the total cross section is shown for comparison. The potential phase shift is varied from 0 to $-\pi/6$.

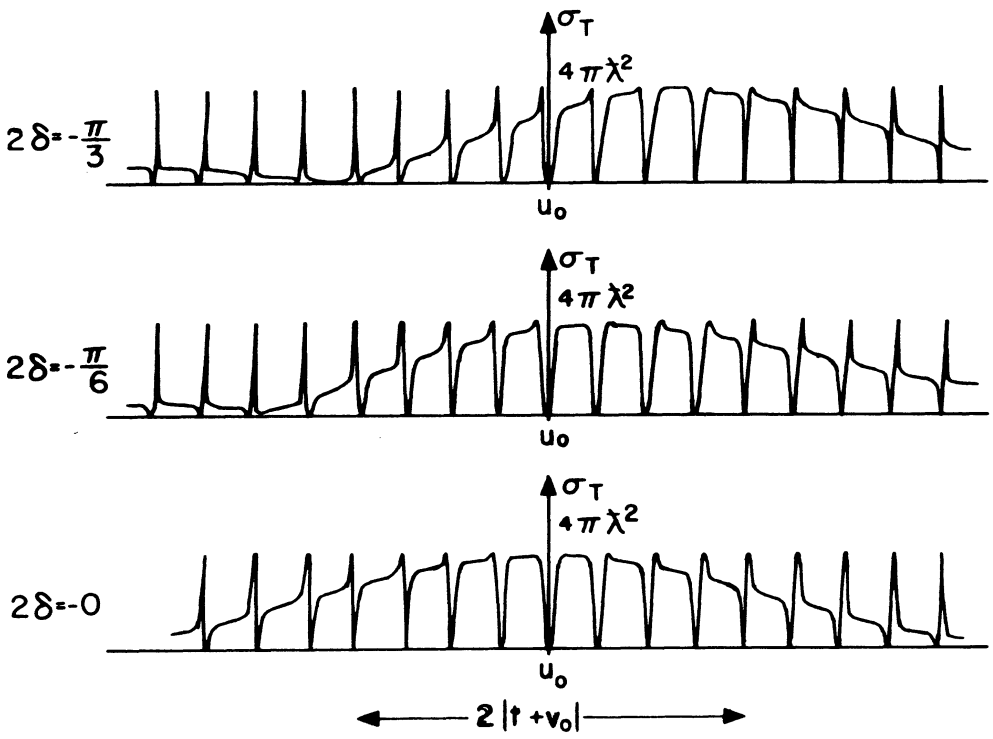

Figure II. 17a. Fine Structure of Total Cross Sections at WC.

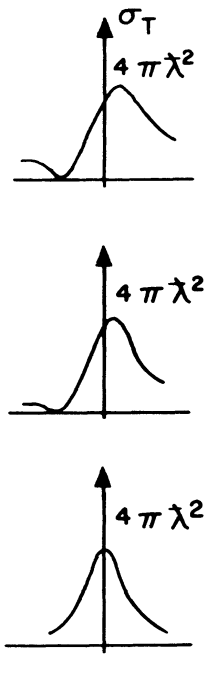

Figure II.17b. Breit-Wigner Forms.

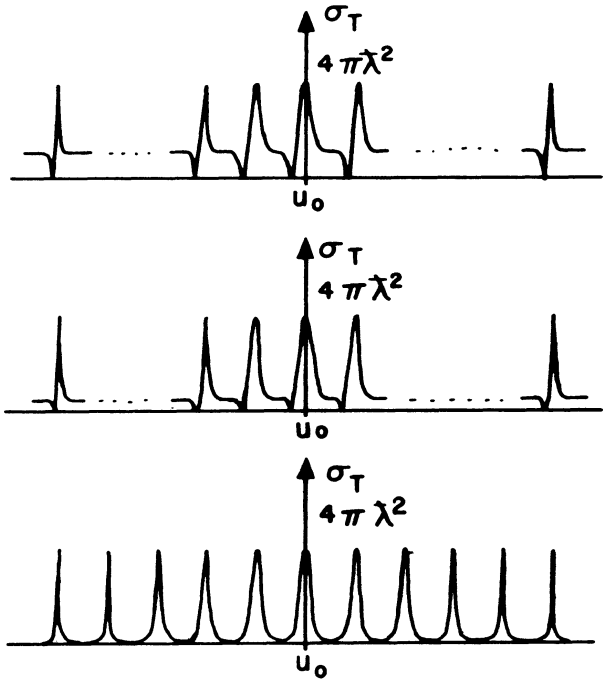

Figure II.17c. Fine Structure of Total Cross Section at SC.

In the case of WC , there is a background cross section which is mainly composed of the doorway state cross section, Equation (3.1.7). The dips near the doorway state are negative resonances and not interferences. Far from the doorway state the resonances approach to the Breit-Wigner form.

At $\delta = 0$, the dips which lie on the right hand side of the peaks (r.h.s. dips) exist below the doorway state energy. The l.h.s. dips exist above the doorway state energy. As δ increases, the l.h.s dips appear in both the lower and higher energy regions away from the doorway state energy. The r.h.s. dips exist only around the doorway state energy. These dips are the negative resonances.

The shape of the fine resonances with the r.h.s. dips greatly deviates from the Breit-Wigner form.

In the case of SC , there is no background cross section. As discussed in the last chapters, the shape of all the resonances approaches the Breit-Wigner form in the SCL . Even if the situation of the coupling strengths is not the SCL , the resonance shapes in SC are approximated by the Breit-Wigner form. In particular, all the dips are the l.h.s. dips for $|\tan 2\delta| < -U_0/\sqrt{t^2 + t - U_0^2}$, as may be inferred from Equation (2.3.13).

3.3 Intermediate Structure of Cross Sections

The total cross section averaged over a small energy interval, (for instance the resonance spacing), is approximately given by

$$\langle \sigma^T \rangle = \begin{cases} \sigma^T_{D.S.} + \langle \sigma^T_{R.P.} \rangle_{Area} \equiv \langle \sigma^T \rangle_{WC} & \text{for } t < t_\alpha \\ \langle \sigma^T_{R.P.} \rangle_{Area} \equiv \langle \sigma^T \rangle_{SC} & \text{for } t > t_\alpha \,, \end{cases} \tag{3.3.1}$$

where $\langle \sigma^T_{R.P.} \rangle_{Area}$ and $\sigma^T_{D.S.}$ are given by Equations (3.1.7) and (3.1.8), respectively, and the E-independent terms are not taken into account. In this section, these results will be compared with the average total cross section obtained in Part I which we will denote by $\langle \sigma^T \rangle_{Part\,I}$.

Now, with the application of Equation (2.0.3), $\langle \sigma^T \rangle_{Part\,I}$ at $\delta = 0$ becomes

$$\langle \sigma^T \rangle_{Part\,I} = \frac{-2 U_0 (t - U_0)}{(z - u_0)^2 + (t - U_0)^2} \,. \tag{3.3.2}$$

The relative error of Equations (3.3.1) and (3.3.2) at $\delta = 0$ and with SC is

$$\frac{\langle \sigma^T \rangle_{Part\,I} - \langle \sigma^T \rangle_{SC}}{\langle \sigma^T \rangle_{SC}} = \frac{-U_0 \left\{ t - U_0 t + U_0^2 + (z - u_0)^2 \right\}}{t \left\{ t^2 + t + U_0^2 + (z - u_0)^2 \right\}} \,. \tag{3.3.3}$$

Therefore, the error is of the order of $(U_0/t)^2$ for $z \sim u_0$ and of the order of $-U_0/t$ for $|z - u_0| \gg t$. The difference between $\langle \sigma^T \rangle_{Part\,I}$ and $\langle \sigma^T \rangle_{WC}$ is approximately equal to $\langle \sigma^T_{R.P.} \rangle_{Area}$;

$$\langle \sigma^T \rangle_{Part\,I} - \langle \sigma^T \rangle_{WC} \cong \langle \sigma^T_{R.P.} \rangle_{Area} \,. \tag{3.3.4}$$

The relative error is of the order of $t/-U_0$. To illustrate the magnitude of this rather large discrepancy, we will estimate the widths of the average cross section of Equations (3.3.1) and (3.3.2), in § 3.5. The reason for the discrepancy is difficult to understand. One possibility is that the explanation may lie in the different energy intervals used for the E-averaging in Part I and Part II. (The interval Δ' in Part I encompasses many resonances). However, the situation is still unclear.

3.4 Distribution of Resonance Widths and the Doorway State Constants

One of the characteristics of the fine structure of doorway states is the distribution of the poles of the T-matrix. The distribution of the imaginary parts of the poles is well approximated by a Lorentzian except at the intermediate coupling. In this section, the constants of the doorway state, $\Gamma^{\uparrow}$ and $\Gamma^{\downarrow}$, will be related to the two parameters specifying the Lorentzian, the peak value and the width.

For WC , the distribution of the fine resonance widths is obtained from Equations (2.2.6) and (2.0.6) with the result:

$$\Gamma_n \equiv -2\frac{\bar{D}}{\pi}\zeta_n^{i}$$

$$= \frac{\bar{D}}{2\pi}\Gamma^{\uparrow}\Gamma^{\downarrow}\left\{1-\frac{2\bar{D}\Gamma^{\downarrow}}{\pi(\Gamma^{\uparrow})^2}\left(1+\frac{\pi\Gamma^{\downarrow}}{6\bar{D}}\right)L(E_n)\right\}\times$$

$$\times 1\Big/\left[(E_n-E_0')^2\left\{1+\frac{2\bar{D}\Gamma^{\downarrow}}{\pi(\Gamma^{\uparrow})^2}\left(1+\frac{\pi\Gamma^{\downarrow}}{6\bar{D}}\right)L(E_n)\right\}^2+\right.$$

$$\left.+\frac{(\Gamma^{\uparrow})^2}{4}\left\{1-\frac{2\bar{D}\Gamma^{\downarrow}}{\pi(\Gamma^{\uparrow})^2}\left(1+\frac{\pi\Gamma^{\downarrow}}{6\bar{D}}\right)L(E_n)\right\}^2\right], \qquad (3.4.1)$$

where

$$L(E_n) \equiv \frac{\frac{1}{4}(\Gamma^{\uparrow})^2}{(E_n - E_o')^2 + \frac{1}{4}(\Gamma^{\uparrow})^2} \cdot \tag{3.4.2}$$

The distribution given by Equation (3.4.1) can be approximated by a Lorentzian (see Appendix C) with the peak value, $(\Gamma)_P$,

$$(\Gamma)_P = \frac{2\bar{D}}{\pi} \cdot \frac{\Gamma^{\downarrow}}{\Gamma^{\uparrow} - \frac{2\bar{D}\Gamma^{\downarrow}}{\pi\Gamma^{\uparrow}}\left(1 + \frac{\pi\Gamma^{\downarrow}}{6\bar{D}}\right)} , \tag{3.4.3}$$

and the half width,

$$W = \Gamma^{\uparrow} - \frac{2\bar{D}\Gamma^{\downarrow}}{\pi\Gamma^{\uparrow}}\left(1 + \frac{\pi\Gamma^{\downarrow}}{6\bar{D}}\right) . \tag{3.4.4}$$

If we define

$$S \equiv \frac{\pi(\Gamma)_P}{2\bar{D}} , \tag{3.4.5}$$

$\Gamma^{\uparrow}$ and $\Gamma^{\downarrow}$ are expressed as follows:

$$\Gamma^{\downarrow} = S\,W , \tag{3.4.6}$$

and

$$\Gamma^{\uparrow} = \frac{W}{2}\left\{1 + \sqrt{1 + \frac{4}{3}S^2 + \frac{4(\Gamma)_P}{W}}\right\} . \tag{3.4.7}$$

For SC , the distribution of the fine resonance widths is obtained from Equations (2.2.11) and (2.0.6),

$$\Gamma_n = \frac{\bar{D}}{2\pi}\Gamma^{\uparrow}(\Gamma^{\downarrow}+2\Gamma^{\uparrow})\Big/\Big[(E_n^{\infty}-E_0')^2 + \frac{\Gamma^{\downarrow}}{4}(\Gamma^{\downarrow}+2\Gamma^{\uparrow}) + \frac{1}{8}\frac{\Gamma^{\uparrow}(\Gamma^{\uparrow}+\Gamma^{\downarrow})^2\left(\frac{4\bar{D}}{3\pi}-\Gamma^{\uparrow}\right)}{(E_n^{\infty}-E_0')^2+\frac{\Gamma^{\downarrow}}{4}(\Gamma^{\uparrow}+\Gamma^{\downarrow})}\Big] . \qquad (3.4.8)$$

The Lorentzian parameters are given by

$$(\Gamma)_p = \frac{2\bar{D}}{\pi}\frac{\Gamma^{\uparrow}}{\Gamma^{\downarrow}+\frac{2\Gamma^{\uparrow}}{\Gamma^{\uparrow}+\Gamma^{\downarrow}}\left(\frac{4\bar{D}}{3\pi}-\Gamma^{\uparrow}\right)} , \qquad (3.4.9)$$

and

$$W = \Gamma^{\uparrow}+\Gamma^{\downarrow}+\frac{1}{3}\frac{\Gamma^{\uparrow}}{\Gamma^{\uparrow}+\Gamma^{\downarrow}}\left(\frac{4\bar{D}}{3\pi}-\frac{5}{2}\Gamma^{\uparrow}\right) . \qquad (3.4.10)$$

Applying Equation (3.4.5), we have that

$$\Gamma^{\downarrow} = \frac{1+2S^2}{1+S+\frac{7}{6}S^2}W - \frac{4}{9}\frac{\bar{D}}{\pi}S\frac{1+3S-\frac{S^2}{2}}{1+S+\frac{7}{6}S^2} , \qquad (3.4.11)$$

and

$$\Gamma^{\uparrow} = \frac{S}{1+2S^2}\Gamma^{\downarrow} + \frac{8}{3}\frac{\bar{D}}{\pi}\frac{S^2}{1+2S^2} . \qquad (3.4.12)$$

For IC , the doorway state pole joins the distribution of the regular poles. Therefore, the measured resonance width which is locally largest is the width of the doorway state even though the pole distribution

is not Lorentzian. Let us denote the measured resonance width by $(\Gamma)_L$. U_α is related to $(\Gamma)_L$ by

$$U_\alpha = -\frac{\pi(\Gamma)_L}{2\bar{D}} \tag{3.4.13}$$

We may then estimate $\Gamma^\uparrow (= -2\bar{D}U_0/\pi)$ and $\Gamma^\downarrow (= 2\bar{D}t_\alpha/\pi)$ using Figure II.8 and Table II.1. Because t^* (see §§2.2.1) depends on U_0, $\Gamma^\downarrow$ is not definite but

$$\frac{2\bar{D}t_\alpha}{\pi} \leq \Gamma^\downarrow \leq \frac{2\bar{D}(t_\alpha+1)}{\pi} . \tag{3.4.14}$$

The above results will be applied in the next section.

3.5 Doorway States at Low Energies

In the energy region where fine resonances may be observed, the doorway states have been identifed by taking the average of the total cross section[92] and of the total and differential elastic scattering cross sections.[93] In this section, we will apply some consequences of our study of the fine structure of the doorway state to the analysis of cross sections exhibiting fine resonances. First, the doorway state constants, E_0', $\Gamma^\uparrow$, and $\Gamma^\downarrow$, will be estimated from the distributions of the fine resonance widths. Then, the total cross section of the doorway state will be calculated to show the consistency of the theory. Finally, we will illustrate the difference in the widths of the intermediate structure obtained in § 3.3 and in Part I.

The experimental data on fine resonance parameters for isotopes ranging from Ca to Ni and in the energy range from 100 to 600 kev are available in Reference 85. Based on the theoretical results of the pole distribution, we have discovered a systematic fluctuation of resonance widths over the above energy and mass ranges.(63) Two examples are shown in Figure II.18 where the histograms indicate the measured resonance widths as a function of resonance energies.

The doorway state constants will be estimated by the following steps: (a) For each situation of coupling strength, $\Gamma^{\uparrow}$ and $\Gamma^{\downarrow}$ will be estimated. (b) From the values obtained, the SCS which applies will be chosen.

For WC and SC , the width distributions can be approximated by a Lorentzian. The curves in Figure II.18 are superpositions of Lorentzians which are locally fitted to the width distribution. The doorway state energies, E_0' , are obtained at the peaks of the curves. The curves also give the peak value and the half width of each Lorentzian. These values are listed in Table II.2. Then, the values of $\Gamma^{\uparrow}$ and $\Gamma^{\downarrow}$ with WC and SC are estimated from Equations (3.4.5), (3.4.6), (3.4.7), (3.4.11), and (3.4.12). The results are listed in Table II.2.

Assuming IC , we may also estimate $\Gamma^{\uparrow}$ and $\Gamma^{\downarrow}$. Taking as an example the doorway state of Ni^{58} at 410 kev, we have $(\Gamma)_L = 8$ kev and $\bar{D} = 18.6$ kev . Applying these values to Equation (3.4.13), we have $U_\alpha = -0.68$. From Figure II.8 and Table II.1, we obtain the following values of t_α and U_0

$$\begin{cases} t_\alpha = 0.53 \\ -U_0 = 1.58 \end{cases} \quad \therefore \quad \begin{cases} \Gamma^{\uparrow} = 18.7 \text{ kev} \\ 6.3 \le \Gamma^{\downarrow} \le 18.1 \text{ kev} \end{cases}$$

where we have applied Equation (3.4.14).

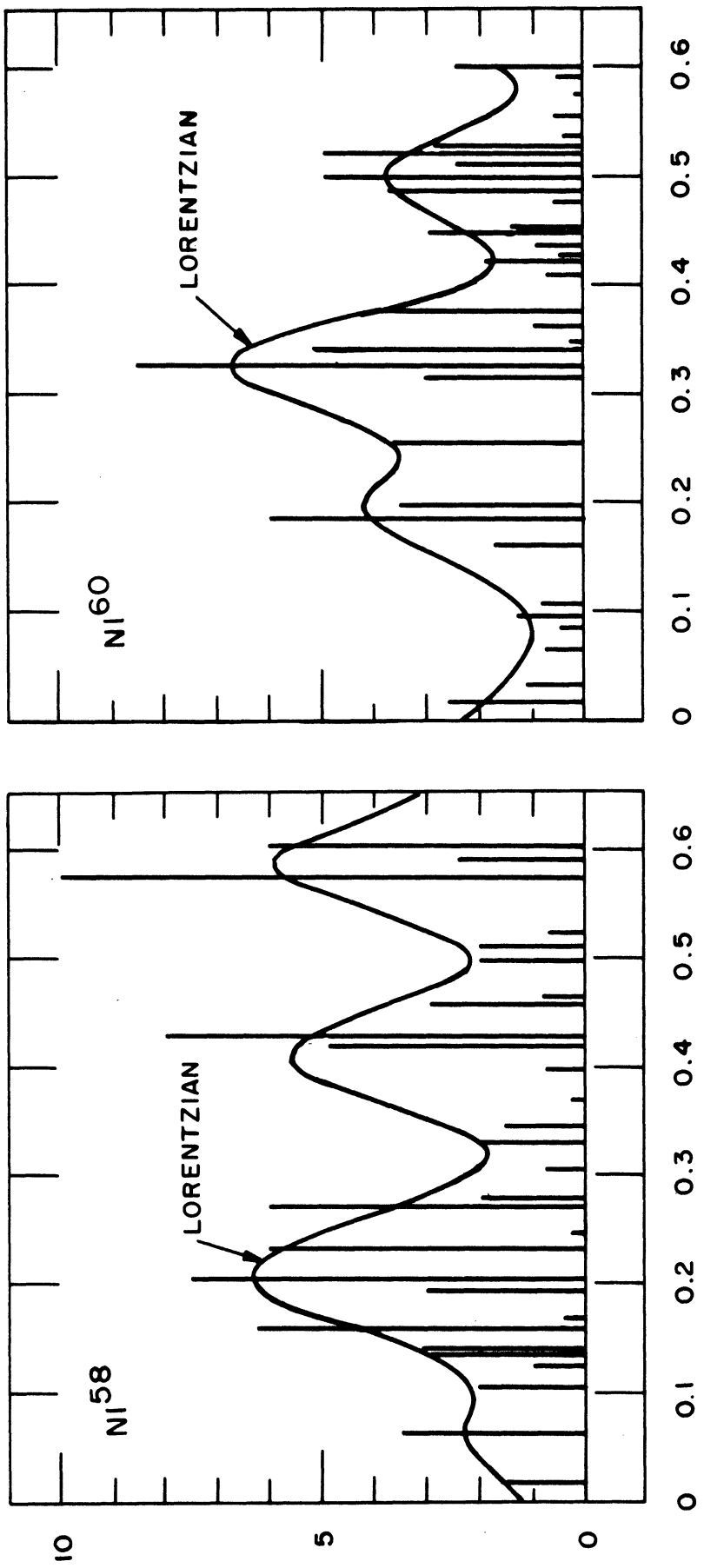

Figure II.18. Resonance Width Distributions.

TABLE II.2

CONSTANTS OF THE WIDTH DISTRIBUTION AND $\Gamma^{\uparrow}$ AND $\Gamma^{\downarrow}$

Experiments (kev)					Weak Coupling		Strong Coupling	
E_0'	W	$(\Gamma)_p$	$\bar{D}$	s	$\Gamma^{\uparrow}$	$\Gamma^{\downarrow}$	$\Gamma^{\uparrow}$	$\Gamma^{\downarrow}$
205	140	6.4	17.5	0.574	158.	80.	42	113
410	130	5.6	18.6	0.473	144.	61.	37	103
580	120	5.7	15.0	0.597	137.	72	37	98

Experiments (kev)					Weak Coupling		Strong Coupling	
E_0'	W	$(\Gamma)_p$	$\bar{D}$	s	$\Gamma^{\uparrow}$	$\Gamma^{\downarrow}$	$\Gamma^{\uparrow}$	$\Gamma^{\downarrow}$
195	130	4.2	32.5	0.203	136.	.26	32	109
320	130	6.8	18.5	0.574	146.	75	39	104
500	110	3.8	11.0	0.543	123	60	32	92

Next, we will evaluate the SCS applying the sum rules of Equations (1.3.13) and (1.3.14) as well as the properties of the fine structure of the total cross section.

For IC , the sum rule of Equation (1.3.13) is violated because the sum of resonance widths near the doorway state at 410 kev is already larger than $\Gamma^{\uparrow} = 18.7$ kev . The same is true for the other doorway states. Thus, IC is excluded from the case of SCS to apply.

For a given Lorentzian distribution common to both WC and SC , the value of $\Gamma^{\downarrow}$ obtained for WC is equal to the sum over the fine resonance widths under the Lorentzian, where Equations (2.2.5) and (1.3.13) are applied. For either WC or SC , $\Gamma^{\uparrow}$ must be larger than the value of $\Gamma^{\downarrow}$ for WC to satisfy the sum rule of Equation (1.3.14). In Table II.2, $\Gamma^{\uparrow}$ for WC satisfies this requirement for all the doorway states of N_i^{58} and N_i^{60} , while $\Gamma^{\uparrow}$ for SC does not except for the doorway state of N_i^{60} at 195 kev. Therefore, the SCS of the doorway states at 320 and 500 kev for N_i^{60} and at 410 and 580 kev for N_i^{58} is WC . However, the SCS of the doorway state of N_i^{60} at 195 kev is undetermined. That of N_i^{58} at 205 kev is WC according to the above criterion.

Now, let us apply the second criterion: as pointed out in the beginning of § 3.2, a background cross section exists only for WC where the anomalous pole yields a contribution distinct from the regular poles. The measured cross section for N_i^{58} shown in Figure II.19 indicates that a background cross section exists around 400 and 600 kev but not around 200 kev. The cross section of N_i^{60} is quite

similar to that of Ni^{58}, a background cross section existing around 350 and 500 kev but not around 200 kev.

Therefore, both criteria for the doorway states of Ni^{60} at 320 to 500 kev and those of Ni^{58} at 410 and 580 kev indicate WC. The second criterion indicates SC for the doorway state of Ni^{60} at 195 kev. For the SCS of the doorway state of Ni^{58} at 205 kev, the two criteria lead to a contradiction. In this case, we chose the result of the second criterion, for the following reason: According to the results of Appendix C (§ C.4 and Figure C.1), for the given values of $\Gamma^{\uparrow}$ and $\Gamma^{\downarrow}$, the average width distribution around the doorway state is almost independent of the number of the more complicated states. However, the deviation of $\sum_{\mu} \Gamma_{\mu}$ from $\Gamma^{\downarrow}$ for WC depends much on the number of these states. Thus, the first criterion can not be thought of as absolute, and violations of it can be explained in terms of the finite Picket Fence model.

The chosen values of $\Gamma^{\uparrow}$ and $\Gamma^{\downarrow}$ are underlined in Table II.2.

The background cross section is caused mainly by $\sigma^{T}_{D.S.}$, Equation (3.1.7). We can estimate $\sigma^{T}_{D.S.}$ for the doorway states at 410 and 580 kev by using the values of $\Gamma^{\uparrow}$, $\Gamma^{\downarrow}$, and the potential phase shift. The potential phase shifts of Ni^{58} are estimated using the square well potential given in Part III with the results that $2\delta \cong -\pi + \frac{\pi}{3}$ at 410 kev and $2\delta \cong -\pi + \frac{\pi}{6}$ at 580 kev. The results of $\sigma^{T}_{D.S.}$ are shown in Figure II.19 with satisfactory quantitative agreement with the measured cross section. (Notice that the fine structure of the measured total cross section around the doorway states at 410 and 480 kev (Figure II.19) roughly resemble the inverse of the cross sections in

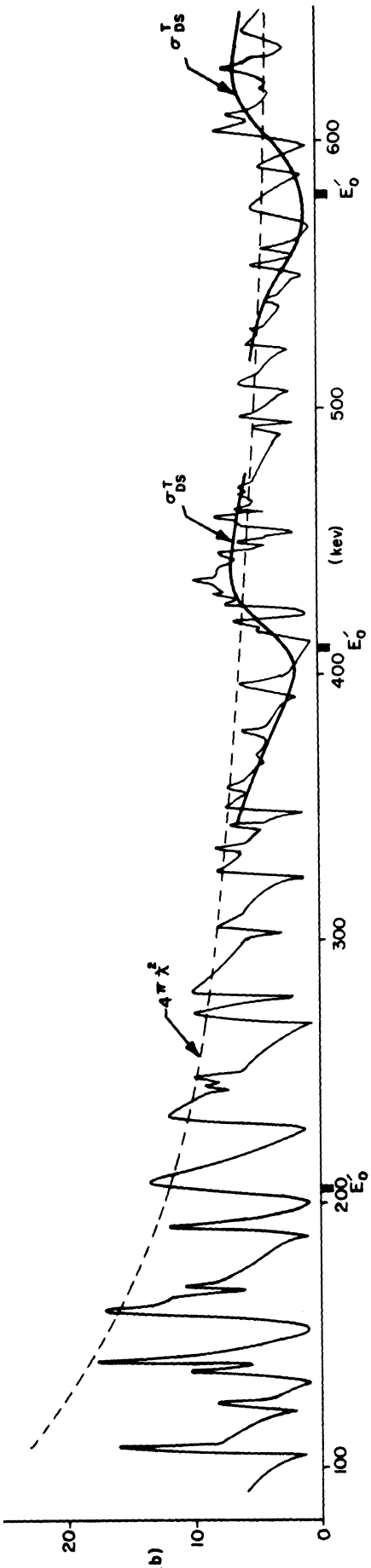

Figure II.19. Total Cross Section and the Background Cross Sections of N_i-58.

Figure II.17a for $2\delta = -\pi/3$ and $-\pi/6$ respectively, where the energy scale is measured from right to left.) This result verifies that the treatment of the resonance width distribution, and the evaluation of its constants $\Gamma^{\uparrow}$ and $\Gamma^{\downarrow}$ are correct.

Finally, the intermediate structure of the doorway state will be briefly discussed. The intermediate resonance around 410 kev is actually a wide dip due to the potential phase shift. According to the results of Part I, the dip width is equal to $\Gamma^{\uparrow} + \Gamma^{\downarrow}$ (= 205). On the other hand, the intermediate resonance given by Equation (3.3.1) is a sum of two dips with widths of 83 and 162 kev, where these values are obtained from Equations (3.3.1), (3.1.6), and (3.1.7). Since the ratio of the cross section $\sigma^{T}_{D.S.}$ to $\langle \sigma^{T}_{R.P} \rangle_{Area}$ around the doorway state is approximately $\Gamma^{\uparrow}/\Gamma^{\downarrow}$, we take a weighted average for the dip width of Equation (3.3.1)

$$\frac{83\,\Gamma^{\uparrow} + 162\,\Gamma^{\downarrow}}{\Gamma^{\uparrow} + \Gamma^{\downarrow}} = 103 \text{ kev}.$$

These two values, 205 and 103 kev, illustrate the difference between the average cross sections obtained in Part I and in this part. The latter value agrees well with the E-averaged cross section of N_i^{58} around 410 kev.

3.6 Doorway States at High Energies

In the continuum region, the number of open channels including the inelastic channels is large.(91) $\Gamma^{\uparrow}$ becomes large (see Equation (1.1.19)), while $\Gamma^{\downarrow}$ is expected to be approximately independent of

energy (see § 2.3). The situation of coupling strengths is therefore the WCL and the poles are given by Equation (2.2.4) and (2.2.5). In this section, the branching ratio will be studied. This ratio determines whether the bumps of the total cross section are caused by the doorway states.

For a given doorway state, the quantum numbers, J^π , are specified. Therefore, the open channels with channel indices $(\alpha l S J M) \equiv (\alpha c)$ may be coupled to the doorway state where $\pi = (-)^l$.

Taking energy units, we will denote the absolute value of the residue of the diagonal element of the resonant part of the T-matrix by $G_{\mu(\alpha c)}$. We have

$$G_{\mu(\alpha c)} = \frac{2\bar{D}}{\pi} |b_\mu| \left| (\underset{\sim}{G})_{(\alpha c)(\alpha c)} \right|$$

$$= -\frac{|b_\mu|}{U_0} \left| (\underset{\sim}{S}^P \cdot \underset{\sim}{\Gamma}^\uparrow)_{(\alpha c)(\alpha c)} \right| , \qquad (3.6.1)$$

where μ refers to the μ-th level, and $\underset{\sim}{G}$ is defined by Equation (1.1.15). The notations of § 1.1 is used throughout this section. The total width is given by the imaginary part of the μ-th pole.

For the WCL , $|b_\mu|$ of the anomalous pole and of the regular poles are given by Equation (2.3.17) and by Equation (2.3.8) respectively. For a given channel (αc) , the values of $G_{\mu(\alpha c)}$ are proportional to $|b_\mu|$; i.e. $G_{a(\alpha c)} >> G_{n(\alpha c)}$, where the subscripts a and n refer to the anomalous and the n-th regular pole. Actually, $G_{\mu(\alpha c)}$ is obtained with the results:

$$G_{a(\alpha c)} \cong 2 \left| (\underset{\sim}{S}^P \cdot \underset{\sim}{\Gamma}^{\uparrow})_{(\alpha c)(\alpha c)} \right| , \tag{3.6.2}$$

and

$$G_{n(\alpha c)} \cong \frac{\Gamma^{\downarrow} \left| (\underset{\sim}{S}^P \cdot \underset{\sim}{\Gamma}^{\uparrow})_{(\alpha c)(\alpha c)} \right|}{(E-E_0')^2 + \frac{1}{4}\left(\Gamma^{\uparrow 2} + \Gamma^{\downarrow 2} + \frac{4\bar{D}}{\pi}\Gamma^{\downarrow}\right)} . \tag{3.6.3}$$

For simplicity, we will limit the problem to the case that there is no direct reaction: $\underset{\sim}{S}^P$ is diagonal and unitary. Thus, Equation (3.6.2) becomes

$$G_{a(\alpha c)} = 2\,\Gamma^{\uparrow}_{(\alpha c)(\alpha c)} \tag{3.6.4}$$

The amplitude of a bump in the total cross section, Equation (2.2.29) of Part I, is approximately given by

$$\text{Amplitude} = 2\pi \lambda^2 g^J_{\alpha_0} \sum_c{}' \frac{G_{a(\alpha_0 c)}}{\Gamma^{\uparrow}}$$

$$= 4\pi \lambda^2 g^J_{\alpha_0} \sum_c{}' \frac{\Gamma^{\uparrow}_{(\alpha_0 c)(\alpha_0 c)}}{\Gamma^{\uparrow}} , \tag{3.6.5}$$

where α_0 refers to the ground state of the target nucleus and the sum over c includes all channel indices obeying the selection rules. This indicates that the amplitude of a bump can be large only if the doorway state is preferencially coupled to the elastic channels.

PART III

CALCULATION OF THE DOORWAY STATE FORMATION PROBABILITY

Introduction

In this part of the thesis, we take N_i-58 as an example of the target nucleus and calculate the doorway state formation probability, $\Gamma^{\uparrow}$. The model Hamiltonian is composed of a pairing force plus $P_L - P_L$ forces. This type of Hamiltonian has been developed by Kisslinger and Sorensen,[99] Baranger,[100] and Yoshida[97] to explain the low excited levels of vibrational type nuclei. The result of this calculation will be seen to agree reasonably well with the measured value of the doorway state formation probability.

In Chapter 1, we determine the low excited states of N_i-58 in order to obtain the force constants. The doorway states of N_i-59 are shown to be composed of three quasi-particles. In Chapter 2, the open channel wave function is represented in terms of shell model eigenfunctions and $\Gamma^{\uparrow}$ is expressed in a form suitable for computation. The doorway state formation probability is calculated and the results are briefly discussed in relation to the Lande-Brown model.

CHAPTER 1

A MODEL HAMILTONIAN AND THE DOORWAY STATES

For convenience of calculation, we will adopt the second quantization formalism.[48] The basis set may be the set of the O.M. wave functions or the set of the single-particle shell model wave functions. The former was chosen by Lemmer, Shakin, and Lovas.[71.77,80] The latter does not apply for the open channels. However, the low excited states have been explained on the basis of the latter representation and calculations of matrix elements of an observable using this basis are easy. In order to exploit this advantage, we will apply the shell model representation with a modification for the open channels. Namely, the bound states are expressed immediately in terms of the shell model wave functions, while the open channel wave functions are calculated from the O.M. Schrödinger equation and then the shell model expansion is applied.

The Hamiltonian we assume is:

$$H = K + U + H^A + H_{int}$$

$$\cong P(K + U_{OM} + H^A)P + Q(K + U_{SM} + H^A + H_{int})Q$$

$$+ PH_{int}Q + QH_{int}P \,, \qquad (1.1.1)$$

where U_{OM} is the real part of the O.M. potential and U_{SM} is the shell model potential.

The first term of the Hamiltonian will be treated in the next chapter. We will further specify the last three terms of Equation (1.1.1) by the model Hamiltonian developed by Kisslinger&Sorensen,[99] Baranger,[100] and Yoshida[97] for the low excited states of vibrational type nuclei:

The residual interaction potential is expanded into a tensor series,[72]

$$V(|\underline{r}_1-\underline{r}_2|)=\sum_{LM}\frac{4\pi x_L}{2L+1}U_L(r_1)\,U_L(r_2)\,Y^*_{LM}(\hat{\underline{r}}_1)\,Y_{LM}(\hat{\underline{r}}_2)\,, \tag{1.1.2}$$

and the Hamiltonian is

$$\mathcal{H}=\mathcal{H}_0+\mathcal{H}^{(4)}_{L-L}\,, \tag{1.1.3}$$

where

$$\mathcal{H}_0\equiv\sum_{\alpha}e_\alpha\,b^+_\alpha\,b_\alpha\,, \tag{1.1.4}$$

and

$$\begin{aligned}\mathcal{H}^{(4)}_{L-L}\equiv-\sum_{LM}\frac{2\pi x_L}{(2L+1)^2}\sum_{j_1\cdots j_4}&\langle N_1\ell_1j_1\|U_L\,Y_L\|N_3\ell_3j_3\rangle\times\\ &\times\langle N_2\ell_2j_2\|U_L\,Y_L\|N_4\ell_4j_4\rangle(-)^{L-M+j_1+j_2+j_3+j_4}\times\\ &\times\Big\{-U_{j_1}U_{j_2}V_{j_3}V_{j_4}\,B^+(j_1j_3;L-M)\,B^+(j_2j_4;LM)-\\ &-V_{j_1}V_{j_2}U_{j_3}U_{j_4}\,B(j_1j_3;L-M)\,B(j_2j_4;LM)+\\ &+2\left(U_{j_1}U_{j_2}V_{j_3}U_{j_4}-V_{j_1}V_{j_2}U_{j_3}V_{j_4}\right)B^+(j_1j_3;L-M)\,A^+(j_2j_4;LM)+\\ &+2\left(U_{j_1}V_{j_2}U_{j_3}U_{j_4}-V_{j_1}U_{j_2}V_{j_3}V_{j_4}\right)A^+(j_1j_3;L-M)\,B(j_2j_4;LM)-\\ &-2U_{j_1}V_{j_2}V_{j_3}U_{j_4}\,B^+(j_1j_3;L-M)\,B(j_2j_4;LM)\Big\}.\end{aligned} \tag{1.1.5}$$

The notations are as follows: b^+_α and b_α are creation and annihilation operators of a qusi-particle associated with a state specified by quantum numbers $\alpha\equiv(N\ell sjm)$ which are often abbreviated by (jm). These are related to the particle operators a^+_α and a_α[88] by the following relations (BCS-transformation[67]),

$$\left.\begin{aligned} b_\alpha &= u_\alpha a_\alpha - v_\alpha a_{\tilde{\alpha}}^+ \\ b_{\tilde{\alpha}} &= u_{\tilde{\alpha}} a_{\tilde{\alpha}} - v_{\tilde{\alpha}} a_\alpha^+ \\ &\text{etc.} \end{aligned}\right\} \qquad (1.1.6a)$$

where $a_{\tilde{\alpha}}^+$ is the time reversed operator of a_α^+ ; e.g.

$$a_{\tilde{\alpha}}^+ = (-)^{j-m} a_{j-m} \qquad (1.1.6b)$$

and where

$$\left.\begin{aligned} \{b_\alpha, b_{\alpha'}\} = \{b_\alpha^+, b_{\alpha'}^+\} &= 0 \ , \\ \{b_\alpha^+, b_{\alpha'}\} &= \delta_{\alpha\alpha'} \ , \\ \{A, B\} &\equiv AB + BA \ , \end{aligned}\right\} \qquad (1.1.6c)$$

and the real positive numbers, u_α, $v_{\tilde{\alpha}}$, v_α, $v_{\tilde{\alpha}}$, satisfy

$$\left.\begin{aligned} u_\alpha^2 + v_\alpha^2 &= 1 \\ u_{\tilde{\alpha}} = u_\alpha \ , \quad v_{\tilde{\alpha}} &= v_\alpha \end{aligned}\right\} \qquad (1.1.6d)$$

For given values of G (pairing force constant) and N (particle number), the single quasi-particle energy, e_α , and the constants u_α and v_α are obtained from the following relations,

$$e_\alpha = \sqrt{(\tilde{\varepsilon}_\alpha - \lambda)^2 + \Delta^2} \ , \qquad (1.1.7a)$$

$$\frac{G}{2} \sum_j \frac{2j+1}{\sqrt{(\tilde{\varepsilon}_\alpha - \lambda)^2 + \Delta^2}} = 1 \ , \qquad (1.1.7b)$$

$$N = \sum_{\alpha>0} 2 v_\alpha^2 \ , \qquad (1.1.7c)$$

where

$$\sum_{\alpha>0} \equiv \sum_{j} \sum_{m>0} \tag{1.1.8}$$

$$V_\alpha^2 = \frac{1}{2}\left(1 - \frac{\tilde{\varepsilon}_\alpha - \lambda}{\sqrt{(\tilde{\varepsilon}_\alpha - \lambda)^2 + \Delta^2}}\right) \tag{1.1.9}$$

$$\tilde{\varepsilon}_\alpha \equiv E_\alpha - G V_\alpha^2 \tag{1.1.10}$$

$$\Delta \equiv G \sum_{\alpha>0} U_\alpha V_\alpha \qquad \text{(gap parameter)}, \tag{1.1.11}$$

and E_α is the shell model single particle energy of a state α. The above relations of the BCS transformation are given in various articles (References 67, 97, and 100). The values of the parameters for N = 2 and various values of G are determined by solving Equations (1.1.7)-(1.1.11) by successive approximation and are listed in Tables III.1 and III.2, and shown in Figure III.1, where the values of E_α are taken from Table III.3. $\langle N'\ell'j' \| U_L Y_L \| N\ell j \rangle$ is the reduced matrix element defined by(97)

$$\langle N'\ell's'j'm' | U_L Y_{LM} | N\ell s j m \rangle$$

$$\equiv \frac{(-)^{L-j'+m}}{\sqrt{2L+1}} \langle j' j\ m'-m | LM \rangle \langle N'\ell'j' \| U_L Y_L \| N\ell j \rangle, \tag{1.1.12}$$

and will be often abbreviated by $\langle j' \| U_L Y_L \| j \rangle$, where $|N\ell s j m\rangle$ is the shell model single particle vector, Equation (D.18). B^+, B, and A^+ are vector coupled two quasi-particle operators defined by Equations (D.7)-(D.10).(67) Finally, χ_L is the $P_L - P_L$ (long-range) force constant.

The reduced matrix element is further related to the radial integral of the shell model wave function, Equation (D.15).(97) The formulae for the radial integrals are given in Appendix D.6.

TABLE III.1

QUASI-PARTICLE PARAMETERS AND PAIRING FORCE (MEV).

λ	-0.4	-0.6	-0.7	-1.0
Δ	0.859	1.066	1.173	1.455
G	0.328	0.390	0.421	0.505
$e_{3/2}$	0.947	1.223	1.366	1.765
$e_{5/2}$	1.460	1.744	1.888	2.299
$e_{1/2}$	1.712	1.989	2.130	2.538
$e_{9/2}$	3.700	3.946	4.072	4.444

TABLE III.2

QUASI-PARTICLE PARAMETERS FOR G = 0.421 (MEV)

α	e_α	V_α^2	U_α^2	V_α	U_α
$p_{3/2}$	1.366	0.244	0.756	0.494	0.870
$f_{5/2}$	1.888	0.108	0.892	0.329	0.944
$p_{1/2}$	2.130	0.082	0.918	0.287	0.958
$g_{9/2}$	4.073	0.021	0.979	0.146	0.989
$d_{5/2}$	6.507	0.008	0.992	0.091	0.996
$s_{1/2}$	7.790	0.006	0.994		
$d_{3/2}$	9.772	0.004	0.996		

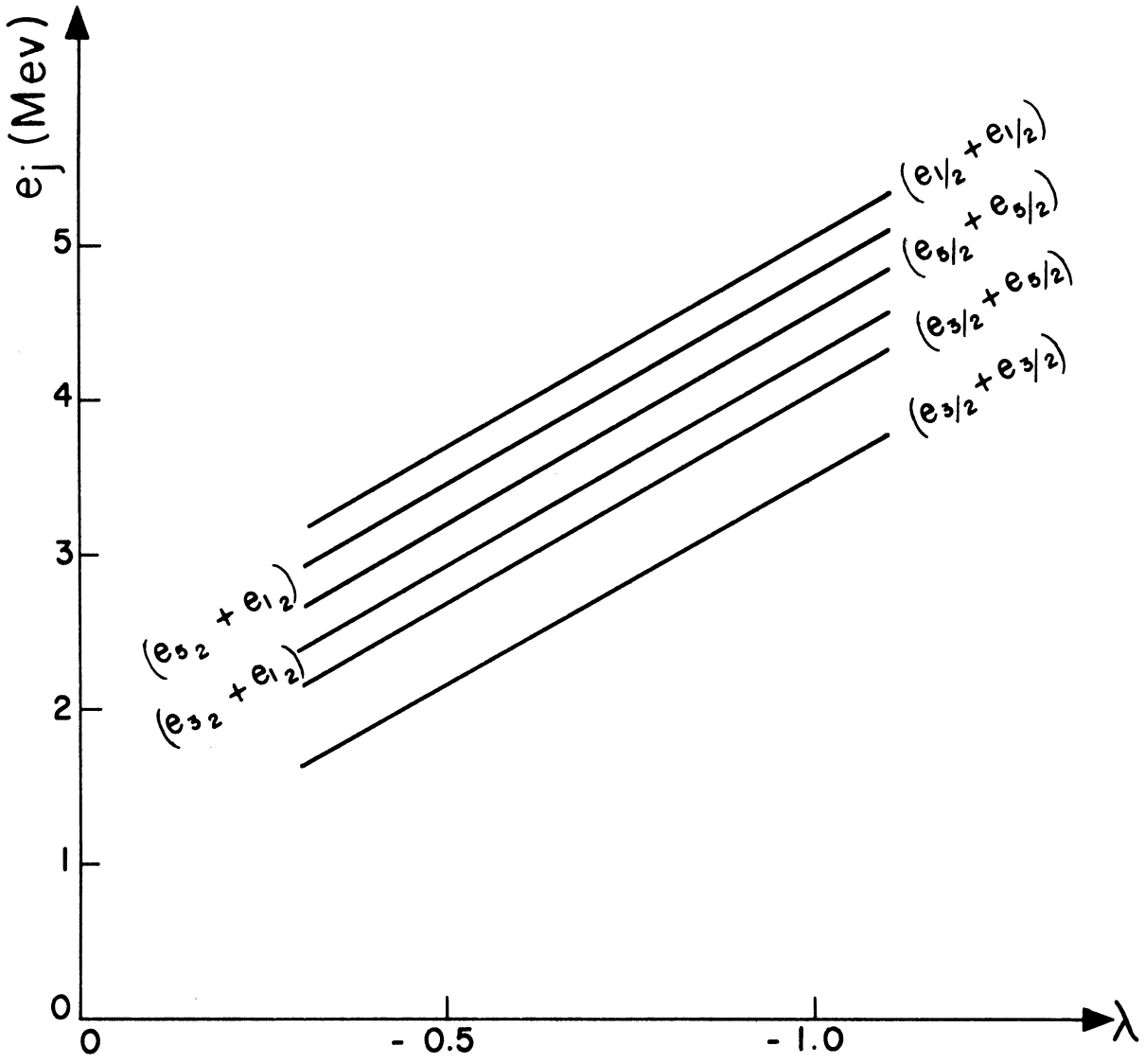

Figure III.1. Independent Two Quasi-Particle Energies $(e_\alpha + e_{\alpha'})$.

The single particle frequency, $\hbar\omega$, for the shell model radial wave function (Equation (D.20)) is obtained by[107]

$$\hbar\omega = 41/A^{1/3} = 10.6 \text{ (Mev)}.$$

The single particle energies, $E_{N\ell j}$, of interest to us are those of $2p_{3/2}$, $1f_{5/2}$, $2p_{1/2}$, $1g_{9/2}$, $2d_{5/2}$, $3s_{1/2}$, and $2d_{3/2}$. The values, which are obtained from the analysis of the direct reaction experiment; $Ni^{58}(d,p)Ni^{59}$,[11-16] are listed in Table III.3.

The neutron separation energy, B , of Ni^{59} is taken to be 9.00 Mev.[12]

TABLE III.3

$E_{N\ell j}$ WITH N_i-56 CORE (Mev)

	$p_{3/2}$	$f_{5/2}$	$p_{1/2}$	$g_{9/2}$	$d_{5/2}$	$s_{1/2}$	$d_{3/2}$
Ref. 11	0.3	0.6	2.2	3.5	6.0	7.3	9.3
Ref. 12	0.3	0.6	2.0	3.5	6.0	7.3	9.3
Ref. 13 - 16	0	0.78	1.08				
Our Choice	0	0.78	1.08	3.2	5.7	7.0	9.0

The second part of the Hamiltonian of Equation (1.1.1) may be decomposed into two parts:

$$\mathcal{H}^{(4)}_{L-L} = \mathcal{H}^{(4)}_{RPA} + \mathcal{H}^{(4)}_{rest} \tag{1.1.13}$$

where

$$\mathcal{H}^{(4)}_{RPA} \sim B^+B^+ + BB + B^+B$$

and

$$\mathcal{H}^{(4)}_{rest} \sim B^+A^+ + A^+B \tag{1.1.14}$$

In Equation (1.1.14), the terms of $\mathcal{H}^{(4)}_{L-L}$ proportional to B^+B, for example, are denoted by $\sim B^+B$. $\mathcal{H}^{(4)}_{RPA}$ will be approximated by $\mathcal{H}^{(4)}_{TD}$ where

$$\mathcal{H}^{(4)}_{TD} \sim B^+B \tag{1.1.15}$$

which is the Tamm-Dancoff approximation[67] for $\mathcal{H}^{(4)}_{L-L}$ and then

$$\left[\sum_\beta C_{\alpha\beta} B^+_\beta , \mathcal{H}_0 + \mathcal{H}^{(4)}_{TD} \right] = \hbar\omega_\alpha \sum_\beta C_{\alpha\beta} B^+_\beta \tag{1.1.16}$$

with $[A, B] \equiv AB - BA$.

Denote the quasi-vacuum state by $|\tilde{0}\rangle$; i.e. $b_\alpha |\tilde{0}\rangle = 0$ for all α. From Equation (1.1.16), we notice that $\{\sum C_{\alpha\beta} B^+_\beta\}^n |\tilde{0}\rangle$ is an n phonon state with the frequency ω_α.[67] $\mathcal{H}^{(4)}_{rest}$ may then be treated by perturbation theory. We write the Schrödinger equation in the form

$$\left(\mathcal{H}_0 + \mathcal{H}^{(4)}_{TD} + \mathcal{H}^{(4)}_{rest} \right) \Psi^{(n)}_{JM} = E^J_{(n)} \Psi^{(n)}_{JM} \tag{1.1.17}$$

where $\mathcal{H}_0 + \mathcal{H}^{(4)}_{TD}$ is explicitly

$$\mathcal{H}_0 + \mathcal{H}^{(4)}_{TD} = \sum_\alpha e_\alpha b^+_\alpha b_\alpha - \sum_{LM} \frac{4\pi\chi_L}{(2L+1)^2} \times$$

$$\times \sum_{j_1 \cdots j_4} \langle j_1 \| U_L Y_L \| j_3 \rangle \langle j_2 \| U_L Y_L \| j_4 \rangle U_{j_1} V_{j_2} V_{j_3} U_{j_4} \times$$

$$\times B^+(j_1 j_3; L-M)\, B(j_2 j_4; LM). \tag{1.1.18}$$

For the system with two quasi-particles, the zero-th order solution of Equation (1.1.17) is straightforward: The ground state is immediately known to be $|\tilde{0}\rangle$, while the excited states are given by

$$\Psi^{(n)}_{JM} = \sum_{j'j} C^{JM(n)}_{j'j} B^+(j'j; JM) |\tilde{0}\rangle , \tag{1.1.19}$$

where

$$\langle \psi^{(n)}_{JM} \mid \psi^{(n')}_{J'M'} \rangle = \delta_{nn'}\,\delta_{JJ'}\,\delta_{MM'}, \qquad (1.1.20)$$

and the coefficients are obtained in Reference 97;

$$C^{(n)}_{J} \equiv \sum_{j'j} (-)^{j+j'} (U_{j'}V_{j} + V_{j'}U_{j}) \langle j' \| U_L Y_L \| j \rangle C^{JM(n)}_{j'j}, \qquad (1.1.21)$$

$$C^{JM(n)}_{j'j} = C^{(n)}_{J} \frac{2\pi\chi_J}{(2J+1)^2} (-)^{j'+j} \frac{(U_{j'}V_{j} + V_{j'}U_{j}) \langle j' \| U_L Y_L \| j \rangle}{E^{J}_{(n)} - (e_{j'} + e_{j})}, \qquad (1.1.22)$$

$$C^{(n)}_{J} C^{(n')}_{J} \left(\frac{2\pi\chi_J}{(2J+1)^2} \right)^2 \sum_{j'j} \frac{(U_{j'}V_{j} + V_{j'}U_{j})^2}{\{ E^{J}_{(n)} - (e_{j'} + e_{j}) \}^2} \times$$

$$\times \left(\langle j' \| U_L Y_L \| j \rangle \right)^2 = \delta_{nn'}, \qquad (1.1.23)$$

$$1 = \frac{2\pi\chi_J}{(2J+1)^2} \sum_{j'j} \frac{(U_{j'}V_{j} + V_{j'}U_{j})^2 (\langle j' \| U_L Y_L \| j \rangle)^2}{E^{J}_{(n)} - (e_{j'} + e_{j})}, \qquad (1.1.24)$$

and

$$C^{JM(n)}_{j'j} = (-)^{l+j'+j-J}\, C^{JM(n)}_{jj'} \qquad \text{for } j \neq j'. \qquad (1.1.25)$$

The zero-th order results turn out to be exact solutions of Equation (1.1.17) because

$$\langle \underset{\sim}{0} \mid \mathcal{H}^{(4)}_{rest}\, B^{+} \mid \underset{\sim}{0} \rangle = \langle \underset{\sim}{0} \mid B^{+}\, \mathcal{H}^{(4)}_{rest}\, B^{+} \mid \underset{\sim}{0} \rangle = 0.$$

The low excited levels with positive parity of Ni^{58} are formed by two quasi-particles in (pf) states. The estimated values of the reduced matrix elements for these states are listed in Table III.4 (see Equations (1.1.12) and (D.15) and Table D.1).

TABLE III.4

RADIAL INTEGRALS (R.I.), AND REDUCED MATRIX ELEMENTS (R.M.E)

J	ℓ_j	$\ell_{j'}$	R.I.	R.M.E.
2	$p_{3/2}$	$p_{3/2}$	9/2	$9/2\sqrt{\pi}$
	$p_{3/2}$	$f_{5/2}$	$-\sqrt{14}$	$-\sqrt{6}/\sqrt{\pi}$
	$p_{3/2}$	$p_{1/2}$	9/2	$-9/2\sqrt{\pi}$
	$p_{1/2}$	$f_{5/2}$	$-\sqrt{14}$	$\sqrt{21}/\sqrt{\pi}$
	$f_{5/2}$	$f_{5/2}$	9/2	$9\sqrt{3}/\sqrt{7\pi}$
4	$p_{3/2}$	$f_{5/2}$	$-33\sqrt{14}/4$	$-99/2\sqrt{\pi}$
	$f_{5/2}$	$f_{5/2}$	99/4	$-297/4\sqrt{14\pi}$

Solving the secular Equation (1.1.24), we determine the force constants, G, χ_2, and χ_4, such that the levels $E^J_{(n)}$ agree with the measured excited levels of Ni^{58} as well as the levels calculated by Lawson et. al.*(107) (See Figure III.3). The determined values are $G = 0.421$ (Mev), $x_2 = -0.337$ (Mev), and $x_4 = -0.021$ (Mev), and the energy levels, $E^J_{(n)}$, are shown in Figure III.2. The values of $E^J_{(n)}$, $C^{(n)}_J$, and $C^{J(n)}_{j'j}$ for $J = 2$ are listed in Tables III.5 and III.6.

For the highly excited states of the compound nucleus, Ni^{59}, more than three quasi-particles are expected to be excited. The eigenfunctions of $\mathcal{H}_0 + \mathcal{H}^{(4)}_{TD}$ of the odd neutron system are given by

$$\sim b^+|\tilde{0}\rangle,\ \sim b^+B^+|\tilde{0}\rangle,\ \sim b^+B^+B^+|\tilde{0}\rangle,\ \cdots\cdots .$$

The elastic channel and the remaining channels are spanned by $\sim b^+|\tilde{0}\rangle$ and $\sim (b^+B^+ + b^+B^+B^+ + \cdots)|\tilde{0}\rangle$ respectively; i.e.

$$P \sim b^+|\tilde{0}\rangle\langle\tilde{0}|b$$

and

$$Q \sim (b^+B^+ + b^+B^+B^+ + \cdots)|\tilde{0}\rangle\langle\tilde{0}|(Bb + BBb + \cdots).$$

Since

$$\langle\tilde{0}|b\,\mathcal{H}\,b^+B^+|\tilde{0}\rangle = \langle\tilde{0}|b\,\mathcal{H}^{(4)}_{rest}\,b^+B^+|\tilde{0}\rangle \neq 0$$

and

$$\langle\tilde{0}|b\,\mathcal{H}\,b^+\overbrace{B^+\cdots B^+}^{N}|\tilde{0}\rangle = 0 \quad \text{for } N=0 \text{ and } N\geq 2,$$

then the subspace q_1 is formed by $\sim b^+B^+|\tilde{0}\rangle$ and the doorway states are composed of the three quasi-particle states.

---

*The author appreciates Dr. Lawson's information on his calculation and matrix elements before publication.

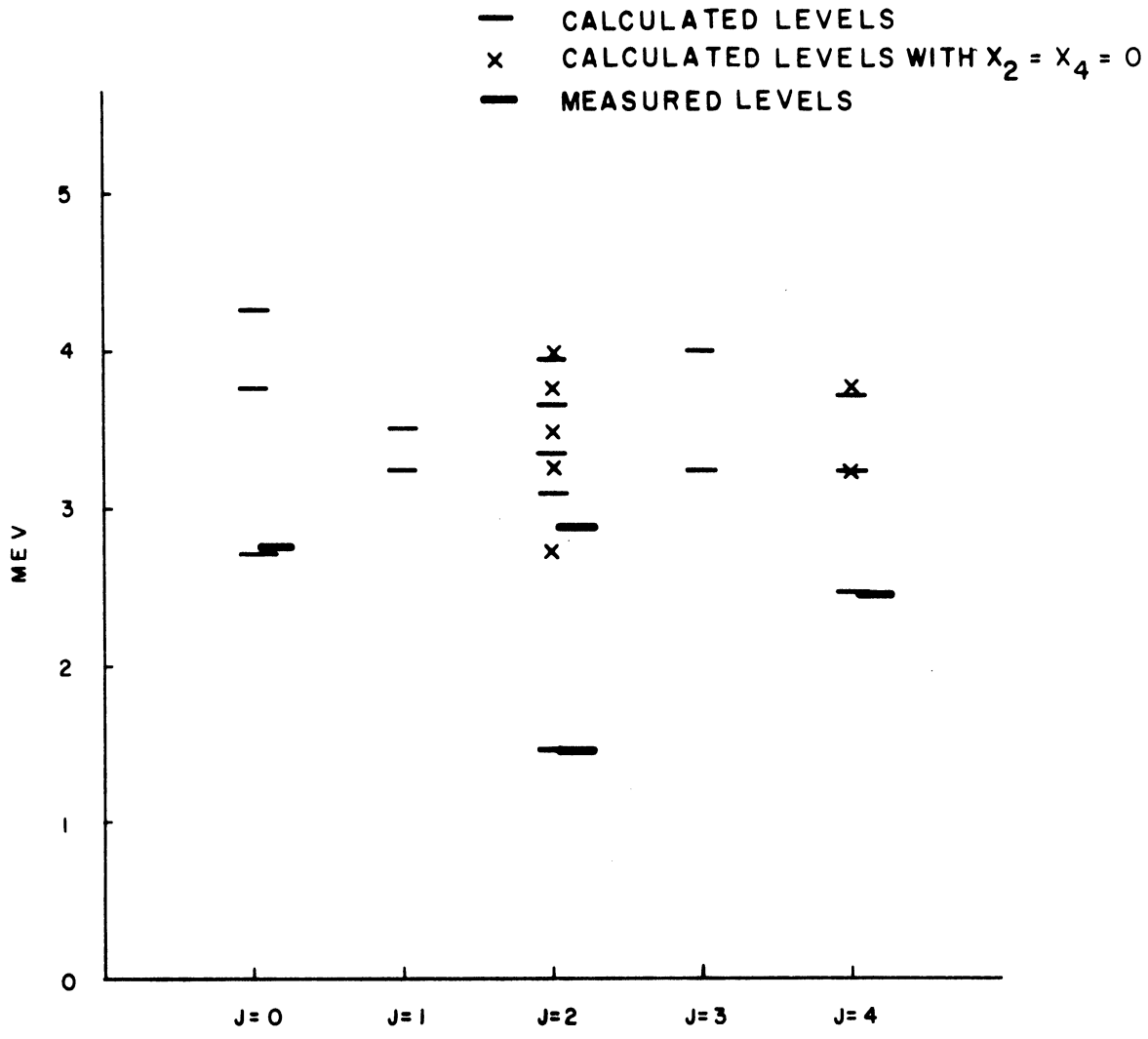

Figure III.2. Low Excited Energy Levels of N_i-58.

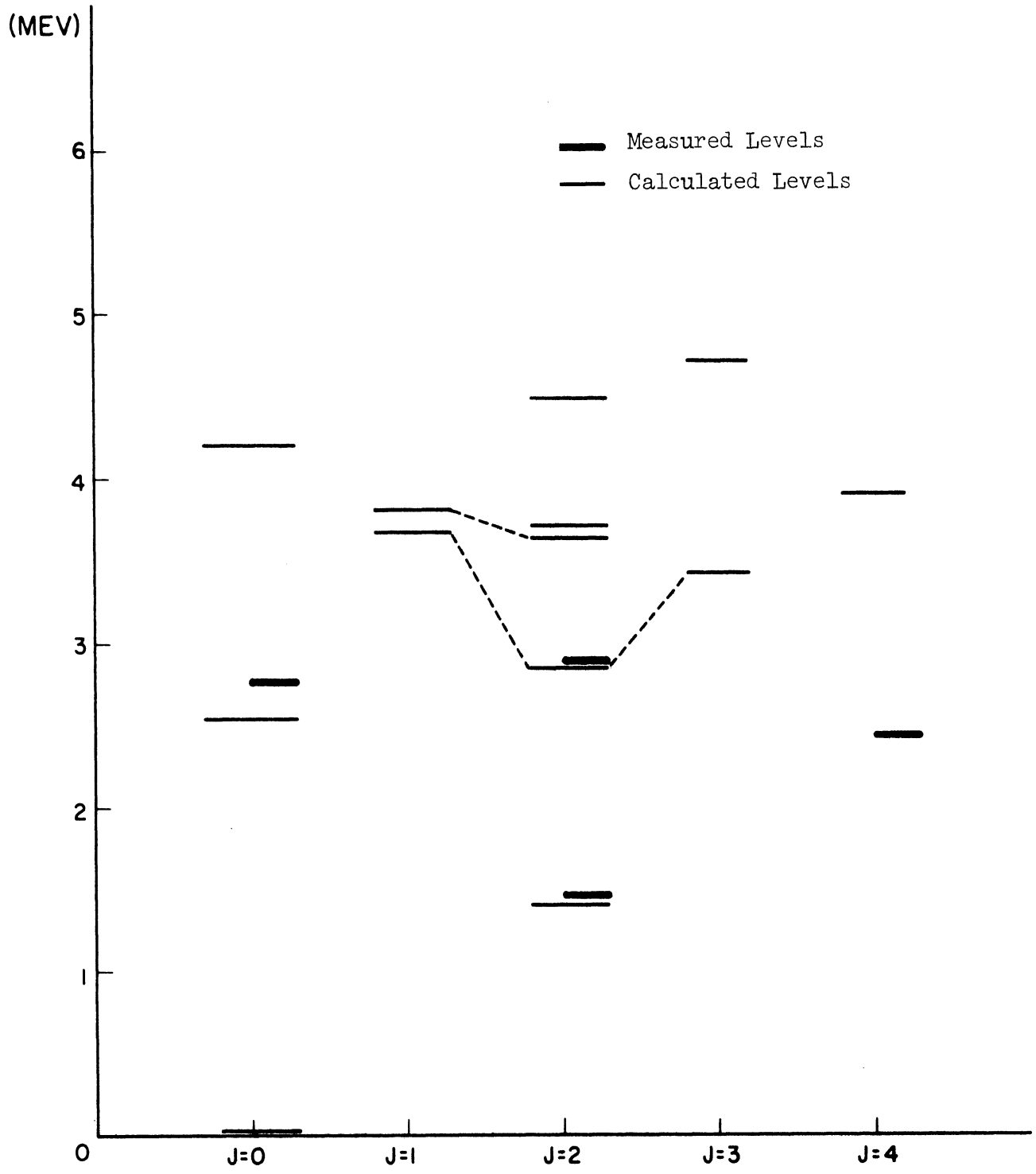

Figure III.3. Calculated Levels by Lawson et. al.[107]

TABLE III.5

$E^{J}_{(n)}$ AND $C^{(n)}_{J}$ FOR J = 2 AT x_2 = -0.337 (MEV)

n	$E^{2}_{(n)}$ (Mev)	$C^{(n)}_{2}$
1	1.45	3.24
2	2.98	0.701
3	3.32	0.299
4	3.68	0.311
5	3.94	0.267

TABLE III.6a

$C^{J(1)}_{j'j}$ FOR $J = 2$

j' \ j	$p_{3/2}$	$f_{5/2}$	$p_{1/2}$
$p_{3/2}$	0.466	0.158	0.246
$f_{5/2}$	-0.158	0.248	0.161
$p_{1/2}$	-0.246	0.161	0

TABLE III.6b

$C^{J(2)}_{j'j}$ FOR $J = 2$

j' \ j	$p_{3/2}$	$f_{5/2}$	$p_{1/2}$
$p_{3/2}$	-0.517	0.227	0.212
$f_{5/2}$	-0.227	0.154	0.087
$p_{1/2}$	-0.212	0.087	0

TABLE III.6c

$C^{J(3)}_{j'j}$ FOR $J=2$

j' \ j	$p_{3/2}$	$f_{5/2}$	$p_{1/2}$
$p_{3/2}$	-0.094	-0.410	0.261
$f_{5/2}$	0.410	0.114	0.055
$p_{1/2}$	-0.261	0.055	0

TABLE III.6d

$C^{J(4)}_{j'j}$ FOR $J=2$

j' \ j	$p_{3/2}$	$f_{5/2}$	$p_{1/2}$
$p_{3/2}$	-0.060	-0.064	-0.261
$f_{5/2}$	0.064	0.569	0.118
$p_{1/2}$	0.261	0.118	0

TABLE III.6e

$C^{J(5)}_{j'j}$ FOR $J=2$

j' \ j	$p_{3/2}$	$f_{5/2}$	$p_{1/2}$
$p_{3/2}$	-0.41	-0.034	-0.093
$f_{5/2}$	0.034	-0.283	0.446
$p_{1/2}$	0.093	0.446	0

For our case of $\eta + Ni^{58}$ reaction with $J^{\pi} = (1/2)^{+}$, parity and angular momentum conservations restrict the possible three quasi-particle states as follows: One and only one of the quasi-particles is either $g_{9/2}$, $d_{5/2}$, $s_{1/2}$, or $d_{3/2}$. Each of the other two is either $p_{3/2}$, $f_{5/2}$, or $p_{1/2}$.

CHAPTER 2

DOORWAY STATE FORMATION PROBABILITY

2.1 Single Particle Potential and the Distorted Wave

We choose the single particle potential for the incident neutron to be a three dimensional (3-D) square well. The two parameters, radius and depth, are chosen as follows: The nuclear radius is taken from the result of the O.M. calculation,[43]

$$a = 1.16\, A^{1/3} + 0.6 \quad fm. \tag{2.1.1}$$

The value is 5.06 fm which is also obtained by $a = 1.30\, A^{1/3}$ fm. The potential depth will be determined such that the energy level of $3S_{1/2}$ lies at 2 Mev below zero incident neutron energy to agree with the measured single particle level (see Table III.3). The estimated value is

$$V_0 = -51.3 \quad Mev. \tag{2.1.2}$$

The depth of the Wood-Saxon potential[43] is 46 Mev in good agreement with our result. Figurative comparison of the potentials is given in Figure III.4.

The distorted wave χ is expanded in terms of shell model wave functions:

$$\chi^{(+)}_{lsjm} = \sum_N C_N^{lj} \, | N l s j m \rangle \, \Psi_{0^+}^{N_i - 58}, \tag{2.1.3}$$

where we have used the fact that the ground state of N_i^{58} is 0^+. Since the incident neutron wave function does not belong to L_2, it may not be expanded by the set of $|Nlsjm\rangle$. However, the couplings between the open and closed channels are spatially limited because the bound state wave function approaches zero as e^{-r^2} when $r \to \infty$.

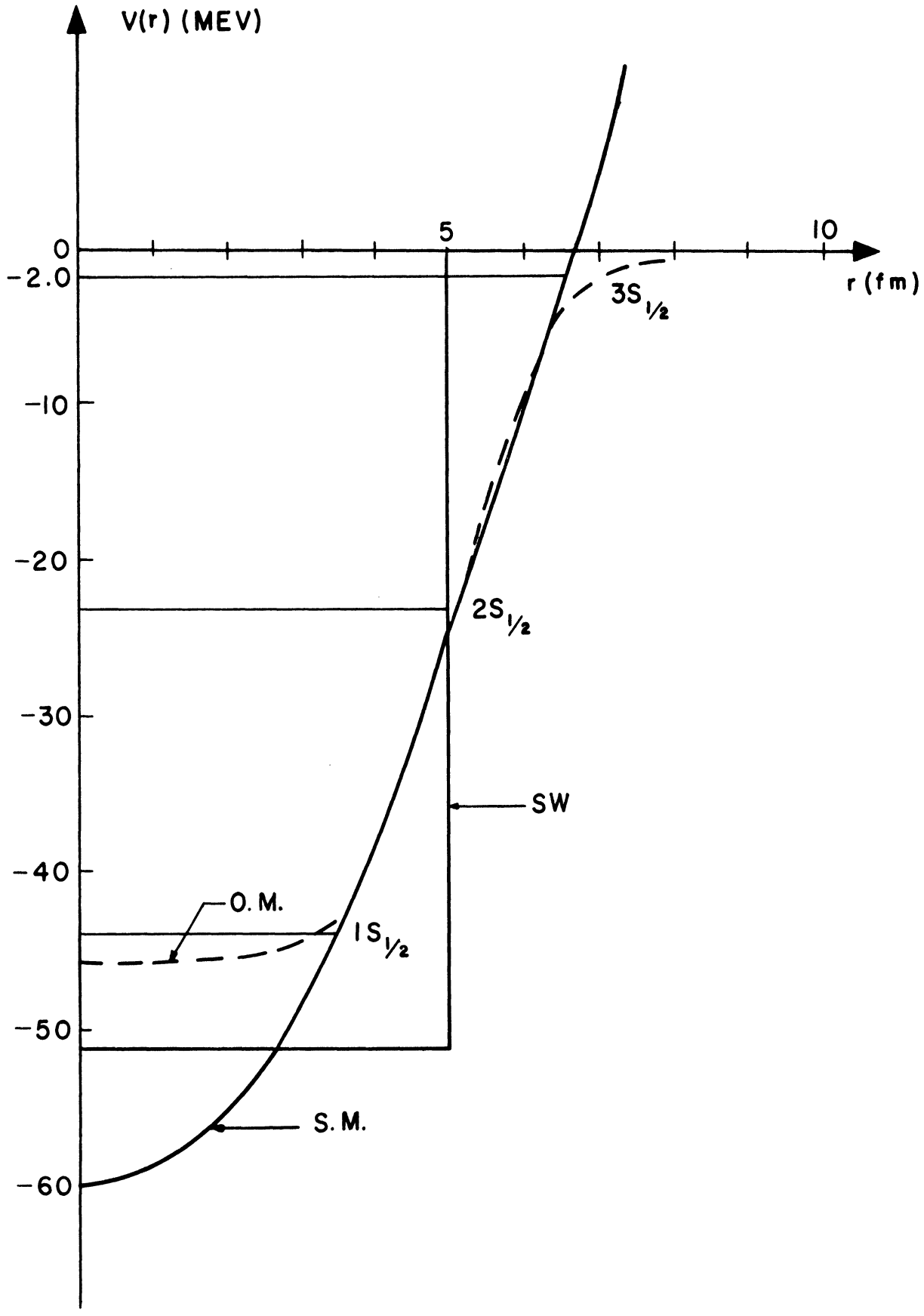

Figure III.4. Single Particle Potentials; 3-D Square Well (S.W.), Shell Model (S.M.), and Optical Model (O.M.) Potentials.

Hence, we may replace $\chi^{(+)}_{\ell s j m}$ by $\chi^{(+)}_{\ell s j m}\,\theta$ where θ is the step function defined by

$$\theta(r_0, R) \equiv \begin{cases} 1 & \text{for } r_0 < R \\ 0 & \text{for } r_0 > R \end{cases} \tag{2.1.4}$$

and then expand:

$$\chi^{(+)}_{\ell s j m}\,\theta(r_0, R) = \sum_N C_N^{\ell j} |N \ell s j m\rangle \Psi_{0^+}^{N_i - 58}. \tag{2.1.5}$$

In the second quantization, the open channel vector is thus effectively given by

$$|\chi^{(+)}_{\ell_k s_k j_k m_k}\rangle = \sum_N C_N^{\ell_k j_k}\, b^{+}_{(k)} |0\rangle \tag{2.1.6}$$

where the subscripts $(N \ell_k s_k j_k m_k)$ are abbreviated by (k).

Now, the distorted wave with $(\nu_2)^+$ is easily obtained from Equation (2.2.35) of Part I[87] with the result,

$$\chi^{(+)}_{E 0 \nu_2 \nu_2 m_k} = \beta^{\nu_2} N_k \frac{R_\chi(r_0)}{r_0} Y_{00}(\hat{r}_0)\, u_{\nu_2 m_k} \Psi_{0^+}^{N_i - 58}, \tag{2.1.7}$$

where

$$R_\chi(r_0)\,\theta(r_0, R) = \begin{cases} \sin \varkappa r_0 & \text{for } r_0 \le a, \\ -\varkappa (r_0 - a)\cos\mu_0 + \sin\mu_0 & \\ & \text{for } a < r_0 < R, \\ 0 & \text{for } r_0 > R, \end{cases} \tag{2.1.8}$$

$$\kappa \equiv \sqrt{\frac{2\mu}{\hbar^2}(E + V_0)}\,, \tag{2.1.9}$$

$$\mu_0 \equiv \kappa a\,, \tag{2.1.10}$$

$$N_k \equiv \sqrt{\frac{2}{\pi}}\sqrt{\frac{k}{\kappa}}\frac{1}{\gamma\hbar\omega}\cdot\frac{\mu_0 e^{-i\rho_0}}{\rho_0 \sin\mu_0 + i\mu_0 \cos\mu_0}\,, \tag{2.1.11}$$

$$\rho_0 \equiv k a \tag{2.1.12}$$

$$\gamma \equiv \kappa/\sqrt{\beta} \tag{2.1.13}$$

and β is defined by Equation (D.22). As will be seen later, the radial integrals, § 2.2, converge rapidly as R becomes large so that the results turn out to be insensitive to the choice of cut-off R .

2.2 Formulation of $\Gamma^{\uparrow}$

The doorway state formation probability, $\Gamma^{\uparrow}$, is defined in Part I.

$$\Gamma^{\uparrow}_{s} = 2\pi \sum_{lsjm} \left| \langle \chi^{(+)}_{lsjm} | PHq_1 | \varphi_s \rangle \right|^2 . \tag{2.2.1}$$

The doorway states of $(1/2)^+$ are composed of three quasi-particles:

$$|\varphi_s\rangle \equiv |(J(n)\, j_\alpha)(1/2)^+ m\rangle = \sum_{m' m_\alpha} \langle j_\alpha J m_\alpha M' | \tfrac{1}{2} m\rangle \times$$

$$\times b^+_\alpha \sum_{j'j} C^{J(n)}_{j'j} B^+(j'j; JM') |0\rangle, \tag{2.2.2}$$

where the low excited states, Equation (1.1.19), are vector coupled to a one quasi-particle state. In this section, $\Gamma_s^{\uparrow}$ will be reduced to a form suitable for practical calculation. Since $PHq_1 = \mathcal{H}^{(4)}_{nest}$, we have

$$\Gamma^{\uparrow}_{(J(n)\, j_\alpha)\, 1/2^+} = 2\pi \sum_{l_k j_k m_k} \Big| \sum_N C_N^{(k)} \sum_{LM} \frac{4\pi \chi_L}{(2L+1)^2} \times$$

$$\times \sum_{j_1 j_2 j_3 j_4} (-)^{L-M+j_1+j_2+j_3+j_4} \langle j_1 \| U_L Y_L \| j_3 \rangle \langle j_2 \| U_L Y_L \| j_4 \rangle \times$$

$$\times \left(U_{j_1} V_{j_2} U_{j_3} U_{j_4} - V_{j_1} U_{j_2} V_{j_3} V_{j_4} \right) \sum_{m_\alpha M'} \langle j_\alpha J\, m_\alpha M' | \tfrac{1}{2}\, m \rangle \times$$

$$\times \langle \underset{\sim}{0} | b_{(k)} A^+(j_2 j_3; L-M) B(j_3 j_4; LM)\, b^+_\alpha \sum_{j' j} C^{J(n)}_{j' j} B^+(j' j; J M') | \underset{\sim}{0} \rangle \Big|^2 . \qquad (2.2.3)$$

For the doorway state to have positive parity, j' and j run over (pf) states and α over (sdg) states. For even L, parities of j_1 and j_3, and of j_2 and j_4 must be the same because the reduced matrix element has the property:

$$\langle N' l' j' \| U_L Y_L \| N l j \rangle \sim 1 + (-)^{l+l'+L}$$

Also, by similar parity considerations, we can show that $[B(j_2 j_4; LM), b^+_\alpha] = 0$

In view of these selection rules, the expression (2.2.3) reduces to

$$\Gamma^{\uparrow}_{(J(n)\, j_\alpha)\, 1/2^+} = 2\pi \sum_{l_k (=\text{even})\, j_k m_k} \Big| \sum_N C_N^{(k)} \sum_{LM} \frac{4\pi \chi_L}{(2L+1)^2} \times$$

$$\times \sum_{j_2 j_4} (-)^{L-M+j_k+j_2+j_\alpha+j_4} \langle j_k \| U_L Y_L \| j_\alpha \rangle \langle j_2 \| U_L Y_L \| j_4 \rangle \times$$

$$\times \left(U_{j_k} V_{j_2} U_{j_\alpha} U_{j_4} - V_{j_k} U_{j_2} V_{j_\alpha} V_{j_4} \right) \sum_{m_\alpha} \langle j_k j_\alpha\, m_k - m_\alpha | L - M \rangle (-)^{j_\alpha + m_\alpha} \times$$

$$\times \sum_{M'} \langle j_\alpha J\, m_\alpha M' | \tfrac{1}{2}\, m \rangle \sum_{j' j} C^{J(n)}_{j' j} \langle \underset{\sim}{0} | B(j_2 j_4; LM) \times$$

$$\times B^+(j' j; J M') | \underset{\sim}{0} \rangle \Big|^2 ,$$

$$= \frac{(4\pi)^3 \chi_J^2}{2(2J+1)^3(2j_k+1)} \left| \sum_N C_N^{(k)} \langle j_k \| U_L Y_L \| j_\alpha \rangle \sum_{j_2 j_4} (-)^{j_2+j_4} \times \right.$$

$$\left. \times \langle j_2 \| U_L Y_L \| j_4 \rangle Z C_{j_2 j_4}^{J(n)} \left(U_{j_k} V_{j_2} U_{j_\alpha} U_{j_4} - V_{j_k} U_{j_2} V_{j_\alpha} V_{j_4} \right) \right|^2, \qquad (2.2.4)$$

where $j_k = 1/2$ otherwise $\Gamma^\uparrow = 0$. In the above derivation, we have applied Equations (D.13), (1.1.25), and (2.1.5).

We will make the approximation that $U_{j_k} \cong 1$ and $V_{j_k} \cong 0$ for all N. This is valid for $N > 3$. For $N < 3$, the reduced matrix elements are small, so that there is little contribution to $\Gamma^\uparrow$. Applying Equations (1.1.21) and (1.1.25), we have

$$\Gamma^\uparrow_{(J(n) j_\alpha) 1/2^+} = \frac{(4\pi)^3 \chi_J^2}{2(2J+1)^3(2j_k+1)} \left| \langle k \| U_J Y_J \| j_\alpha \rangle U_{j_\alpha} \right|^2 \times$$

$$\times \left(C_J^{(n)} \right)^2, \qquad (2.2.5)$$

where we have defined:

$$\langle k \| U_J Y_J \| j_\alpha \rangle \equiv \sum_N C_N^{\ell_k j_k} \langle N \ell_k j_k \| U_J Y_J \| N_\alpha \ell_\alpha j_\alpha \rangle. \qquad (2.2.6)$$

By Equations (D.15), (2.1.5), and (2.1.9), this reduced matrix element is calculated with the result:

$$\langle k \| U_J Y_J \| j_\alpha \rangle = (-)^{j_\alpha - j_k} \frac{1+(-)^{\ell_\alpha + \ell_k + J}}{2} \sqrt{\frac{(2J+1)(2j_k+1)}{4\pi}} \times$$

$$\times \langle j_k J \; 1/2 \; 0 | j_\alpha \; 1/2 \rangle \langle k | U_J | N_\alpha \ell_\alpha \rangle, \qquad (2.2.7)$$

where in the above derivation we have used the following relation of the radial integrals

$$\sum_N C_N^{l_k j_k} \langle N l_k | U_J | N_\alpha l_\alpha \rangle = \langle k | U_J | N_\alpha l_\alpha \rangle$$

$$= N_k \int_0^\infty \beta^{1/4} dr_0 \; \vartheta(r_0, R) R_\chi(r_0) (\beta^{1/2} r_0)^J R_{n_\alpha l_\alpha}(r_0)$$

$$= N_k C_{n_\alpha l_\alpha} I_{J n_\alpha l_\alpha}, \qquad (2.2.8)$$

and where

$$C_{n_\alpha l_\alpha} \equiv \left[\frac{2 n_\alpha !}{\Gamma(n_\alpha + l_\alpha + 3/2)} \right]^{1/2} \qquad (2.2.9)$$

and

$$I_{J n_\alpha l_\alpha} \equiv \int_0^\infty dy \; \vartheta(y, R/\gamma) R_\chi(y/\gamma) e^{-\frac{y^2}{2}} \times$$

$$\times y^{J+l+1} L_{n_\alpha}^{l+1/2}(y^2). \qquad (2.2.10)$$

The estimated values of $C_{n_\alpha l_\alpha} I_{J n_\alpha l_\alpha}$ for $J = l_\alpha = 2$ and $n_\alpha = 1$ and for $J = l_\alpha = 4$ and $n_\alpha = 1$ are -6.11 and 14.96 respectively.

By the triangular relation of the reduced matrix element of Equation (2.2.7), for $j_k = 1/2$ and a given J, the states of j_α are selected as follows: For $J = 2$, these are $d_{3/2}$ and $d_{5/2}$ and for $J = 4$, $g_{9/2}$.

Finally, $\Gamma^\uparrow$ becomes

$$\Gamma^\uparrow_{(J(n) j_\alpha) 1/2^+} = \frac{4\pi^2 \chi_J^2}{2(2J+1)^2} \left(C_J^{(n)}\right)^2 |N_k|^2 \times$$

$$\times \left(\langle \tfrac{1}{2} J \tfrac{1}{2} 0 | j_\alpha \tfrac{1}{2} \rangle \right)^2 \left(C_{n_\alpha l_\alpha} I_{J n_\alpha l_\alpha} \right)^2, \qquad (2.2.11)$$

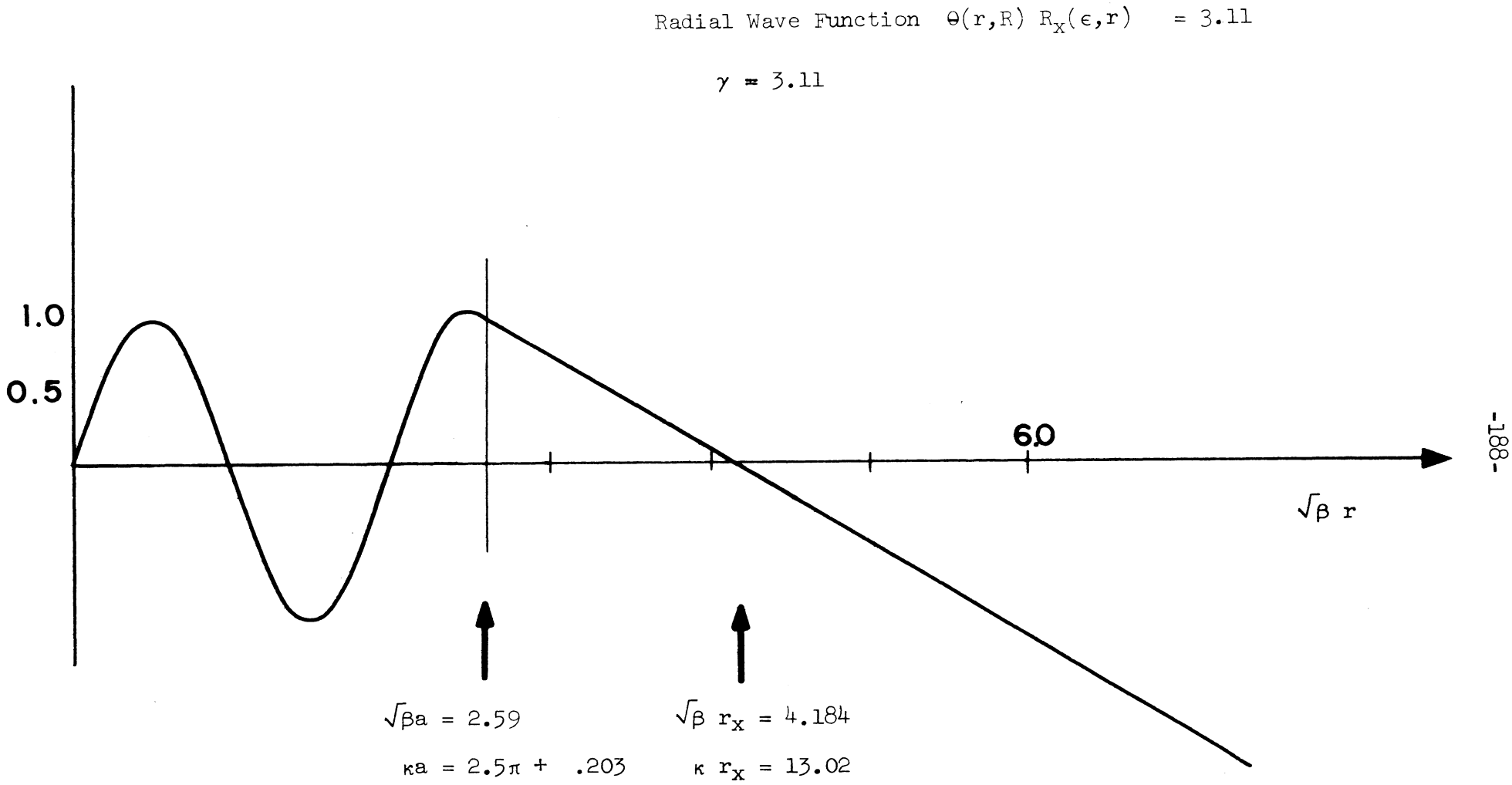

Figure III.5. Radial Wave Function of the Incident Neutron.

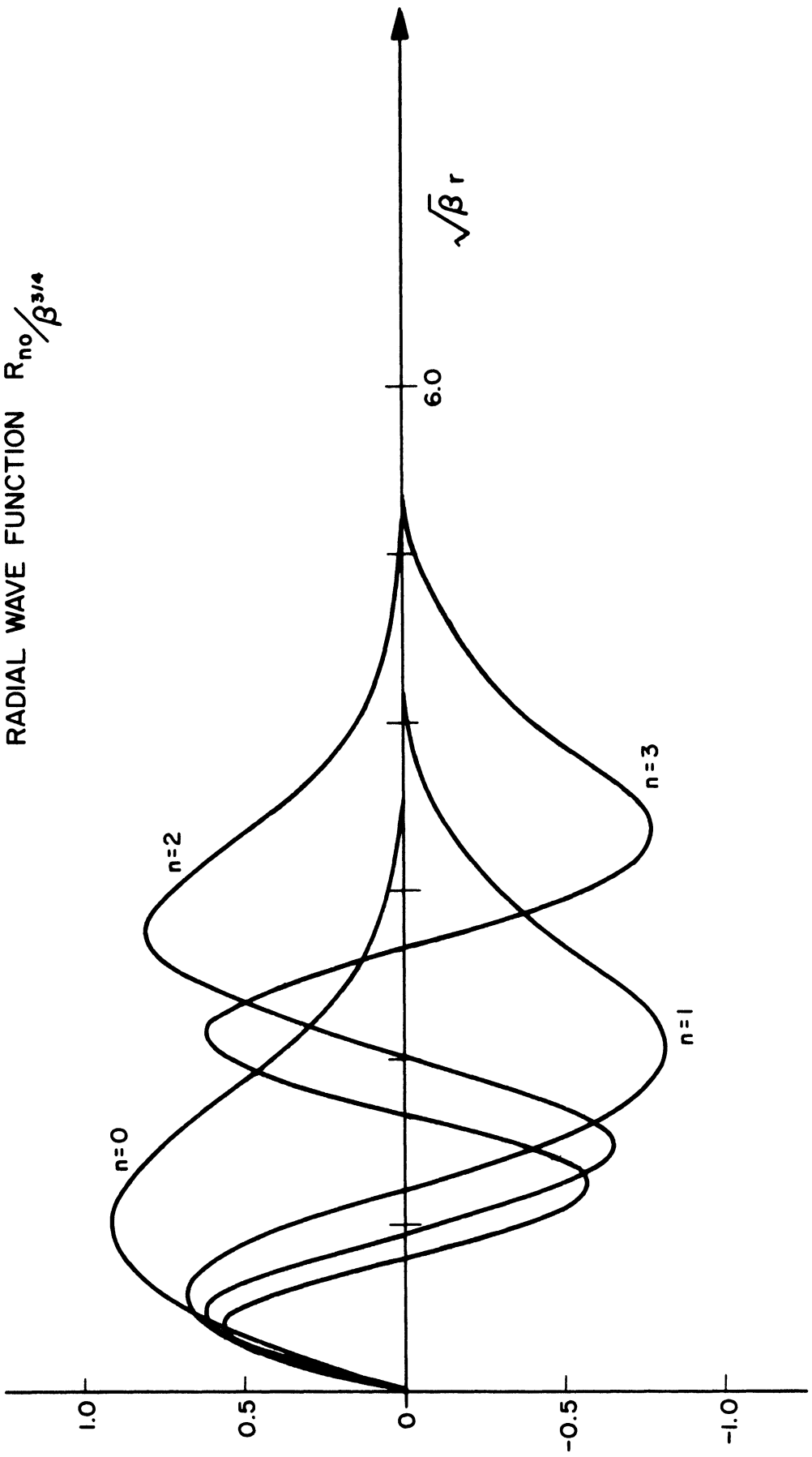

Figure III.6. Bound State Radial Wave Functions.

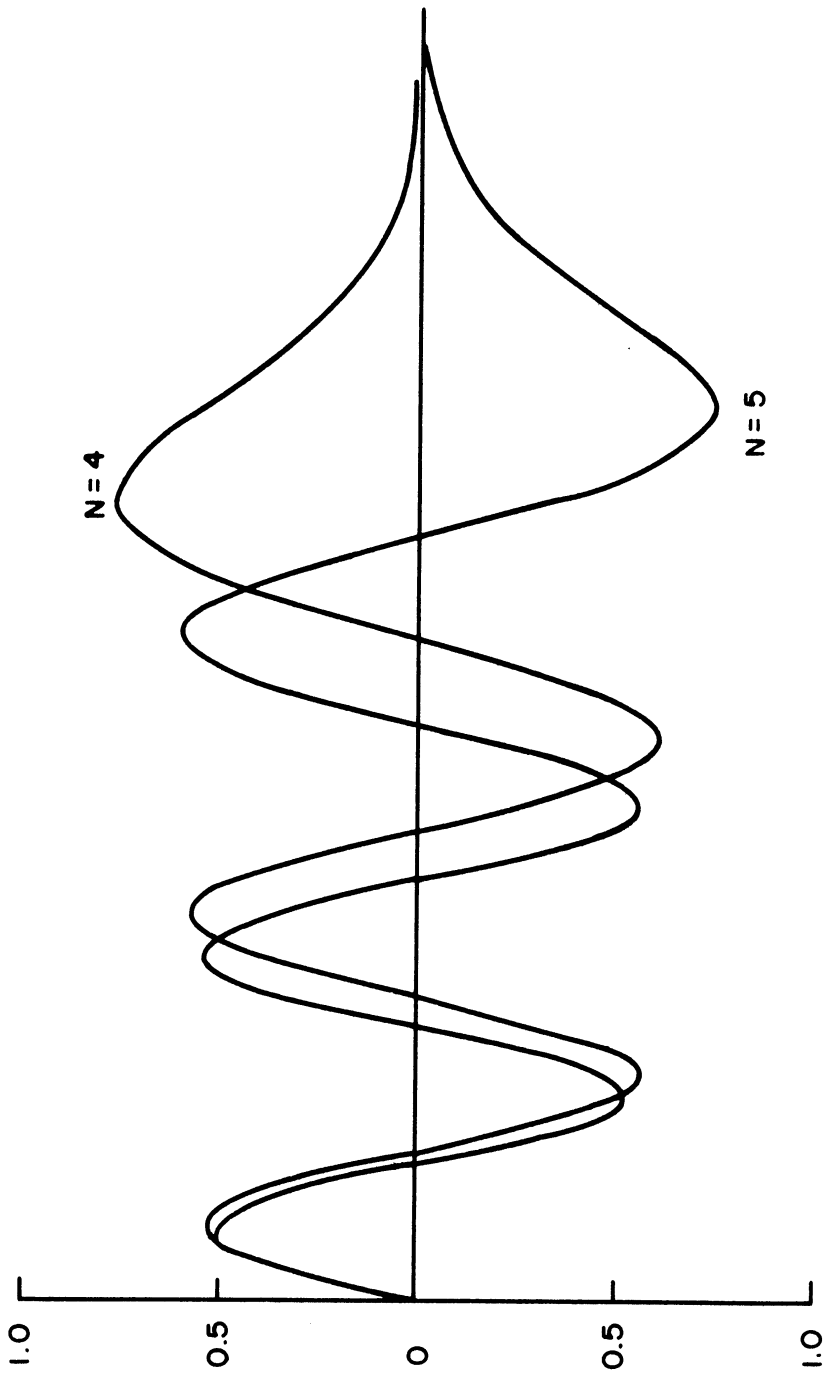

Figure III.7. Bound States Radial Wave Functions.

where

$$|N_k|^2 = \frac{2}{\pi}\frac{1}{\gamma\hbar\omega}\cdot\frac{\mu_0^2}{\rho_0^2\sin^2\mu_0 + \mu_0^2\cos^2\mu_0} \quad . \qquad (2.2.12)$$

The relative doorway state energy is given by $e_{j\alpha} + E^J_{(n)}$. We will adjust the absolute values of $e_{j\alpha}$ and the doorway state energies measured from the zero incident neutron energy, as follows: We assume that the absolute values of the single quasi-particle energies of N_i^{59} in the higher energy range, (sdg) levels, are approximately equal to those of the single particle energies of N_i^{57} which are $E_{N\ell_\alpha j_\alpha} - B$, and also that the former is given by $e_{j\alpha} - B$. Since the energy of the two quasi-particles relative to the vacuum state energy is given by $E^J_{(n)}$, the absolute value of the doorway state energy becomes

$$E_s(j\alpha, n) = e_{j\alpha} + E^J_{(n)} - B. \qquad (2.2.13)$$

2.3 Results and Discussions

For $J = 4$, the doorway state energies are far below the zero incident neutron energy. For $J = 2$, the states of the single quasi-particles are $2d_{3/2}$ and $2d_{5/2}$. From these two single quasi-particle states and five two quasi-particle states, there are made up nine three quasi-particle doorway states with energies above the zero incident neutron energy. These states are listed in Table III.7 along with the estimated values of the doorway state energies and formation probabilities. These results are also pictured in Figure III.8 together with the experimental values.

TABLE III.7

$\Gamma^{\uparrow}$ AND THE DOORWAY STATE ENERGIES

$(j_\alpha\ n)$	$E_{(j_\alpha n)}$ (Mev)	$\Gamma^{\uparrow}_{(J(n)j_d)\ 1/2^+}$ (kev)
$(d_{5/2}\ 2)$	0.49	109.
$(d_{5/2}\ 3)$	0.83	25.
$(d_{5/2}\ 4)$	1.19	32.
$(d_{5/2}\ 5)$	1.45	26.
$(d_{3/2}\ 1)$	2.22	2010.
$(d_{3/2}\ 2)$	3.75	113.
$(d_{3/2}\ 3)$	4.09	21.
$(d_{3/2}\ 4)$	4.45	23.
$(d_{3/2}\ 5)$	4.71	17.

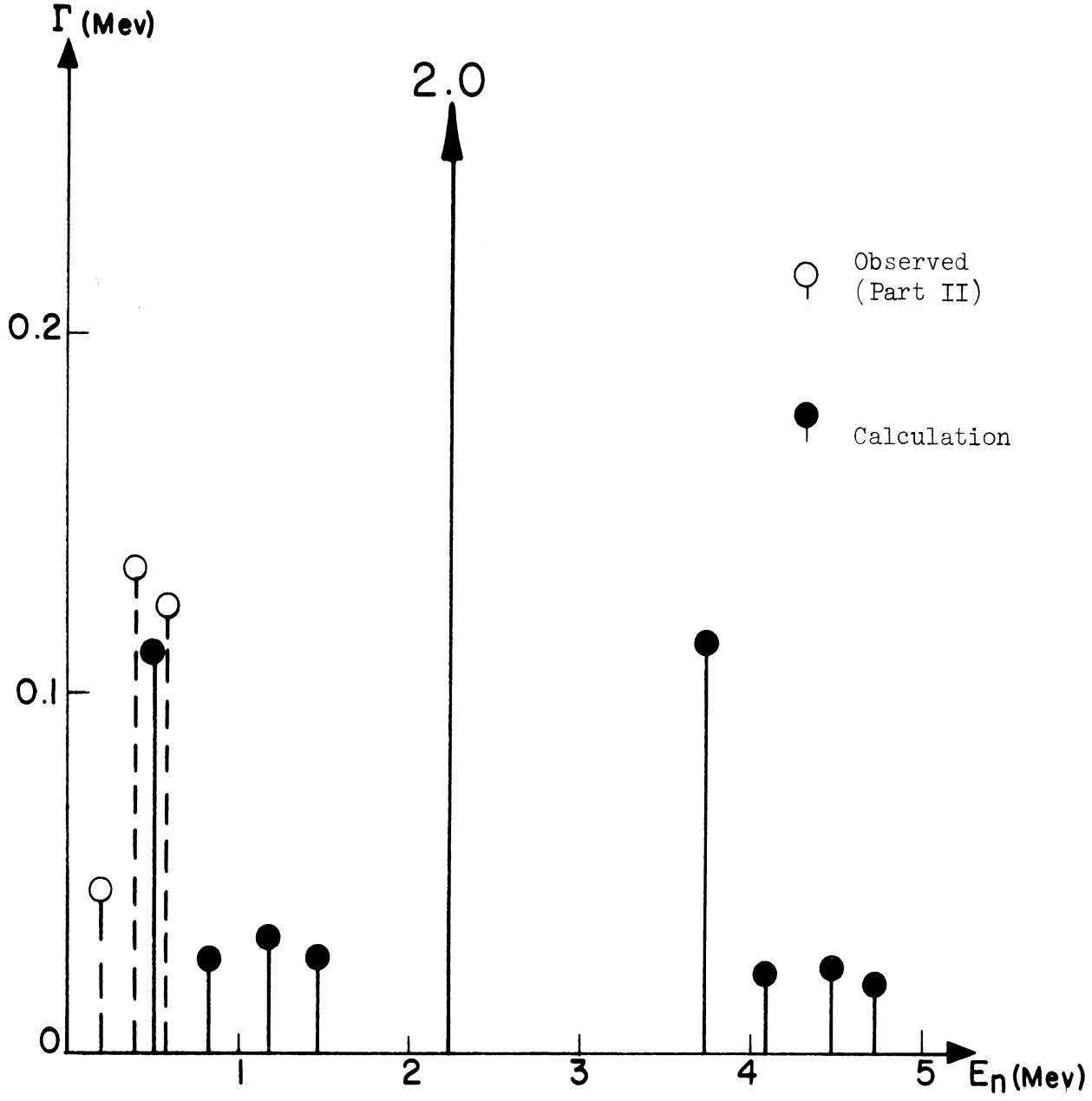

Figure III.8. $\Gamma^{\uparrow}$ and Doorway States.

We obtain two levels with $\Gamma^{\uparrow} \sim 100$ kev and six levels with $\Gamma^{\uparrow} \sim 30$ kev. In addition there is one level with a very large $\Gamma^{\uparrow}$ (~ 2 Mev) at ~ 2 Mev which resembles a giant resonance in the energy range of $2 \sim 3$ Mev. Accurate experimental values for $\Gamma^{\uparrow}$ are only available for the energy range less than 600 kev. The three identified values of $\Gamma^{\uparrow}$ (see Part II) are shown in Figure III.8 and they are seen to confirm the theory reasonably well. There is, in addition, a broad bump (its width $\sim$Mev) in the observed total cross section of natural $Ni^{(51)}$ around $1 \sim 2$ Mev which may very likely be associated with the predicted "giant" doorway state.

We will now briefly compare our calculations with other attempts at obtaining information about intermediate structures.

The elastic scattering cross sections of N^{15} and C^{12} are estimated by Lemmer and Shakin[71] and by Lovas.[80] Their estimated cross sections give excellent fits to the measured values. Compared to these fits, our results are not so good. However, our target nucleus is much more complicated than the C^{12} or N^{15} nucleus. In addition the SCS for C^{12} and N^{15} doorway states is WCL, so that the measured values of $\Gamma^{\uparrow}$ are just the widths of the individual fine resonances.

More complicated nuclei are treated by Shakin[77] who calculated $\Gamma^{\uparrow}$ values for Pb and Sn. As in the work of Lemmer and Shakin,[71] the author assumed that the SCS was WCL, and, in fact, in the case of Pb, there was an order of magnitude agreement between the calculated values of $\Gamma^{\uparrow}$ and the measured fine resonance widths. However, the calculated values of $\Gamma^{\uparrow}$ for Sn did not agree with the measured fine

widths. Our calculation is about as successful as Shakin's Pb calculation. However, our particular interest lies in treating examples of SCS (e.g. WC and SC) which are more general than the limiting case of WCL . In retrospect, it seems reasonable that Shakin's values for $\Gamma^{\uparrow}$ in Sn might prove more nearly correct if the Sn data had first been analyzed to determine the SCS .

Lande and Brown[106] calculated the spectroscopic factor of individual excited levels of Ni^{61} . Their results did not yield the intermediate structure. Briefly, the Lande-Brown model for the highly excited states of Ni^{61} is composed of one particle plus many phonons with a single frequency. The interaction Hamiltonian changes the phonon number by one. Thus, there is only one doorway state associated with a single particle state, resulting in the very low density of the doorway state levels. Presumably, we could use our model to calculate the fine resonance widths by abandoning the Picket Fence model and taking into account the excitation of more particles from the nuclear core. Although we would expect to obtain the intermediate structure (resonance width distribution (Part II)), the calculation would be very complicated.

Summary

The doorway state constants $\Gamma^{\uparrow}$ and $\Gamma^{\downarrow}$ of Ni^{58} and Ni^{59} are obtained from the analysis of the distribution of fine resonance widths (Part II). From the values obtained, the background cross section of Ni^{58} is estimated and is in good agreement with the measured cross section (Part II). The values of $\Gamma^{\downarrow}$ are incorporated into the modified O.M. imaginary potential in Part I and the result leads to the discovery the double $1/v$ total cross section of the

experimental measurements. Finally, in Part III, $\Gamma^{\uparrow}$ is estimated by means of a nuclear structure calculation and agrees fairly well with the experimental results. With these results, we may support the doorway state ansatz.

APPENDIX A

DISTORTED WAVE T-MATRIX AND SCATTERING AMPLITUDES

The T-matrix, T , may be defined by[73]

$$P\Psi^{(+)}_{[i]} = U_{[i]} + \frac{1}{E^{(+)} - H_0}\frac{P}{2\pi} T U_{[i]} . \qquad (A.1)$$

The scattering amplitudes, $\mathcal{F}$, may be defined by the asymptotic form of $P\Psi$:

$$P\Psi^{(+)}_{[i]} \sim U_{[i]} + \sum_{j=0}^{N} \mathcal{F}([i]\to[f]) \times$$

$$\times \frac{e^{ikr_0}}{r_0} \mathcal{U}_{s\nu_j} \Psi_j^{A}(r_1,\cdots,r_A), \qquad (A.2)$$

where notations may be seen in § 2.1 and 2.2 of Part I.

In this appendix, the T-matrix elements which are represented by the free waves will be related to the scattering amplitudes. Then, the T-matrix elements will be related to the distorted wave T-matrix (see Equation (2.2.22) of Part I)*. Finally, the cross section will be related to the scattering amplitudes and the T-matrix elements.

The T-matrix elements will be first related to the scattering amplitudes by comparing the asymptotic form of the solution of Equation (A.1) with Equation (A.2). Since the completeness relation on the subspace of $\mathcal{E}' \otimes \tilde{\mathcal{E}}^A$ projected by P is given by

$$\sum_{j=0}^{N} \sum_{\nu_j} \int d\underline{k}_j \, U_{[\alpha(j)\,\underline{k}_j s\nu_j]}(\underline{r}_0) \rangle\langle U_{[\alpha(j)\,\underline{k}_j s\nu_j]}(\underline{r}_0')$$

$$= P\,\delta(\underline{r}_0 - \underline{r}_0'), \qquad (A.3)$$

---

*Equations referred to in this appendix are in Part I of this thesis.

then Equation (A.1) becomes

$$P\Psi_{[i]}^{(+)} = U_{[i]} + \sum_{j=0}^{N} \sum_{\nu_j} \frac{1}{2\pi} \int d\underline{k}_j \frac{1}{E^{(+)} - E_j^A - \frac{\hbar^2 k_j^2}{2\mu}} \times$$

$$\times U_{[\alpha(j)\underline{k}_j s\nu_j]} \langle U_{[\alpha(j)\underline{k}_j s\nu_j]} T U_{[i]} \rangle \qquad (A.4)$$

$$\sim U_{[i]} - \frac{\mu}{\sqrt{2\pi}\hbar^2} \sum_{j=0}^{N} \sum_{\nu_j} \frac{e^{ik_j r_0}}{r_0} u_{s\nu_j} \Psi_j^A \langle U_{[f]} T U_{[i]} \rangle, \qquad (A.5)$$

where Equation (2.2.21) has been applied. By comparing Equation (A.5) with Equation (A.2), we have

$$\mathcal{F}([i] \to [f]) = -\frac{\mu}{\sqrt{2\pi}\hbar^2} \langle U_{[f]} T U_{[i]} \rangle . \qquad (A.6)$$

By means of the distorted wave given by Equation (2.2.22), the Schrödinger Equation of Equation (2.2.17) becomes

$$P\Psi_{[i]}^{(+)} = U_{[i]} + \frac{1}{E^{(+)} - H_0} U\chi_{[i]}^{(+)} + \frac{1}{E^{(+)} - PHP} W P\Psi_{[i]}^{(+)}$$

$$= U_{[i]} + \frac{1}{E^{(+)} - H_0} P \Big[U\chi_{[i]}^{(+)} +$$

$$+ \Big(1 + U \frac{1}{E^{(+)} - PHP}\Big) W P\Psi_{[i]}^{(+)} \Big], \qquad (A.7)$$

where we have applied the operator identity,

$$\frac{1}{E^{(+)} - PHP} P = \frac{1}{E^{(+)} - H_0} P + \frac{1}{E^{(+)} - H_0} PU \frac{1}{E^{(+)} - PHP} P ,$$

and the facts that $[U, P] = 0$, $PW = W$, and $P\chi^{(+)} = \chi^{(+)}$

Comparing Equation (A.7) to Equation (A.1), we have

$$\langle U_{[f]} T U_{[i]} \rangle = 2\pi \left\{ \langle U_{[f]} U \chi^{(+)}_{[i]} \rangle + \right.$$

$$\left. + \langle \chi^{(-)}_{[f]} W P \Psi^{(+)}_{[i]} \rangle \right\} , \qquad \text{(A.8)}$$

where

$$\chi^{(-)}_{[f]} = U_{[f]} + \frac{1}{E^{(-)} - H_0} U \chi^{(-)}_{[f]} . \qquad \text{(A.9)}$$

As far as the incident neutron is treated as a distinguishable one from those of the target nucleus, the incident and scattered wave currents (the first and second terms of Equation (A.2)) may be calculated as usual.[70] The results are

$$I_{inc} \sim \frac{\hbar k}{(2\pi)^3 \mu} \qquad (n/cm^2 sec) , \qquad \text{(A.10)}$$

and

$$I_{sc} \sim \sum_{j=0}^{N} \frac{\hbar k_j}{\mu} \left| f([i] \to [f]) \right|^2 \qquad (n/rad\ sec) . \qquad \text{(A.11)}$$

Thus, the differential cross section is obtained:

$$\frac{d\sigma([i] \to [f])}{d\Omega} = (2\pi)^3 \frac{k_j}{k} \left| f([i] \to [f]) \right|^2$$

$$= \frac{(2\pi)^2 \mu^2}{\hbar^4} \frac{k_j}{k} \left| \langle U_{[f]} T U_{[i]} \rangle \right|^2 . \qquad \text{(A.12)}$$

APPENDIX B

CROSS SECTIONS AND PARTIAL WAVE ANALYSIS

In § B.1, the wave functions of Appendix A will be transformed to the channel spin representation. Then, the partial wave analysis of the free wave will be given according to Goldberger and Watson[73] in § B.2. In § B.3, various cross sections will be expressed by the partial waves so that Blatt and Biedenharn's expression[76] will be derived. In § B.4, partial wave analysis of the distorted wave will be given. The orthonormality and completeness of the distorted waves[73] are given in § B.1 and § B.4. These relations are useful for later development of the unified theory.

B.1 Channel Spin

The channel spin is given by a vector couple of the incident neutron spin and the target nuclear spin[4] and its state vector is denoted by $\mathcal{U}_{\alpha s \nu}(s', s_\alpha)$:

$$\mathcal{U}_{\alpha s \nu}(s', s_\alpha) \equiv \sum_{\nu' \nu_\alpha} \langle s' s_\alpha \nu' \nu_\alpha | s \nu \rangle \, \mathcal{U}_{s' \nu'} \, \Psi^{A}_{\alpha(j)}(s_\alpha \nu_\alpha), \qquad \text{(B.1)}$$

where the indices (s', s_α) will be often suppressed.

The wave function of Equation (2.2.21)* is transformed by

$$\mathcal{U}_{\alpha(j) k_j s \nu} = \sum_{\nu_j \nu_\alpha} \langle s' s_\alpha \nu_j \nu_\alpha | s \nu \rangle \, \mathcal{U}_{[\alpha(j) k_j s' \nu_j]}$$

$$= \mathcal{U}_{k_j} \, \mathcal{U}_{\alpha(j) s \nu}, \qquad \text{(B.2)}$$

*Equations referred to in this appendix are in Part I of the thesis.

where

$$\upsilon_{\underline{k}_j} \equiv (2\pi)^{-3/2} e^{i \underline{k}_j \cdot \underline{r}_0} . \tag{B.3}$$

We define

$$\chi^{(+)}_{\alpha(j)\underline{k}_j s\nu} \equiv \sum_{\nu'\nu_\alpha} \langle s' s_\alpha \nu_j \nu_\alpha | s\nu \rangle \chi^{(+)}_{[\alpha(j)\underline{k}_j s'\nu_j]} , \tag{B.4}$$

and

$$P\Psi^{(+)}_{\alpha(j)\underline{k}_j s\nu} \equiv \sum_{\nu'\nu_\alpha} \langle s' s_\alpha \nu_j \nu_\alpha | s\nu \rangle P\Psi^{(+)}_{[\alpha(j)\underline{k}_j s'\nu_j]} . \tag{B.5}$$

The inverse relation to Equation (B.2) is

$$\upsilon_{[\alpha(j)\underline{k}_j s'\nu_j]} = \sum_{s\nu} \langle s' s_\alpha \nu_j \nu_\alpha | s\nu \rangle \upsilon_{\alpha(j)\underline{k}_j s\nu} . \tag{B.6}$$

We have the following orthonormality and completeness on $\mathcal{E}^1 \otimes \tilde{\mathcal{E}}^A$

$$\langle \upsilon_{\alpha(j)\underline{k}_j s\nu} | \upsilon_{\alpha'(j')\underline{k}'_j s'\nu'} \rangle$$

$$= \delta_{(\alpha s\nu;\alpha' s'\nu')} \delta(\underline{k}_j - \underline{k}'_j) , \tag{B.7}$$

and

$$\sum_{j=0}^{N} \sum_{s\nu} \int d\underline{k}_j \, \upsilon_{\alpha(j)\underline{k}_j s\nu}(\underline{r}) \rangle\langle \upsilon_{\alpha(j)\underline{k}_j s\nu}(\underline{r}')$$

$$= P\, \delta(\underline{r} - \underline{r}') . \tag{B.8}$$

By Equations (B.2), (B.4), and (B.5), Equation (A.1) becomes

$$P\Psi^{(+)}_{\alpha\underline{k}s\nu} = \upsilon_{\alpha\underline{k}s\nu} + \frac{1}{E^{(+)} - H_0} \frac{P}{2\pi} T \upsilon_{\alpha\underline{k}s\nu} . \tag{B.9}$$

Similarly, Equation (A.2) becomes

$$P\Psi^{(+)}_{\alpha \underline{k} s\nu} \sim U_{\alpha \underline{k} s\nu} + \sum_{j=0}^{N} \mathfrak{f}(\alpha \underline{k} s\nu \to \alpha(j) \underline{k}_j s_f \nu_f) \times \frac{e^{ik_j r_0}}{r_0} U_{\alpha(j) s_f \nu_f}, \tag{B.10}$$

where

$$\mathfrak{f}(\alpha \underline{k} s\nu \to \alpha(j) \underline{k}_j s_f \nu_f) \equiv \sum_{\nu' \nu_\alpha \nu_j \nu_\alpha} \langle s' s \nu' \nu_\alpha | s\nu \rangle \times \langle s'' s_\alpha \nu_j \nu_\alpha | s_f \nu_f \rangle \mathfrak{f}([\alpha \underline{k} s'\nu'] \to [\alpha(j) \underline{k}_j s'' \nu_j])$$

$$= -\frac{\mu}{\sqrt{2\pi}\, \hbar^2} \langle U_{\alpha(j) \underline{k}_j s_f \nu_f} \top U_{\alpha \underline{k} s\nu} \rangle. \tag{B.11}$$

Similar to Appendix A, we have the following differential cross section

$$\frac{d\sigma}{d\Omega}(\alpha \underline{k} s\nu \to \alpha(j) \underline{k}_j s_f \nu_f)$$

$$= \frac{(2\pi)^2 \mu^2}{\hbar^2} \frac{k_j}{k} \left| \langle U_{\alpha(j) \underline{k}_j s_f \nu_f} \top U_{\alpha \underline{k} s\nu} \rangle \right|^2. \tag{B.12}$$

A set of the solutions of the following equation,

$$\chi^{(+)}_{\alpha \underline{k} s\nu} = U_{\alpha \underline{k} s\nu} + \frac{1}{E^{(+)} - H_0} U \chi^{(+)}_{\alpha \underline{k} s\nu}, \tag{B.13}$$

satisfies the othonormality,

$$\langle \chi^{(+)}_{\alpha \underline{k} s\nu} | \chi^{(+)}_{\alpha' \underline{k}' s'\nu'} \rangle = \delta_{(s\nu; \alpha' s'\nu')} \delta(\underline{k} - \underline{k}'), \tag{B.14}$$

and the completeness,

$$\sum_{s\nu} \int d\underline{k}\, \chi^{(+)}_{\alpha \underline{k} s\nu}(\underline{r}) \rangle\langle \chi^{(+)}_{\alpha \underline{k} s\nu}(\underline{r}') + B.S. = P_\alpha\, \delta(\underline{r}-\underline{r}'), \qquad (B.15)$$

where B.S. is an abbreviation of a similar term to the first term which is sum over the bound states of the last neutron. The proof may be seen in the text by Goldberger and Watson.(73)

B.2 Free Wave in Partial Wave Analysis

The plane wave $v_{\underline{k}}$ expanded into a series:(73)

$$v_{\underline{k}} = \sqrt{\frac{2}{\pi}} \sum_{\ell m} i^\ell j_\ell(kr)\, Y_{\ell m}(\hat{\underline{r}})\, Y^*_{\ell m}(\hat{\underline{k}}), \qquad (B.16)$$

from which we may write:

$$v_{\alpha \underline{k} s\nu} = \sqrt{\frac{2}{\pi}} \sum_{\ell m} i^\ell j_\ell(kr)\, Y_{\ell m}(\hat{\underline{r}}) Y^*_{\ell m}(\hat{\underline{k}})\, u_{\alpha s\nu}. \qquad (B.17)$$

Let us define the partial wave by(73)

$$v_{\alpha \varepsilon \ell s J M} \equiv \sqrt{\rho_\varepsilon} \sum_{m\nu} \langle \ell s\, m\nu | JM \rangle \int d\hat{\underline{k}}\, Y_{\ell m}(\hat{\underline{k}})\, v_{\alpha \underline{k} s\nu}, \qquad (B.18)$$

where

$$\varepsilon = E - E_j^A = \frac{\hbar^2 k^2}{2m}. \qquad (B.19)$$

The inverse relation to Equation (B.18) is

$$v_{\alpha \underline{k} s\nu} = \frac{1}{\sqrt{\rho_\varepsilon}} \sum_{\ell m J M} \langle \ell s\, m\nu | JM \rangle\, Y^*_{\ell m}(\hat{\underline{k}})\, v_{\alpha \varepsilon \ell s J M}. \qquad (B.20)$$

The orthonormality and completeness of Equations (B.7) and (B.8) become

$$\langle \mathcal{U}_{\alpha\varepsilon\ell sJM} | \mathcal{U}_{\alpha'\varepsilon'\ell's'J'M'} \rangle = \delta_{(\alpha\ell sJM;\alpha'\ell's'J'M')} \delta(\varepsilon-\varepsilon') \qquad \text{(B.21)}$$

and

$$\sum_{\alpha\ell sJM} \int d\varepsilon \, \mathcal{U}_{\alpha\varepsilon\ell sJM}(\underline{r}) \rangle\langle \mathcal{U}_{\alpha\varepsilon\ell sJM}(\underline{r}')$$

$$= P\,\delta(\underline{r}-\underline{r}') . \qquad \text{(B.22)}$$

If we make use of the abbreviation,

$$\mathcal{U}_{\varepsilon\ell}(r) \equiv \sqrt{\frac{2}{\pi}} \sqrt{\rho_\varepsilon}\; i^\ell j_\ell(kr) , \qquad \text{(B.23)}$$

then the free wave may be written in the following form:

$$\mathcal{U}_{\alpha\varepsilon\ell sJM} = \sum_{m\nu} \langle \ell s m\nu | JM \rangle \, \mathcal{U}_{\varepsilon\ell}(r) Y_{\ell m}(\hat{\underline{r}}) \, \mathcal{U}_{\alpha s\nu} . \qquad \text{(B.24)}$$

B.3 Cross Sections

The cross section of Equation (B.12) will be reduced to the form of the Blatt and Biedenharn's expression.(76)

From Equation (B.20), we have

$$\langle \mathcal{U}_{\alpha'\underline{k}'s'\nu'} T \mathcal{U}_{\alpha\underline{k}s\nu} \rangle = \frac{1}{\sqrt{\rho_\varepsilon \rho_{\varepsilon'}}} \sum_{\ell m \ell' m' JM} \langle \mathcal{U}_{\alpha'\varepsilon'\ell's'JM} T \mathcal{U}_{\alpha\varepsilon\ell sJM} \rangle \times$$

$$\times \langle \ell' s' m'\nu' | JM \rangle \langle \ell s m\nu | JM \rangle Y_{\ell' m'}(\hat{\underline{k}}') Y_{\ell m}(\hat{\underline{k}}) , \qquad \text{(B.25)}$$

where we have used the fact that $[J,T] = 0$. We choose a coordinate system with the Z-axis parallel to k . Then we have $Y_{lm}^{*}(\hat{k}) = \delta_{m0}\sqrt{(2l+1)/4\pi}$ and hence

$$\langle U_{\alpha' \underline{k}' s' \nu'} T U_{\alpha \underline{k} s \nu} \rangle = \frac{1}{2\pi\sqrt{\rho_\varepsilon \rho_{\varepsilon'}}} \sum_{l m l' m' J M} \sqrt{\frac{2l+1}{4\pi}} \times$$

$$\times T^{J}_{\alpha' l' s'; \alpha l s} \langle l' s' m' \nu' | J M \rangle \langle l s m \nu | J M \rangle Y_{l' m'}(\hat{k}'), \qquad \text{(B.26)}$$

where $T^{J}_{\alpha' l' s'; \alpha l s}$ is defined by Equations (2.2.27) and (2.2.28).

From Equations (B.12) and (B.26), the differential cross section is obtained:

$$\frac{d\sigma}{d\Omega}(\alpha s \nu \to \alpha' \hat{k}' s' \nu') = \pi \lambda^2 \Big| \sum_{l l' m' J M} \sqrt{2l+1} \times$$

$$\times T^{J}_{\alpha' l' s'; \alpha l s} \langle l' s' m' \nu' | J M \rangle \langle l s 0 \nu | J M \rangle Y_{l' m'}(\hat{k}') \Big|^2 . \qquad \text{(B.27)}$$

Averaging over initial polarizations and summing over final polarizations, the result may be written in the form of Blatt and Biedenharn:

$$\frac{d\sigma}{d\Omega}(\alpha \hat{k} s \to \alpha' \hat{k}' s') \equiv \sum_{\nu'} \left\langle \frac{d\sigma}{d\Omega}(\alpha s \nu \to \alpha' \hat{k}' s' \nu') \right\rangle_{\nu}$$

$$= \frac{\lambda^2}{2s+1} \sum_{L} B_L(\alpha' s', \alpha s) P_L(\hat{k}' \cdot \hat{k}), \qquad \text{(B.28)}$$

where

$$B_L(\alpha' S', \alpha S) \equiv \frac{(-)^{S-S'}}{4} \sum_{\ell\ell'\ell''\ell'''} \sum_{JJ'} \bar{Z}(\ell J \ell'' J'; SL) \times$$

$$\times \bar{Z}(\ell' J \ell''' J'; SL) \left(T^J_{\alpha'\ell' S'; \alpha \ell S} \right)^* T^J_{\alpha' \ell''' S'; \alpha \ell'' S}, \qquad \text{(B.29)}$$

and

$$\bar{Z}(\ell J \ell'' J'; SL) \equiv \sqrt{(2J+1)(2J'+1)(2\ell+1)(2\ell''+1)} \times$$

$$\times \langle \ell \ell'' 00 | L 0 \rangle \, W(\ell J \ell'' J'; S L). \qquad \text{(B.30)}$$

The $\bar{Z}$-coefficient is defined by Lane and Thomas.[4] The Wigner W-coefficient[70,81] is related to the Wigner $6\text{-}j$ symmbol by

$$W(\ell J \ell'' J'; SL) = (-)^{J+\ell+J'+\ell''} \begin{Bmatrix} \ell & J & S \\ J' & \ell'' & L \end{Bmatrix}. \qquad \text{(B.31)}$$

By integral of the differential cross section of Equation (B.28) over $\hat{k}'$, the total cross-section becomes

$$\sigma(\alpha S \to \alpha' S') = \frac{\pi \lambda^2}{2S+1} \sum_{\ell\ell' J} (2J+1) \left| T^J_{\alpha'\ell' S'; \alpha \ell S} \right|^2. \qquad \text{(B.32)}$$

The total cross section for $\alpha \to \alpha'$ is then obtained;

$$\sigma(\alpha \to \alpha') \equiv \sum_{S'} \langle \sigma(\alpha S \to \alpha' S') \rangle_S$$

$$= \pi \lambda^2 \sum_J g_\alpha^J \sum_{\ell\ell' S S'} \left| T^J_{\alpha'\ell' S'; \alpha \ell S} \right|^2, \qquad \text{(B.33)}$$

where the statistical weight factor is given by

$$g_\alpha^J \equiv \frac{2J+1}{(2S_1+1)(2S_\alpha+1)}, \tag{B.34}$$

and S_1 and S_α are neutron spin and nuclear spin in the incident channel respectively. The S-matrix and T-matrix are related by

$$\underset{\sim}{S} = \underset{\sim}{1} - i\,\underset{\sim}{T} . \tag{B.35}$$

The total elastic cross section is given by

$$\sigma_\alpha^{EL} \equiv \sigma(\alpha\to\alpha) = \pi\lambda^2 \sum_J g_\alpha^J \sum_{ls} \Big\{ 1 - 2\mathcal{R}e\, S^J_{\alpha ls;\alpha ls} + \sum_{l's'} \big| S^J_{\alpha l's';\alpha ls} \big|^2 \Big\}, \tag{B.36}$$

and the total reaction cross section is

$$\sigma_\alpha^R \equiv \sum_{\alpha'(\neq\alpha)} \sigma(\alpha\to\alpha')$$

$$= \pi\lambda^2 \sum_J g_\alpha^J \sum_{ls} \Big\{ 1 - \sum_{l's'} \big| S^J_{\alpha l's';\alpha ls} \big|^2 \Big\}, \tag{B.37}$$

where the unitarity of S-matrix has been applied. The total cross section is given by

$$\sigma_\alpha^T = \sigma_\alpha^{EL} + \sigma_\alpha^R$$

$$= 2\pi\lambda^2 \sum_J g_\alpha^J \sum_{ls} \mathcal{R}e\left(i\, T^J_{\alpha ls;\alpha ls} \right). \tag{B.38}$$

B.4 Distorted Wave in Partial Wave Analysis

Let us define the partial wave of the distorted wave by

$$\chi^{(+)}_{\alpha\varepsilon\ell sJM} \equiv \sqrt{\rho_\varepsilon} \sum_{m\nu} \langle \ell s m\nu | JM\rangle \int d\hat{\underline{k}}\, Y_{\ell m}(\hat{\underline{k}})\, \chi^{(+)}_{\alpha \underline{k} s\nu} . \tag{B.39}$$

The inverse relation is obtained:

$$\chi^{(+)}_{\alpha \underline{k} s\nu} = \frac{1}{\sqrt{\rho_\varepsilon}} \sum_{\ell m JM} \langle \ell s m\nu | JM\rangle\, Y^*_{\ell m}(\hat{\underline{k}})\, \chi^{(+)}_{\alpha\varepsilon\ell sJM} . \tag{B.40}$$

Applying Equation (B.40) to Equations (B.14) and (B.15), we have the following orthonormality and completeness;

$$\left\langle \chi^{(+)}_{\alpha\varepsilon\ell sJM} \middle| \chi^{(+)}_{\alpha'\varepsilon'\ell's'J'M'} \right\rangle = \delta_{(\alpha\ell sJM;\alpha'\ell's'J'M')}\, \delta(\varepsilon-\varepsilon'), \tag{B.41}$$

and

$$\sum_{\ell sJM} \int d\varepsilon\, \chi^{(+)}_{\alpha\varepsilon\ell sJM}(\underline{r}) \rangle \langle \chi^{(+)}_{\alpha\varepsilon\ell sJM}(\underline{r}')$$

$$= P_\alpha\, \delta(\underline{r}-\underline{r}') . \tag{B.42}$$

APPENDIX C

DEVIATION FROM THE INFINITE PICKET FENCE MODEL

In Part II, we have applied the infinite Picket Fence model for the more complicated states. In this appendix, we will study the effects of the deviation of the model from the infinite Picket Fence model by relaxing two assumptions: the infinity of the number of the compounded states and the equality of the coupling strengths, a_n^2. We assume $(2N + 1)$ more complicated states, equi-spacing, $\bar{D}$, and that $|\xi/\bar{D}| < 1$, where ξ is defined in Equation (1.3.4)*. In § C.1, the equation for ξ will be derived. For WC, the poles will be obtained in § C.2. Then, assuming no fluctuation of a_n^2, we will evaluate the edge effects in § C.3.

C.1 Poles of the T-matrix

From the condition $F(E_k + \xi_k) = 0$ of Equation (1.3.1), we have

$$\xi_k = \frac{a_k^2}{E_k + \xi_k - E_0 - \sum_{\substack{l=-N \\ (\neq k)}}^{N} \frac{a_l^2}{E_k - E_l + \xi_k}}$$

$$= \frac{a_k^2}{E_k + \xi_k - E_0 - \langle a_l^2 \rangle_k \sum_{\substack{l=-N \\ (\neq k)}}^{N} \frac{a_l^2}{E_k - E_l + \xi_k}} , \qquad \text{(C.1)}$$

*Equations referred to in this appendix are in Part II of this thesis.

where we have defined the average $\langle a_\ell^2 \rangle_k$:

$$\sum_{\substack{\ell=-N \\ (\neq k)}}^{N} \frac{a_\ell^2}{E_k - E_\ell + \xi_k} = \langle a_\ell^2 \rangle_k \sum_{\substack{\ell=-N \\ (\neq k)}}^{N} \frac{1}{E_k - E_\ell + \xi_k} \,. \qquad \text{(C.2)}$$

The average value $\langle a_\ell^2 \rangle_k$ is complex in general and depends upon ξ_k . If we neglect fluctuations in the values of the coupling constants, then $\langle a_\ell^2 \rangle_k$ becomes independent of k and is given simply by a_k^2 $(= a_\ell^2$ for all ℓ) which is equivalent to another average:

$$\langle a_\ell^2 \rangle \equiv \frac{1}{2N+1} \sum_{\ell=-N}^{N} a_\ell^2 \,, \qquad \text{(C.3)}$$

while

$$\Gamma^{\downarrow} = \frac{2\pi}{\bar{D}} \langle a_\ell^2 \rangle \,. \quad \text{(see Equation (1.1.23)).} \qquad \text{(C.4)}$$

To illustrate the edge effects, we write, using Equation (2.0.3),

$$\sum_{\substack{\ell=-N \\ (\neq k)}}^{N} \frac{1}{E_k - E_\ell + \xi_k} = -\frac{1}{\xi_k} + \frac{\pi}{\bar{D}} \cot \frac{\pi \xi_k}{\bar{D}} +$$

$$+ \frac{1}{\bar{D}} \sum_{n=N+1}^{\infty} \left\{ \left[n - \left(\frac{\xi_k}{\bar{D}} + k \right) \right]^{-1} - \left[n + \left(\frac{\xi_k}{\bar{D}} + k \right) \right]^{-1} \right\} . \qquad \text{(C.5)}$$

Denoting the last term by $F(k, N, \xi_k/\bar{D})$, we have, using the Euler-Maclaurine sum formula,

$$F(k, N, x) \simeq -\frac{2}{\bar{D}} \tanh^{-1} \frac{k+x}{N+1} \,. \qquad \text{(C.6)}$$

Applying Equations (C.5) and (C.6) to Equation (C.1), we have

$$\xi_k (E_k + \xi_k - E_0) \tan \frac{\pi \xi_k}{D} = \langle a_l^2 \rangle_k \frac{\pi \xi_k}{D} +$$

$$+ (a_k^2 - \langle a_l^2 \rangle_k) \tan \frac{\pi \xi_k}{D} + \xi_k \langle a_l^2 \rangle_k F \tan \frac{\pi \xi_k}{D} . \qquad (C.7)$$

As $N \to \infty$, the function F approaches zero. If also $a_k^2 = \langle a_k^2 \rangle$, then Equation (C.7) is reduced to Equation (2.1.1). The second and third terms of r.h.s. of Equation (C.7) contain the fluctuation and edge effects.

We now expand F into a power series of x :

$$F(k, N, x) = \frac{1}{D} F_0(k, N) + x \left\{ F_1(k, N) + \right.$$

$$\left. + \frac{x}{2} F_2(k, N) + \frac{x^2}{3} F_3(k, N) + \cdots \right\} , \qquad (C.8)$$

where

$$F_0(k, N) \equiv \ln \frac{N+1-k}{N+1+k} , \qquad (C.9)$$

$$F_1(k, N) \equiv (N+1+k)^{-1} + (N+1-k)^{-1} , \qquad (C.10)$$

$$F_2(k, N) \equiv (N+1-k)^{-2} - (N+1+k)^{-2} , \qquad (C.11)$$

and $$F_3(k, N) \equiv (N+1+k)^{-3} + (N+1-k)^{-3} . \qquad (C.12)$$

C.2 Weak Coupling

For WC , the regular poles are obtained from Equation (C.7) with the result:

$$\xi_k \cong \frac{a_k^2}{E_k - E_0} + \frac{1}{(E_k - E_0)^3}\left\{ a_k^4 + \frac{1}{3}\left(\frac{\pi}{\bar{D}}\right)^2 a_k^6 \right\} +$$
$$+ \frac{1}{3}\left(\frac{\pi}{\bar{D}}\right)^2 \frac{a_k^4 \left(a_k^2 - \langle a_l^2 \rangle_k\right)}{(E_k - E_0)^3} +$$
$$+ \frac{\langle a_l^2 \rangle_k \, a_k^2}{(E_k - E_0)^2} \frac{1}{\bar{D}} F_0(k, N) +$$
$$+ \frac{\langle a_l^2 \rangle_k \, a_k^4}{(E_k - E_0)^3} \frac{1}{\bar{D}^2} F_1(k, N) . \qquad \text{(C.13)}$$

C.3 Edge Effects

If there is no fluctuation of a_k^2, then

$$a_k^2 = \langle a_l^2 \rangle_k = \langle a_k^2 \rangle = \frac{\bar{D}}{2\pi} \Gamma^{\downarrow} , \qquad \text{(C.14)}$$

and there remains only edge effects in Equation (C.13):

$$\xi_k \cong \frac{\frac{\bar{D}}{2\pi}\Gamma^{\downarrow}}{E_k - \frac{\Gamma^{\downarrow}}{2\pi} F_0 - E_0 + \frac{\frac{\bar{D}}{2\pi}\Gamma^{\downarrow}\left\{1 + \frac{\Gamma^{\downarrow}}{2\pi\bar{D}}\left(\frac{\pi^2}{3} - F_1 + F_0^2\right)\right\}}{E_k - E_0}} ,$$

$$\text{for } \frac{\Gamma^{\downarrow} F_0}{2\pi\Gamma^{\uparrow}} \ll 1 . \qquad \text{(C.15)}$$

C.4 Summary

Equation (C.13) is the generalization of Equations (1.4.8) and (2.2.6): If we ignore terms higher than first order in $a_k^2/(E_k - E_0)$, it is reduced to Equation (1.4.8). By assuming the Picket Fence (P.F.) model, it is reduced to Equation (C.15) and, by setting $N \to \infty$ further, Equation (2.2.6) is rederived.

The pole distributions of the P.F. models are shown in Figure C.1, where $\Gamma^{\uparrow}$ = 143.5 kev, $\Gamma^{\downarrow}$ = 61.5 kev and $\overline{D}$ = 18.0 kev. The open circles are the poles of the infinite P.F. model. The poles of the finite P.F. model are obtained by varying N as indicated in Figure C.1. The black circles are the poles of the infinite P.F. model but the distributinn is approximated by a Lorentzian (see Equations (3.4.3) and (3.4.9)).

The peak values of the distributions are almost independent of N . The deviation of Γ_k of the finite P.F. models from that of the infinite P.F. model becomes maximum at the edges. These results are consistent with those of Moldauer's R-matrix P.F. model. In our case, however, the values of Γ_k itself become small as the poles become farther from the doorway state. Consequently, the deviation does not affect the overall distribution significantly and the distribution may be approximated by that of the infinite P.F. model. Of course, this approximation becomes better as N increases. In Figure C.2, W (width of the distribution) and $\sum_k \Gamma_k$ as functions of N are shown. Relative error of W is less that 10 percent if $(2N+1)\overline{D} \gtrsim 2W$, while $\sum_k \Gamma_k$ depends on N to a somewhat greater extent.

In the above example, $\Gamma^{\downarrow}/\Gamma^{\uparrow} \cong 0.36$ and $U_0 = -38.0$. From the latter value, we have that the IC is attained when $\Gamma^{\downarrow}/\Gamma^{\uparrow} \cong 0.90$ (see Table II.1). Therefore, our example is fairly close to the IC . But the width distribution of the infinite P.F. model is still approximated well by the Lorentzian of which parameters are given by Equations (3.4.3) and (3.4.4).

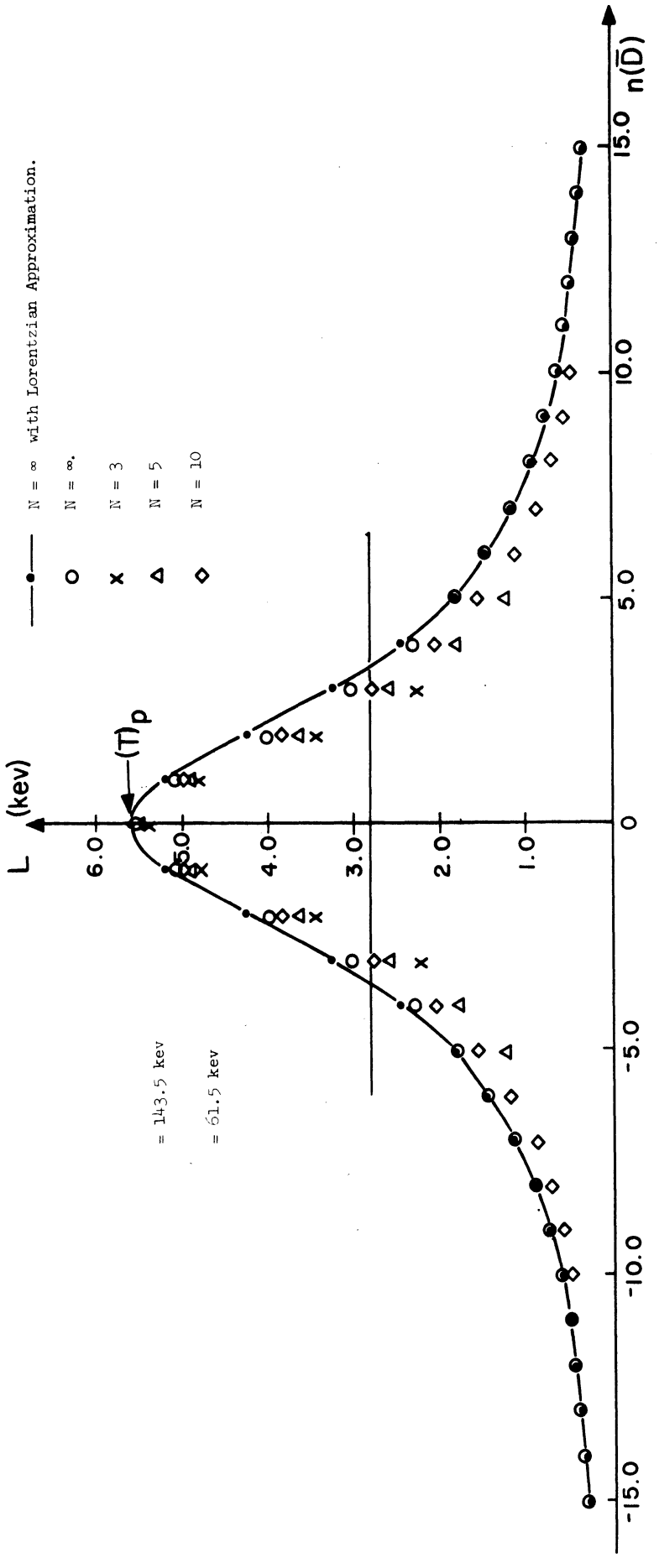

Figure C.1. Width Distribution (Edge Effects).

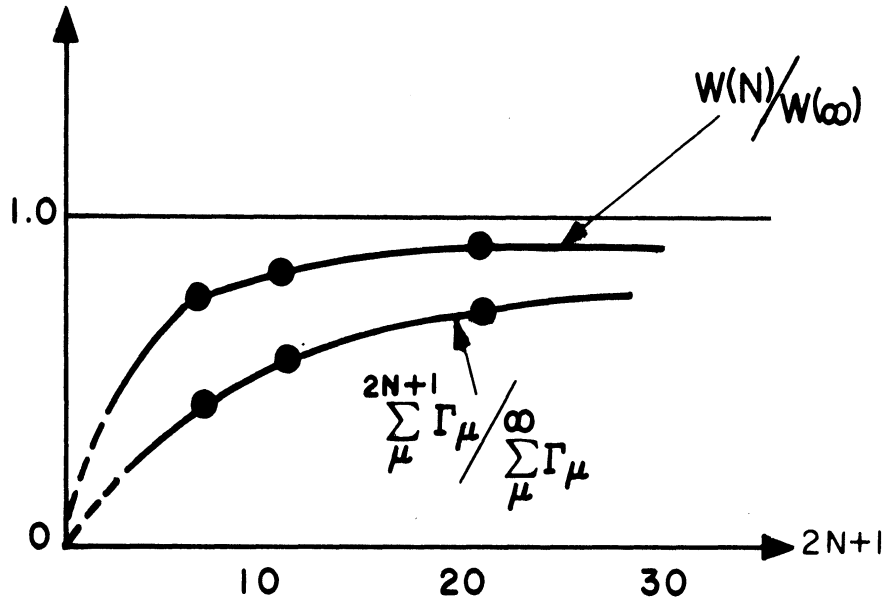

Figure C.2. W and $\sum_{\mu} \Gamma_\mu$ of the Finite Picket Fence Model.

Finally, we briefly discuss effects of fluctuations of a_ℓ^2 upon the average distribution of the poles for the case of an infinite number of poles $(F \to 0)$. Define a distribution function for the value of a_ℓ^2 by $P(a_\ell^2)$ such that

$$\int P(a_\ell^2)\, da_\ell^2 = 1,$$

and

$$\int a_\ell^2 P(a_\ell^2)\, da_\ell^2 = \langle a_\ell^2 \rangle .$$

Then, the probability for the values of the coupling strength of all the levels to be in $(a_\ell^2,\ a_\ell^2 + da_\ell^2)$ for $\ell = -N, -N+1, \ldots, N$ is given by

$$\prod_{\ell=-N}^{N} P(a_\ell^2),$$

and we will denote the expectation value of $F(a_{-N}^2, \cdots, a_N^2)$ by $(F(a_{-N}^2, \cdots, a_N^2))_{AV}$:

$$\left(F(a_{-N}^2, \cdots, a_N^2)\right)_{AV} \equiv \prod_{\ell=-N}^{N} \int F(a_{-N}^2, \cdots, a_N^2)\, P(a_\ell^2)\, da_\ell^2 .$$

E.g.

$$(a_k^2)_{AV} = \prod_{\ell=-N}^{N} \int a_k^2\, P(a_\ell^2)\, da_\ell^2 = \langle a_\ell^2 \rangle ,$$

$$(\langle a_\ell^2 \rangle_k)_{AV} = \langle a_k^2 \rangle ,$$

$$(a_k^6)_{AV} = (d_k^3)_{AV} + 3\langle a_k^2 \rangle (d_k^2)_{AV} + \langle a_k^2 \rangle^3 ,$$

$$(a_k^4)_{AV} = (d_k^2)_{AV} + \langle a_k^2 \rangle^2 ,$$

$$(a_k^4 \langle a_\ell^2 \rangle_k)_{AV} = (a_k^4)_{AV} \langle a_k^2 \rangle ,$$

where

$$d_k \equiv a_k^2 - \langle a_k^2 \rangle ,$$

and, for the last equation, we have used Equation (C.2) multiplied by a_k^4 and then averaged.

Limiting outselves to the case when $\Gamma^{\uparrow} \gg \bar{D}$, we may estimate the average of ξ_k from Equation (C.13) with the result:

$$(\xi_k)_{Av} \cong \xi_k|_{I.P.F.} + \frac{(d_k^2)_{Av} + \frac{1}{3}\left(\frac{\pi}{\bar{D}}\right)^2 \left\{ 2(d_k^3)_{Av} + 5\langle a_k^2 \rangle (d_k^2)_{Av} \right\}}{(E_k - E_0)^3} ,$$

where $\xi_k|_{I.P.F.}$ is given by Equation (2.2.6). Thus, the fluctuation effects are of the order of

$$\frac{(d_k^3)_{Av}}{(\langle a_k^2 \rangle)^3} \left\{ \frac{\bar{D}}{2\pi} \frac{\Gamma^{\downarrow}}{\Gamma^{\uparrow}} \right\}^2 .$$

For our case of the above example, the value in the braces is approximately 1. For further development, we need to know higher moments of the function P . However, from the above result, we conclude that the flucturation effects are smaller for weaker coupling and that the average pole distribution is expressed well by the infinite P.F. model if the fluctuation is small.

APPENDIX D

THE FORMULAE FOR PART III

In this appendix, some formulae which are applied in Part III are listed. These are mainly based on Lane's text.[67]

D.1 Tensor Expansion of the Two-Body Interaction Potential

The residual two-body interaction potential, $V(|\underline{r}_1 - \underline{r}_2|)$, is expanded into a tensor series.[72]

$$V(|\underline{r}_1-\underline{r}_2|) = \chi \sum_{LM} \frac{4\pi}{2L+1} U_L(r_1, r_2) Y^*_{LM}(\hat{\underline{r}}_1) Y_{LM}(\hat{\underline{r}}_2). \qquad (D.1)$$

If we may separate the radial dependence of the potential,[72]

$$U_L(r_1, r_2) = U_L(r_1)\, U_L(r_2), \qquad (D.2)$$

then the two-body interaction is reduced to a sum of products of single particle potentials.

In the second quantization formalism, the corresponding part of the Hamiltonian[69, 88] becomes

$$\begin{aligned} H_{L-L} &= -\frac{1}{2} \sum_{\alpha\beta\gamma\delta} \langle \alpha\beta | V(|\underline{r}_1 - \underline{r}_2|) | \gamma\delta \rangle_{NAS}\, a^+_\alpha a^+_\beta a_\gamma a_\delta \\ &= -\frac{\chi}{2} \sum_{LM} \frac{4\pi}{2L+1} \sum_{\alpha\cdots\delta} \langle \alpha | U_L(r_1) Y^*_{LM}(\hat{\underline{r}}_1) | \gamma \rangle \times \\ &\quad \times \langle \beta | U_L(r_2) Y_{LM}(\hat{\underline{r}}_2) | \delta \rangle\, a^+_\alpha a^+_\beta a_\gamma a_\delta , \end{aligned} \qquad (D.3)$$

where a^+_α and a_α are creation and annihilation operators of a state indicated by α, and $|\gamma\delta\rangle_{NAS}$ means the two particle wave function which is not anti-symmetrized.[67]

By applying Equation (1.1.11)* to Equation (D.3), we have

$$H_{L-L} = -\sum_{LM} \frac{2\pi \varkappa_L}{(2L+1)^2} \sum_{\substack{j_1 j_2 j_3 j_4 \\ m_1 m_2 m_3 m_4}} (-)^{L-M} (-)^{-j_1 - j_2 + m_3 + m_4} \times$$

$$\times \langle j_1 j_3\, m_1 -m_3 | L-M\rangle \langle j_2 j_4\, m_2 -m_4 | LM\rangle \langle j_1 \| U_L Y_L \| j_3\rangle \times$$

$$\times \langle j_2 \| U_L Y_L \| j_4\rangle a^+_{j_1 m_1} a^+_{j_2 m_2} a_{j_3 m_3} a_{j_4 m_4} , \qquad (D.4)$$

where the amplitude of the radial potential has now been incorporated into the force constant $\varkappa_L$

D.2 Normal Products

The four operators in Equation (D.4) are transformed by the BCS-transformation, Equation (1.1.5), to the quasi-particle creation and annihilation operators. Denoting normal products(98) with respect to the quasi-particle operators by $N(\text{-----})$, a^+a^+aa becomes

$$\begin{aligned} a_1^+ a_2^+ a_3 a_4 &= N(a_1^+ a_2^+ a_3 a_4) + \\ &+ \Big[V_1^2 \{ \delta_{14} N(a_2^+ a_3) - \delta_{13} N(a_2^+ a_4) \} + \\ &\quad + V_2^2 \{ \delta_{23} N(a_1^+ a_4) - \delta_{24} N(a_1^+ a_3) \} + \\ &\quad + \delta_{1\tilde{2}} V_1 U_2 N(a_3 a_4) + \delta_{3\tilde{4}} U_3 V_4 N(a_1^+ a_2^+) \Big] + \\ &+ \Big[(\delta_{14}\delta_{23} - \delta_{13}\delta_{24}) V_1^2 V_2^2 + \delta_{1\tilde{2}}\delta_{3\tilde{4}} V_1 U_2 V_3 U_4 \Big] \\ &\equiv (a_1^+ a_2^+ a_3 a_4)^{(4)} + (a_1^+ a_2^+ a_3 a_4)^{(2)} + (a_1^+ a_2^+ a_3 a_4)^{(0)} . \end{aligned} \qquad (D.5)$$

*Equations referred to in this appendix are in Part III of this thesis.

This decomposition of products of four operators into terms with normal products of 4, 2, and 0 operators is used to write H_{L-L} as a sum of terms $H^{(4)}_{L-L}$, $H^{(2)}_{L-L}$, and $H^{(0)}_{L-L}$ respectively. For example,

$$H^{(4)}_{L-L} = -\sum_{LM} \frac{4\pi \chi_L^2}{(2L+1)^2} \sum_{\substack{j_1 \cdots j_4 \\ m_1 \cdots m_4}} (-)^{L-M} \langle j_1 \| U_L Y_L \| j_3 \rangle \times$$

$$\times \langle j_2 \| U_L Y_L \| j_4 \rangle \langle j_1 j_3 \, m_1 - m_3 | L-M \rangle \langle j_2 j_4 \, m_2 - m_4 | LM \rangle \times$$

$$\times (-)^{j_1 + j_2 - m_3 - m_4} N\left(a^+_{j_1 m_1} a^+_{j_2 m_2} a_{j_3 m_3} a_{j_4 m_4} \right) . \qquad \text{(D.6)}$$

D.3 Vector Coupled Two Quasi-Particle Operators

A creation operator a^+_{jm} and an annihilation operator $(-)^{j-m} a_{j-m}$ have the rotation property of an angular momentum (jm).[88] So do b^+_{jm} and $(-)^{j-m} b_{j-m}$ (see Equation (1.1.5)). Therefore, two of these operators may be coupled by the C-G coefficients. We will denote

$$B^+(j_1 j_2 ; JM) \equiv \sum_{m_1 m_2} \langle j_1 j_2 m_1 m_2 | JM \rangle \, b^+_{j_1 m_1} b^+_{j_2 m_2} , \qquad \text{(D.7)}$$

$$B(j_1 j_2 ; JM) \equiv \sum_{m_1 m_2} \langle j_1 j_2 m_1 m_2 | JM \rangle (-)^{j_1 - m_1} b_{j_1 - m_1} \times$$

$$\times (-)^{j_2 - m_2} b_{j_2 - m_2} , \qquad \text{(D.8)}$$

$$A^+(j_1 j_2 ; JM) \equiv \sum_{m_1 m_2} \langle j_1 j_2 m_1 m_2 | JM \rangle \, b^+_{j_1 m_1} \times$$

$$\times (-)^{j_2 - m_2} b_{j_2 - m_2} , \qquad \text{(D.9)}$$

and

$$A(j_1 j_2; JM) \equiv -\sum_{m_1 m_2} \langle j_1 j_2 m_1 m_2 | JM \rangle b^{\dagger}_{j_2 m_2} \times$$

$$\times (-)^{j_1 - m_1} b_{j_1 - m_1} . \qquad (D.10)$$

The Hermitian conjugates of B^+ and A^+ are related to B and A according to

$$\left\{ B^+(j_1 j_2; JM) \right\}^{\dagger} = (-)^{J-M} B(j_1 j_2; J\,-M) , \qquad (D.11)$$

and

$$\left\{ A^+(j_1 j_2; JM) \right\}^{\dagger} = (-)^{J-M} A(j_1 j_2; J\,-M) . \qquad (D.12)$$

The commutation relations of these operators are complicated. However, we do have[67]

$$\left[B(j_1 j_2; JM),\, B^+(j_1' j_2'; J'M') \right] | \underset{\sim}{0} \rangle$$

$$= \delta_{JJ'} \delta_{MM'} \left\{ (-)^{J-M} \delta_{j_1 j_1'} \delta_{j_2 j_2'} - (-)^{j_1 + j_2 - M} \delta_{j_1 j_2'} \delta_{j_2 j_1'} \right\} | \underset{\sim}{0} \rangle . \qquad (D.13)$$

After some algebra, Equation (D.6) is reduced to the following form:

$$H^{(4)}_{L-L} = -\sum_{LM} \frac{2\pi \chi_L}{(2L+1)^2} \sum_{j_1 \cdots j_4} \langle j_1 \| U_L Y_L \| j_3 \rangle \langle j_2 \| U_L Y_L \| j_4 \rangle \times$$

$$\times (-)^{L-M+j_1+j_2+j_3+j_4} \left\{ -U_{j_1} U_{j_2} V_{j_3} V_{j_4} B^+(j_1 j_3; L\,-M) B^+(j_2 j_4; L\,M) - \right.$$

$$\left. - V_{j_1} V_{j_2} U_{j_3} U_{j_4} B(j_1 j_3; L\,-M) B(j_2 j_4; L\,M) + \right.$$

$$+ 2\left(U_{j_1}U_{j_2}V_{j_3}U_{j_4} - V_{j_1}V_{j_2}U_{j_3}V_{j_4}\right) B^{+}(j_1 j_3; L\,-M) A^{+}(j_2 j_4; LM) +$$

$$+ 2\left(U_{j_1}V_{j_2}U_{j_3}U_{j_4} - V_{j_1}U_{j_2}V_{j_3}V_{j_4}\right) A^{+}(j_1 j_3; L\,-M) B(j_2 j_4; LM) -$$

$$- 2\,U_{j_1}V_{j_2}V_{j_3}U_{j_4}\, B^{+}(j_1 j_3; L\,-M) B(j_2 j_4; LM) \Big\} +$$

$$+ \sum_{L} \frac{2\pi\,\chi_L}{(2L+1)^2} \sum_{\nu\kappa} (-)^{\nu-\kappa} \sum_{j_1 \cdots j_4} \mathcal{U}(j_1 j_2 j_3 j_4; L\nu) \times$$

$$\times \Big\{ \langle j_1 \| U_L Y_L \| j_2 \rangle \langle j_3 \| U_L Y_L \| j_4 \rangle (-)^{L+j_3+j_4} \times$$

$$\times \left(\frac{1}{\sqrt{2j_3+1}} U_{j_1}U_{j_2}U_{j_3}U_{j_4} + \frac{(-)^{j_1+j_2+j_3+j_4}}{\sqrt{2j_4+1}} V_{j_1}V_{j_2}V_{j_3}V_{j_4} \right) -$$

$$- \langle j_1 \| U_L Y_L \| j_4 \rangle \langle j_2 \| U_L Y_L \| j_3 \rangle U_{j_1}V_{j_2}V_{j_3}U_{j_4} \times$$

$$\times \left(\frac{1}{\sqrt{2j_3+1}} + \frac{(-)^{j_1+j_2+j_3+j_4}}{\sqrt{2j_4+1}} \right) \Big\} B^{+}(j_1 j_3; \nu\kappa) B(j_2 j_4; \nu\,-\kappa), \qquad (D.14)$$

where $\mathcal{U}(j_1 j_2 j_3 j_4; L\nu)$ is the Racah coefficient.[52,81]

D.4 The Reduced Matrix Elements and the Radial Integrals

The reduced matrix elements defined by Equation (1.1.11) may be related to the radial integral:[52]

$$\langle N'\ell'j' \| U_L Y_L \| N\ell j \rangle = (-)^{j-j'} \frac{1+(-)^{\ell+\ell'+L}}{2} \times$$

$$\times \sqrt{\frac{(2L+1)(2j'+1)}{4\pi}} \langle j' L\, \tfrac{1}{2}\, 0 | j\, \tfrac{1}{2} \rangle \langle N'\ell' | U_L | N\ell \rangle, \qquad (D.15)$$

where formulae for the 6-j and 3-j symbols[81] have been applied in the derivation.

The following property may be obtained from the above equation and the fact that the radial integral is real:

$$\langle j' \| U_L Y_L \| j \rangle = (-)^{j'-j} \langle j \| U_L Y_L \| j' \rangle \tag{D.16}$$

D.5 Shell Model Wave Functions

The single particle shell model Hamiltonian[72] is

$$H_{S.P.} = -\frac{\hbar^2}{2m}\Delta + \frac{m\omega^2}{2} r^2 + \underset{\sim}{l}\cdot\underset{\sim}{s}\, V_{l\text{-}s}(r) = H^{(0)}_{S.P.} + \underline{l}\cdot\underline{s}\, V_{l\text{-}s}. \tag{D.17}$$

The eigenfunctions of $H_{S.P.}\,|N l s j m\rangle = E_{Nlj}\,|N l s j m\rangle$ are usually obtained by perturbation theory[72] and the zero-th order solution is

$$|N l s j m\rangle = \sum_{m_l m_s} \langle l s m_l m_s | j m\rangle \frac{R_{nl}(r)}{r} Y_{l m_l}(\hat{\underline{r}})\, U_{s m_s}, \tag{D.18}$$

where the radial wave functions, R_{nl} , satisfy

$$-\frac{d^2 R_{nl}}{dr^2} + \frac{l(l+1)}{r^2} R_{nl} + r^2\beta^2 R_{nl} = \frac{2m}{\hbar^2} E_{nl} R_{nl}, \tag{D.19}$$

and where

$$E_{nl} \equiv E_N = \left(N + \frac{3}{2}\right)\hbar\omega, \tag{D.20}$$

[101,102]

$$\left.\begin{aligned} N &= 2n + l, \\ l &= N,\ N-2,\ \cdots,\ (0 \text{ or } 1) \end{aligned}\right\} \tag{D.21}$$

$Y_{lm}(\hat{\underline{r}})$: spherical Harmonics,

and $\beta \equiv \frac{m\omega}{\hbar}$ (D.22)

The principal quantum numbers N and n are used interchangably. The radial wave functions are given by[101,102]

$$R_{n\ell}(r) = A_{n\ell}\, r^{\ell+1} e^{-\frac{\beta}{2}r^2} L_n^{\ell+\frac{1}{2}}(\beta r^2), \tag{D.23}$$

where $L_n^{\ell+\frac{1}{2}}(\beta r^2)$ is the Laguerre polynomial:[103]

$$L_n^{\alpha}(z) \equiv \frac{e^z z^{-\alpha}}{n!} \frac{d^n}{dz^n}\left(e^{-z} z^{\alpha}\right). \tag{D.24}$$

The orthonormality relation is[103]

$$\int_0^{\infty} z^{\alpha} e^{-z} L_m^{\alpha}(z) L_n^{\alpha}(z)\, dz = \delta_{mn} \frac{\Gamma(\alpha+n+1)}{n!} \tag{D.25}$$

for $\alpha > -1$. The normalization constant of Equation (D.23) is given by

$$A_{n\ell} = \sqrt{\frac{2\,\beta^{\ell+3/2}\, n!}{\Gamma(n+\ell+3/2)}}\,. \tag{D.26}$$

To first order of $V_{\ell\text{-}s}$, the eigenvalues of $H_{s.p.}$ are[72]

$$E_{n\ell j} = E_{n\ell} + \frac{1}{2}\left\{ j(j+1) - \ell(\ell+1) - \frac{3}{4} \right\} \zeta_{n\ell}, \tag{D.27}$$

where

$$\zeta_{n\ell} \equiv \left\langle \frac{R_{n\ell}}{r} \middle| V_{\ell\text{-}s} \middle| \frac{R_{n\ell}}{r} \right\rangle . \tag{D.28}$$

The relation between the energy E_N and the quantum numbers is sketched in Figure D.1.

The completeness of the shell model wave functions is given by

$$\sum_{N\ell s j m} |N\ell s j m\rangle\langle N\ell s j m| = \underset{\sim}{1}\, \delta(\underset{\sim}{r} - \underset{\sim}{r}') . \qquad (\text{in spin} \otimes L_2) \tag{D.29}$$

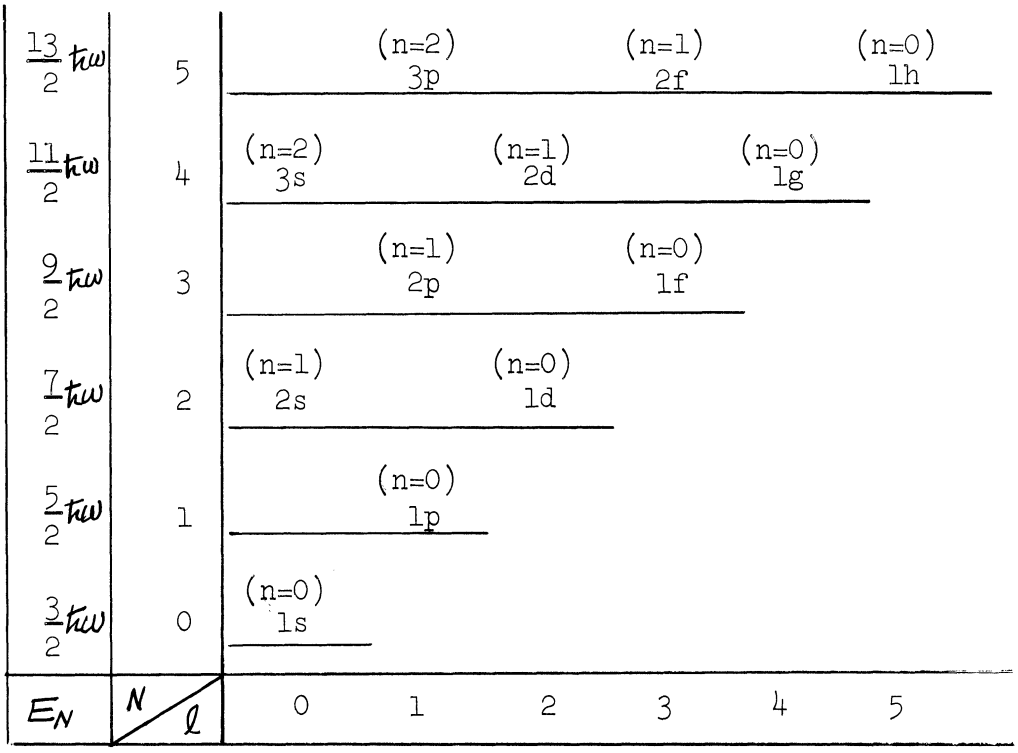

Figure D.1. E_N and Quantum Numbers.

D.6 Radial Integrals

Applying the formulas for the integrals of products of Laguerre polynomials,[101] we may obtain the radial integrals for Equation (D.15). In general, we have:

$$\langle N'\ell' | (\beta^{1/2} r)^{\lambda} | N\ell \rangle = \int_0^{\infty} (\beta^{1/2} r)^{\lambda} R_{n'\ell'}(r) R_{n\ell}(r)\, dr$$

$$= \left[\frac{n!\, n'!}{\Gamma(n+\ell+\frac{3}{2})\Gamma(n'+\ell'+\frac{3}{2})}\right]^{1/2} (-)^{n+n'} \left(\frac{\lambda+\ell'-\ell}{2}\right)! \left(\frac{\lambda+\ell-\ell'}{2}\right)! \times$$

$$\times \sum_{\sigma} \frac{\Gamma\left(\frac{\ell+\ell'+\lambda}{2}+\sigma+\frac{3}{2}\right)}{\sigma!\,(n-\sigma)!\,(n'-\sigma)! \left(\sigma+\frac{\ell'-\ell+\lambda}{2}-n\right)! \left(\sigma+\frac{\ell-\ell'+\lambda}{2}-n'\right)!}, \quad \text{(D.30)}$$

provided that the following conditions are satisfied:

$$\left.\begin{array}{l} n \\ n' \end{array}\right\} \geq \sigma \geq \begin{cases} n - \dfrac{\ell'-\ell+\lambda}{2} \\ n' - \dfrac{\ell-\ell'+\lambda}{2} \end{cases} , \qquad \text{(D.31)}$$

$$\ell-\lambda \leq \ell' \leq \ell+\lambda ,$$

and $$n - \frac{\ell'-\ell+\lambda}{2} \leq n' \leq n + \frac{\ell-\ell'+\lambda}{2} .$$

Otherwise, the integrals vanish. For $\lambda=2$, the non-zero radial integrals occur for $N'=N$, $N\pm2$ and for $\ell'=\ell$, $\ell\pm2$, and for $\lambda=4$, $N'=N$, $N\pm2$, $N\pm4$, and $\ell'=\ell$, $\ell\pm2$, $\ell\pm4$. The formulas are listed in Table D.1. In calculation of the matrix elements of V_L to use in the determination of $\Gamma^{\uparrow}$ as well as the low excited energy levels of Ni^{58}, we made the assumption

$$V_L \sim r^L .$$

This is equivalent to writing H_{L-L} as a sum of 2^Lpole-2^L pole forces. (References 97 and 99).

TABLE D.1a

RADIAL INTEGRALS ($\lambda = 2$)

N'	ℓ'	$\langle N'\ell' \mid \beta r^2 \mid N\ell \rangle$
N	ℓ	$N + \frac{3}{2}$
	$\ell+2$	$-\sqrt{(N+\ell+3)(N-\ell)}$
$N+2$	ℓ	$-\frac{1}{2}\sqrt{(N+\ell+2\pm1)(N-\ell+1\pm1)}$
	$\ell+2$	$-\frac{1}{2}\sqrt{(N+\frac{1}{2}\pm(\ell+\frac{5}{2}))(N+\frac{5}{2}\pm(\ell+\frac{5}{2}))}$

TABLE D.1b

RADIAL INTEGRALS ($\lambda = 4$)

N'	ℓ'	$\langle N'\ell' \mid \beta^2 r^4 \mid N\ell \rangle$
N	ℓ	$\frac{1}{2}\left\{(N+\frac{5}{2})(N+\ell+3) + (N-\ell)(2N+\ell+\frac{7}{2})\right\}$
	$\ell+2$	$-\frac{3}{2}\sqrt{(N+\ell+3)(N-\ell)}\ (N+\ell+\frac{3}{2})$
	$\ell+4$	$\frac{3}{2}\sqrt{(N+\ell+5)(N+\ell+3)(N-\ell)(N-\ell-2)}$
$N\pm2$	ℓ	$-\sqrt{(N+\ell+2\pm1)(N-\ell+1\pm1)}\ (N+\frac{3}{2}\pm1)$
	$\ell+2$	$\frac{1}{2}\sqrt{\{N+\frac{5}{2}\pm(\ell+\frac{5}{2})\}\{N+\frac{1}{2}\pm(\ell+\frac{5}{2})\}}\ \{2N+3\pm(\ell+\frac{1}{2})\}$
	$\ell+4$	$-\sqrt{(N-\ell)(N+\ell+3)\{N+\frac{5}{2}\pm(\ell+\frac{9}{2})\}\{N+\frac{1}{2}\pm(\ell+\frac{9}{2})\}}$
$N\pm4$	ℓ	$\frac{1}{4}\sqrt{(N+\ell+3\pm2)(N+\ell+1\pm2)(N-\ell\mp2)(N-\ell+2\mp2)}$
	$\ell+2$	$\frac{-1}{4}\sqrt{(N+\ell+4\pm3)(N-\ell-1\pm3)\{N+\frac{5}{2}\pm(\ell+\frac{5}{2})\}\{N+\frac{1}{2}\pm(\ell+\frac{5}{2})\}}$
	$\ell+4$	$\frac{1}{4}\sqrt{\{N+\frac{9}{2}\pm(\ell+\frac{9}{2})\}\{N+\frac{5}{2}\pm(\ell+\frac{9}{2})\}\{N+\frac{1}{2}\pm(\ell+\frac{9}{2})\}\{N-\frac{3}{2}\pm(\ell+\frac{9}{2})\}}$

REFERENCES

1. Feshbach, H. Ann. Phys. 5, 357 (1958).

   _____ . Ann. Phys. 19, 287 (1962).

2. Block, B. and Feshbach, H. Ann. Phys. 23, 47 (1963).

3. Blatt, J. B. and Weisskopf, V. F. Theoretical Nuclear Physics. New York: John Wiley and Sons, 1952.

4. Lane, A. M. and Thomas, R. G. Rev. of Mod. Phys. 30, 257 (1958).

5. Breit, G. Encyclopedia of Physics. Vol. XLI/1, Berlin: Springer-Verlag, 1959.

6. Evans, R. D. The Atomic Nucleus. New York: McGraw-Hill, 1955.

7. Darrow, K. K. Rev. Sci. Instr. 4, 58 (1933), and 5, 66 (1934).

8. Rutherford, E. Phil. Mag. 37, 581 (1919).

9. Pose, H. Z. Physik. 64, 1 (1930).

10. Bothe W. and Becker, H. Z. Physik, 66, 289 (1930).

11. Chadwick, J. Proc. Roy. Soc. A136, 692 (1932).

12. Nuclear Data Tables, Part I, USAEC. (1960).

13. Moon, P. B. and Tillman, J. R. Nature. 135, 904 (1935).

    _____ . Nature. 136, 66 (1935)

    _____ . Proc. Roy. Soc. A135, 476 (1936).

14. Bohr, N. Nature. 137, 344 (1936).

15. Breit, G. and Wigner, E. Phys. Rev. 49, 519 (1936).

16. Bethe, H. A. Rev. Mod. Phys. 9, 69 (1937).

    Bethe, H. A. and Placzek, G. Phys. Rev. 51, 450 (1937).

17. Weisskopf, V. F. Phys. Rev. 52, 295 (1937).

    Weisskopf, V. F. and Ewing, D. H. Phys. Rev. 57, 472, 935 (1940).

18. Konopinski, E. J. and Bethe, H. Phys. Rev. 54, 130 (1938).

19. Kapur, P. L. and Peierls, R. E. Proc. Roy. Soc., A166, 277 (1938).

20. Breit, G. Rev. of Mod. Phys. 36, 1071 (1964).

21. Weisskopf, V. F. Phys. Today. 14, 18 (1961).

22. Block, B. and Feshbach, H. Ann. Phys. 23, 47 (1963).

23. Moldauer, P. A. Phys. Rev. 135, B642 (1964).

24. Feshbach, H. Ann. Rev. Nucl. Sci. 8, 49 (1958).

25. Bethe, H. A. Phys. Rev. 47, 747 (1935).

26. Bethe, H. A. Phys. Rev. 57, 1125 (1940).

27. Ford, K. W. and Bohm, D. Phys. Rev. 79, 745 (1950).

28. Barshall, H. H. Phys. Rev. 86, 431 (1952).

29. Feshbach, H., Porter, C. E. and Weisskopf, V. F. Phys. Rev. 96, 448 (1954).

30. Lane, A. M., Thomas, R. G. and Wigner, E. P. Phys. Rev. 98, 693 (1955).

31. Elliot, J. P. and Skylm, T. H. R., Proc. Roy. Soc. A232, 561 (1955).

32. Thomas, R. G. Phys. Rev. 97, 224 (1955).

33. Lane, A. M., Thomas, R. G. and Wigner, E. P. Phys. Rev. 98, 693 (1955).

34. Moldauer, P. A., Phys. Rev. 157, 907 (1967).

35. Freidman, F. L. and Weisskopf, V. F. Niels Bohr and Development of Physics. London: Pergamon Press, 1955.

36. Wolfenstein, L. Phys. Rev. 82, 690 (1951).

Hauser, W. and Feshbach, H. Phys. Rev. 87, 366 (1952).

37. Moldauer, P. A. Rev. of Mod. Phys. 36, 1079 (1964).

38. Bjorklund, F. and Fernback, S. Phys. Rev. 109, 1295 (1958).

39. Amster, H. J. Phys. Rev. 113, 911 (1959).

40. Khanna, F. C. and Tang, Y. C. Nucl. Phys. 15, 337 (1960).

41. Krueger, T. K. and Margolis, B. Nucl. Phys. 28, 578 (1961).

42. Fiedeldey, H. and Fralm, W. E. Nucl. Phys. 38, 868 (1962).

43. Moldauer, P. A. Nucl. Phys. 47, 65 (1963).

44. Vladiminsky, V. V. and Ilyiann, I. L. Nucl. Phys. 6, 295 (1958).

45. Magolis, B. and Tronbetzkoy, E. S. Phys. Rev. 106, 105 (1958).

46. Chase, D. M., Willets, L. and Edmonds, A. R. Phys. Rev. 110, 1080 (1958).

47. Buck, B. Phys. Rev. 130, 712 (1963).

48. Perey, F. and Buck, B. Nucl. Phys. 32, 353 (1962).

49. Reference 24 and references in it.

50. Porter, C. E. Phys. Rev. 100, 935 (1955).

51. BNL-325 (1958) and (1966).

KFK-120 (1962).

52. Yoshida, S. Proc. Roy. Soc. A69, 668 (1956).

53. Lemmer, R. H. and Shakin, C. M. Ann. Phys. 27, 13 (1964).

54. BNL-904 (N-8) (1965).

55. ABACUS II-Code (BNL-6562).

56. Feshbach, H. Nuclear Spectroscopy, (F. Ajzenberg-Selve, ed., (F. Ajzenburg-Selve, ed.), New York: Academic Press, 1960.

57. Porter, C. E. Rev. of Mod. Phys. 36, 1094 (1964).

58. Porter, C. E. Statistical Theories of Spectra; New York: Academic Press, 1965.

59. Porter, C. E. Phys. Rev. 100, 935 (1955).

60. Tobocman, W. Theory of Direct Nuclear Reactions. London: Oxford University Press (1961).

61. Lemmer, R. H. BNL-948 Vol III (1965).

Feshbach, H. Nuclear Structure Study with Neutrons. Amsterdam: North Holland Pub., 1966.

Feshbach, H., Kerman, A. K. and Lemmer, R. H. Ann. Phys. 41, 230, (1967).

62. Kerman, A. K., Rodberg, L. S. and Young, J. E. Phys. Rev. Lett. 11, 422 (1963).

63. Takeuchi, K. Bull. Am. Phys. Soc., II, 12 (1966).

64. Austern, N. Fast Neutron Physics, Part II, (I.N. Morison and J. L. Flower, ed.), New York: Interscience Pub., 1963.

65. Nagasaki, M. Progr. Theoret. Phys. 16, 429 (1956).

Ui, H. Progr. Theoret. Phys. 16, 299 (1956).

Brown, G. E. and deDominicis, C. T. Proc. Phys. Soc. (London) 70A 668, 681, 686 (1957).

Block, C. Nucl. Phys. 4, 503 (1957).

66. Hecht, K. T. Selected Topics in Nuclear Spectroscopy. (B. J. Verhaar, ed.), Amsterdam: North-Holland Pub., 1964.

67. Lane, A. M. Nuclear Theory. New York: Benjamin, 1964.

68. For all this section, see Reference 67.

69. Dirac, P. A. M. The Principle of Quantum Mechanics. London: Oxford University Press, 1947.

70. Messiah, A. Quantum Mechanics I and II. New York: John Wiley and Sons, 1962.

71. Lemmer, R. H. and Shakin, C. M. Ann. Phys. 27, 13 (1964).

72. de-Shalit, A. and Talmi, I. Nuclear Shell Theory. New York: Academic Press, 1963.

73. Goldberger, M. L. and Watson, K. M. Collision Theory. New York: John Wiley and Sons, 1964.

74. Emmerich, W. S. "Optical Model Theory." Fast Neutron Phys. Part II. (J. M. Morison and J. L. Fowler, ed.), New York: Interscience Pub., 1963.

75. Moldauer, P. A. Phys. Rev. 123, 968 (1961).

76. Blatt, J. M. and Biedenharn, L. C. Rev. of Mod. Phys. 24, 258 (1952).

77. Shakin, C. M. Ann. Phys. 22, 373 (1964).

78. Whittaker, E. T. and Watson, G. N. A Course of Modern Analysis. London: Cambridge Press, 1963.

Knopp, K. Theory of Functions. Part I and II, New York: Dover Pub., 1947.

Churchill, R. G. Complex Variables and Applications. New York: McGraw-Hill, 1960.

79. Perlis, S. Theory of Matrices. New York: Addison-Wesley, 1958.

80. Lovas, I. Nucl. Phys. 81, 353 (1966).

81. Rotenberg, M. The 3-j and 6-j Symbols. MIT Press, 1959.

82. Mahaux, C. and Weidenmüller, H. A. Nucl. Phys. A91, 241 (1967).

83. Smith, A. B. private communication.

84. Humblet, J. and Rosenfeld, L. Nucl. Phys. 26, 529 (1961).

85. Bilpuch, E. G., Seth, K. K., Bowman, C. D., Tabony, R. H., Smith, R. C., and Newson, H. W. Ann. Phys. 14, 387 (1961).

Bowman, C. D., Bilpuch, E. G. and Newson, H. W. Ann. Phys. 17, 319 (1962).

Farrell, J. A., Bilpuch, E. G. and Newson, H. W. Ann. Phys. 37, 367 (1966).

86. Divadeenam, M. and Newson, H. W. Bull. Am. Phys. Soc. 12, GD10 (1966).

87. Schiff, L. I. Quantum Mechanics. New York: McGraw-Hill, 1955.

88. Brink, D. M. and Satchler, G. R. Nouvo Cimento IV No. 3 (1956).

89. Moldauer, P. A. Bull. Am. Phys. Soc. 12, 27 (1966) and References in it.

90. Singh, P. P., Hoffman-Pinther, P. and Lang, D. W. Phys. Lett. 23, 255 (1966).

91. Ericson, T. Phys. Rev. Lett. 5, 430 (1960).

_____ . Am. Phys. 23, 290 (1963).

_____ . Phys. Lett. 4, 258 (1963).

Brink, D. B. and Stephen, R. O. Phys. Lett. 5, 77 (1963).

_____ . Nucl. Phys. 54, 577 (1964).

Moldauer, P. A. Phys. Lett. 8, 70 (1964).

92. Smith, A. B. and Whalen, J. F. Bull. Am. Phys. Soc. 12, GD16 (1966).

93. Cox, S. A. Bull. Am. Phys. Soc. 12, GD15 (1966), Phys. Lett. to be published.

94. Peierls, R. E. Proc. Roy. Soc. A253, 16 (1959).

LeCouteur, E. J. Proc. Roy. Soc. A256, 115 (1960).

Davies, K. T. R. and Baranger, M. Ann. Phys. 19, 383 (1962).

Weidenmüller, H. A. Ann. Phys. 28, 60 (1964), 29, 378 (1964).

95. Wigner, E. P. and Eisenbud, L. Phys. Rev. 72, 29 (1947).

96. Newton, R. G. J. of Math. Phys. 1, 319 (1960).

97. Yoshida, S. Phys. Rev. 123, 2122 (1961).

98. Schweber, S. S. An Introduction to Relativistic Quantum Field Theory. New York: Harper and Row Pub., 1962.

99. Kisslinger, L. S., and Sorensen, R. A. Mat. Fys. Medd. Dan. Vid. Selsk. 32, no. 9 (1960).

100. Baranger, M. Phys. Rev. 120, 957 (1960).

101. Morse, P. M. and Feshbach, H. Methods of Theoretical Physics. Part I and II, New York: McGraw-Hill, 1953.

102. Nilsson, S. G. Dan. Mat. Fys. Medd. 29, no. 16 (1955).

103. Handbook of Mathematical Functions. (M. Abramowitz and I. A. Stegun, ed.) National Bureau of Standards, Washington, D. C., 1964.

104. Russell, J. B. J. of Math. and Phys. 12, 291 (1933).

105. Fullmer, R. H., McCarthy, A. L., Cohen, B. L., and Middelton, R. Phys. Rev. 133, B955 (1964).

106. Lande, A. and Brown, G. E. Nucl. Phys. 75, 344 (1966).

107. Cohen, S. Lawson, R. D., Macfarlane, M. N., Pandya, S. P., and Soga, M. Phys. Rev. to be published.

108. Hsu L. S. and French, J. B., Phys. Lett. 19, 135 (1965).

109. Plastino, A., Arvieu, R. and Moszkowski, S. A. Phys. Rev. 145, 837 (1966).

110. Auerbach, N. Nucl. Phys. 74, 321 (1966).